Identification and functional characterization of ICS1-dependent metabolites in *Arabidopsis thaliana* (L.) HEYNH.

Inaugural-Dissertation

zur Erlangung des Doktorgrades
der Mathematisch-Naturwissenschaftlichen Fakultät
der Heinrich-Heine-Universität Düsseldorf

vorgelegt von

Nicola Scholten

aus Essen

Düsseldorf, Mai 2021

aus dem Institut für Molekulare Ökophysiologie der Pflanzen
der Heinrich-Heine-Universität Düsseldorf

Gedruckt mit der Genehmigung der
Mathematisch-Naturwissenschaftlichen Fakultät der
Heinrich-Heine-Universität Düsseldorf

Berichterstatter:
1. Prof. Dr. Jürgen Zeier
2. Prof. Dr. Georg Groth

Tag der mündlichen Prüfung: 28.10.2021

Danksagung

An dieser Stelle möchte ich mich bei den Personen bedanken ohne die, die Erstellung der Arbeit nicht möglich gewesen wäre.

Ganz herzlich möchte ich mich bei Herrn Prof. Dr. Jürgen Zeier für die Vergabe und Betreuung eines so interessanten Promotionsthemas bedanken. Ebenso bedanke ich mich für die guten Ratschläge, anregenden Disskussionen und die freie Arbeitsweise.
Herrn Prof. Dr. Georg Groth danke ich herzlichst für die freundliche Erstellung des Zweitgutachtens.

Ein weiterer Dank geht an iGRAD*plant*, welches mir nicht nur die Promotion ermöglicht hat, sondern auch darüberhinaus geholfen hat meine eigenen Fähigkeiten auszubauen. An dieser Stelle geht ein ganz besonderer Dank an Frau Prof. Dr. Susanne Hoffmann-Benning. Ich bedanke mich für die nette Aufnahme und gute Betreuung in ihrer Arbeitsgruppe während meines Aufenthaltes an der Michigan State University. Aus ihrer Arbeitsgruppe bedanke ich mich besonders bei Dr. Jie Li, der mich in die Floureszenzmikroskopie eingeführt hat.

Der größte Dank geht an alle ehemaligen und akutellen Mitglieder des Instituts Molekulare Ökophysiologie der Pflanzen. Dr. Michael Hartmann und Dr. Stefan Schuk danke ich für jedgliche Unterstützung, ob bei schwierigen Fragen im Labor oder als Mentoren bei kniffeligen Problemen. Für ein offenes Ohr und die gute Laune bedanke ich mich bei Karin Kiefer. Des Weiteren danke ich Dr. Elia Stahl, Dr. Ziba Ajam, Ipek Yildiz und Anika Schnake die mich auf dem Weg zur Promotion begleitet haben. Für die zuverlässige und motivierte Arbeitsweise möchte ich mich bei meinen Studentinnen Melissa Mantz, Sarah Zerres und Marie Löwe bedanken. Mit euch allen hat es wirklich Spaß gemacht!

Zum Schluss möchte ich mich bei meinen Freunden und meiner Familie bedanken. Meinen Eltern, die mich in all meinen Entscheidungen unterstützten und meinen Schwestern, auf die ich mich immer verlassen kann. Bei meiner eigenen kleinen Familie bedanke ich mich dafür, dass sie mir jeden Tag zeigt wie vielfältig Liebe ist.

Table of contents

Abbreviations

Units and abbreviations from the International System of Units (SI) are not listed as well as dimensional units, which are specified by the International Union for Pure and Applied Chemistry (IUPAC). The single- and three-letter code is used for amino acids.

3-CaBA	3-carboxybenzoic acid, isophthalic acid
3-CaMeBA	3-(carboxymethyl)-benzoic acid
3-FBA	3-formylbenzoic acid
5-CaMeSA	5-(carboxymethyl)-salicylic acid
5-CaSA	5-carboxysalicylic acid, 4-hydroxyisophthalic acid, hydroxyterephthalic acid
5-FSA	5-formylsalicylic acid
A.	*Arabidopsis*
AA	amino acids
ABA	abscisic acid
ALD1	AGD2-LIKE DEFENSE RESPONSE PROTEIN1
AM	ante meridiem
avir	avirulence
BA	benzoic acid
bp	base pair
BSMT	salicylic acid/benzoic acid carboxyl methyltransferase
CA	chorismic acid
CAM	camalexin
cDNA	complementary DNA
CFP	cyan fluorescent protein
cfu	colony forming units
CM	chorismate mutase
CoA	coenzyme A
Col	Columbia
c_T	cycle threshold
DHBA	dihydroxybenzoic acid
DIW	deionized water
DP	dehydropipecolic acid
dpi	day post inoculation
EDS	ENHANCED DISEASE SUSCEPTIBILITY
EDTA	ethylendiaminetetraacetic acid
EIC	extracted ion chromatogram
ET	ethylene
ETI	effector-triggered immunity
FMO1	FLAVIN-DEPENDENT MONOOXYGENASE 1
FW	fresh weight
GDG1	GH3-LIKE DEFENSE GENE 1
GH3	Gretchen Hagen 3
Glc	glucose
h	hour

Hpa	*Hyaloperonospora arabidopsidis*
hpi	hours post inoculation
HR	hypersensitive response
IAA	indole acetic acid, auxin
IC	isochorismic acid
ICC	indole-3-carbaldehyde
ICA	indole-3-carboxylic acid
IC-Glu	isochorismoyl-glutamate
ICS1	ISOCHORISMATE SYNTHASE 1
IPL	isochorismate pyruvate lyase
IR	induced resistance
JA	jasmonic acid
JA-Ile	jasmonoyl-isoleucine
KAC	ε-amino-α-ketocaproic acid
LRR	leucine-rich repeat
M	$mol*L^{-1}$
M^+	molecular ion
MA HCl	methoxyamine hydrochloride
Mal	malic acid
MAMP	microorganism-associated molecular patterns
MAP	mitogen-activated protein
MAPK/MPK	mitogen activated protein kinase
MATE	multidrug and toxin extrusion
MeJA	methyl jasmonate
MeOH	methanol
MES	MeSA esterase
MeSA	methyl salicylate
min	minute
mRNA	messenger RNA
MSTFA	*N*-Methyl-*N*-(trimethylsilyl)trifluoroacetamide
MW	mass weight
m/z	mass-to-charge ratio
NahG	salicylate hydroxylase 191 from *Pseudomonas putida*
NB	nucleotide-binding site domain
NB-LRR	nucleotide-binding–leucine rich repeats
nd	not detected
NDR1	NON RACE SPECIFIC DISEASE RESISTANCE 1
NHP	*N*-hydroxypipecolic acid
NLR	NB and LRR-containing protein
NPR1	NON-EXPRESSOR OF PR GENES 1
N-pyr-Glu	*N*-pyruvoyl-glutamate
ON	overnight
OPDA	*cis*-12-oxo-phytodienoic acid
P.	*Pseudomonas*
PA	polyamine
PAL	phenylalanine ammonia-lyase
PAMP	pathogen-associated molecular patterns
PBS3	AvrPphB SUSEPTIBLE 3
PCR	polymerase chain reaction
Pip	pipecolic acid
PR	pathogenesis-related

PRR	pattern recognition receptors
Psm avir	*Pseudomonas syringae* pv. *maculicola* ES4326 avrRpm1
Psm lux	*Pseudomonas syringae* pv. *maculicola* luxCDABE
Psm	*Pseudomonas syringae* pv. *maculicola* ES4326
Psp	*Pseudomonas syringae* pv. *phaseolicola* strain 3121
PTI	PAMP-triggered immunity
pv.	pathovar
qRT-PCR	quantitative real-time-PCR
R	resistance
rmp	rounds per minute
ROS	reactive oxygen species
RT	retention time
S3H	SA 3-hydroxylase
SA	salicylic acid
SAG	salicylic acid 2-*O*-ß-D-glucoside
SAGT	salicylic acid glucosyltransferases
SA-Mal	salicylic acid malic acid
SAMT	SA methyltransferase 1
SAR	systemic acquired resistance
SARD4	SAR-DEFICIENT 4
sCA	small carboxylic acid
SD	standard deviation
SGE	salicyloyl glucose ester
SID	salicylic acid induction deficient
T3SS	bacterial Type-III secretion system
TAE	tris-acetate-ethylenediamine tetraacetic acid
*t*CA	*trans*-cinnamic acid
tDNA	transposable DNA
TIC	total ion chromatogram
TMCS	trimethylsilyl chloride
TMS	trimethylsilylation
TMV	tobacco mosaic virus
U	unknown molecular species
UGT	UDP-dependent glycosyltransferases
v/v	volume per volume
w/v	weight per volume
WIN 3	HOPW1-1-INTERACTING3
YFP	yellow fluorescent protein

α	alpha
β	beta
Δ	delta
ε	epsilon
λ	lamda
ν	nu

1 Introduction

The plant immune system consists of a complex regulatory network for constitutive and inducible defense mechanisms against phytopathogens. A large group of plant pathogens, next to herbivores, such as insects, includes pathogenic microorganisms. During the race of co-evolution, plants developed different levels of defense to combat microbial pathogens. Constitutive plant defense against microbial pathogens consists of a series of physical and chemical barriers that hamper the entry of pathogens. These barriers include a waxy cuticle, lignification of cell walls, but also antimicrobial secondary metabolites, so called phytoanticipins, embedded in the apoplast [1]. The inducible plant defense implies specific receptors on a plant cell surface, which recognize conserved structures, metabolites or proteins of a microbe and allow a plant to initiate a direct defense response. Depending on how the plant recognized the pathogen, either pattern triggered or effector triggered immunity (PTI or ETI) is activated (Figure 1.1.1). At the site of a local infection, PTI and ETI are considered to play a crucial role in the development of defense-relevant metabolites [2]. A local infection can immunize the whole plant and protects the plant against further pathogen attacks. This phenomenon is called systemic acquired resistance (SAR). Activation and establishment of SAR is mediated through plant metabolites. Important SAR metabolites are known; however, the active SAR-signal and full biosynthetic pathways remain to be determined.

The phytohormone salicylic acid (SA) is a key player to establish a full SAR reaction. Moreover, *N*-hydroxypipecolic acid (NHP), and its precursor the non-proteogenic amino acid pipecolic acid (Pip) are essential defense metabolites in plant immunity [3–5]. There is growing evidence that NHP is mobile and induces SAR [6]. The following chapters introduce how plants battle microbial infections on a local level and develop a whole plant immunization through the establishment of SAR. Hereinafter, the role of crucial defense-related metabolites is explained in more detail.

1.1 Defense strategies against microbial plant pathogens

An efficient immune response is based on the exact recognition of the attacking microbe. Due to a constant co-evolution between plant resistance and microbial virulence, a plants immune system can be described as a zig-zag-model (Figure 1.1.1). Meaning, on the one hand, plants can recognize microbial structures on different molecular levels to build up an immunity and on the other hand pathogens try to overcome the established barriers [7].

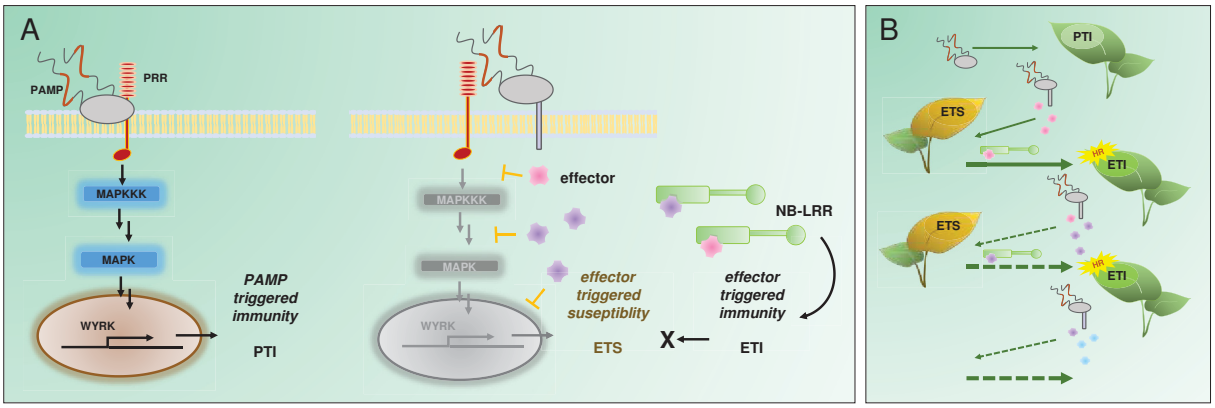

Figure 1.1.1: Establishment of local defense responses PTI and ETI
(A) PAMP triggered immunity (PTI), is induced by general molecular elicitors, so called pathogen associated molecular patterns (PAMPs). These PAMPs are recognized by pathogen recognition receptors (PRR). A signal cascade mitogen-activated protein kinases (MAPK) is initiated, and defense genes are expressed. On the second step of co-evolution, pathogens introduce specific effector proteins into the plant cell to suppress the formation of PTI and induce an effector triggered susceptibility (ETS). Plants on the other hand, evolved resistance proteins, including NB-LRR receptors, which recognize and inhibit these effector proteins. (B)The zig-zag-model after Jones and Dangl 2006 depicts the plant-pathogen-co-evolution-race, where the level of pathogen recognition induces a more severe defense response. Whereas PTI alone results in lower defense, ETI activates and strengthens PTI-related gene expression combined with antimicrobial defenses resulting in a stronger immune response ending with a hypersensitive response (HR) and local cell death.

On the first level of a basal resistance, plants can identify microbe or pathogen associated molecular patterns (MAMPs or PAMPs), structures that are essential for the vitality or virulence of the microbe, through pathogen recognition receptors (PRR) on a plant cell surface (Figure 1.1.1 A). The recognition of PAMPs through PRRs induces the mitogen-activated protein kinases (MAPK) cascade and directly provokes a PTI [8,9]. The local activation of MAPK can induce an immunization on the whole plant level. The induction of SAR through MAPK includes the crucial signaling compounds SA and NHP and the expression of the corresponding genes (see Figure 1.2.1) [8,10].

Pathogens, on the other hand, bypass PTI by releasing effector proteins which inhibit the formation of basal resistance and induce an effector triggered susceptibility (ETS) in the plant (Figure 1.1.1) [7]. The next evolutionary step on a plant level is the direct identification of effector proteins or indirect identification of the interaction of effector proteins, through specialized

nucleotide binding leucine-rich repeat (NB-LRR) protein receptors. The NB-LRRs are highly variable disease resistance proteins and induce the second layer of defense called ETI [2]. Both PTI and ETI have the accumulation of defense metabolites and expression of defense-related genes to inhibit the spread and growth of the disease as consequence. In contrast to PTI, the immune response in ETI is strong and often results in the hypersensitive response (HR), a local programmed cell death to inhibit the spread of a pathogen (Figure 1.1.1 B) [11]. HR is locally induced by avirulent or non-host pathogens whereas virulent pathogens trigger a stronger response in non-infected distal plant tissue [12].

1.1.1 Systemic acquired resistance

Following a local infection, an immunization on a whole plant level is established. The SAR provides an enhanced pathogen protection and builds up a board immunization against further infections in plant tissue distal to the infection side [13]. The plant reacts with a *de novo* synthesis of defense metabolites and an increase of defense-related gene expression. The expression of SAR-genes is activated in local and distal tissue. Furthermore, SAR is associated with defense priming, a state that enables the plant to more effectively induce defense responses [5,14,15]. After virulent bacterial infection SA and NHP are biosynthesized in local and systemic plant tissue (Figure 1.1.2) [3,5,16]. In the following paragraphs, the crucial defense regulators SA and NHP and their role in plant immunity will be introduced.

1.2 Crucial regulators of plant immunity

The local infection of a leaf triggers the expression of more than 3,000 defense-associated genes in uninfected systemic leaves [17]. Among the highest upregulated genes are positive regulators of plant defense genes like: *NDR1*, *EDS1* and *PAD4* and also essential genes for NHP biosynthesis: *ALD1*, *SARD4 and FMO1* as well as crucial genes for SA biosynthesis: *ICS1, EDS5, PBS3*, *NPR1* and *PR1*. The upregulation of these genes in local and systemic tissue emphasizes the important role of both metabolites in plant defense [15,17,18]. The positive regulators in SA and NHP biosynthesis in the model plant *A. thaliana* will be introduced shortly. An overview of the most relevant genes and their interplay is given in Table 1.2.1 and Figure 1.2.1.

SAR-genes are not only induced by (hemi)biotrophic microbes like bacteria or fungal pathogens but can be activated after oviposition of arthropod eggs. The oviposition on a local leaf triggers a SAR response, making the whole plant more resistant to further infections [19,20].

Table 1.2.1: Important SAR-genes in *A. thaliana*

	defense gene	short description
ALD1	*AGD2-LIKE DEFENSE RESPONSE PROTEIN 1*	encodes α-aminotransferase which converts Lys to KAC followed by a cyclization and isomerization to form DP.
EDS1	*ENHANCED DISEASE SUSCEPTIBILITY 1*	encodes a disease resistance signaling protein with homology to eukaryotic lipases. EDS1 is a component of resistance gene-mediated disease resistance and interacts directly with PAD4.
EDS5	*ENHANCED DISEASE SUSCEPTIBILITY 5*	encodes an orphan MATE. Expression is induced by SA. EDS5 is essential for SA dependent signaling. Mutants (*eds5* or *sid1*) are SA deficient.
FMO1	*FLAVIN-DEPENDENT MONOOXYGENASE 1*	encodes pipecolate *N*-hydroxylase which converts Pip to NHP.
ICS1	*ISOCHORISMATE SYNTHASE 1*	encodes isochorismate synthase. Mutants (*sid2*) are SA deficient.
NDR1	*NON-RACE-SPECIFIC DISEASE RESISTANCE 1*	encodes a plasma membrane-anchored integrin-like protein which is required for non-race-specific resistance to bacterial and fungal pathogens. Positivly influences local defense and mediates SAR response. The mRNA is cell-to-cell mobile.
NPR1	*NONEXPRESSER OF PR GENES 1*	encodes the transcriptional co-regulator induced by SA. NPR1 is a key regulator of SA signal transduction in SAR. Mutants (*npr1*) fail to express *PR1* genes.
PAD4	*PHYTOALEXIN DEFICIENT 4*	encodes a lipase-like gene which is important for SA signaling and function in resistance gene-mediated and basal plant disease resistance. PAD4 can interact directly with EDS1. The mRNA is cell-to-cell mobile.
PBS3	*AVRPPHB SUSCEPTIBLE 3*	encodes an amino acid conjugase. PBS3 conjugates Glu to isochorismate which breaks down to SA and *N*-pyruvoyl-Glu. *In vitro* PBS3 conjugates 4-substituted benzoates to AA. Mutants (*pbs3*) are very suceptible against pathogenes, show a weakend SAR and lack *PR1* expression and SAG fromation.
PR1	*PATHOGENESIS-RELATED GENE 1*	genetic marker for SAR response, *PR1* is induced after various (hemi)-biotrophic pathogens. *PR1* expression is SA responsive.
SARD4	*SAR DEFICIENT 4*	encodes a reductase which converts DP to Pip.

DP: 2,3-dehydropipecolic acid, KAC: ε-amino-alpha-ketocaproic acid, MATE: multidrug and toxin extrusion transporter, NHP: *N*-hydroxypipecolic acid, Pip: pipecolic acid, SA: salicylic acid, SAG: salicylic acid 2-*O*-ß-D-glucoside, SAR: systemic acquired resistance, *sid*: salicylic acid induction deficient

Moreover, pathogen recognition induces the production of hydrogen peroxide (H_2O_2) in the chloroplast. The reactive oxygen species (ROS) induces accumulation of phytoalexins like camalexin (CAM) and is also involved in the expression of further defense genes (Figure 1.2.1) [21].

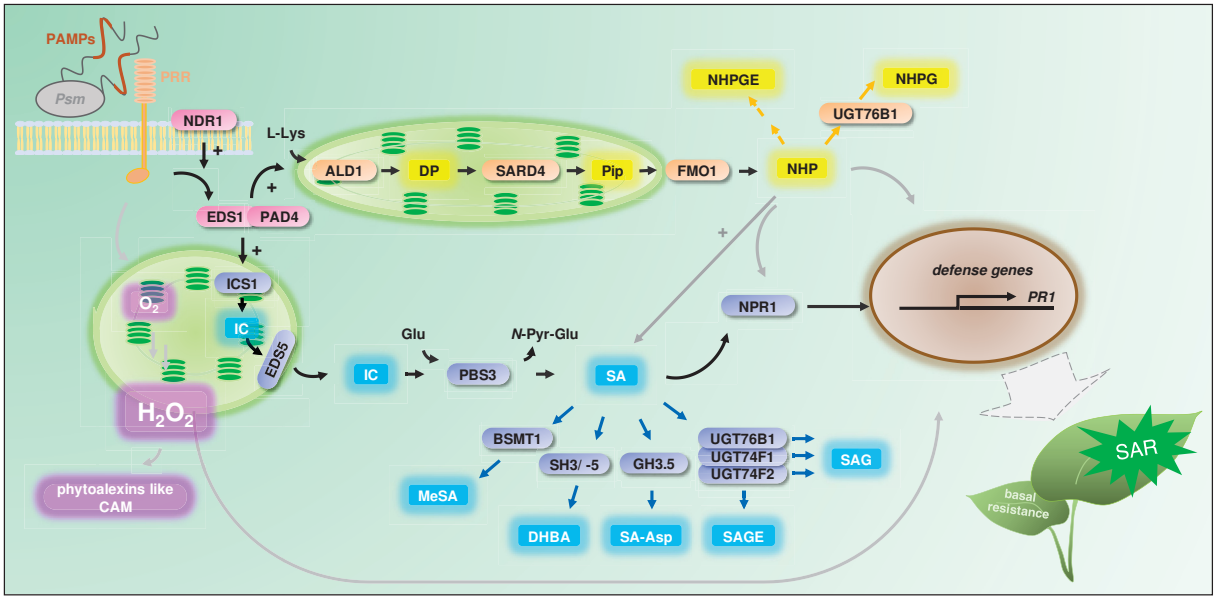

Figure 1.2.1: Interplay of defense-related genes in plant resistance
Overview of the interaction of defense-related genes in *A. thaliana* after infection with the (hemi)biotrophic bacterium *Psm*. Positive regulators in local defense are indicated in red, activations through ROS are indicated in pink, NHP-associated genes are highlighted in orange and SA-associated genes are colored in blue. Abbreviations are explained in the corresponding text parts and in Table 1.2.1.

1.2.1 NDR1, EDS1 and PAD4 - positive regulators of local defense

A positive regulator of basal resistance is the plasma membrane–anchored integrin-like protein NON-RACE-SPECIFIC DISEASE RESISTANCE 1 (NDR1) [22]. NDR1 is a key signaling component against multiple bacterial, fungal, oomycete and nematode plant pathogens [23,24]. NDR1 promotes basal resistance through the activation of multiple NB and LRR-containing proteins (NLR) which are required for defense responses [22,25]. Moreover, NDR1 positively regulates resistance genes and is SA-dependent. NDR1 positively influences the SA accumulation and the establishment of a SAR response. Further functions and associations of NDR1 include formation of HR after incompatible plant-pathogen interactions and the accumulation of ROS [26].

Local defense is mainly under the control of the nucleocytoplasmic lipase-like protein ENHANCED DISEASE SUSCEPTIBILITY 1 (EDS1). EDS1 closely interacts with its co-regulators PHYTOALEXIN DEFICIENT 4 (PAD4) and SENESCENSE-ASSOCIATED GENE 101 (SAG101) [27–29]. EDS1 and PAD4 promote defense gene expression of *ISOCHORISMATE SYNTHASE 1* (*ICS1*), *ALD1* and *FMO1*, triggering the accumulation of crucial defense metabolites SA and NHP [3,9,30]. Therefore, EDS1 and PAD4 are necessary to establish a full SAR response. The activation of EDS1 and PAD4 is not only induced by

(hemi)biotrophic pathogens, but can also be stimulated by chemical treatment [31]. EDS1 and PAD4 are positioned upstream of SA and NHP pathways, but their actual role remains still elusive [4,9,30]. Newest studies showed the interaction of EDS1 with AvrPphB SUSEPTIBLE 3 (PBS3). Here, PBS3 protects EDS1 from degradation through poly-ubiquitination and is essential for the accumulation of EDS1 [32]. PAD4 is required for Pip-inducible resistance to bacterial infection and promotes a defense amplification loop of NHP and Pip in local and in systemic tissue after local infection [4,5]. Moreover, EDS1 and PAD4 have a positive influence on the transcription of *ALD1* and *FMO1* [3].

The development of a local defense is complex and involves the interplay of various regulatory elements. Current research results point out the positive influence of tocopherols known as vitamin E biosynthesis to SA. Tocopherols are required to establish an effective basal resistance against (hemi)biotrophic pathogens like *Pseudomonas syringae* in *A.thaliana.* Further, the immune regulators EDS1 and PAD4 promote accumulation of tocopherols in plants [33].

1.2.2 NHP – a crucial SAR metabolite

The non-proteinogenic amino acid Pip and its active form NHP, were identified as crucial player in plant defense [3,5,15,34]. NHP and Pip are derived from L-lysine and their common biosynthetic pathway is illustrated in Figure 1.2.1. The α-aminotransferase AGD2-LIKE DEFENSE RESPONSE PROTEIN 1 (ALD1) catalyzes the α-NH_2-group of L-Lys to an acceptor oxoacid, which preferentially is pyruvate, to form alanine [4,35]. The generated ε-amino-α-ketocaproic acid (KAC) cycles to the dehydropipecolic acid (DP) isomers 1,2-DP and 2,3-DP, which are detectable *in planta* [4]. A reductase, as SAR-DEFICIENT 4 (SARD4) and probably other non-identified plant reductases, reduce DP-intermediates to Pip [34]. The final step in the biosynthetic pathway is the *N*-hydroxylation form Pip to its active form NHP, which is performed by the pipecolate-*N*-hydroxylase FLAVIN-DEPENDENT MONOOXYGENASE1 (FMO1) in the presence of oxygen and NAD(P)H [3]. NHP can further be glycosylated to NHP-*O*-β-D-glucoside (NHPG) and NHP glucose ester (NHPGE) *in planta* [4,36,37]. For both glucosides SA-biosynthesis is essential [36]. UGT76B1 is able to glycosylate both stress hormones SA as well as NHP to SAG and NHPG [36] (Figure 1.2.1). It does not seem like the glycolyzed forms are required for long-distance signaling of NHP, nevertheless NHP glycosides might have a regulation purpose in plant defense [37].

Both key genes *ALD1* and *FMO1* are highly upregulated locally and systemically in SAR and after Pip treatment, emphasing their role in plant immunity [18]. The SAR deficient *ald1* knockout

mutant lacks NHP and Pip but can regain its immune resistance via exogenously applied NHP and Pip. Therefore, the pathway is positively regulated by NHP and Pip. However, in *fmo1* knockout mutants SAR is completely abolished and can only be restored by exogenously applied NHP [3,5,38]. Preparing for SAR, NHP induces a complex signal amplification loop, to promote plants to react faster and stronger against further pathogen attacks and brings plants to a primed stage [4,18]. The relevance of NHP as central plant defense metabolite shows its conservation throughout the angiosperm group. NHP accumulates in various representative di- and monocotyledonous plants after infection with a compatible pathogen, like tobacco, cucumber and the grass *Brachypodium distachyon* [39]. NHP is discussed to be a mobile SAR signal in plant defense [6,40].

Interplay of SA, NHP and Pip

Exogenously applied SA, NHP and Pip promote plants to a primed stage, enabling a faster and stronger defense reaction [3,5,15]. Pip applied to the soil induces an FMO1-dependent transcriptional response, including regulatory SAR genes *ALD1*, *SARD4* and *FMO1* as well as *ICS1* and *EDS5* as SA related genes. Moreover, the application of NHP leads to a rising expression of the same genes, indicating a self-regulation of NHP via a feedback loop and ensuring new production of the crucial SAR-metabolite. This substantiates the importance of NHP in the establishment of SAR and its positive influence on SA biosynthesis [3,18]. Treatment with exogenously applied SA induces *PR1* gene expression and enhances the expression of *EDS1* and *PAD4* as well as *SARD4*. The data shows that NHP and Pip are required to trigger SA related defense and lead to SA depended defense in uninfected systemic tissue of the plant [15,18].

1.2.3 Salicylic acid – a central player in plant immunity

2 SA plays a crucial role in the plant immune system against a broad spectrum of biotrophic and (hemi)biotrophic pathogens as viruses, bacteria, fungi and oomyces, in local defense and in the establishment of SAR. SA derives in *A. thaliana* from two distinct biosynthetic pathways (Figure 1.2.2). After pathogen treatment, 90 % of the accumulated SA derives through isochorismic acid or the IC-pathway and only 10 % of SA is synthesized through a second route over phenylalanine ammonia lyase or the PAL-pathway [41]. Both routes originate from chorismic aid (CA), an intermediate of the shikimate pathway [42].

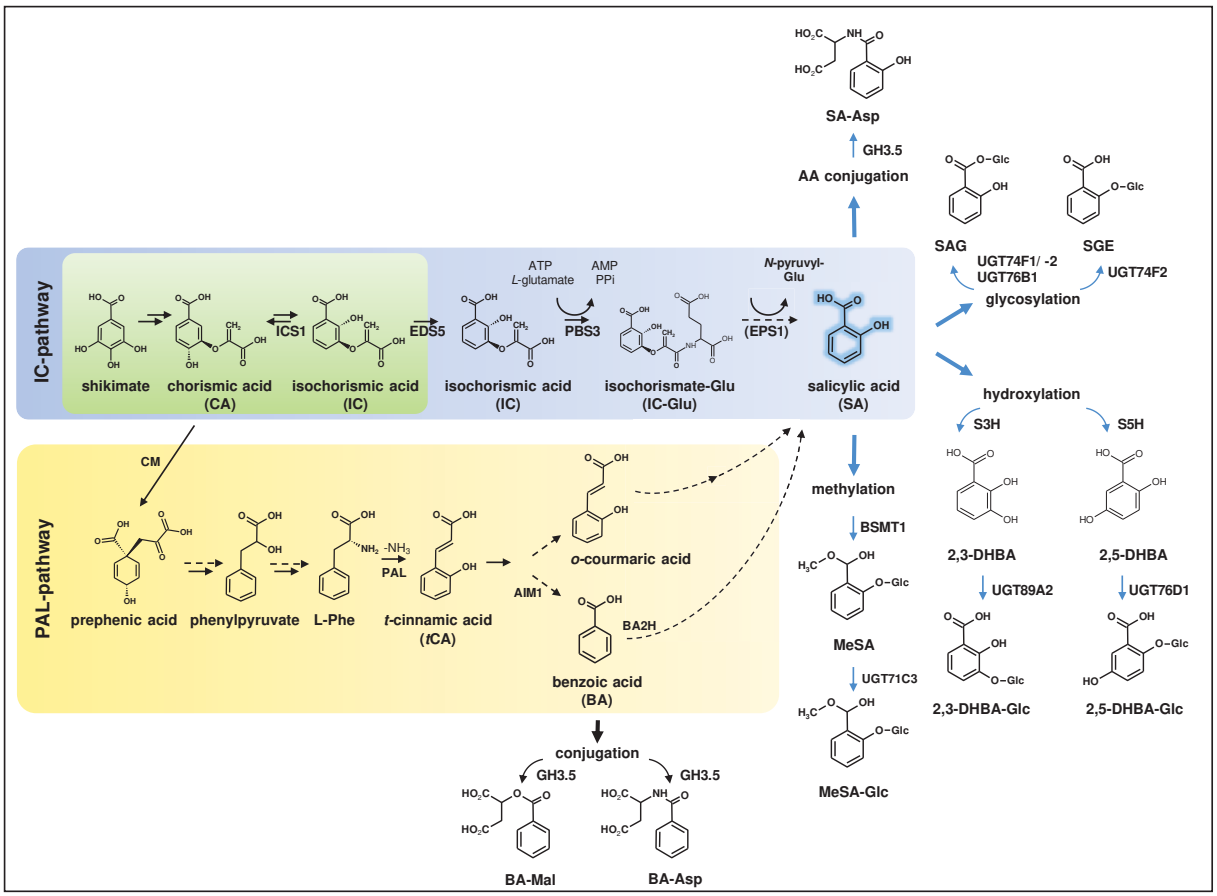

Figure 1.2.2: Biosynthesis of SA in plants
SA biosynthesis via the IC-pathway is shaded in blue, via the PAL-pathway is shaded in orange. SA as central metabolite is highlighted in blue. Dashed arrows indicate putative reactions, blue arrows indicate direct SA modifications and corresponding reactions. Reactions localized to the chloroplast are shaded in green. Abbreviations are explained in the corresponding text parts.

IC-pathway

Located in the chloroplast, ICS1 catalyzes a *de novo* synthesis of SA through the conversion of CA to its constitutional isomer IC in local and in distal leaves after infection [41,43,44]. The second isochorismate synthase ICS2 is also localized in the plastid but its contribution to biosynthesis of IC is not as significant [18,41]. Knockout of the ICS1-gene in *SA induction-deficient 2* (*sid2*) mutant, leads to a loss of local and systemic SA accumulation. Therefore, a forfeiture of SAR points out the importance of ICS1 in response to pathogens in plant immunity [15,43,45]. In bacteria IC is converted to SA through isochorismate pyruvate lyase (IPL), a similar way was proposed but has not been confirmed so far for plants [46]. Rekhter and colleagues proposed that IC is transported out of the chloroplast into the cytosol through the multidrug and toxin extrusion (MATE) transporter ENHANCED DISESE SUSCEPTIBILITY 5 (EDS5) [47]. In native plants the *EDS5* expression is very low, whereas it is strongly induced after pathogen, UV-C light or SA treatment, indicating an important role for plant immunity. *EDS5* expression is dependent on EDS1, PAD4 and NDR1 [48–50].

PBS3 – the missing link in SA-biosynthesis

Latest improvement in SA biosynthesis research enabled the description of PBS3 as missing link in converting IC to SA [47,51]. In the cytoplasm, PBS3 conjugates IC to glutamate forming isochorismoyl-Glu (IC-Glu) [47]. This construct spontaneously and with the influence of ENHANCED PSEUDOMONAS SUSCEPTIBILTY 1 (EPS1) decays to SA and *N*-pyruvoyl-Glu (*N*-pyr-Glu) [47,51]. The approval of these reaction steps *in planta*, fill a long unknown gap in SA biosynthesis (Figure 1.2.1 and Figure 1.2.2). PBS3 or GH3.12 is a member of the GH3 acyl adenylase family and is required for a full SA-related response after pathogen stimuli. PBS3 is one of 19 proteins belonging to the firefly-luciferase protein superfamily, which is wide spread throughout the plant kingdom [52–54]. The monomeric, soluble enzyme PBS3 is also known as HOPW1-1-INTERACTING3 (WIN 3) or GH3-LIKE DEFENSE GENE 1 (GDG1) [55–57]. The *pbs3* knockout mutant shows a weakened SAR reaction and a higher susceptibility against (hemi)biotrophic pathogens, such as *P. syringae*. Furthermore, the *pbs3* mutant lacks *PR1* gene expression and SAG formation [52]. Unlike the broad substrate diversity of GH3.5, PBS3 substance acceptance has been described to be rather narrow [53]. *In vitro* assays revealed that PBS3 conjugates amino acids (AA) to 4-substituted benzoic acids, whereas SA showed an inhibiting influence on the enzymatic activity of PBS3 [58]. However, latest findings concerning PBS3 research propose further roles for the involvement of the enzyme. As mentioned before PBS3 interacts with EDS1 and suppresses EDS1 degradation [32]. Moreover, PBS3 is not only involved in biotic stressed SA accumulation but also interferes with abiotic stressors as salt, drought and temperature stress. The PBS3 enzyme protects young rosette leaves of *A. thaliana* from the immune suppression of the phytohormone ABA, which is involved in stomatal closure due to abiotic stresses [59].

PAL-pathway

The second route described for SA biosynthesis is the PAL-pathway which only plays a minor role for SA accumulation in plant defense (Figure 1.2.2). Here, chorismate mutase (CM) converts CA to prephenic acid. Further intermediates in this pathway include phenylpyruvate and phenylalanine. In the next step, phenylalanine ammonia lyase, PAL, converts Phe to *trans*-cinnamic acid (*t*CA) releasing NH_3 [60]. There are several biosynthetic pathways proposed for *t*CA conversion forming SA. For some plant species one proposed route leads over *ortho*-courmaric acid as intermediate to SA formation [61]. Another route is described over benzoic acid (BA) to synthesize SA [46,62]. For rice and in *A. thaliana* seeds, a 3-hyhroxyacyl-CoA dehydrogenase and

peroxisomal protein (AIM1), is involved to convert *t*CA to BA [63,64]. The final step from BA to SA has been proposed to occur via an inducible BA 2-hydroxylase (BA2H) but it remains unclear for *A. thaliana* [62].

NPR1 - regulator of pathogen induced gene expression

Downstream SA biosynthesis the accumulation of SA induces expression of defense-related genes via the transcriptional co-regulator NONEXPRESSOR OF PR GENES1 (NPR1). As a crucial element in SA-dependent signal transduction, NPR1 has been described as a direct SA receptor [65–67]. The role of NPR1 has been discovered through the *npr1* mutant, which fails to activate *PATHOGENESIS-RELATED 1* (*PR1)* genes and is therefore unable to establish neither a local nor a systemic resistance [68,69]. Latest findings showed, that besides SA the mobile SAR activator NHP induces NPR1-dependent transcriptional reprogramming [6].

In naïve plants, NPR1 occurs in the cytosol as oligomer connected through intermolecular disulfide bridges. After pathogen infection and in the presence of enhanced SA levels, the reduction of NPR1 is triggered by concomitant redox changes and is transported to the nucleus. In the nucleus, NPR1 forms a complex with transcription factors (TF) TGA2, TGA5, TGA6 and CDK8 forming a bridge between the RNA polymerase and the *PR1* promoter inducing *PR1* gene transcription [70–73]. To establish a complete SAR, NPR1 as well as TGA2/5/6 are necessary [74]. Next to NPR1, its paralogues NPR3 and NPR4 accept SA as well but were described as SA repressors [40]. Likewise, NPR3/NPR4 interact with TGA2/5/6 with different binding affinities to the molecule [75]. Consequently, all three enzymes regulate SA accumulation: NPR1 positively and NPR3/NPR4 negatively. Therefore, NPR3 and NPR4 are, in contrast to NPR1, independent transcriptional co-repressors of defense-related gene expression [66]. Latest research results show that the perception of SA by NPR1 and NPR4 is essential for initiation of NHP biosynthesis, which is crucial for SAR induction [40].

SA modifications in *A. thaliana*

SA homeostasis has a significant role, not only as a regulator in plant immunity, but it also directly affects further biological functions, such as development, leaf senescence, flowering and photosynthesis. To regulate SA homeostasis, the released cytosolic SA is further modified. Especially, conjugations of SA to sugars or AA, but also further metabolization are known and are introduced in the following text parts (Figure 1.2.2).

Methylation of SA

A major amount of SA is methylated to methyl salicylate (MeSA) during the first 12 h after pathogen infection through the BENZOIC ACID/SA METHYL TRANSFERASE 1 (BSMT1). The methylation of SA enhances the volatility and membrane permeability of the metabolite. Therefore, MeSA was thought to be a long distance signal, but plants lacking *bsmt1* are still able to establish a SAR response, diminishing the role of MeSA in plant resistance as signaling molecule [76]. The accumulation of MeSA and BSMT1 expression seems to be light-dependent [77]. Moreover, the glycosylation of MeSA through uridine diphosphate-glycosyltransferase (UGT) UGT71C3 has been proposed to negatively regulate plant systemic defense signaling. Here, knockout mutants of *ugt71c3* accumulated a higher amounts of systemic SA and MeSA as wild-type plants [78].

Glycosylation of SA

The main part of accumulated SA is glycolyzed through SA glycosyltransferases (SAGT) either to SA-2-*O*-β-D-glucose (SAG) or SA glucose ester (SGE), whereas SAG seems to be the primary SA derived metabolite in *A. thaliana*. Two SAGTs were described for *A. thaliana*, UGT74F1 and UGT74F2, sharing 77 % of identity at the sequence level [79]. UGT74F1 is only designated to form SAG, UGT74F2 forms both, SAG and SGE but is more active on SGE formation [80,81]. SAG and SGE differ in the position of the conjugated sugar. SAG is also formed by UGT76B1, which has recently been identified to form NHPG as well [36,82]. SAG is known to be a stable glycosylation whereas the glycosylation on the carboxylic acid group in SGE is rather described as a high-energy compound. Therefore, SGE might occur as potential biosynthetic or metabolic intermediate [80]. The attached sugar enhances the water solubility of the molecules, so a surplus of SA can be stored in the vacuole to prevent a rise of toxic concentrations of SA in the cytoplasm. Here, SAG, rather than SGE, is proposed to be transported to the vacuole. Due to the negative charge of the molecule it is more likely for SAG to be accepted by vacuolar transporters. Moreover, in *N. tabacum* it has been described that SAG can reach the apoplast and be re-converted to SA through extracellular β-glycosidase and released back into the cytoplasm as a signaling molecule [83,84].

Hydroxylation of SA

SA can be hydroxylated to dihydroxybenzoic acids (DHBA). As direct SA derivatives 2,3-DHBA catalyzed through SA 3-hydroxylase (S3H) and 2,5-DHBA or gentisate converted via SA 5-hydroxylase (S5H, former DMR6) are described [46,85,86]. Evidence for an origin of

2,5-DHBA from SA in various plant species has been described nearly sixty years ago [87]. Cellular amounts of both DHBAs increase with plant age and after pathogen attack. 2,3-DHBA predominantly exists as a xylose conjugation, 2-hydroxy-3-β-*O*-D-xylopyranosyloxy-BA, which is structurally distinct from known SA-glucose conjugates [88]. The glycoside form of 2,5-DHBA has been described as 2,5-DHBA 2-*O*-β-D-glucose (DHB2G) as metabolite in plants [80]. For the glycosylation of 2,3-DHBA and 2,5-DHBA the glycosyltransferases UGT89A2 and UGT76D1 are under discussion [89,90]. The direct roles of 2,3-DHBA and 2,5-DHBA remain unclear. However, 2,3-DHBA induces a weak *PR1* gene expression leading to the suggestion that 2,3-DHBA is a deactivated form of SA. On the contrary 2,5-DHBA enhances the expression of a different set of *PR* genes that is not induced by SA [88].

Amino acid conjugations of SA

Conjugations of phytohormones to AA have been reported to play important roles in fine tuning the activity and function of a hormone Family members of the acyl adenylase protein family Gretchen Hagen 3 (GH3) conjugate AA to the carboxylic acid group of the hormone substrate forming an amide bond. The combination of phytohormone and conjugated AA decides upon the activation or inactivation of the hormone signal [91]. GH3.11 or JAR1 connects jasmonic acid (JA) to Ile to form the bioactive signal JA-Ile [92,93]. In contrast, GH3.5 conjugates AA to the major growth regulator indole-3-acetic acid (IAA) or auxin to inactivate the hormone. In this case, the conjugation of auxin to different AA results in various levels of inhibition. The conjugation of IAA to Asp or Glu leads to the degradation of the molecule, whereas IAA conjugations to Ala or Val occur as inactive storage forms which can be hydrolyzed back to the free, active hormone [94]. Unlike other GH3 proteins which are substrate specific GH3.5 has been described to accept multiple molecules. In the developmental and growth pathway it accepts not only IAA but also the natural auxin form phenylacetic acid. Further GH3.5 conjugates benzoates such as SA and BA to AA [95–97]. Here, conjugations to Asp have been described for SA and BA through GH3.5 (Figure 1.2.2). Out of all examined GH3 proteins GH3.5 is the only protein which accepts SA as substrate, indicating a specialized role of GH3.5. Nevertheless, GH3.5 uses BA as a more efficient substrate [95]. The occurrence of SA-Asp and BA-Asp in plants has been detected about three decades ago in beans (*Phaseolus vulgaris*) and duckweed (*Lemna paucicostata)* as well as in grapevines (*Vitis riparia* and *Vitis rupestris*) [98–100]. For BA further conjugations to small aliphatic acids like malic acid (Mal) have been described back then, as *O*-benzoyl malate (BA-Mal) and *O*-benzoyl isocitrate [98]. It was proposed for BA-Asp and BA-Mal to be involved in the auxin biosynthesis [101]. So far SA-Asp is the only known

in planta occurring AA-conjugation to SA. SA-Asp is not converted back to free SA and has, like SA, positive influence on disease resistance. Therefore, SA-Asp has been reported as putative activator of plant immunity but this hypothesis remains to be confirmed [97]. The AA Asp plays an important role in plant immunity as precursor of NHP and Pip biosynthesis.

NahG – a bacterial SA hydroxylase used to study immunity in transgenetic plants

The influence of SA in SAR has been shown about a quarter of a century ago. One mayor approach was the genetic introduction of the bacterial salicylate hydroxylase *NAHG* gene into *Nicotiana tabacum* and *A. thaliana*, forming *NahG* plants. The enzyme NAHG has been isolated from *Pseudomonas putida*. There, NAHG catalyzes the transformation of SA to catechol, where it is involved in the naphthalene degradation pathway [67,102]. *NahG* plants are therefore impaired in SA accumulation. Both *NahG* transgenic plant types showed an enhanced susceptibility towards bacterial infections and a strongly reduced *PR* gene expression compared to their corresponding wild-type plants, underscoring the importance of induced SA in plant immunity. Furthermore, *NahG* plants are compromised in SAR establishment. Compared to other SA deficient mutants like *sid2* and *eds5*, *NahG* plants exhibit more severe symptoms, including lesions and a strong HR reaction, after most pathogen infections [45]. Especially high amounts of catechol influence the hydroxyl peroxide production in *A. thaliana* plants [103]. The strong phenotypic reaction of *NahG* plants is therefore not only attributed to the lack of SA but also to the negative influence of accumulating catechol. The question remains to be open, to which extent it is possible to study the particular role of SA on the basis of an introduced hydroxylase, without the consideration of putative involved side reactions.

1.2.4 Further defense metabolites

In addition, to phytohormones such as SA, AA play an important role in the plant immune system. Many AA are used as precursors of phytohormones and antimicrobial phytoalexins. These include Trp which acts as a precursor for indole derivatives such as CAM and indole-3-carboxylic acid (ICA) [104]. In many representatives of the *Brassicaceae* family the phytoalexin CAM is strongly accumulated after necrotrophic and (hemi)biotrophic pathogen contact [105]. The formation of CAM is complex and is influenced by SA, ROS production and the glutathione content of the cell (Figure 1.2.1) [106]. SA content has a positive influence on CAM biosynthesis. However, SA is necessary, but not sufficient for the synthesis of CAM. For

example, the *pad4* mutant is impaired in SA and CAM accumulation. Moreover, the *ald1* mutant also shows inhibited accumulation of CAM [45,107].

In addition, AA themselves are involved in defense mechanisms. After pathogen contact, Pro contributes to the production of ROS enhancing the induction of HR [108]. The non-proteinogenic AA Pip and NHP as described previously, which are synthesized from L-Lys (Figure 1.2.1). Next to AA, polyamines (PA) have been described to play a role in plant defense, especially spermine which accumulates in *N. tabacum* after tobacco mosaic virus infection (TMV) and is able to induce HR and *PR* genes. Spermine derives from ornithine, with putrescine as intermediate (reviewed in Zeier, 2013).

Moreover, a conjugation of AA to phytohormones can influence circuit of a signal. For example does the already mentioned conjugation between auxin and AA inhibit signal transduction, whereas the conjugation between JA and Ile forms active signal JA-Ile [59,110,111]. JA is derived from membrane lipids in the chloroplast, with α-linolenic acid as starting substance. Through several intermediates *cis*-12-oxo-phytodienoic acid (OPDA) forms the direct precursor of JA. OPDA is reduced in the peroxisome to JA through the OPDA reductase OPR3. Accumulation of the phytohormones JA and ethylene (ET) occurs after wounding caused by necrotrophic or herbivorous organisms, mostly due to insect grub. The through wounding induced JA/ ET signaling pathway proceeds antagonistic to the SA defense pathway induced by (hemi)biotrophic pathogens like bacteria, fungi and oomycetes [112].

1.3 *Arabidopsis thaliana* and *Pseudomonas syringae* pathosystem

Thale cress or *Arabidopsis thaliana* (L.) HEYNH. forms together with the (hemi)biotrophic bacterium *Pseudomonas syringae* a well-studied host-pathogen model system. Both interaction partners within this model are phenotypically and genetically completely identified. *A. thaliana* belongs to the family of *Brassicaceae* and is an annual dicot. *A. thaliana* is a small, undemanding plant with a short life cycle of six to eight weeks. The simple cultivation of *A. thaliana* and its fully sequenced genome of 30,000 genes, allocated on five chromosomes make *A. thaliana* a suitable model plant for genetic engineering including forward and reverse genetic manipulations. Due to simple manipulation of the *A. thaliana* genome, a great variety of mutants is available through stock centers as for example The European Arabidopsis Stock Centre (NASC) that distribute and conserve seeds of *A. thaliana* mutants and ecotypes. Ecotypes are natural occurring variants of *A. thaliana* and are distributed widely on the northern hemisphere. As background for all mutants in this study served the wild-type form of Colombia 0 (Col-0).

P. syringae is an aerobic, rod-shaped, gram negative bacterium with polar flagella. *P. syringae* enters the host through wounds or stomata and proliferates in the apoplast. The bacteria channels toxins and effector proteins into the host plant through a type-3-secretion-system (T3SS) into the plant cell. There are several pathovar (pv) forms of *P. syringae* that interact with specific host plants. Through the combination of *P. syringae* strains and *A. thaliana* accessions different host-pathogen responses can be studied, including non-host resistance, incompatible and compatible interactions.

In this work, the model system between the host *A. thaliana* Col-0 and the virulent, *Psm* ES4326 strain (*Psm vir*) was used to develop the compatible interaction that overcomes basal resistance. For incompatible interaction studies, *Psm* carring the *pLAFR3* plasmid containing the avirulence gene *avrRpm1 (Psm avir)* was used to infect Col-0.

1.4 Objectives of this thesis

After infection with the virulent, (hemi)biotrophic bacterial pathogen *Psm vir, A. thaliana* wild-type Col-0 shows a shift on the metabolic level compared to mock treated control plants. The accumulation of a large number of defense-related metabolites helps the plant to build up an immune response and establish a full SAR to protect itself against further infections. A fraction of these metabolites has been identified but the majority remains elusive.
The major focus of this study is to examine the identification and characterization of new putative regulators in plant immunity, with a specific attention on the involvement of PBS3. Here, a more precise characterization of the PBS3 protein, including subcellular protein localization and *in vitro* analysis of the recombinant protein is one goal. A further aim of this thesis is the analysis of *NahG*, especially regarding the influence of NHP and Pip on the transgenic line, carrying a SA-hydroxylase. Taken together the three main subjects of this thesis are:

1) Identification and characterization of ICS1-dependent molecular species in plant immunity
2) Characterization of the PBS3 protein in plant immunity
3) Investigation of the influence of NHP and Pip on the transgenic SA-hydroxylase line *NahG* in plant immunity

The overall goal of this thesis is a contribution to unravel the complex system of plant immunity and to gain greater knowledge of the sensitive interplay between plants and plant pathogens.

2 Results

This study is focused on three major questions regarding the role of defense-metabolites in plant defense. The first part discusses the identification and characterization of previously unknown ICS1-dependent molecular species and their potential role in plant defense (chapter 2.1). A further goal was a more precise characterization of the active PBS3 protein, including enzymatic studies and the subcellular localization of PBS3 (chapter 2.2). The last part debates the influence of the *A. thaliana* transgenic mutant line *NahG* in plant resistance (chapter 2.3). The following chapters display the results gained during this study to answer the three questions.

2.1 Identification and characterization of ICS1-dependent molecular species in plant immunity

Plants accumulate phytohormones and defense metabolites after pathogen infections and establish a SAR to for protection against further attacks. SA is a key regulator in plant immunity. Two major pathways have been described for SA biosynthesis in plants. Chorismate poses the precursor of SA in both pathways. The PAL-pathway leads through the conversion of Phe to *t*CA. However, after pathogen infection most of the accumulated SA is synthesized through the IC-pathway, named after its key enzyme ICS1 which converts chorismate to isochorismate. ICS1 mutants (*sid2*) are unable to synthesize SA and cannot establish a SA-dependent SAR [43]. Downstream of the IC-pathway NPR1, leads to a SA-mediated activation of SAR-related genes [72]. Moreover, NPR1 acts as a negative feedback regulator for the IC-pathway and *npr1* mutants tend to over-accumulate metabolites involved in the SA-dependent SAR.

In this study, we focused on the following main questions concering newly identified molecular species that accumulate after pathogen infection in *A. thaliana*: (I) Which molecular species accumulate*?* (II) How fast accumulate the molecular species after pathogen treatment? (III) How are the molecular species involved in the IC-pathway? (IV) How do the molecular species influence plant immunity? (V) What is the origin of the molecular species?

Awnsering these questions we could identifiy nine new ICS1-dependent molecular species accumulating after bacterial treatment. Most of the metabolites are structurally related to SA and BA. Therefore, we included structural similar metabolites like 2,3- and 2,5-DHBA and the BA conjugations BA-Asp and BA-Mal as comparison for further characterization studies. We examined the metabolites in question regarding time-dependent accumulation in locally infected and systemic non-infected *A. thaliana* wild-type tissue. Moreover, we established accumulation patterns including SAR and defense-related *A. thaliana* knockout mutants to compile a metabolic profile of the molecular species. To examine the influence of the identified compounds on plant resistance, leaves were pre-infiltrated with the commercially available authenic substance. The impact of the molecular species was determined by induced resistance assays and *PR1* gene expression. Finally, feeding studies with the isotope-labeled putative precursors D_5-BA, D_4-SA and D_5-Phe should clarify the origin of molecular species in plants.

2.1.1 Identification and verification of unknown molecular species U1 to U9

In this study we aimed to identify SAR-related unknown molecular species that accumulate after *Psm vir* treatment in *A. thaliana*. Therefore, we compared the metabolome of infected and uninfected *A. thaliana* Col-0 with *sid2* and *npr1* plants which are impaired in SA response to pathogen treatment (Figure 2.1.1 A). Analysis of the metabolome was achieved using a combination of gas chromatography (GC) connected mass spectrometry (GC-MS) and Fourier transform infrared spectroscopy (GC-FTIR) of extracted leaf samples. Here, the extracted metabolome was separated by the GC-column in order to volatility and compound size. Due to the order of the metabolites and resulting retention times (RT), peaks of unknown molecular species could be easily recognized. In total, we identified nine unknown SAR-related metabolites by comparison of the total ion chromatogram (TIC) and extracted ion chromatogram (EIC) of the metabolomes (Figure 2.1.1 B and C). To gain information about their structure the GC-separated metabolites were subsequentially analyzed by MS and/or FTIR (Figure 2.1.1 D and E). MS spectra of the metabolites provide information about the mass of the metabolite and its fragments. Here, the molecular ion (M^+) and the mass-to-charge ratio (m/z) of the ion fragments provide guidance in identifing the metabolite. The M^+ is usally complys to the mass weight (MW) of a molecule (Figure 2.1.1 D). FTIR spectroscopy gave us information about the present and absent of chemical groups (Figure 2.1.1 E). Here, molecular vibrations are stimulated by infrared radiation (IR). The frequency of vibration depends on mass and binding, whereas the location of absorbed peaks indicates functional groups of a compound (Table S1). Combining all the analytical and spectroscopic data, we reconstructed the chemical structure of the nine accumulating compounds. Authentic standard substances or chemical or enzymaical synthesis verified the identification of a substance. The following subchapters describe the identification and verification of each unknown molecular species in detail.

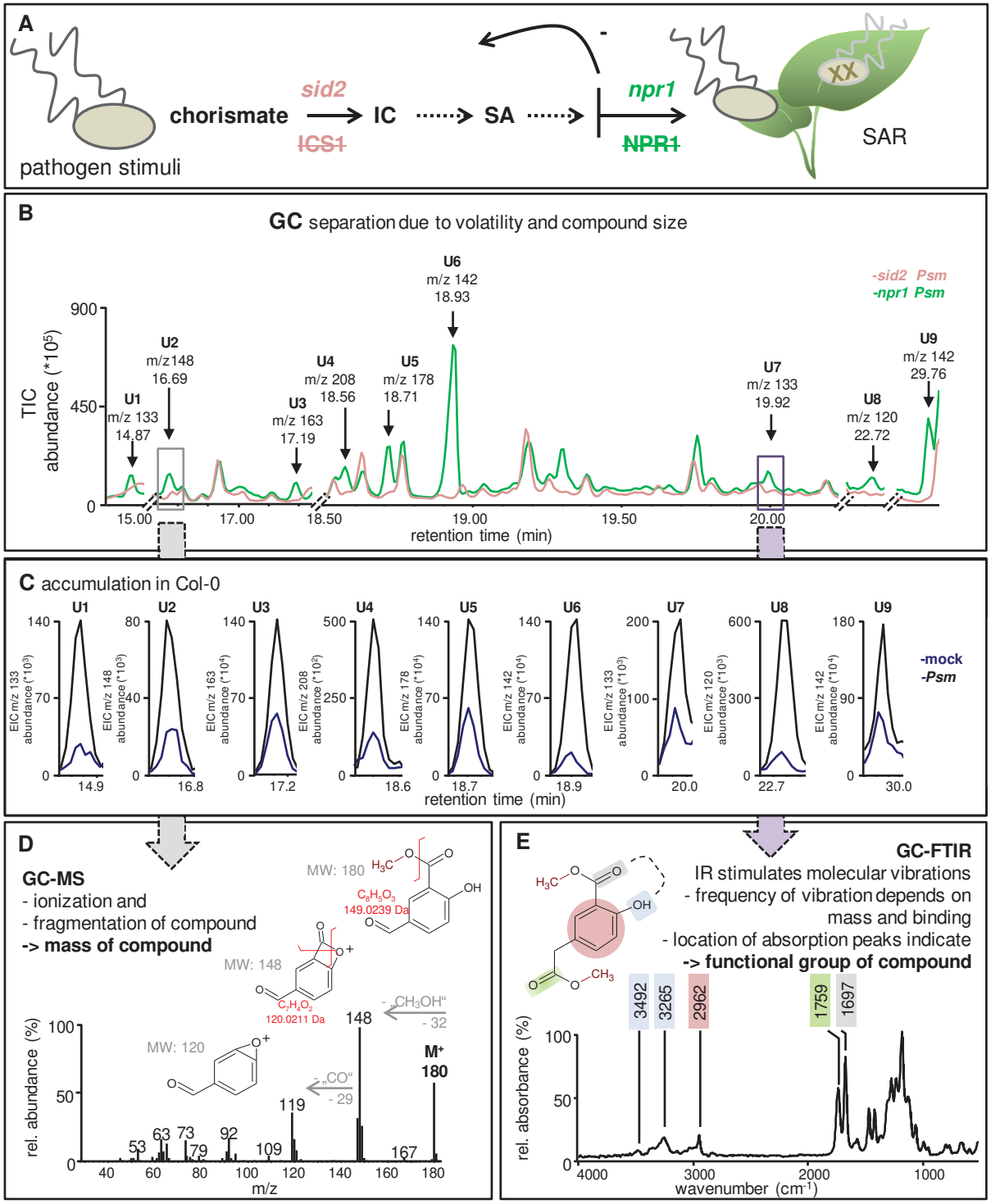

Figure 2.1.1: Graphical workflow of molecular species identification
(A) After pathogen attack defense-related molecules like SA accumulate due to up regulation of defense-related genes. Important pathogen-related genes are ICS1, which is responsible for pathogenic induced SA production and NPR1. The interplay of gene regulation and metabolites leads to an increase in immunity and establishment of SAR. (B) Extracted leaf samples have been analyzed through GC methods. The TIC depicts the accumulation pattern of nine unknown molecular species U1-9, in *Psm vir* infected *A. thaliana* knockout mutants *sid2* and *npr1*. Samples were methylated with trimethylsilyl diazomethane for derivatization. (C) EICs of specific main ion fragments (m/z) of U1 to U9, represent the pathogenic accumulation of examined molecular species in pathogen-stressed in wild-type Col-0 compared to non-stressed mock control plants. For a more detailed characterization of the molecular species, a combination of GC-MS (D) and GC-FTIR (E) was used. (D) Data about mass and fragmentation of a molecular species was gained by GC-MS analytics. The MS depicts the exemplary ion fragmentation of the molecular species U2 with a of $M^+$of m/z 180 and main ion fragments m/z 148

and m/z 119. The displayed compound, with a MW of 180 g*mol^{-1} (180 Da) reflects the plausible fragmentation pattern of the MS, after separation of a methanol group („CH_3OH“, MW: 32 Da) leading to a compound fragment of 148 Da. A further separation of a carbonyl group („CO“, MW: 28 Da) results in a compound fragment of about 120 Da. (E) Information about the composition of a compound, with occurrence or absence of functional groups, were acquired through GC-FTIR spectroscopic analysis. The IR spectrum of molecular species U7 exemplary illustrates the assignments of main IR bands to functional group vibrations (wave number/ vibration). The functional groups and appropriate vibration are shaded for clarification: 3,492 cm^{-1}/ O-H stretching and 3,265 cm^{-1}/ O-H stretching in hydrogen bonding (blue); 2,962 cm^{-1}/ C-H (aliphatic) stretching (red); 1,759 cm^{-1}/ C=O stretching (green) and 1,697 cm^{-1}/ C=O in hydrogen bonding (gray).

U1 is 3-formylbenzoic acid

The unknown molecular species U1 was identified as 3-formylbenzoic acid (3-FBA) through comparative metabolic analysis of GC-MS and GC-FTIR. Using GC-FTIR spectrum of *Psm vir* infected and methylated plant samples, we deduced chemical groups and identified the potential molecular structure. Characteristic for the identification of U1 were IR bands at 2,963 cm^{-1} indicating an aliphatic stretch. Followed by the two small bands at 2,807 cm^{-1} and 2,723 cm^{-1} describing an aldehyde stretch. Later, a strong carbonyl group stretch at 1,747 cm^{-1} and 1,724 cm^{-1} appears in the GC-FTIR spectrum (Figure 2.1.2 A). The GC-MS spectrum of U1 depicts the main ion fragments m/z 105, m/z 133 with a M^+ of m/z 164. The fragmentation indicates a loss of methyl group (31 Da), and a carbonyl group (28 Da). Due to the combination of gained information we concluded that the structure must be a formylbenzoic acid (FBA) with a total molecular mass of 164 Da. Unknown remained the substituted position of the formyl group on the aromatic ring. Therefore, we methylated authentic standard substances covering three possible formyl group positions, 2-FBA (152080250, Acros) 3-FBA (296560010, Acros) and 4-FBA (A15277, Alfa Aesar) and analyzed the substances via GC-MS (Figure 2.1.2 C). The RT of the three analyzed FBAs gained through GC, lay between 14.64 min for 2-FBA, 14.76 min for 4-FBA and 14.87 min for 3-FBA, close to the RT of U1 with 14.87 min (Figure 2.1.1 B/ Figure 2.1.2 D, E). We verified that U1 truly is 3-FBA, by co-injection of 3-FBA to a *Psm vir* infected plant sample, which led to an increasement of the peak at 14.87 min. To exclude 4-FBA being the molecular species of interest, we also added 4-FBA (b) to the plant extract, resulting in a distinct peak for 4-FBA (14.76 min) and a dilution of the 3-FBA peak (Figure 2.1.2 E). *In planta* infiltration of authentic 3-FBA into Col-0 leaves, showed four hours after infiltration an accumulation in 3-FBA, which was missing in water and SA treated plant leaves. GC-MS and GC- FTIR spectra of the authentic 3-FBA substance are found at the appendix of this thesis (Figure S1, S3).

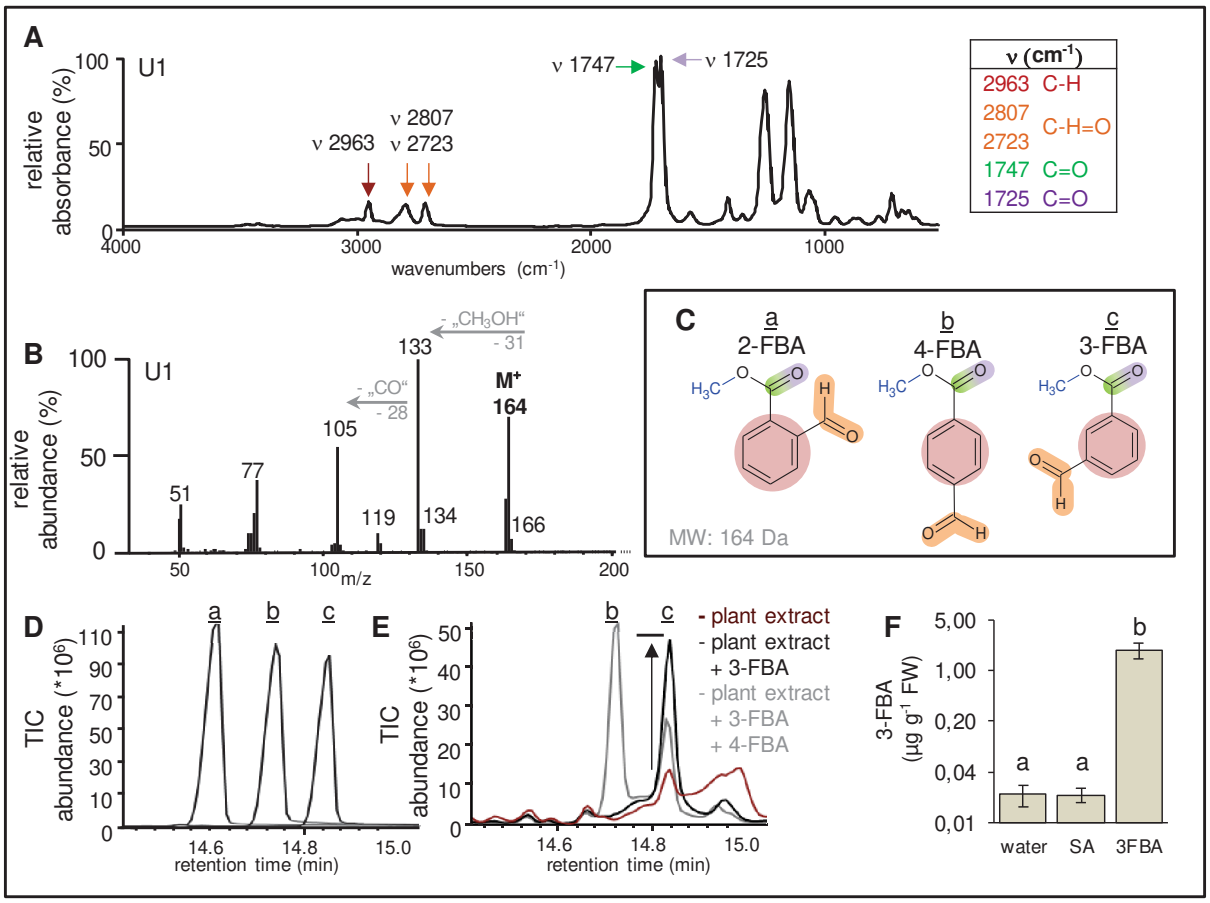

Figure 2.1.2: Identification of U1 as 3-formylbenzoic acid through comparative chromatographic analysis

(A) The GC-FTIR spectrum of U1 in methylated *Psm vir* plant samples, assignments of main IR bands to functional groups vibrations (wavenumber/ vibration) are listed in the table on the right. (B) The GC-MS mass spectrum depicts the main ion fragments m/z 105, m/z 133 with a molecular ion M^+ of m/z 164. The fragmentation indicates a loss of methanol group (31 Da), and a carbonyl group (28 Da). Samples for GC-FTIR and GC-MS analytics have been extracted the same way and were methylated by trimethylsilyl diazomethane for derivatization. (C) Three differently substituted FBAs have a MW of 164 Da. (D) Through derivatization introduced methyl groups are indicated in blue. Comparison of GC-MS total ion chromatogram (TIC) of the three FBAs by retention time (min): (a) 2-FBA (14.64 min), (b) 4-FBA (14.76 min), (c) 3-FBA (14.87 min). (E) The U1 peak in *Psm vir* plant extract (red line) has a retention time of 14.87 min. To verify that U1 is 3-FBA (c), the plant sample was co-injected with 3-FBA (black line), which led to an increasement of the peak at 14.87 min. To exclude 4-FBA being the molecular species of interest, we also added 4-FBA (b) to the plant extract, resulting in a distinct peak for 4-FBA (14.76 min) and a dilution of the 3-FBA peak (gray line). (F) Col-0 plants were infiltrated with 0.5 mM SA and 3-FBA and water as control. Leaf samples harvested 4 hpi yield to an increase of 3-FBA in 3-FBA infiltrated leaf samples, whereas SA and water showed low levels of 3-FBA. Different letters denote significant differences ($p < 0.05$, ANOVA and post hoc Tukey HSD test). The y-axis has a $\log_2$ scaling.

U2 is 5-formylsalicylic acid

Through the comparison of the analytical technics of GC-MS and GC-FTIR 5-formylsalicylic acid (5-FSA) has been identified as ICS1 depended molecular species U2, accumulating *Psm vir* infection in wild-type Col-0 plants and over-accumulates in *npr1* knockout mutants. Comparing the FTIR-spectrum of SA with the IR-spectrum of the identified molecular species 3-FBA and U2, overlapping characteristics in main IR-bands were noticed (Figure 2.1.3 A-C). SA and U2 share similar IR bands at 3,208 cm^{-1} (SA: 3,262 cm^{-1}) indicating an O-H stretching in hydrogen bonding and at 1,699 cm^{-1} (SA: 1,697 cm^{-1}) indicating a carbonyl stretching in hydrogen bonding. The characteristic molecular groups are marked in the molecular formula of each metabolite, the hydrogen group is shaded in blue while the carbonyl group in hydrogen bonding is shaded in gray and the aromatic ring is shaded in red and the formyl group is indicated on the molecular structure of 3-FBA in orange. With 3-FBA, U2 shares the characteristic aldehyde stretching at 2,807 cm^{-1} and 2,727 cm^{-1} (3-FBA: 2,807 cm^{-1} and 2,723 cm^{-1}). This data suggests molecular species U2 as 5-FSA. The GC-MS reflects the fragmentation of the plausible metabolite of 5-FSA (Figure 2.1.3 D, E). The M^+ of m/z 164 concurs to the MW of 164 Da of 5-FSA. Further the ion fragmentation pattern agrees to the molecular fragmentation. Here, a loss of a methanol group (32 Da) leads to m/z 148 and a carbonyl group (28 Da) to m/z 119. The characteristic chemical groups are colored in the molecular formula of 5-FSA (Figure 2.1.3 E). For a specific verification of U2, authentic 5-FSA standard substance (F17601, Sigma) has been methylated and co-analyzed with plant extract, leading an enhancement of the peak (Figure 2.1.3 F). *In planta* infiltration of 0.5 mM 5-FSA led to an increasement of 5-FSA in plant leaves after 4 hpi, compared to plants treated with water or SA. The GC-MS mass spectrum of authentic 5-FSA is identical to the mass spectrum of the plant extract (Figure 2.1.3 D) and is attached to the appendix of this thesis (Figure S1).

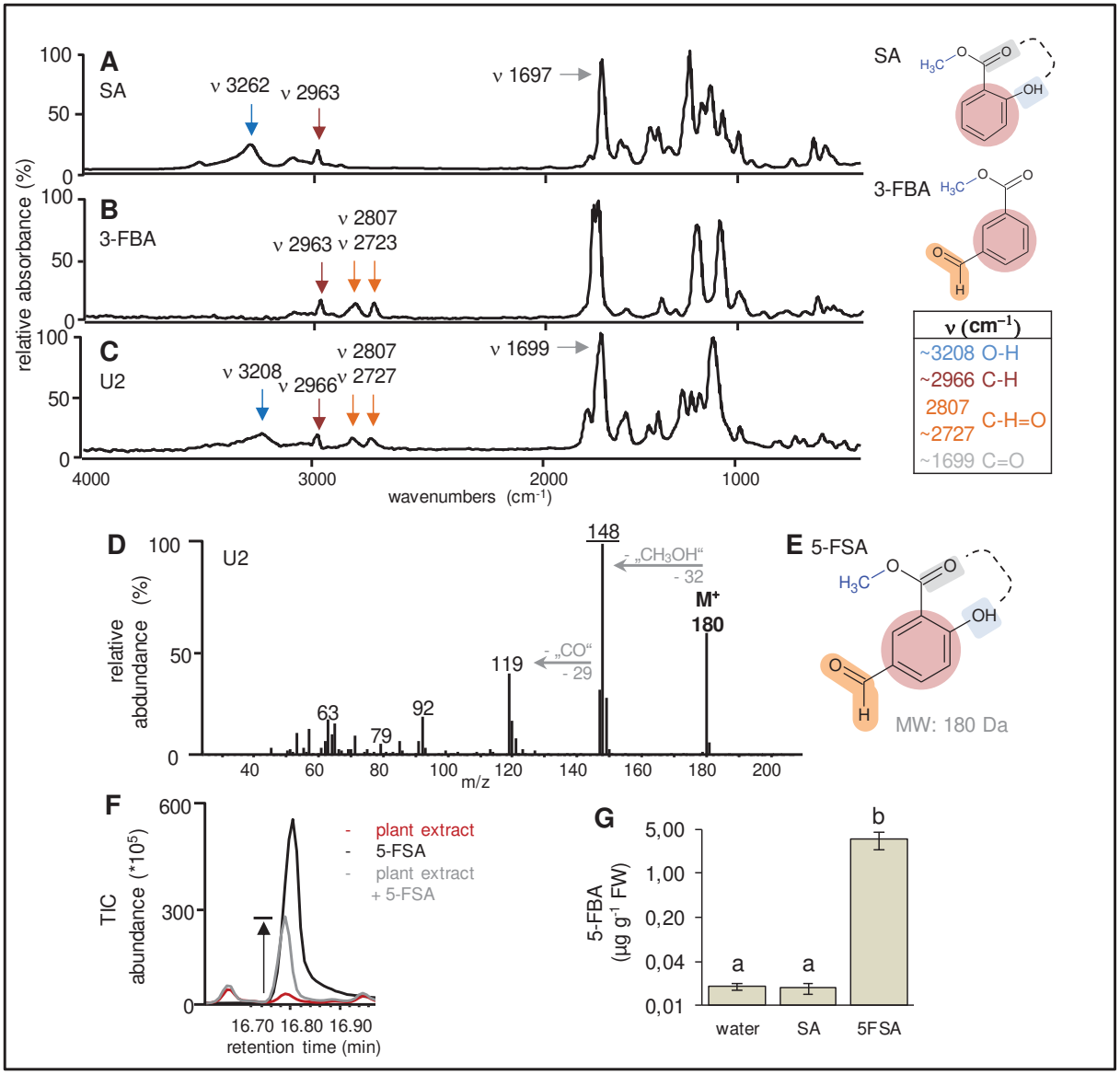

Figure 2.1.3: Identification of 5-formylsalicylic acid through comparative chromatographic analysis of SA and 3-FBA

(A-C) Comparison of the FTIR-spectra of SA with the identified molecular species 3-FBA and U2. On the right, are molecular structures of the comparative metabolites. Chemical groups are colored for clarification. Introduced methyl groups are indicated in blue. Assignments of main IR bands to functional groups vibrations (wavenumber/ vibration) are listed in the table on the right. (D) The GC-MS mass spectrum of U2, depicts the molecular ion M^+ of m/z 180 and main ion fragments m/z 148, m/z 119. The methylated molecular structure of 5-FSA confirms the MW of 180 Da. For analysis with GC-FTIR and GC-MS, samples were derivatized with trimethylsilyl diazomethane. (E) Molecular formula of 5-FSA. (F) Verification that U2 truly is 5-FSA, *npr1* plant extract (red line) was co-injected with 5-FSA authentic substance (black line) resulting in an increased peak of the plant extract (gray line). (G) Col-0 plant leaves were treated with 0.5 mM SA and 5-FSA and water as control, yields to accumulation of 5-FBA *in planta*. Different letters denote significant differences ($p < 0.05$, ANOVA and post hoc Tukey HSD test). The y-axis has a $\log_2$ scaling.

U3 and U5 are 3-carboxybenzoic acid and 5-carboxysalicylic acid

To examine the molecular species U1 (3-FBA) and U2 (5-FSA) we infiltrated *A. thaliana* wild-type Col-0 plants with 0.5 mM SA, 3-FBA, 5-FSA, or water as control (Figure 2.1.2 F and 2.1.3 G). Interestingly, we observed an increased accumulation of the unknown molecular species U3 and U5 after infiltration of 3-FBA and 5-FSA (Figure 2.1.4 A, B). Through GC-MS analysis we could detect a strong accumulation of molecular species U3 (27.44 µg * gFW^{-1}) after infiltration with 3-FBA, 224 times higher compared to U3 in water infiltrated leaf sample (0.12 µg * gFW^{-1}). Further, after infiltration with 5-FSA a strong accumulation of molecular species U5 (11.42 µg * gFW^{-1}) 45 times higher compared to U5 in water infiltrated leaf sample (0.25 µg * gFW^{-1}) (Figure 2.1.4 B) was noticed. Leaf treatment with SA or water had no impact on the accumulation of U3 or U5 (Figure 2.1.4 A, B). These results indicate that *in plana* U3 is derived of 3-FBA and U5 is a derivative of 5-FSA. Using GC-MS we identified U3 as isophthalic acid or 3-carboxybenzoic acid (3-CaBA) (Figure 2.1.4 C). The molecular ion M^+ of m/z 194 correlates to the molecular weight of 3-CaBA of 194 Da. A cleavage of a methanol group (31 Da) matches the main ion fragment of m/z 163 and a further carbonyl loss (28 Da), leads to ion m/z 135. The GC-MS spectrum of authentic 3-CaBA (A14445, Alfa Aesar) agrees to U3 GC-MS spectrum and is attached to the appendix as well as an IR-spectrum of authentic 3-CaBA (Figure S1, S3). A long with 3-CaBA, U5 was identified as 5-carboxysalicylic acid (5-CaSA) or 4-Hydroxyisophthalic acid by GC-MS (Figure 2.1.4 D). The mass loss from M^+ of m/z 210 to m/z 178 and m/z 147 can be explained by cleavage of the two methanol groups (32 Da). A further loss of a carbonyl group (28 Da) leads to m/z 119. The MW of 210 Da matches the M^+ of m/z 210 and the fragmentation pattern of the corresponding molecular element 5-CaSA. GC-MS fragmentation pattern of 5-CaSA was confirmed with the authentic standard substance (4-Hydroxyisophthalic acid, 278270, Sigma) (Figure S1). In conclusion our data indicate that the aldehyde forms 3-FBA and 5-FSA are potential precursors of the carbon acids 3-CaBA and 5-CaSA.

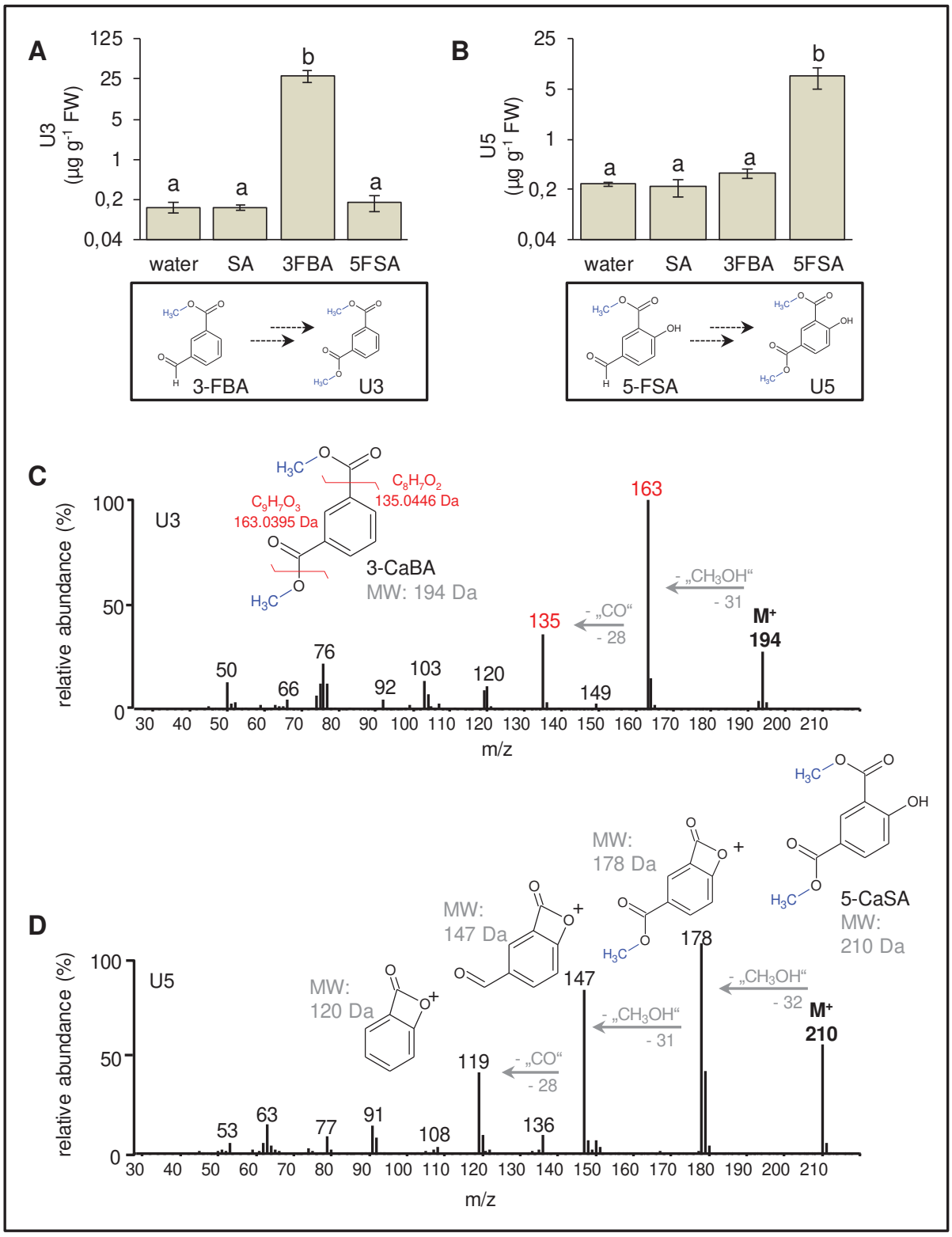

Figure 2.1.4: Identification of 3-CaBA and 5-CaSA through accumulation after 5-FSA and 3-FBA infiltration

(A and B) GC-MS analysis of *A. thaliana* leaf samples showed a significant increase in 3-CaBA after 3-FBA infiltration and an enhancement of 5-CaSA after 5-FSA infiltration. Samples were taken 4 hpi and prepared via VPE and have been methylated for derivatization. Different letters denote significant differences ($p < 0.05$, ANOVA and post hoc Tukey HSD test). The y-axes have a $\log_2$ scaling. (C) Through the fragmentation of the GC-MS mass spectrum, molecular species U3 was clearly identified as 3-CaBA with a M^+ of m/z 194 according to the MW of 3-CaBA of 194 Da. The ion fragmentation pattern of a cleavage of methyl group (31 Da) leading to m/z 163 and a cleavage of carbonyl group (28 Da) leading to m/z 135 emphasis the molecular structure. (D) In the same way, U5 was identified as

5-CaSA with a MW of 210 Da according to the M^+ of m/z 210. Losses of two methyl groups, leads to m/z 178 and m/z 147. A Further cleavage of a carbonyl group makes m/z 119.

U4 and U7 are 3-(carboxymethyl)-benzoic acid and 5-(carboxymethyl)-salicylic acid

The molecular species U7 and U4 were identified as 5-(carboxymethyl)-SA (5-CaMeSA) and 3-(carboxymethyl)-BA (3-CaMeBA) by spectroscopic analysis using GC-FTIR and GC-MS. Comparing the GC-FTIR spectrum of SA, U7 and U4 revealed distinct similarities in the characteristic IR bands (Figure 2.1.5 A-C). The absorption bands at 3,264 cm^{-1} (SA: 3,262 cm^{-1}) are assigned to a hydroxide stretching conjugated to a hydrogen bonding. Both IR-spectra of SA and U7 indicate vibrations of carbonyl groups, whereas the absorption for a free carbonyl stretching in SA is small, under 20% absorption, (1,751 cm^{-1}) compared to a moderate, about 50% absorption, carbonyl stretching in U7 (1,759 cm^{-1}). The conjugated carbonyl stretching is high in SA (1,696 cm^{-1}) and moderate in U7 (1,697 cm^{-1}). This data indicates that a potential molecular structure of U7 must contain a free carbonyl group, as well as a conjugated carbonyl group, compared to SA. The information gained about U7 through GC-MS mass spectrum revealed a molecular ion $M^+$of m/z 224 (Figure 2.1.5 D). The ion fragments of m/z 192, and m/z 165, indicate a cleavage of a methanol (32 Da) and carbonyl group (28 Da). Through the combined data, we calculated a molecular structure of 5-CaMeSA as U7 with a total MW of 224 $g*mol^{-1}$ (Figure 2.1.5 E). For 5-CaMeSA no authentic substance commercially was available. The GC-FTIR spectrum of U4, differs in the prominent free carbonyl stretching (1,747 cm^{-1}) compared to SA (1,751 cm^{-1}) and 5-CaMeSA (1,759 cm^{-1}) (Figure 2.1.5 C). Further, characteristic vibrations for the hydroxy group, found in SA and 5-CaMeSA, are the missing in the spectrum of U4. The mass spectrum of U4 in indicates a M^+ of m/z 208 (Figure 2.1.5 F). The main ion fragmentation represents the cleavage of methanol group m/z 177 (32 Da) and cleavage of carbonyl group to m/z 149 (28 Da). Together this data leads to the molecular structure of 3-CaMeBA with a MW of 208 $g*mol^{-1}$ (Figure 2.1.5 G). With an authentic standard substance of 3-CaMeBA (446214, fluorochem), we verified that U4 truly is 3-CaMeBA. The GC-MS mass spectrum of authentic 3-CaMeBA matches the mass spectrum of U4 extracted from plant material completely and is attached to the addendum of this thesis (Figure S1). Co-injection of the plant extract with authentic 3-CaMeBA substance leads to an enhanced m/z 208 peak the plant extract verifying U4s identity. Moreover, Col-0 plant leaves treated with 0.5 mM 3-CaMeBA, yield to an accumulation of 3-CaMeBA *in planta* compared to the controls treated with water or 0.5 mM SA. Taken together, 5-CaMeSA and 3-CaMeBA share a basic molecular structure containing a carbonxyl group and share similarities with SA and BA.

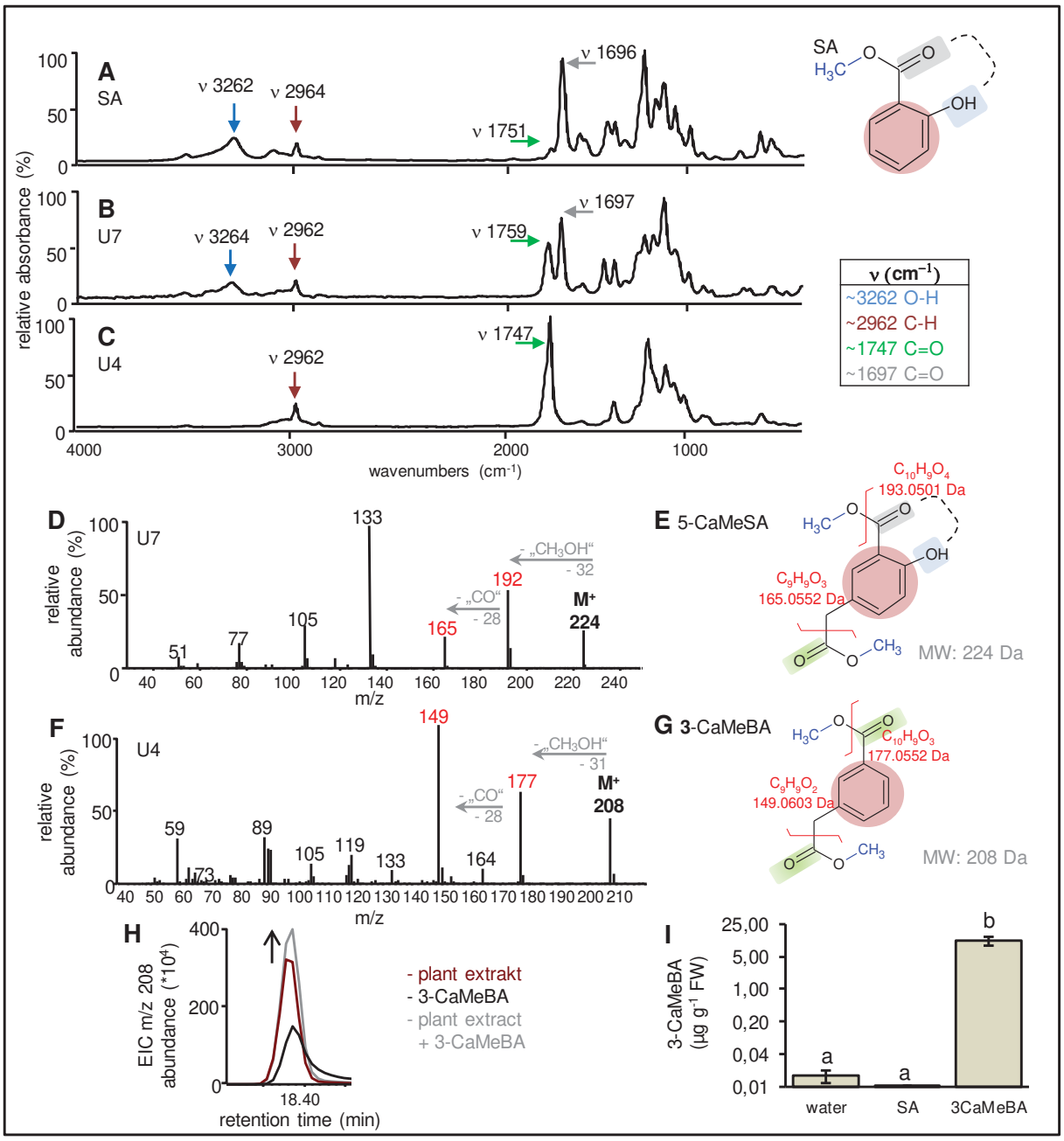

Figure 2.1.5: Identification of (carboxymethyl)benzoic acids through comparative chromatographic analysis of SA

(A-C) The IR spectrum of SA and U7 share characteristic absorption bands, whereas U4 is missing bands compared to SA and U7. Assignments of main IR bands to functional groups vibrations (wavenumber/ vibration) are listed in the table on the right. On the molecular formulas on the right, hydroxy groups are shaded in blue, carbonyl groups in green and a carbonyl group with hydrogen bonding in gray, the aromatic ring is shaded in red. (D) MS fragmentation pattern of U7 with a M^+ of m/z 224 indicates the cleavage of methanol group (32 Da) and a carbonyl group (28 Da). (F) The mass spectrum of U4 indicates a M^+ of m/z 208. The main ion fragments (m/z 177 and 149) indicate also the cleavage of a methanol group (32 Da), and a carbonyl group (28 Da). (E and G) Chemical groups identified by GC-FTIR and potential MS fragment sizes are highlighted on the molecular formulas of 5-CaMeSA (E) and 3-CaMeBA (G). Introduced methyl groups are indicated in blue. (H) Co-injection of the plant extract (red line) with authentic 3-CaMeBA substance (black line) leads to an enhanced m/z 208 peak the plant extract (gray line). (I) *A. thaliana* Col-0 plant leaves treated with 0.5 mM 3-CaMeBA, yield to an accumulation of 3-CaMeBA *in planta* compared to the controls treated with water or 0.5 mM SA. Different letters denote significant differences ($p < 0.05$, ANOVA and post hoc Tukey HSD test). The y-axis has a $\log_2$ scaling.

U6 is *N*-pyruvoyl-glutamate and U9 is putatively isochorismoyl-glutamate

In *Psm vir* infected *npr1* plant material we observed a strong accumulation of the molecular species U6 and a moderate accumulation of U9 in GC-MS analysis. Through the combination of GC-MS and GC-FTIR analzysis we could identify U6 as *N*-pyruvoyl-Glu (*N*-pyr-Glu) and U9 as putative isochorismoyl-Glu (IC-Glu). The FTIR spectrum of U6 revealt a small vibration for an amino stretching at 3,412 cm^{-1}, a small aliphatic stretching at 2,962 cm^{-1}, a strong carbonyl stretching at 1,762 cm^{-1} and a moderate secondary amino stretching at 1,710 cm^{-1} (Figure 2.1.6 A). A comparison to IR spectra of *N*-acetylated amino acid especially *N*-acetyl-Glu and *N*-acetyl-aminoadipic acid (AAD) indicates molecular structure of U6 having two carboxy groups and a nitrogen conjugation and a carbon skeleton of four molecules. FTIR spectra of *N*-acetyl-Glu and *N*-acetyl-AAD are attached to the appendix (Figure S2). In detail, the strong absorbance intensity of the IR band at 1,762 cm^{-1} indicates two carbonyl groups for U6, and a substitution at the amino group (1,710 cm^{-1}). One potential molecule for U6 is *N*-pyruvoyl-L-glutamate, which fulfills the proposed molecular groups identified through IR-spectroscopy. The GC-MS mass spectrum of molecular species U6, with a RT of 18.93 min shares similarities in ion fragmentation pattern of molecular species U9 with a RT of 29.76 min (Figure 2.1.6 B, C). The higher RT of U9 indicates a lager molecule than U6. Similar MS part and ion fragments of U6 and U9 are indicated in purple. Interestingly, the first part of U9s MS spectrum includes mass fragments of m/z 150 which corresponds to the MW of SA (Figure S1). Taking this data together, we speculated that U9 is a conjugation of U6 and SA. The conjugation of chorismate or IC with Glu are possible structures for U9. Strikingly, the accumulation of U9 is ICS1-dependend and ICS1 is converting chorismate to isochorismate, a precursor of SA. Therefore, U9 is most likely IC-Glu. Comparing the molecular structure of IC-Glu with the MS fragmentation pattern of U9 the MW of IC-Glu (395 Da) is in line with the potential M^+ of m/z 396. Further molecular fragmentation patterns of IC-Glu are indicated in the structure and correspond to the MS ion fragmentation of U9 and U6 (Figure 2.1.6 D). For *N*-pyr-Glu and IC-Glu no authentic standard substance was commercially available. However, in protein assays with active PBS3, pyruvic acid and Glu we detected traces of *N*-pyr-Glu (see chapter 2.2.1) emphasizing our hypothesis for U6 as *N*-pyr-Glu and supporting the hypothesis of U9 beeing IC-Glu.

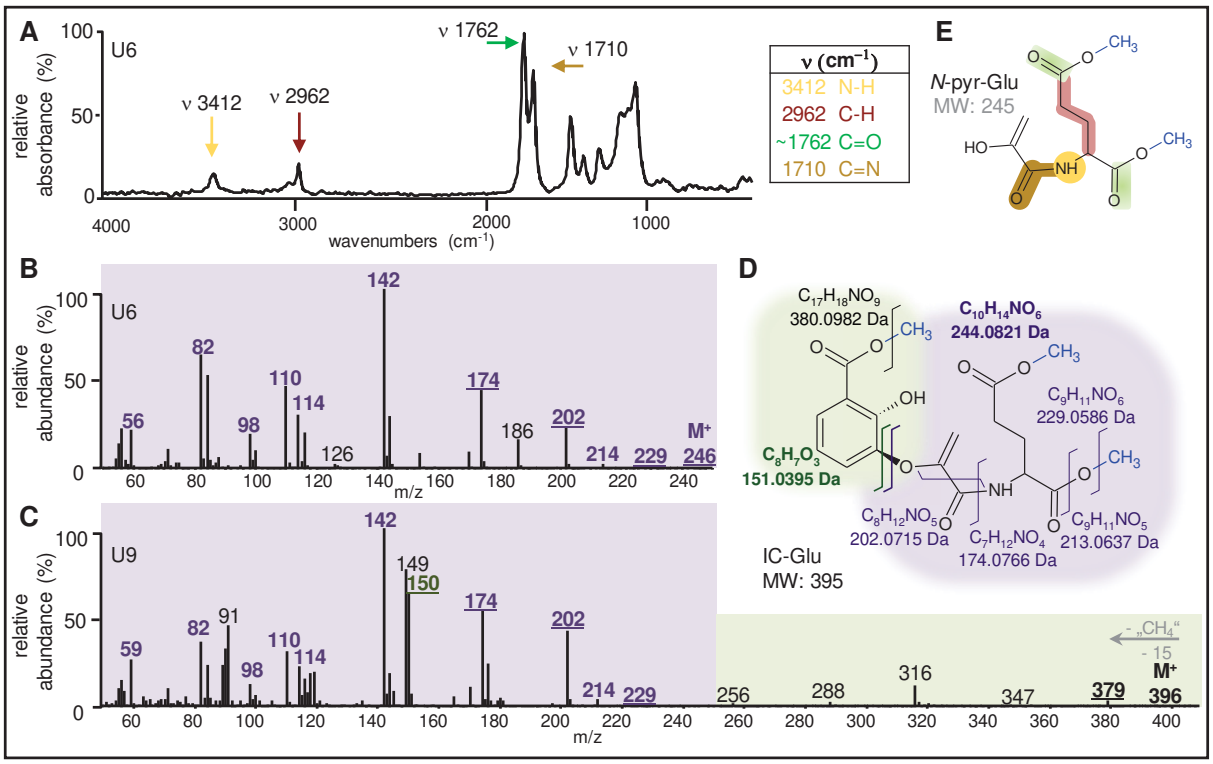

Figure 2.1.6: Identification of U6 and U9 through comparative chromatographic analysis
(A) The GC-FTIR spectrum of molecular species U6. Assignments of main IR bands to functional group vibrations (wavenumber/ vibration) are explained in the table on the right. (B) The GC-MS spectrum of molecular species U6 shares similarities in ion fragmentation pattern of molecular species U9 (C). Similar MS ion fragments are indicated in purple. All samples were extracted from pathogen induced plant tissue and methylated for derivatization with trimethylsilyl diazomethane. (D) Potential structure of U9 as a conjugation of IC with Glu forming IC-Glu with a MW of 395 Da. Putative structure of U6 as *N*-pyr-Glu is shaded in purple and drawn in E.

U8 is salicylic acid and malic acid

Metabolic GC-MS analysis of *Psm vir* infected leaf tissue, revealed a *Psm*-dependent accumulation of molecular species U8 in *A. thaliana* wild-type Col-0 plants. The molecular species is missing in knockout mutants *sid2* and is over-accumulating in *npr1* (Figure°2.1.7°A). The mass spectra of U8, resembles the ion fragmentation of SA (Figure 2.1.7 A, Figure S1). Both MS include the ion fragments of m/z 120/121, m/z 92, m/z 65, indicating a putative molecular relationship. Moreover, the MS of U8 differs in only one mass compared to the MS of the SA amino acid conjugation SA-Asp emphasizing the connection to SA (Figure S1). The M^+ of m/z 282 corresponds to the formula weight of SA-Mal 282 Da. Also, the cleavage of a methanol group (32 Da), and Mal (161 Da) concur with the fragmentation pattern, supporting this hypothesis. To prove that U8 is SA derived, we infiltrated isotope labeled D_4-SA *in planta* and chemically conjugated SA with Mal synthesizing salicyloyl-malate (SA-Mal). Compared to *Psm vir* treated *npr1* plants, we detected a shift of four mass units of U8 in *npr1* after infiltration with 2 mM D_4-SA (Figure 2.1.7 A, B). The molecular fragmentation, indicated in the molecular structure, resembles the fragmentation in U8. To verify the identity of U8, we chemically synthesized SA-Mal. Therefore, 100 µM malic acid in acetonitrile (ACN) was mixed with 20 µM salicyloylchloride, dissolved in DCM, at ambient temperature. Samples were taken after 1 h, 2 h and the next day (overnight: ON). Compared to the *in planta* accumulation of U8, the SA-Mal synthesis resulted in a small accumulation of m/z 120 at 24.2 min (Figure 2.1.7 D,E). Mal in acetonitrile served as control. The MS mass spectrum of SA-Mal synthesis, main ions of U8, m/z 120 and M^+ of m/z 282, were detectable (Figure 2.1.7 C).

Taking together, this data indicates that U8 is SA-Mal. First, the fragmentation pattern of U8 shares characteristics to SA fragmentation as well SA-Asp. Second, U8 is a direct SA derivate and was labeled through D_4-SA infiltration. And third, the synthesis of SA-Mal proves the previous suggestions.

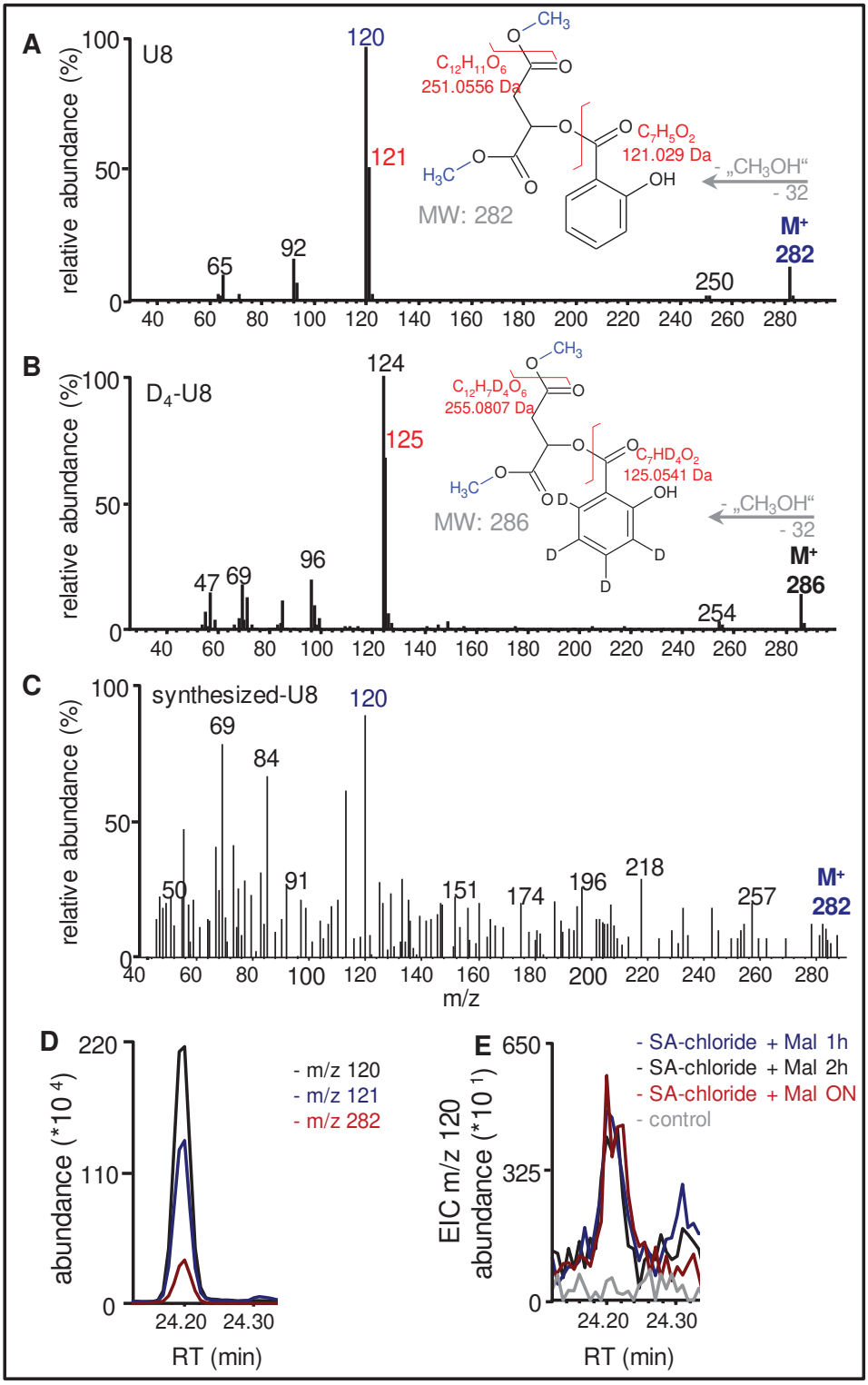

Figure 2.1.7: Identification of SA-Mal as ICS1- and PBS3-dependent molecular species U8

(A) GC-MS mass spectra of U8 derived from *Psm vir* infected *npr1* plant tissue. The molecular fragmentation, indicated on the molecular structure in red, concur with the MS fragmentation. Cleavage of methanol group leads to a 251 Da fragment and the cleavage of malate leads to 121 Da. Introduced methyl groups are indicated in blue. (B) To prove that U8 is a SA derivate, we infiltrated *npr1* leaves with 2 mM SA and isotope labeled D_4-SA and harvested samples 4 hpi. (C) The mass spectra of SA-Mal synthesis (2 h) highlights the characteristic ions of SA-Mal m/z 120 and M^+ of m/z 282 in blue. Accumulation of U8 in *npr1 Psm vir* plant extract (D) has identical RT at 24.2 min as synthesized SA-Mal (E). For SA-Mal synthesis, samples were taken after 1h, 2h and ON. ACN and malic acid served as a control.

Benzoic acid-malate and benzoic acid-aspartate in *A. thaliana*

Due to the structural relation, SA and BA were promising precursors candidates of the novel molecular species. Therefore, plants were infiltrated with isotope labeled D_4-SA and D_5-BA to solve this question. Here, the previously described U8 has been identified as SA-Mal. After D_5-BA infiltration we could observe an accumulation of tow BA-derivates. One of the derivates was identified as conjugation of BA to Mal forming BA-Mal and the other as putative BA-Asp. Both BA derivates accumulate also after pathogen infection in *A. thaliana* tissue (see chapter 2.1.2, Table 2.1.1). The molecular fragmentation of BA-Mal is consistent with the MS ion fragmentation pattern (Figure 2.1.8 A). M^+ of m/z 266 concurs with the total MW of 266 DA of BA-Mal, also the main ion m/z 105 depicts the benzol skeleton. Ions m/z 235 and m/z 207 represent the cleavage of methanol group (31 Da) and a carbonyl group (28 Da). Moreover, a shift of five masses was observed in the MS spectrum of plant tissue pretreated with D_5-BA (Figure 2.1.8 B). The BA-derivate was confirmed as BA-Mal through chemical synthesis with bezoyl chloride (7456.1, Roth) and malic acid (3034.1, Roth) (Figure 2.1.8 C). The overlay of the EIC of m/z 105 depicts the peak at 23.29 min for synthesized BA-Mal compared to the extracted peak in plant extract. No accumulation of m/z 105 has been determined in the control consisting of Mal and pyridine (Figure 2.1.8 D). BA-Asp was identified through pre-infiltration of isotope labeled D_5-BA. Comparing MS spectrum of BA-Asp to verified BA-Mal , we found great similarities concerning the ion fragmentation pattern (Figure 2.1.8 A and E). Mal is the corresponding dicarboxylic acid of Asp, carrying a hydroxy group instead of an amino group. Therefore, BA-Asp is one mass unit smaller compared to BA-Mal. The molecular fragmentation of BA-Asp concurs with the ion fragmentation pattern. Here, the molecular ion M^+ of m/z 265 concurs with the MW of 265 Da of BA-Asp, m/z 234 describes the cleavage of methanol group (31 Da), m/z 206 cleavage of a carbonyl group, whereas the main ion m/z 105 describes the benzoyl fragment (Figure 2.1.8 E). After *in planta* infiltration with isotope labeled D_5-BA, the mass spectrum of BA-Asp shifts about five masses (Figure 2.1.8 F).

In conclusion, mass spectrum of BA-Asp compared to the very similar mass spectrum of confirmed BA-Mal underlines the close relationship. The further labeling of BA-Asp through isotope labeled D_5-BA emphasizes BA-Asp identity. Although, an incontestable identification of BA-Asp through an authentic standard substance or a chemical synthesis is still pending.

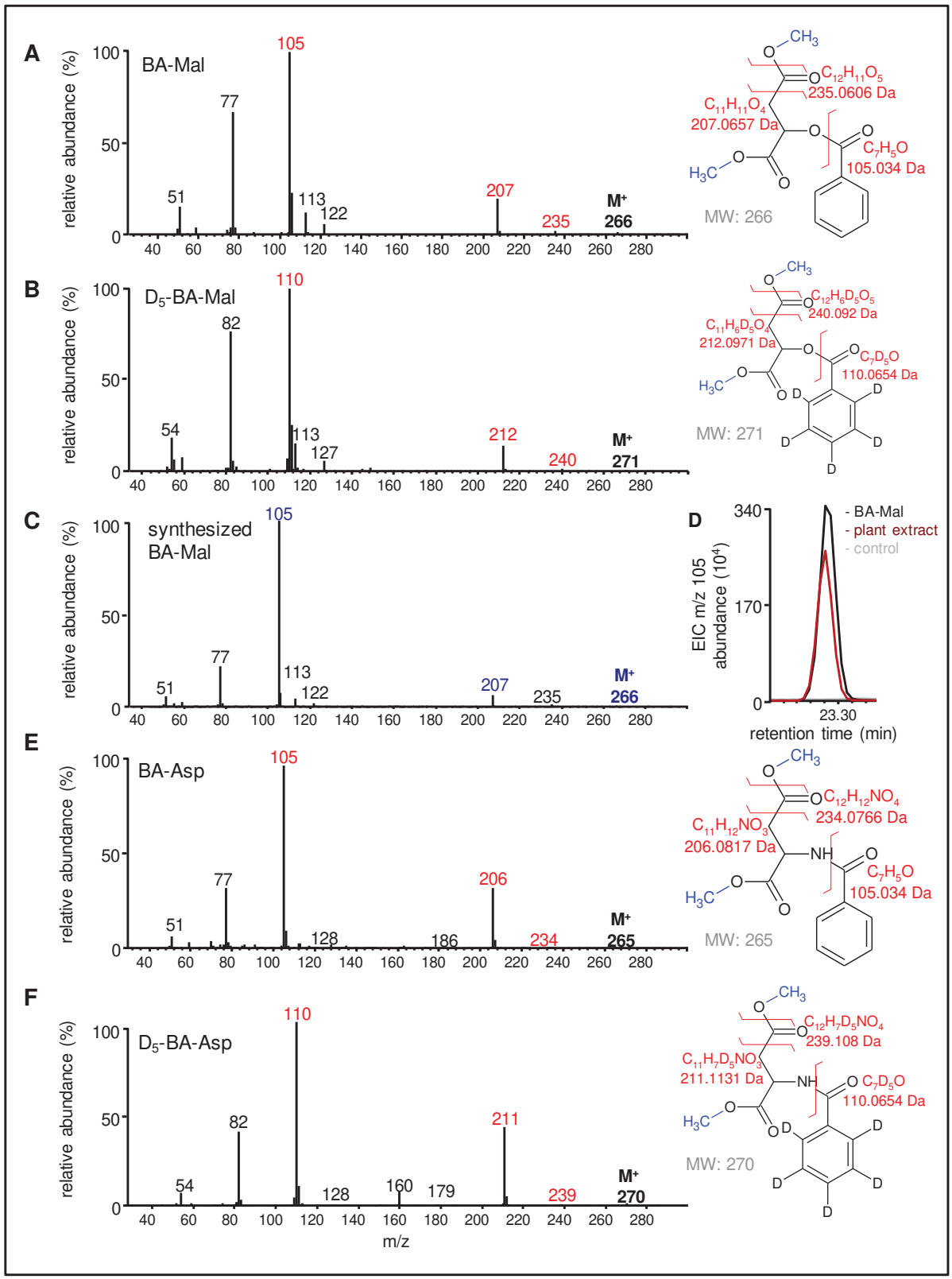

Figure 2.1.8: Identification and synthesis of BA-Mal and identification of BA-Asp
(A) The MS of the metabolite in question depicts ion fragmentation going along with the molecular fragmentation indicated on the molecular structure shown on the right. (B) Leaf infiltration with 2 mM isotopic labeled D_5-BA 4 hours before infection with *Psm vir*, results in a shift of five masses of the metabolite Plant samples were harvested 48 hpi with *Psm vir*. For the chemical synthesis of BA-Mal, 0.5 M benzoyl chloride and 0.5 M Mal were added to dry pyridine. Reaction proceeded at room temperature and washed and with MeOH. All samples were methylated with trimethylsilyl diazomethane and analyzed via GC-MS. (C) The mass spectrum of synthesized BA-Mal exactly concurs with the MS of the plant metabolite in A. (D) Overlay of the EIC)of m/z 105 depicts that plant extract and synthesized

BA-Mal share the same RT of 23.28 min. (E) Mass spectrum and molecular structure of BA-Asp and isotope labeled D_5-BA-Asp after *in planta* infiltration of 2 mM D_5-BA (F). Samples were harvested 4 hpi and methylated for derivatization. All samples have been methylated with trimethylsilyl diazomethane for derivatization, indicated in red.

2.1.2 Characterization of identified ICS1-dependent molecular species

A common feature of the newly identified molecular species is the ICS1-dependent accumulation after pathogen treatment in *A. thaliana*. Strikingly, the identified molecular species 3-FBA (U1), 5-FSA (U2), 3-CaBA (U3), 3-CaMeBA (U4), 5-CaSA (U5), 5-CaMeSA (U7), SA-Mal (U8) and IC-Glu (U9) share all, except *N*-pyr-Glu (U6), structural similarities to SA or BA. Therefore, we included additional SA and BA derivates to our further investigations. Here, we especially focused on SA glycoside conjugations, SA 2-*O*-β-glucoside SAG and SA glucose ester SGE as well as the SA and BA conjugations to Mal and Asp. Moreover, we included the plant defense-related SA derivates 2,3-DHBA and 2,5-DHBA and their glycosolic conjugations. The following overview, Figure 2.1.9, shall illustrate the structural relationship of the molecular compounds.

For a more detailed characterization of the origin and function of the metabolites we analyzed the accumulation pattern in further *A. thaliana* mutants of the SA-, NHP and Pip pathways and checked the influence of the molecular species on SA-biosynthesis and SAR formation and priming against pathogen attacks. To confirm the *in planta* occurrence of the identified molecular species we applied two different leaf extraction and derivatization methods: vapor phase extraction (VPE) and trimethylsilyl (TMS) method (Table 2.1.1). Time-dependent and systemic accumulation of certain molecular species in wild-type Col-0 underlines a potential role in defense activity. Infiltration studies with authentic standard substances should help to clarify the direct influence in plant immunity. Investigations of metabolic accumulation patterns of important defense mutant plants should help specify the role of each molecular species in plant-defense. To identify the origin of the molecular species we infiltrated *A. thaliana* wild-type plants with radioactive labeled versions of the putative molecular precursors: D_4-SA, D_5-BA and D_5-Phe.

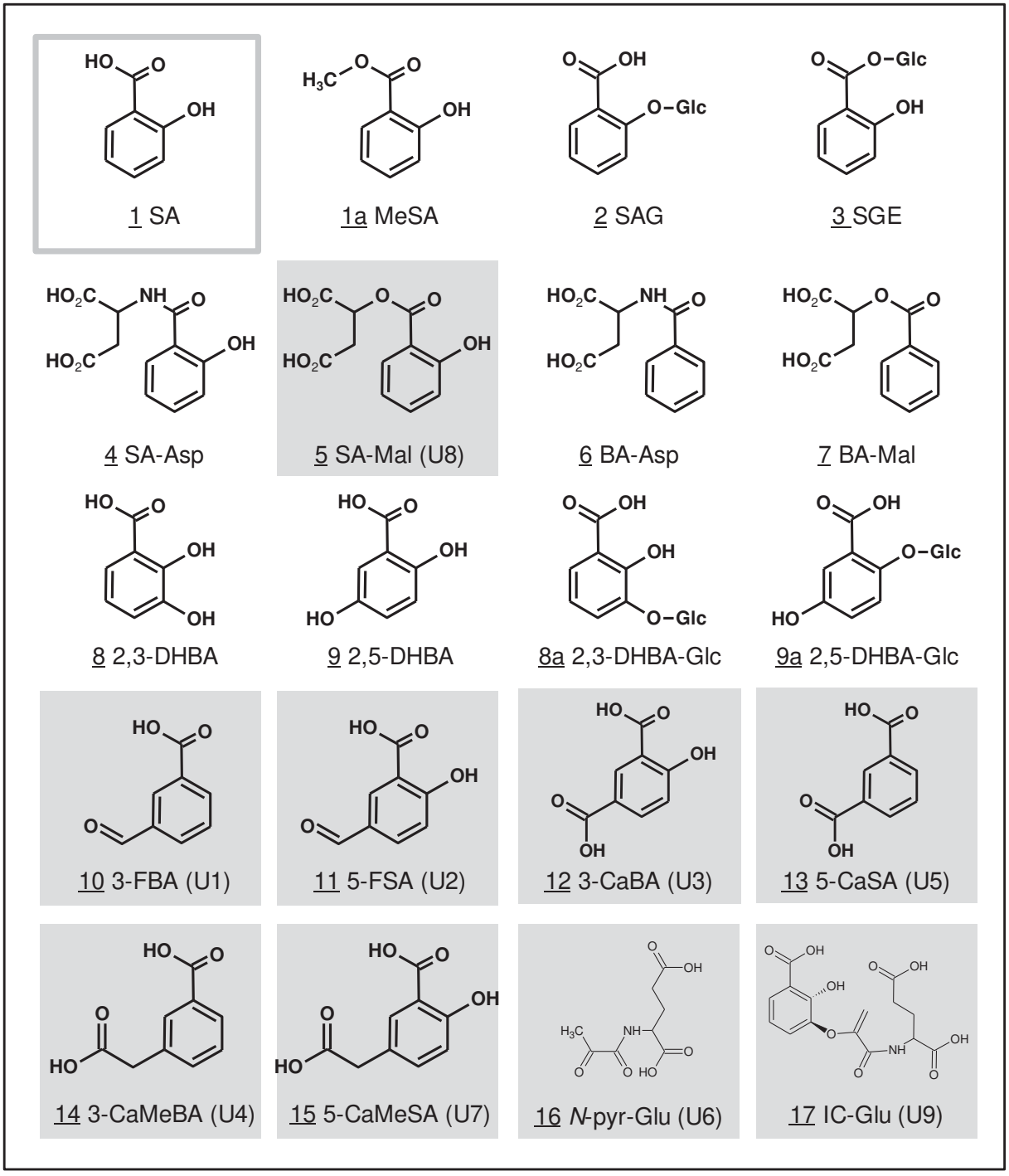

Figure 2.1.9: Chemical structures of identified molecular species and structural relatives
Overview of aromatic metabolites that accumulate after *Psm vir* treatment in *A. thaliana* wild-type plants Col-0. All compounds, besides *N*-pyr-Glu, share structural similarities to SA or BA. In this study, we describe the identification of nine new *ICS1*-dependent metabolites (highlighted in gray). The results were achieved using a combination of GC-MS and GC-FTIR. With help of the mass spectra and RT given by GC-MS analytics, we gained information about the possible mass and structure of the compounds in question. Due to the characteristic mass spectra of each metabolite we could quantify the accumulation of metabolites. FTIR spectroscopy gave us information about the present and absent of chemical groups. Combining all the analytical and spectroscopic data, we could reconstruct the chemical structure of nine previously unknown molecular species U1-9.

Time-dependent accumulation of identified molecular species

For a more detailed characterization of the defense-related metabolites, a time-dependent accumulation of the molecular species was analyzed in *A. thaliana* wild-type Col-0 (Figure 2.1.10). Plant leaves infiltrated with the bacterial strains *Psm vir* or the HR inducing avirulent strain *Psm avir*. Samples were harvested 6, 10, 24 and 48 hpi and subsequently analyzed by GC-MS. Samples of untreated plants and leaves infiltrated with 10 mM $MgCl_2$ served as controls. The results of the time course analysis depict a time-dependent accumulation of SA and its derivates. SA is rapidly accumulating after *Psm vir* and *Psm avir* infection reaching the highest amounts 24 hpi, whereby the SA response is faster after *Psm avir* inoculation. The data indicates a decrease 48 hpi, however the difference to 24 hpi is not significant. Since the metabolites were methylated for GC-MS analysis we were unable to distinguish between SA and its natural methylated form MeSA. Compared to SA the accumulation of SA glycosides (SA-Glc including SAG and SGE), SA-Mal and SA-Asp is delayed and tends to steadily increase over time. SA-Glc accumulates significantly after 10 hpi and stays accumulated after 24- and 48 hpi after *Psm vir* (25.72 µg*g FW^{-1}/ 24.61 µg*g FW^{-1}) and *Psm avir* (29.33 µg*g FW^{-1}/ 38.44 µg*g FW^{-1}) infection. The glycosylic conjugation of SA enhances the solubility of SA in water. Therefore, SA-glycoside conjugations were found in the aqueous phase of VPE extracts, whereas free SA and MeSA are found in the organic phase. Added HCl to the aqueous phase, led to a cleavage of the sugars through the acid and detach sugars form SA. Therefore, only released SA was analyzable and the previous glycosylic form remains undetermined. The SA conjugations SA-Mal and SA-Asp reach the climax after 48 hpi and *Psm vir* inoculation (1.44 µg*g FW^{-1}/ 0.51 µg*g FW^{-1}). The corresponding BA conjugations BA-Asp and BA-Mal were not detected in this experiment. The amounts of the SA derivates 2,3-DHBA and 2,3-DHBA-glycoside (2,3-DHBA-Glc) revealed a steady increase over time. In contrast, accumulation of 2,5-DHBA reached the maximum at 6 hpi with *Psm vir*. However, after infection with *Psm avir* highest amounts of 2,5-DHBA were detected 48 hpi. 2,5-DHBA-Glc could not be detected in this experiment. The significantly highest amount of 3-FBA was detected 10 hpi with *Psm vir* and 24 hpi with *Psm avir*. The levels of 3-FBA decreased at 48 hpi. Contrarily, 5-FSA tends to steadily increase after infection with *Psm vir* or *Psm avir* and reached a climax at 48 hpi after bacterial infection. 5-CaSA and 5-CaMeSA accumulate significantly at 48 hpi with *Psm vir*. Interestingly no significant accumulation was observed for 5-CaSA and 5-CaMeSA after infection with *Psm avir*. 3-CaBA tents to a rising accumulation at 48 hpi with *Psm vir* or *Psm avir*. The metabolites *N*-pyr-Glu and IC-Glu continuously increase after pathogen treatment and reach a climax at 48 hpi. An accelerated

accumulation was observed after treatment with *Psm avir*. 3-CaMeBA could not be detected in this experiment.

In summary, the accumulation pattern of the metabolites can be separated into three groups: (I) early accumulation after pathogen treatment included 2.5-DHBA (II) increasing accumulation between 10 and 24 hpi and decrease afterwards included SA and 3-FBA (III) virtually continuous accumulation over time and a climax at 48 hpi included all other analyzed metabolites. Since the level of most metabolites were significantly increased at 48 hpi with *Psm vir,* the time point of 48 hpi and *Psm vir* as bacterial strain was used for following experiments unless indicated otherwise.

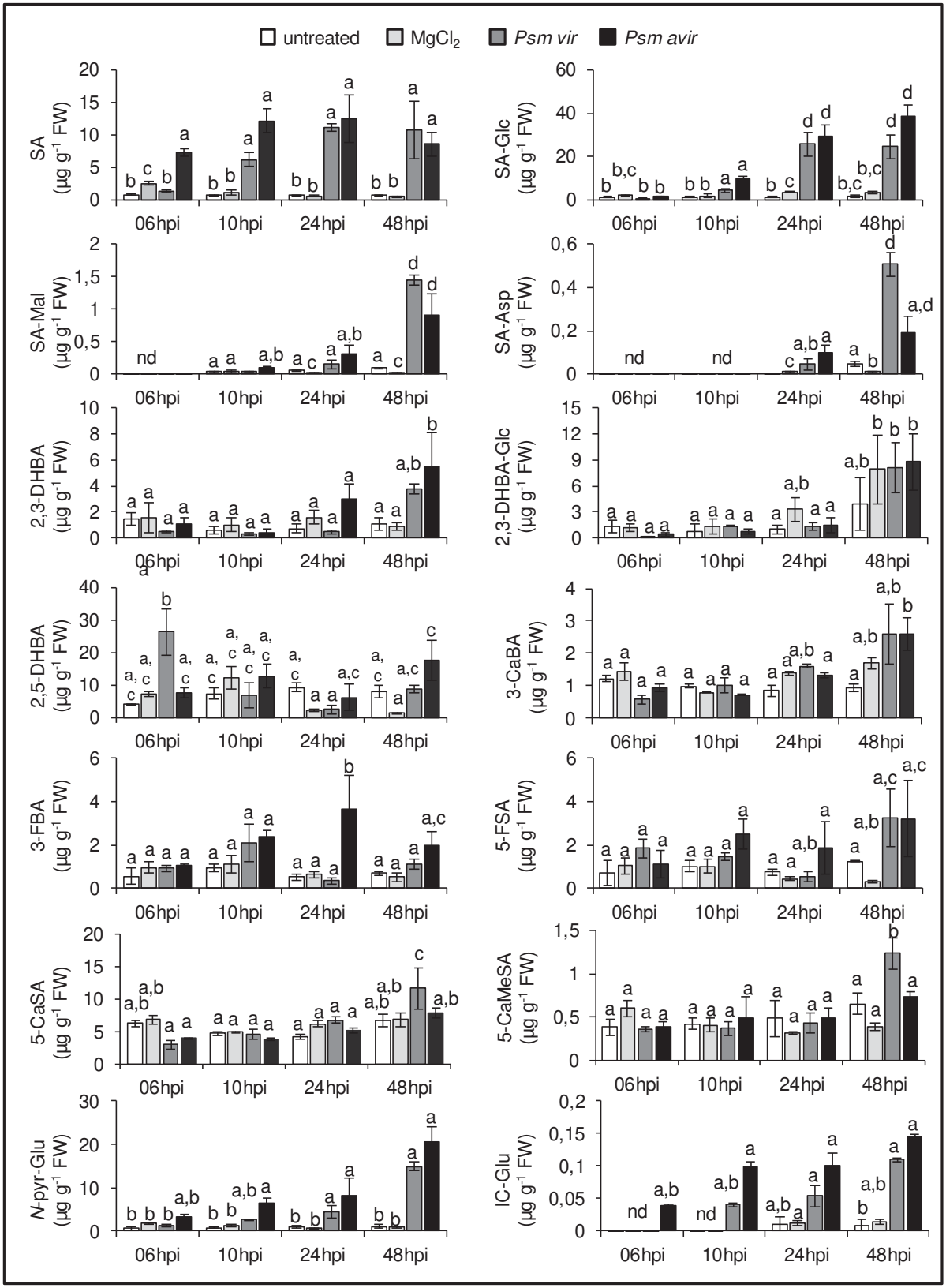

Figure 2.1.10: Time- and pathogen-dependent accumulation of molecular species in *A. thaliana* wild-type Col-0

The time course analysis depicts the accumulation of molecular species after *Psm vir* infection, infection with the hypersensitive response inducing *Psm avir* strain. Infiltration with $MgCl_2$ and untreated leaf samples served as control. Col-0 leaves were infiltrated with a bacterial solution of OD_{600}= 0.005 or 10 mM $MgCl_2$. Leaf samples were harvested 6-, 10-, 24- and 48 hpi and extracted via VPE. Samples have been methylated for derivatization. No analyzable traces of metabolites were declared as not

detected (nd). Bars represent means ± SD an individual experiment consisting of three biological replicates. Letters above bars indicate statistically significant differences ($p < 0.05$, ANOVA and posthoc Tukey's honestly significant difference [HSD] test). Samples were harvested and extracted by Elia Stahl.

Comparable metabolite profiling

All nine novel molecular species are ICS1-dependent and over-accumulate in *npr1* mutants after pathogen infection. To investigate how all nine molecular species are integrated into defense-related pathways we considered a further contemplation of crucial genes in plant immunity. Therefore, we quantified the metabolites in extracts from wild-type *A. thaliana* Col-0 plants and defense-related *A. thaliana* knockout mutants: *sid2* (*ics1*), *eds5* (*sid1*), *pad4*, *ndr1*, *ald1*, *fmo1*, *pbs3*, *npr1*, as well as from the SA-hydroxylase carrying *NahG* transgenic line. Leaf samples were infiltrated with *Psm vir* or 10 mM $MgCl_2$ and were harvested 48 hpi. Since, all identified molecular species were ICS1-dependent they were missing in *sid2* mutant plants. EDS5 and PBS3 are key-players in the SA-biosynthesis pathway. While EDS5 transports isocorismate out of the chloroplast into the cytoplasm, is PBS3 an amino acid conjugase which is important for the conversion of Glu to IC which spontaniously bereaks down to free SA and *N*-pyr-Glu. The positive defense regulators PAD4 and NDR1 were also included. NDR1 is a membrane-associated protein, which is responsible for the resistance establishment after bacterial infection. PAD4 is required for SA- and CAM-dependent defense pathways. ALD1 and FMO1 are essential key enzymes for the crucial SAR metabolites NHP and Pip. Moreover, we included the transgenic *NahG* to the experiments, to examine if the molecular species are directly involved in SA-biosynthesis. In *NahG* plants SA is hydroxylated to catechol. To compile the metabolite profile, six indipendent experiment were considered and analzyed (Figures S4-S9). In each experiment all shown treatments consisted of three biological replicates. Here, three leaves of six plants per treatment were harvested and for each replicate leaves of two plants were pooled to one sample. For quanification a hypothetical correction factor of 1 has been used for all molecular species. Since, most SAR and defense-deficient mutant plants are more susceptible towards pathogen infections, they develop more severe symptoms compared to wild-type plants which results in a proportionally higher metabolic quantity. The higher loss of water in stronger infected tissue was considered and corrected during evaluation of the data. Table2.1.1 conflates all gained data of the individual experimments and represents the to fold change of the accumulation in *Psm vir* infected tissue to the wild-type mock control.

To validate the occurrence of the metabolites *in planta* we used two different leaf extraction and derivatization methods (Table 2.1.1). The VPE method is suitable for low abundant organic

compounds like 3-FBA, 5-FSA and SA-Mal. For subsequent analysis by GC-MS metabolites were methylated with trimethylsilyl diazomethane. Samples were heated up to 70°C and 200°C for complete evaporation. However, this method is not optimal for all metabolites. As mentioned before, using VPE it was not possible to distinguish between glycosylated forms SAG and SGE. Therefore, we established a second leaf extraction and derivation method. For the TMS method samples were silylated for derivatization by adding a TMS-group to the compound through *N*-Methyl-*N*-(trimethylsilyl) trifluoroacetamide (MSTFA) before GC-MS analysis. All analyzed molecular species were upregulated 48 hpi in *A. thaliana* wild-type Col-0 (Table 2.1.1). Nine of the 17 molecular species were previous unknown molecular species (U) *in planta* and were first identified in this thesis.

The identified molecular species are accumulating in *A. thaliana* wild-type Col-0 after *Psm vir* infection more than two times higher compared to mock treated control plants. The majority of the molecular species is ICS1-dependent, and therefore missing in the SA deficient mutant *sid2*, except BA derivates: BA-Asp, BA-Mal. Moreover, most metabolites are missing in *eds5*, the knockout mutant plant of the MATE transporter, responsible for the release of IC from the plastid to the cytosol. SA-Mal displayed a moderate accumulation in *eds5* and 5-CaSA accumulates by a ratio of four times compared to Col-0 mock. The molecular species 3-FBA, 5-FBA, 3-CaBA, 5-CaSA and 3-CaMeBA did not accumulate in *ndr1* and *pad4* mutant plants after pathogen treatment compared to Col-0 mock plants. The Pip biosynthesis mutant *ald1* shared the accumulation pattern similar to the wild-type Col-0. However, *fmo1*, deficient to synthesize NHP from Pip, showed no accumulation of 3-FBA, 3-CaBA and 5-CaSA after *Psm vir* infection compared to Col-0 mock. Therefore, 3-FBA, 3-CaBA and 5-CaSA were missing in SA- and NHP-dependent mutant plants. The *pbs3* mutant showed an over-accumulation especially of 3-FBA, 5-FBA, 3-CaMeBA, 5-CaMeSA. The content of free SA in *pbs3* mutants resembles to wild-type concentrations, whereas strikingly, SA-derived metabolites like SAG, SGE, SA-Mal, SA-Asp 2,3-DHBA as well as IC-Glu and *N*-pyr-Glu are missing or are strongly reduced in *pbs3*. The loss of IC-Glu and *N*-pyr-Glu underlines the PBS3-dependency. Furthermore, all metabolites are over-accumulating in *npr1*, which is in agreement with its previously described function in negative feedback of the IC-pathway and NPR1s function as dircet activator of *PR1* gene expression. To examine a relationship to SA we analyzed the transgenic line *NahG*, which degrades SA to catechol and displayed, as expected, that SA-Mal as direct SA-derivate is absent in *NahG* mutant plants. Moreover, 3-CaBA is not accumulating in *NahG*. 2,5-DHBA could not be detected in any of the experiments probably due to 2,5-DHBAs very early respond after pathogen treatment (Figure 2.1.10). Due to a

relativly low abundancy and a late GC RT the molecular species SA-Asp, BA-Asp, BA-Mal, 2,3-DHBA and IC-Glu were only detectable some experiments.

Taken together it can be summarized that all identified molecular species are ICS1- and EDS5-dependent. Additionally, IC-Glu and *N*-pyr-Glu are depending on PBS3. SA-Mal, as direct SA derivate, is missing in *NahG*. All seven remaining molecular species are over-accumulating in *pbs3* and *npr1* plants, indicating an independency of both proteins. It can be concluded that all identified molecular species have to be involved in metabolic pathways downstream ICS1 and EDS5 and upstream NPR1.

Table 2.1.1: Pathogen-induced molecular species are not induced in *sid2* and *eds5* and are over-accumulating in *pbs3* and *npr1*

	molecular species		method	RT	m/z	Col-0		*sid2*	*eds5 (sid1)*	*pad4*	*ndr1*	*ald1*	*fmo1*	*pbs3*	*npr1*	*NahG*	first description in plant immunity	fold change *Psm* to Col-0 mock
						mock	*Psm vir*											
1	SA		VPE	11.8	120	1	8	0	1	2	6	13	9	10	17	0	Piria, 1838	
2	SAG		TMS	21.6	361	1	20	1	1	6	11	27	21	4	17	0	Klick et al. 1988	
3	SEG		TMS	21.7	193	1	9	0	0	10	23	17	21	2	55	0	Klick et al. 1989	
4	SA-Asp		VPE	24.8	121	1	14	0	nd	nd	nd	nd	nd	4	>100	nd	Steffan, 1988	
5	SA-Mal	U8	VPE	22.5	120	1	>100	1	4	6	16	16	7	1	>100	nd	this study	
6	BA-Asp		VPE	23.7	105	1	4	7	nd	nd	nd	nd	nd	7	7	nd	Suzuki et al. 1988	
7	BA-Mal		VPE	21.6	105	1	2	3	nd	nd	nd	nd	nd	3	3	nd	Suzuki et al. 1988	
8	2,3-DHBA		VPE	14.1	136	1	3	0	nd	nd	nd	nd	nd	1	2	nd	Ibrahim et al. 1959	
9	2,5-DHBA		VPE	17.0	136	nd	nd	nd	nd	nd	nd	nd	nd	nd	nd	nd	Ibrahim et al. 1969	
10	3-FBA	U1	VPE	14.8	133	1	2	1	0	0	0	2	1	63	25	2	this study	
11	5-FSA	U2	VPE	16.8	148	1	3	1	0	1	1	7	4	>100	58	8	this study	
12	3-CaBA	U3	VPE	17.2	163	1	2	1	0	1	1	2	1	20	6	1	this study/ Döring 2015	<1.5
13	5-CaSA	U5	VPE	18.7	178	1	2	1	0	1	1	2	1	28	10	2	this study/ Döring 2015	1.5-3
14	3-CaMeBA	U4	VPE	18.6	208	1	5	1	0	2	0	5	19	>100	>100	23	this study	3-10
15	5-CaMeSA	U7	VPE	20.0	133	1	4	1	4	4	6	6	3	>100	47	10	this study	10-30
16	*N*-pyr-Glu	U6	VPE	18.9	142	1	7	1	1	5	7	22	10	1	56	6	Rekhter et al. 2019/ Torrence-Spence et al. 2019/ this study	30-100
17	IC-Glu	U9	VPE	29.0	142	1	21	0	nd	nd	nd	12	5	nd	>100	nd		>100

Accumulation pattern of molecular species in defense-related mutants. All samples were harvested 48 hours after *Psm* infection and 10 mM $MgCl_2$ infiltrated plants served as mock control. The values indicate the fold change to the wild-type mock control and depict an average of at least three independent replicates. For all values, except SA, a hypothetical correction factor of 1 has been used. The VPE method is based on a separation of a water free organic phase and methylation with trimethylsilyl diazomethane of carboxyl groups. Through evaporation steps (70°C, 200°C/ 2min) only volatile compounds were collected. TMS method extraction with MeOH: H_2O (80:20 (v/v)) and silylated with MSTFA containing 1 % TCMS (70°C/ 30min). Data is based on six individual experiments. In most cases data of several experiments have been considered. Data of individual experiments is shown in the supplemental information (Figure S4-S8). Meaning of *nd: metabolite was not detectable in entire experimental setup.

Systemic accumulation of molecular species

The key defense regulators SA, NHP and Pip accumulate after pathogen infection in local infected plant tissue, as well as in healthy systemic leaf tissue to establish a SAR, which protects the plants against further pathogen attacks. A systemic accumulation of the identified molecular species could indicate a possible role in pathogen defense. Therefore, we harvested systemic leaves of locally *Psm vir* infected *A. thaliana* wild-type plants Col-0 at 48 hpi. Control plants were treated locally with 10 mM $MgCl_2$ (Figure 2.1.11). The results depict a significant accumulation of SA as well as the SA-derivate 2,3-DHBA after bacterial treatment. 2,5-DHBA has been detected in systemic leaf tissue but did not accumulate after pathogen treatment. The newly identified metabolites 3-CaBA, 5-CaSA and *N*-pyr-Glu were found enhanced in systemic tissue after pathogen treatment. However, exclusively the accumulation of *N*-pyr-Glu and 5-CaSA was significant. The other six novel metabolites 3-FBA, 5-FSA, 3-CaMeBA, 5-CaMeSA, and SA-Mal were not detectable in systemic leaf samples. Taken together, 2,3-DHBA, 3-CaBA, 5-CaSA and *N*-pyr-Glu are accumulating locally and systemically after *Psm vir* infection in wild-type plant tissue.

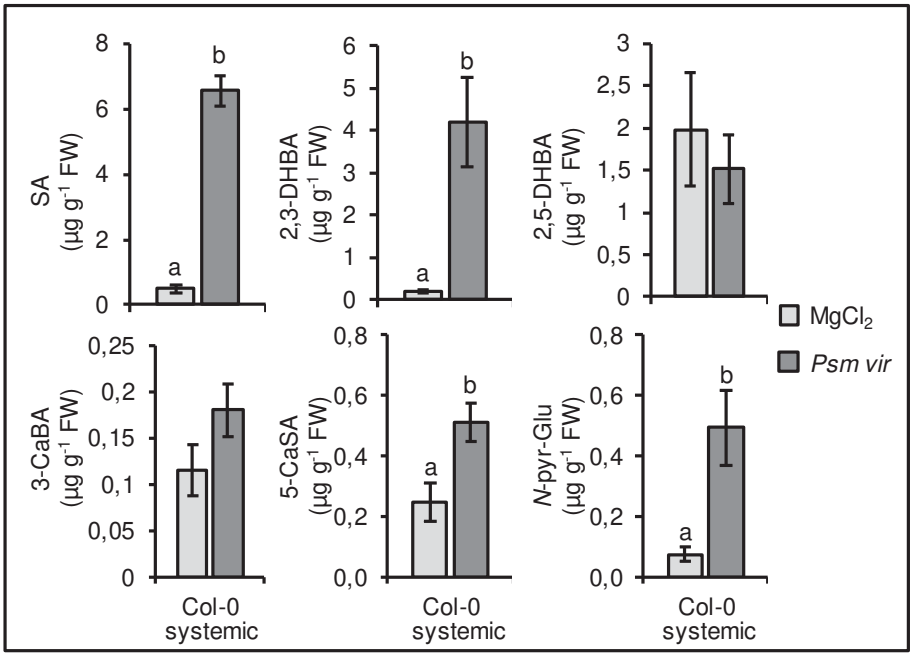

Figure 2.1.11: Systemic accumulation of molecular s pecies in *A. thaliana* wild-type Col-0 indicates a role in pathogen defense
Systemic accumulation of SA, 2,3-DHBA, 2,5-DHBA, 3-CaBA, 5-CaSA and *N*-pyr-Glu in *A. thaliana* Col-0 48 hpi with *Psm vir*. Mock control plants were infiltrated with 10 mM $MgCl_2$. Samples were methylated for derivatization and subsequent analyzed by GC-MS. Data represents one experiment, including three biological replicates. Here, three leaves of six plants per treatment were harvested and for each replicate leaves of two plants were pooled to one sample. Different letters denote statistically significant differences between mock and *Psm vir* infiltrated leaves ($p < 0.05$; two-tailed t test). Samples were harvested and extracted by Denis Kim and Michael Hartmann.

Influence on plant immunity of identified molecular species

So far, we characterized a time-dependent accumulation after pathogen infection of several identified molecular species with an overall accumulation at 48 hpi, a systemic accumulation of 2,3-DHBA, 3-CaBA, 5-CaSA and *N*-pyr-Glu after *Psm vir* infection and determined that most molecular species were dependent on ICS1 and EDS5 and further defense-related genes. Therefore, the resulting question is: how do the molecular species influence plant immunity? Does the exogenious application of authentic molecular species substances has an influence on bacterial resistance and *PR1* gene expression, like SA does? To answer this question, we performed molecular species induced resistance studies and molecular species induced *PR1* gene expression (Figure 2.1.12). In both experimental setups we infiltrated Col-0 and *sid2* plants with a 0.5 mM aqueous solution of 3-FBA, 5-FSA, 3-CaMeBA, 3-CaBA, 5-CaSA as well as 2,3-DHBA and 2,5-DHBA. The infiltration of 0.5 mM SA served as a positive control, deionized water as a negative.

To determine the induced resistance of the named substances, we infected the same leaves 4 hpi with *Psm lux* (OD_{600}= 0.001) and measured the bacterial growth 48 hours later (Figure 2.1.12 A-C). The application of SA 4 h before pathogen infection led to a significant decrease of the bacterial growth in Col-0 and *sid2* plants. The application of 5-CaSA and 2,3-DHBA reduced the bacterial growth significantly in Col-0 but not as strong as SA did. In SA deficient *sid2* plants, none of these five compounds showed a direct influence on bacterial growth. To verify the gained results each resistance assay has been individually repeted at least three times (Figure S10).

To study the influence of the identified molecular species on the immune system on a genetic level, Col-0 and *sid2* plants were infiltrated with the authentic substances as described for the induced resistance assay (Figure 2.1.12 D-F). Leaf samples were harvested 4 h after substance infiltration. The mRNA has been extracted and reverse transcribed to cDNA. With the gained cDNA quantitative real time PCR has been processed and the relative expression of *PR1* has been measured. The application of SA lead to an enhanced *PR1* expression in Col-0 and *sid2* plants. Out of the identified metabolites, 3-CaMeBA inhibits *PR1* expression in Col-0 and *sid2* plants compared to SA and the water control. 3-CaBA influences *PR1* expression negatively in Col-0 plants. The application of the SA derivative 2,3-DHBA enhances *PR1* expression significantly in Col-0 and *sid2* plants compared to the water control, but not as strong as SA did. 2,5-DHBA has a weaker influence on *PR1* than 2,3-DHBA in Col-0 and did not influence *sid2* plants. The application of the remaining molecular species did not significantly influence *PR1* expression neither in Col-0 nor in *sid2* plants.

In conclusion, SA out of the infiltrated molecular species, has the strongest influence to promote bacterial resistance and induce *PR1* expression. 2-3-DHBA has a significant but moderate influence on bacterial resistance and *PR1* expression. 3-CaBA reduced bacterial growth in Col-0 plants but showed no influence on gene expression level. Infiltration of 3-CaMeBA inhibited *PR1* expression but had no influence on the bacterial growth.

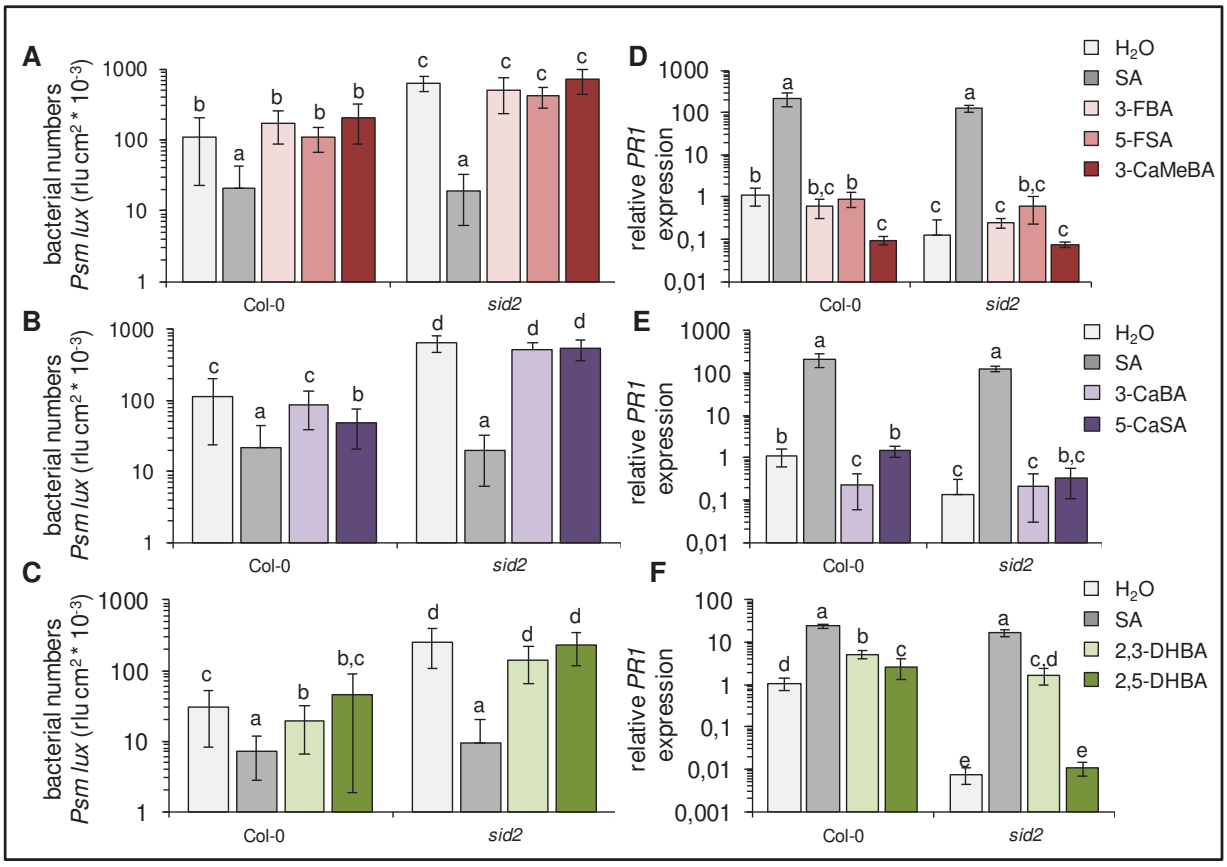

Figure 2.1.12: Identified molecular species have no direct influence on plant immunity
To examine the influence of the identified metabolites to plant resistance, authentic standard substances of the molecular species were infiltrated into Col-0 wild-type and *sid2* mutant plants with aqueous solutions of 0.5 mM 3-FBA, 5-FBA, 3-CaMeBA (A, D), 3-CaBA and 5-CaSA (B, E) and 2,5-DHBA, 2,3-DHBA (C, F). SA has been infiltrated as a positive control, autoclaved deionized water as a negative. For bacterial resistance assays (A, B, C) plants were pretreated with the previously mentioned substance concentrations. 4 hours later the same leaves were infected with *Psm lux* (OD_{600}= 0.001). Bacterial numbers were defined 60 hpi with the bioluminescent virulent *Psm lux* strain and expressed as rlu per cm^2 leaf area. For *PR1* gene expression (D, E, F), plants were treated with the mentioned substances and leaf samples were collected 4 hpi. For bacterial resistance assays bars represent at least three individual experiments, each experiment, consisting of at least 15 leaves (individual experiments are shown in Figure S10). Letters above bars indicate statistically significant differences ($p < 0.05$, ANOVA and posthoc Tukey's honestly significant difference [HSD] test). The y-axes have a log_{10} scaling.

Influence of 3FBA, 5-FSA and 3-CaMeBA on SA-biosynthesis

To further characterize the identified molecular species, an influence of the novel identified metabolites on SA-biosynthesis was analyzed. It is well known, that key SAR metabolites like

SA, NHP and Pip lead to an accumulation of SA after exogenous application or infiltration. Therefore, we quantified cellular SA levels of *A. thaliana* Col-0, *sid2*, *NahG*, *pbs3* and *npr1* after infiltration with SA, 3-FBA, 3-FSA and 3-CaMeBA by GC-MS. As described in the literature, SA infiltration leads to a remarkably increase in SA amounts, in all tested plant lines, except in the SA-hydroxylase carrying mutant *NahG* (Figure 2.1.13 A). Strikingly, Col-0 and *npr1* plants infiltrated with 3-FBA, 3-FSA and 3-CaMeBA reacted with increasing SA levels compared to water infiltrated plants. However, the three molecular species were not able to induce SA accumulation in *sid2*, *pbs3* and *NahG* plants (Figure 2.1.13 B).

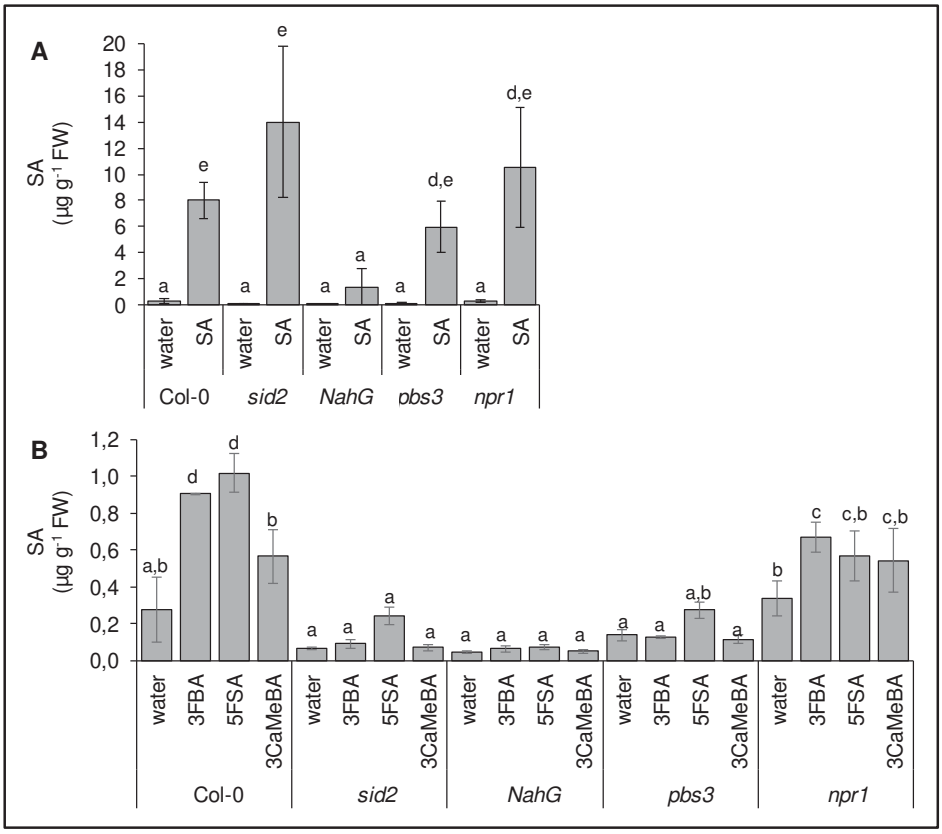

Figure 2.1.13: 3-FBA 5-FBA trigger SA accumulation in wild-type plants
Accumulation of SA after treatment with 0.5 mM SA (A) or 0.5 mM 3-FBA, 5-FSA and 3-CaMeBA (B) compared to water infiltrated plants. Samples were harvested 4 hpi and methylated for analysis via GC-MS. Different letters denote statistically significant differences ($p < 0.05$).

Infiltration of isotope labeled potential precursors

What is the origin of the molecular species?

Moreover, eight of the nine molecular species shared structural similarities to SA or BA, indicating a putative relationship. There are two pathways forming SA: (I) the IC-pathway is accumulating most SA under pathogen stress (II) the PAL-pathway forms SA under non-

stressed conditions. To clarify the origin of the molecular species we infiltrated with the isotope deuterium (D) labeled putative precursors D_4-SA, D_5-BA and D_5-Phe. If the molecular species origin from the putative precursors, the deuterium labeled aromatic ring will be intergrated into the molecular struckture of the molecular species. The enhanced weight of gained D can be measured through a shift in the GC-MS ion fragmentation. In this regard, it is possible to retrace the molecular origin of the identified species through isotope labeling.

The defense hormone SA, with main ion fragmentation of m/z 120/121 and a RT of 11.6 min, accumulated in *npr1* plants 48 hpi with *Psm vir* (Figure 2.1.14 A). In plants pretreated with 2 mM D_4-SA 4 h before pathogen treatment, accumulation leads to a shift of four mass units to m/z 124/125 as main ion fragment (Figure 2.1.14 B). The extracted ion chromatograms revealed the accumulation of the metabolite's characteristic main ion, for SA m/z 120, plus the following five masses, to detect a shift of MW after D_4-SA isotope treatment. Pretreatment with D_5-BA or D_5-Phe did not lead to a shift of molecular masses (Figure 2.1.14 C-D). SA-Mal was identified as SA derivative through pre-infiltration with D_4-SA. SA-Mal has a RT of 22.5 min and a main ion fragment of m/z 120/121 and accumulates after bacterial treatment. A shift of four mass units to *m/z* 124/125 after D_4-SA infiltration verified the direct deduction of SA. Pretreatment with D_5-BA and D_5-Phe did not lead to an isotope labeling of SA-Mal or shift of molecular masses (Figure 2.1.14 E-H). The BA conjugation BA-Mal accumulates after pathogen infection (Figure 2.1.14 I). Moreover, pretreatment with isotope labeled D_5-BA and D_5-Phe leads to an over-accumulation of labeled D_5-BA-Mal, confirming the formation of BA through the PAL-pathway (Figure 2.1.14 K L). Interestingly, we also detected labeled BA-Mal after infiltration with labeled D_4-SA, indicating a re-formation of BA through SA (Figure 2.1.14 J). Similar results were gained for BA-Asp (Figure S11). The remaining eight identified molecular species were not labeled neither through D_4-SA nor D_5-BA or D_5-Phe pre-infiltration. A shift of their molecular masses indicating an origin of SA, BA or Phe was not determined. Exemplarily, the molecular species 5-FSA, did not exhibit an expected mass shift of three mass units after D_4-SA, D_5-BA or D_5-Phe pretreatment (Figure 2.1.14 M-P). Data of remaining molecular species are shown in the supplemental information (Figure S11).

This labeling experiment indicated that the majority of the identified molecular species are not directly derived from SA, BA, or Phe. Therefore, identified ICS1-dependent molecular species most likely occur prior to SA and BA biosynthesis. SA-Mal was identified as direct SA derivate.

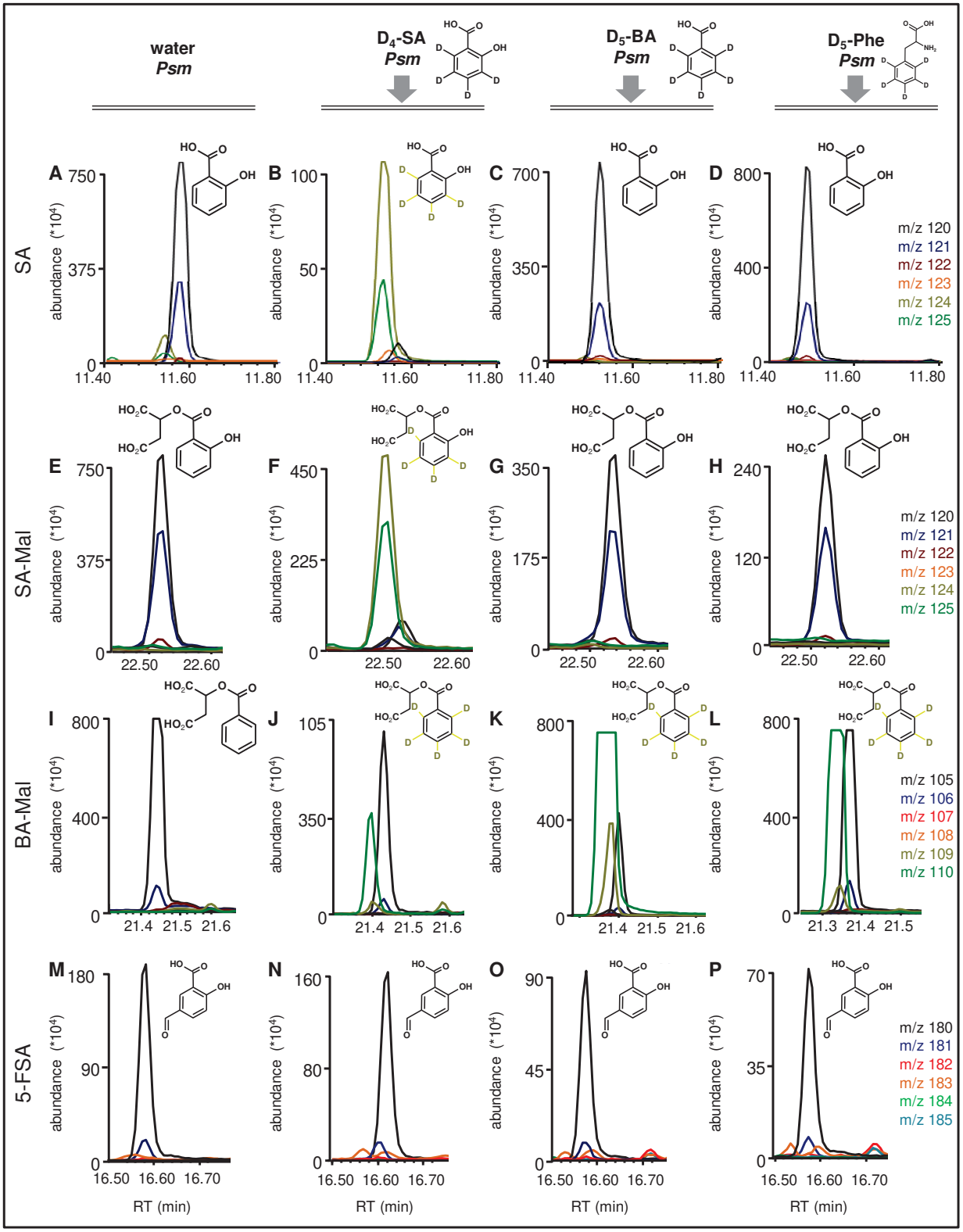

Figure 2.1.14: SA-Mal is the only identified molecular species that derives directly from D_4-SA

The identified molecular species share structural similarities to SA and BA. To clarify their origin, fully grown leaves of five weeks old *npr1* plants were pre-infiltrated with 2 mM of the potential precursors SA, BA and Phe as well as deuterium labeled varieties D_4-SA, D_5-BA and D_5-Phe or water for control. Four hours later, same leaves were infected with *Psm vir* (OD_{600}= 0.005). Infiltrated leaves were harvested 48 hours after second treatment. Plant material has been extracted, methylated for derivatization and was analyzed by GC-MS.

2.1.3 Summarized results of identified molecular species

In conclusion, we could expand the hitherto described metabolic IC-pathway by the identification and characterization of nine novel compounds: 3-FBA, 5-FSA, 3-CaBA, 5-CaSA, 3-CaMeBA, 5-CaMeSA, *N*-pyr-Glu, IC-Glu and SA-Mal. Moreover, we detected the BA conjugations BA-Mal and BA-Asp as *Psm vir*-dependent metabolites in *A. thaliana*. Table 2.1.2 summerizes all results gained about the molecular species in this study. Most of the molecular species were verified through an authentic substance (AS) that was eigther commercially available or validated through nuclear magnetic resonance (NMR) spectroscopy. SA-Mal, BA-Mal and *N*-pyr-Glu were validated through chemical- and biosynthesis (CS, BS). Here, molecular species and synthesized products displayed an identical mass spectra (MS), however, an unequivocal verfication is still pending. The combination of MS and IR and the strong similarities to 3-CaMeBA, strenghens the putative identity of U5 as 5-CaMeSA. Nonetheless, for an unambiguous validation 5-CaMeSA has to be synthesized or assembled through high performance liquid chromatography (HPLC) or solid phase extraction (SPE). The presumed MS of SA-Asp and BA-Asp were comparable to SA-Mal and BA-Mal and differed only in one mass. Both metabolites were deuterium labeled (D) after infiltration with the specific isotope labeled precursor, which supports the identity of the putative substance. The molecular species U9 is most likely IC-Glu, since the MS shares great overlapping ions with the MS of *N*-pyr-Glu. Moreover, current studies described IC-Glu and *N*-pyr-Glu as pivotal metabolites in PBS3 research. Since the detection of the majority of the molecular species was determined by VPE method, this method has been chosen for further analysis. Additionally, we could verify SA, 3-CaBA, 5-CaSA, 3-CaMeBA, 5-CaMeSA *in planta* applying the TMS method. Moreover, SA, SAG, SGE, 3-CaMeBA and 5-CaMeSA could be detected using a similar method to TMS (TMS2). In TMS2, samples were treated with methoxyamine hydrochloride (MA HCl, 30°C/ 90 min), forming oximes upon with ketones and aldehydes. After that, samples were silylated by adding MSTFA (37°C/ 30 min). This method does not expose high temperatures to the plant samples and is more gentle approach to extract the substances. All AS could be verified through all three methods. Appropriate GC-MS mass spectra were attached to the appendix of this thesis (Figure S1 and S2).

The characterization displayed that most of the molecular species accumulated the strongest two days after bacterial treatment. Besides that, 3-CaBA, 5-CaSA and *N*-pyr-Glu were not only accumulating locally but also systemically after *Psm vir* infection in Col-0 plant tissue,

indicating a putative role in plant pathogen interaction. All newly described molecular species were ICS1 and EDS5 depending. Furthermore, all of them over-accumlated *npr1* muntants and the majority also over-accumulated in *pbs3* mutants. The ICS1, EDS5 and PBS3 dependency of *N*-pyr-Glu and IC-Glu support latest descriptions of PBS3 and its crucial role in SA-biosynthesis. Exogeniosly applied 5-FSA and 5-CaSA were able to induce a bacterial resistance in Col-0 plants, besides SA and 2,3-DHBA. None of the novel molecular species had an influence on the expression of the pathogenesis-related marker gene *PR1*. The isotope labeling data revealed that SA-Mal is a direct derivate of SA. Furthermore, BA-Asp and BA-Mal are not only synthesized through BA but also through SA and Phe. All remaining novel molecular species most probably occur prior to SA, BA or Phe biosynthesis.

Table 2.1.2: Summarized results of analyzed molecular species

molecular species	vali-dation	time course								syst. acc.	induced resistance		*PR1* expression		isotope labeling		
		06 hpi		10 hpi		24 hpi		48 hpi									
		vir	*avir*	*vir*	*avir*	*vir*	*avir*	*vir*	*avir*	24hpi	Col-0	*sid2*	Col-0	*sid2*	D_4-SA	D_5-BA	D_5-Phe
SA	AS	( )	(+++)	(+++)	(+++)	(+++)	(+++)	(+++)	(+++)	(+++)	(+++)	(+++)	(+++)	(+++)	(+++)	nd	nd
SAG	AS	( )	( )	(+++)	(+++)	(+++)	(+++)	(+++)	(+++)	nd	-	-	-	-	(+++)	nd	nd
SEG	AS									nd	-	-	-	-	(+++)	nd	nd
SA-Asp	MS + D	( )	( )	( )	( )	(++)	(++)	(+++)	(++)	nd	-	-	-	-	(+++)	nd	nd
SA-Mal	CS + D	( )	( )	( )	( )	( )	(++)	(+++)	(+++)	nd	-	-	-	-	(+++)	nd	nd
BA-Asp	MS + D	nd	nd	nd	nd	nd	nd	nd	nd	nd	-	-	-	-	(++)	(+++)	(++)
BA-Mal	CS + D	nd	nd	nd	nd	nd	nd	nd	nd	nd	-	-	-	-	(++)	(+++)	(+++)
2,3-DHBA	AS	( )	( )	( )	( )	( )	( )	(++)	(+++)	(+++)	(+++)	(++)	(+++)	(+++)	(+++)	nd	nd
2,5-DHBA	AS	(+++)	( )	( )	( )	( )	( )	( )	(+++)	(+)	( )	( )	(+++)	( )	(+++)	nd	nd
3-FBA	AS	( )	( )	( )	(++)	( )	(+++)	( )	(++)	nd	( )	( )	( )	( )	nd	nd	nd
5-FSA	AS	( )	( )	( )	(++)	( )	(++)	(+++)	(+++)	nd	(++)	( )	( )	( )	nd	nd	nd
3-CaBA	AS	( )	( )	( )	( )	( )	( )	(++)	(++)	(++)	( )	( )	(-)	( )	nd	nd	nd
5-CaSA	AS	( )	( )	( )	( )	( )	( )	(+++)	(++)	(+++)	(+++)	( )	( )	( )	nd	nd	nd
3-CaMeBA	AS	nd	nd	nd	nd	nd	nd	nd	nd	nd	( )	( )	(-)	( )	nd	nd	nd
5-CaMeSA	MS + IR	( )	( )	( )	( )	( )	( )	(+++)	( )	nd	-	-	-	-	nd	nd	nd
N-pyr-Glu	BS	( )	(++)	(++)	(+++)	(+++)	(+++)	(+++)	(+++)	(+++)	-	-	-	-	nd	nd	nd
IC-Glu	MS	( )	(++)	(++)	(+++)	(+++)	(+++)	(+++)	(+++)	nd	-	-	-	-	nd	nd	nd

Overview and comparison of central experiments to characterize molecular species identified and described in this thesis. The Summarized overview of the time course experiment after *Psm vir* (*vir*) and *Psm avir* (*avir*) infiltration, systemic accumulation of molecular species, induced resistance and *PR1*-expression in Col-0 and *sid2* plants and detection of the potential precursors through isotopic labeled varieties of D_4-SA, D_5-BA and D_5-Phe. Explanation of key elements: (+) detection, but not significant; (++) tendency not significant accumulation, (+++) significant accumulation; ( ) no influence; (-) significant negative influence; nd not detected; - not tested.

2.2 Characterization of the PBS3 protein

The role of PBS3 the in plant immune system must be important but has still not been fully clarified yet. It is known that PBS3 conjugates 4-substituted BAs as well as small carboxylic acids to AA. PBS3 fullfills the long lasting gap in SA-biosynthesis by conjugating IC to Glu forming IC-Glu. The cleavage of *N*-pyr-Glu from IC-Glu releases free SA. For a more detailed characterization of PBS3 and its involvement in pathogen defense, we purified recombinantly expressed PBS3 and analyzed its enzymatic activity *in vitro*. We tested further substrate combinations to clarify, PBS3 role in the plant metabolic pathway. For *in planta* localization of PBS3, we established transient expression lines in *N. tabacum* as well as stable lines in *A. thaliana*. Therefore, plasmids encoding for PBS3 fluorescent proteins CFP fusion protein were constructed to determine the cellular location of PBS3 via flourescence microscopy.

2.2.1 PBS3 *in vitro* studies

The SAR defective *pbs3* mutant plant is lacking the ICS1-depending metabolites, *N*-pyr-Glu, IC-Glu and SA-Mal. Moreover, SA-derivates like SAG and SGE as well as SA-Asp show lower levels in the *pbs3* knock out mutant compared to *A. thaliana* wild-type Col-0 (Table 2.1.1). Those metabolites might be direct PBS3 products or synthesized downstream and potentially play an important role in plant resistance. To find out whether those metabolites are PBS3 products, biochemical analyses of the *A. thaliana* PBS3 enzyme (AT5G13320) are necessary. We constructed a pET32 expression vector encoding for a PBS3 poly-His affinity tag fusion protein and expressed it in optimized BL21 *Escherichia coli* cells. After cell disruption the protein was purified through affinity chromatography (Figure 2.2.1 B). The extraction and purification of PBS3 was successful and the quantity of the enzyme was with 1.59 mg/mL abundant (Figure 2.2.1 C).

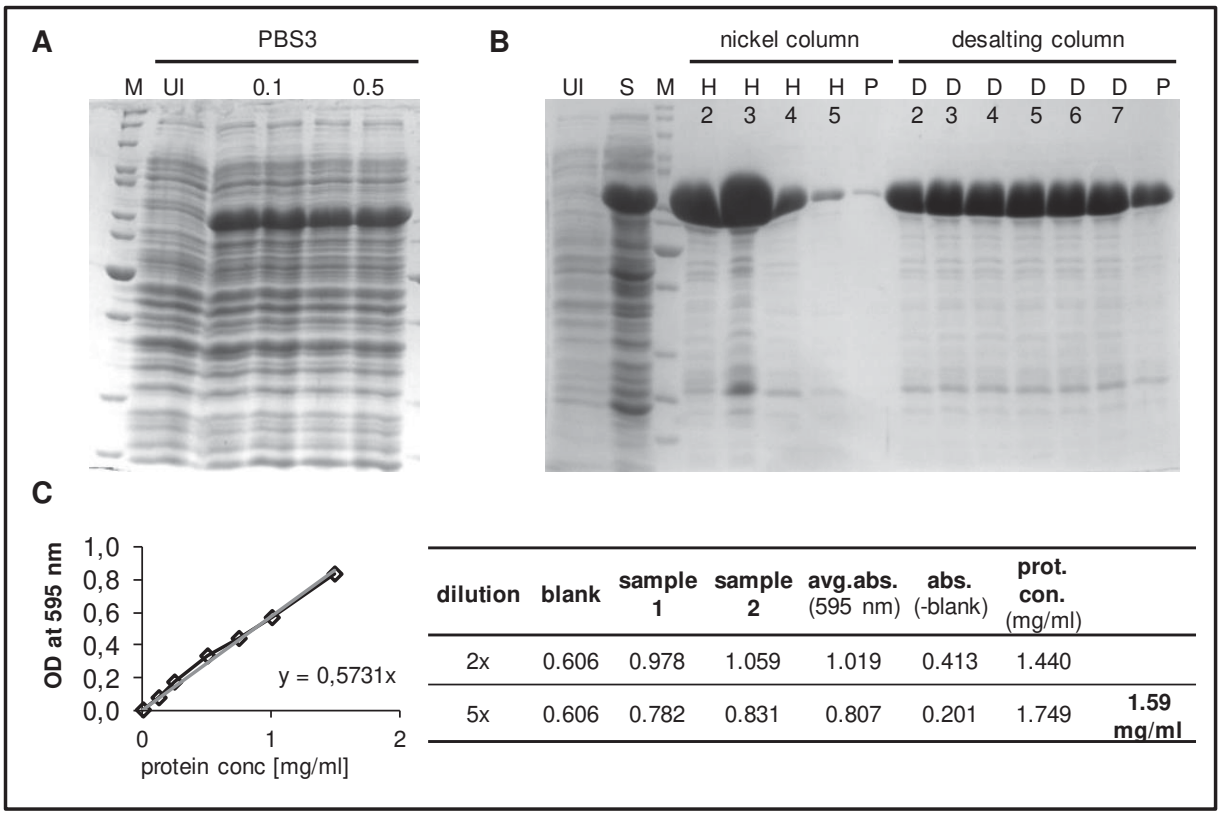

dilution	blank	sample 1	sample 2	avg.abs. (595 nm)	abs. (-blank)	prot. con. (mg/ml)	
2x	0.606	0.978	1.059	1.019	0.413	1.440	
5x	0.606	0.782	0.831	0.807	0.201	1.749	**1.59 mg/ml**

Figure 2.2.1: Protein purification of PBS3
(A) Induction test of PBS3 with two IPTG concentrations 0.1 mM and 0.5 mM, bacteria cultures were grown ON at 16°C. PBS3 protein was purified using a nickel column following a desalting column. Protein concentration was measured using a Bradford assay with bovine serum albumin as standard protein. M: marker, UI: uninduced, S: supernatant, H: His-tag, P: pooled, D: desalting

Confirmation of published PBS3 *in vitro* substrates

The three missing molecular species in *pbs3* mutant plants are putative PBS3 products, *in vitro* recombinant protein studies with the expressed PBS3 enzyme should prove this hypothesis. Therefore, we tested PBS3 amino transferase activity on 21 potential substrate combinations, including combinations of BAs with AA and small carboxylic acids (sCA) with AA (Table S2). We could confirm the PBS3 *in vitro* activity, which was previously described by Okrent et al. 2009, on the known substrates 4-hydroxybenzoic acid with Glu forming 4-HBA-Glu, on 4-hydroxybenzoic acid with Met forming 4-HBA-Met and on *para*-aminobenzoic acid with glutamate forming *p*-ABA-Glu (Figure 2.2.2). Through GC-MS analysis, we were able to confirm the conjugations as *in vitro* products.

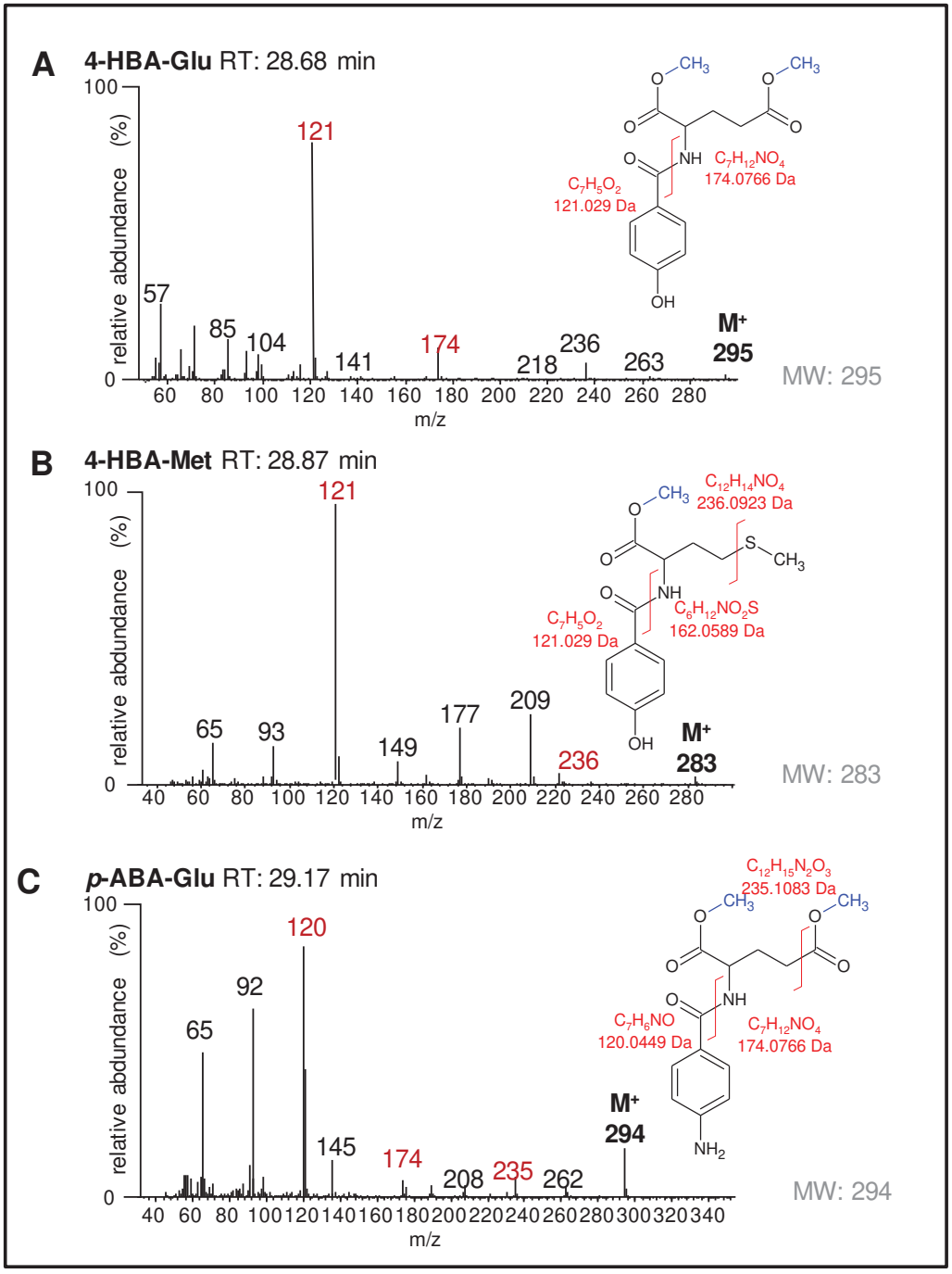

Figure 2.2.2: PBS3 *in°vitro* conjugates 4-substituted benzoic acids to amino acids
The purified PBS3 enzyme was active and conjugated 4-HBA with Glu (A) and 4-HBA with Met (B). Furthermore, PBS3 conjugated 4-*p*ABA with Glu (C). Protein assays have been methylated with trimethylsilyl diazomethane before GC-MS analysis. Introduced methyl groups are indicated in blue. The molecular structures of the resulting PBS3 product are shown. Consisting molecular fragmentation with MS ion fragmentation is indicated in red. The M^+ is bolded and consisting to the corresponding MW of the product structure.

PBS3 accepts small carboxy acids as *in vitro* substrates

On our quest for PBS3 substrates, we confirmed four previously unknown PBS3 *in vitro* substrate combinations between small carboxy acids (sCA) and AA. PBS3 conjugated glutaric acid with glycine or alanine and succinate with alanine or valine (Table S2). GC-MS analysis showed that the molecular fragmentation of all metabolic products was consistent with the ion fragmentation pattern of main ions. For glutaric acid-glycine m/z 59, m/z 129, m/z 101, m/z 158, m/z 185. The RT of the product was at 19.95 min (Figure 4.2.3 A). Glutaric acid-alanine shared the main ion fragments m/z 59, m/z 87, m/z 101, m/z 129 with glutaric acid glycine, also the other ions m/z 145, m/z 172, m/z 200, m/z 217 were consistent with the molecular fragmentation. The RT of the product was at 19.68 min (Figure 4.2.3 B). The main ion fragment for succinate was m/z 115, represented in succinate-alanine and succinate-valine. In both products the molecular fragmentation was consistent with the ion fragmentation pattern, which consisted for succinate-alanine of main ions m/z 59, m/z 87, m/z 115, m/z 158, m/z 186. Moreover, the M^+ of m/z 217 is consistent with the MW of 217 Da. The RT of the product was at 18.15 min (Figure 4.2.3 C). For succinate-valine the ion fragmentation pattern included the main ions m/z 59, m/z 115, m/z 186, m/z 214. Further, the M^+ of m/z 245 is consistent with the MW of 245 Da. The GC-MS RT of the product was at 19.85 min (Figure 4.2.3 D). These finding broadens the substrate acceptance of PBS3 to small caroxylic acids. However, these newly identified PBS3 products glutaric acid-Glu, glutaric acid-Ala, succinate-Ala and succinate-Val, were only detected *in vitro* and have yet not been determined *in planta*.

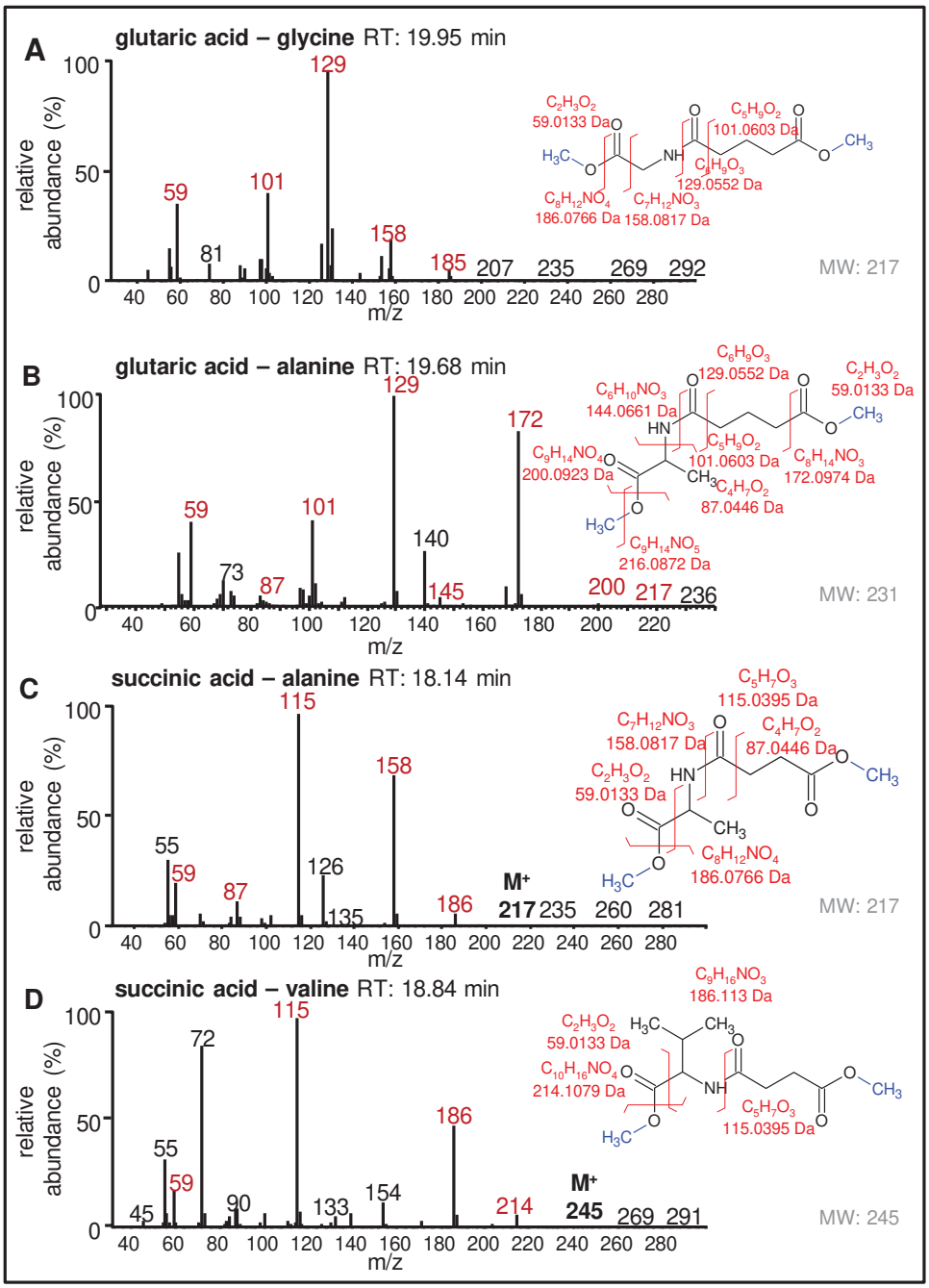

Figure 2.2.3: PBS3 *in°vitro* conjugates carboxy acids to amino acids
GC-MS mass spectrum of new PBS3 *in vitro* conjugations between sCA and AA: (A) glutaric acid with glycine (B) glutaric acid with alanine (C) succinate with alanine (D) succinate with valine. Consistent molecular- and ion fragmentation is indicated in red. Protein assays have been methylated with trimethylsilyl diazomethane before GC-MS analysis. Introduced methyl groups are indicated in blue.

PBS3 forms *N*-pyr-Glu *in vitro*

The activity of PBS3 as a conjugase of sCA to AA and the lack of the molecular species *N*-pyr Glu and IC-Glu in *pbs3* knockout mutants, strengthen the hypothesis that both metabolites are PBS3-dependent. Comparing the EIC and the mass spectrum of *N*-pyr-Glu from *A. thaliana* plant extracts depict similarities to EIC and the mass spectrum gained through *in vitro* analysis of PBS3 protein with pyruvic acid (Pyr) and Glu (Figure 2.2.4 A-B and C-D). Through the *in vitro* assay gained amounts of m/z 142 share the RT at 18.78 min with pathogen induced *N*-pyr-Glu (Figure 2.2.4 A, C). *N*-pyr-Glu from *A. thaliana* plant extracts has the same characteristic main ion at a RT of 18.78 min (Figure 2.2.4 B, C). Moreover, further characteristic ions m/z: 202, 174 and 110 were identified in both spectra. The metabolite was missing in the *in vitro* control sample without substrates (Figure C). We concluded that PBS3 conjugates Pyr and Glu to the newly identified molecular species *N*-pyr-Glu. To strength the hypothesis that *N*-pyr-Glu is a product of PBS3, we co-incubated *pbs3* plant material with the PBS3 enzyme, to examine if the added enzyme can rescue the *N*-pyr-Glu loss in pbs3 mutant plants. For the *in vitro* co-incubation assay with crude *pbs3* plant material, *pbs3* leaf material was incubated with purified PBS3 enzyme and pyridoxal phosphate (PLP) as a co-factor. Using GC-MS, small amounts of *N*-pyr-Glu main ion fragment m/z 142 were detected at the same RT as in Col-0 *Psm vir* plant extract and samples *in vitro* assays at 18.78 min in the crude *pbs3* plant extract incubated with PLP and PBS3 (Figure 2.2.4 E). This molecule was not detectable in control samples of incubated plant extract without PBS3 protein. A closer look at the mass spectrum of the sample, bears further consistent ion fragments with *N*-pyr-Glu from *in vitro* synthesis and *Psm vir* infected Col-0 plant extract (Figure 2.2.4 B, D, F). The PBS3 biosynthesis of *N*-pyr-Glu and the establishment of *N*-pyr-Glu in *pbs3* mutant plant after PBS3 addition, supports the hypothesis that *N*-pyr-Glu is directly PBS3-dependent.

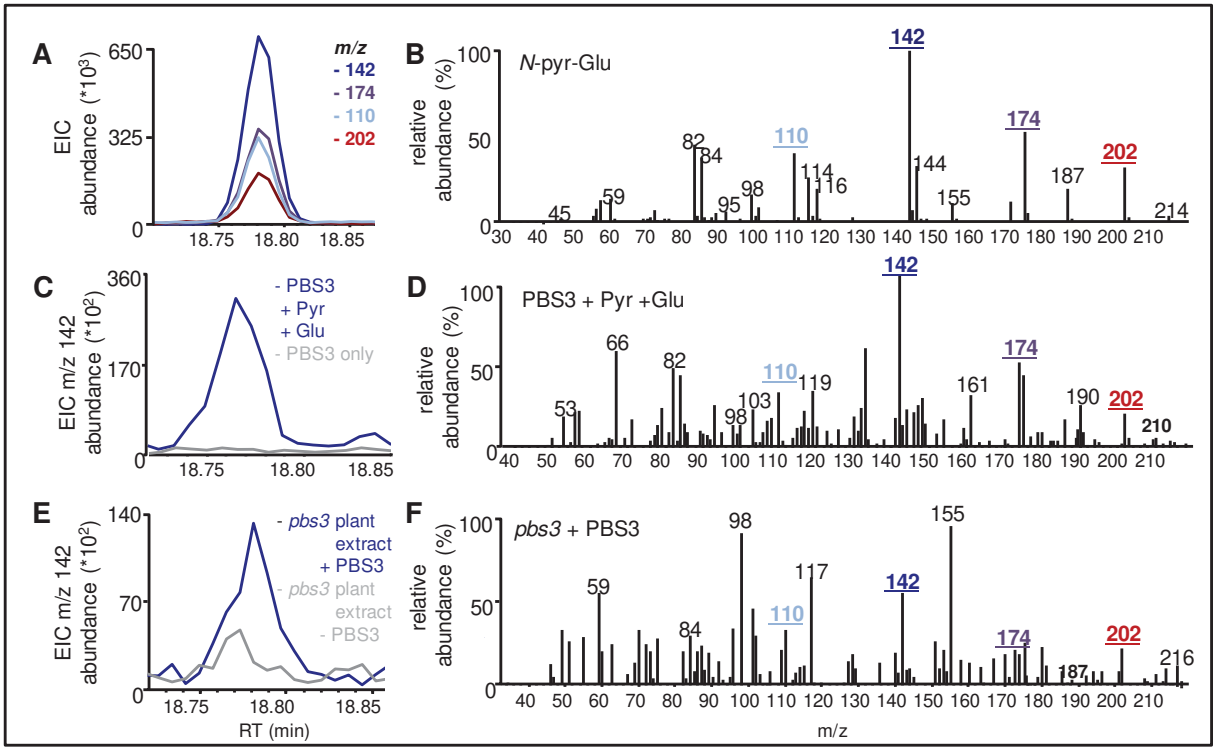

Figure 2.2 4: PBS3 *in vitro* synthesis of *N*-pyr-Glu through pyruvic acid and Glu
(A) EIC of *N*-pyr-Glu consists of the main ion fragments at a RT of 18.78 min extracted from *Psm vir* infected wild-type *A. thaliana* Col-0 plant. (B) Corresponding mass spectra of *N*-pyr-Glu. (C) ECI of *in vitro* incubation of active PBS3 enzyme with Pyr and Glu, led to an accumulation of m/z 142 at the same RT as *N*-pyr-Glu (blue line), enzyme control showed no peak (gray line). (D) Corresponding mass spectrum of the *in vitro* incubation has a consisting ion fragmentation pattern with *N*-pyr-Glu (B). (E) Co-incubation
of active PBS3 enzyme with crude *pbs3* mutant plant extract, EIC depicts an accumulation of m/z 142 at the same RT as *N*-pyr-Glu in *Psm vir* infected Col-0 plants (A). (F) The corresponding mass spectrum of the crude *pbs3* plant material + PBS3 enzyme shares an ion fragmentation pattern with *N*-pyr-Glu in (B). Correlating ion fragments are indicated in similar colors.

2.2.2 Subcellular localization of PBS3

The subcellular localization of the PBS3 enzyme should help to solve PBS3 involvement with other key enzymes in plant resistance. ICS1, for example, has been localized to the plastid of plant cells [41]. With LOCALIZER 1.0 (CSIRO), an online tool to predict subcellular localization of plant and effector proteins in the plant cell, PBS3 could not be assigned to a specific cell compartment (https://suba.live/factsheet.html?id=AT5G13320.1[113]).

To gain further information about PBS3 we analyzed the subcellular localization using fluorescence microscopy (Figure 2.2.5). Therefore, an expression vector for a full-length PBS3-CFP (Cyan Fluorescent Protein) fusion protein under the control of an 35S promoter of cauliflower mosaic virus (CaMV) was constructed using the GATEWAY® cloning system.

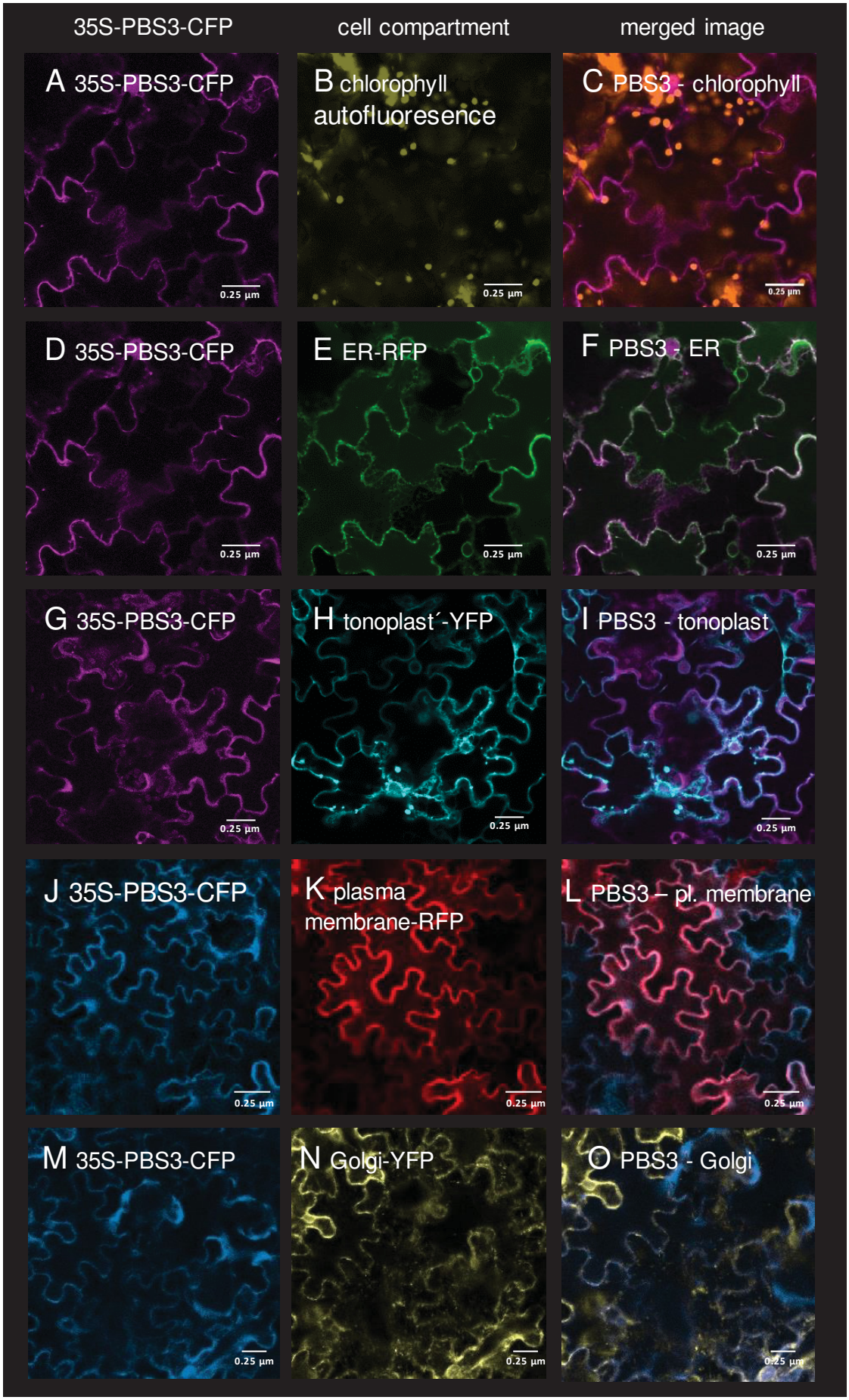

Figure 2.2.5: PBS3 could not be co-localized through transient expression in *N. tabacum*

Transient subcellular localization of PBS3 in *N. tabacum*. 35S-PBS3-CFP and cell compartment specific proteins fused to fluorescence proteins, were transformed into *A. tumefaciens* and co-inoculated into *N. tabacum* leaves. Fluorescence was observed by a confocal laser scanning microscope. A, D, G, J, M: 35S-PBS3-CFP, B: chlorophyll autofluorescence, E: ER-RFP, H: tonoplast-YFP, K: plasma membrane-RFP, N: Golgi-YFP.

Agrobacterium tumefaciens GV3101 carrying the 35S-PBS3-CFP expression vector was infiltrated into *N. tabacum* leaves for transformation. Moreover, *A. tumefaciens* GV3101 carrying one of the expression vectors for marker proteins of the endoplasmic reticulum (ER), tonoplast, plasma membrane or Golgi apparatus was infiltrated into the same leaves for transformation for co-localization studies. All cellular localization markers werer fused eigher Red (RFP) or Yellow Fluorescent Protein (YFP). After two days of incubation, epidermis cells of the transformed *N. tabacum* leaves were analyzed with an Olympus FlouView-1000 confocal fluorescence microscope (Figure 2.2.5). So far it seems like PBS3 is localized in the cytosol, because it did not co-localize with the autofluorescence of chlorophyll in chloroplasts , ER-RFP, tonoplast-YFP, plasma membrane-RFP or Golgi apparatus-YFP markers.

2.2.3 Summarized results of PBS3 in plant immunity

Taken the gained results together, we could show new *in vitro* conjugations of PBS3. PBS3 was active on 4-substituted BAs to AA, here we could confirm the findings as described in Okrent et al. 2009 that PBS3 conjugates 4-*p*ABA with Glu, as well as 4-HBA with Glu and Met. Moreover, we could show, that PBS3 conjugates also sCA to AA. *In vitro* we found four combinations glutaric acid to Gly and glutaric acid to Ala as well as succinate to Ala and succinate to Val. These newly identified, broadens the substance acceptance of PBS3. However, none of the four metabolites has been verified *in planta* yet. Through PBS3 *in vitro* assays we received small amounts of *N*-pyr-Glu. Co-incubation studies with the purified PBS3 protein added to crude *pbs3* leaf extracts was another approach to regain *N*-pyr-Glu. Further, we could narrow down the putative localization of PBS3 to the cytosol. The results of this PBS3 gained in this study, strenghten the role pivotal role of PBS3 in the plant immune system and correlate with major resaerch concernig the enzyme.

2.3 The influence of NHP and Pip on the transgenic SA-hydroxylase line *NahG* in plant immunity

NHP is the hydroxylated form of the non-proteinogenic amino acid Pip and is a critical element in plant systemic immunity [3]. Exogenous application of the three key defense metabolites SA, NHP and Pip, enhances resistance against bacterial pathogens in *A. thaliana* wild-type plants [3,5]. Transgenic *A. thaliana NahG* were established to study the influence of SA on plant immunity. Therefore, the bacterial salicylate hydroxylase NAHG was introduced to the plant genome to degrade SA to catechol [102]. *NahG* plants are known to be defective in non-host pathogen interaction and the absence of SA. However, the enhanced susceptibility of *NahG* plants against bacteria is most likely a result of the accumulation of catechol and not solely the loss of SA [103]. Whether the hydroxylase is capable of degradation a broader range of metabolites is still unknown. In this following chapter, we examined the effect of exogenously applied SA, NHP and Pip on plant resistance of transgenic *A. thaliana NahG* and analyzed the cellular levels of known defense-related metabolites after pathogen treatment.

2.3.1 Influence of SA, NHP and Pip to the bacterial resistance of *NahG*

To examine the influence of exogenously applied defense metabolites SA, NHP and Pip induced resistance assays with *A. thaliana* wild-type Col-0, SA deficient mutant *sid2* and transient salicylate hydroxylase line *NahG* were carried out (Figure 2.3.1). For induced resistance assays plant leaves were infiltrated with the bioluminescent *Psm lux* strain and bacterial growth was analyzed by measuring the bioluminescence 60 hpi. To investigate the effect of exogenous applied SA on bacterial growth, leaves of the *A. thaliana* lines were pre-infiltrated with 0.5 mM SA four hours before infection with *Psm lux* (OD_{600}= 0.001). As already known the SA deficient mutant plants *sid2* and *NahG* were significantly more susceptible to the bacterial pathogen *Psm lux* (Figure 2.3.1 A). Here, the immunity of *NahG* plants was even significantly weaker compared to *sid2* plants. SA pretreatment induces resistance in Col-0 wild-type and in *sid2*, whereas *NahG* plants showed no inhibition of the bacterial growth. NHP and Pip were exogenously applied to the soil of *A. thaliana* (10 mL 1 mM) one day before induced resistance assays were carried out. For *A. thaliana* Col-0 a significant reduction in bacterial growth was observed after application of NHP or Pip, whereby NHP increases the resistance even stronger. In *sid2* as well as in *NahG* plants, the exogenous application of NHP and Pip leads to a slightly decreased bacterial growth, however it was not

significant in both mutant plants (Figure 2.3.1 B). A significant negative effect on bacterial growth after NHP and Pip application to *sid2* plants was previously described [3].

Since the application of NHP leads to a strong increasement of resistance in wild-type plants, but does not affect *sid2* and *NahG* plants, a more detailed influence of NHP was examined. Therefore, we analyzed the influence of pre-infiltrated NHP on bacterial growth in local and systemic leaves of Col-0, *sid2* and *NahG* plants. Here, local leaves were infiltrated with 1 mM NHP or water and one day later we infected either the pre-infiltrated local leaves or untreated systemic leaves with *Psm lux* (OD_{600}= 0.001). The bacterial growth was measured 60 hpi. The mechanical wounding, induced by pre-infiltration of water before bacterial infection in local leaves, lead to a reduction of the bacterial growth in Col-0. Pretreatment of NHP had a significant reduction of locally and systemically infiltrated *Psm lux* as compared to systemic leaves of water treated Col-0. No significant difference was observed compared to local leaves; however, the tendency of bacterial growth reduction is stronger after NHP pretreatment.

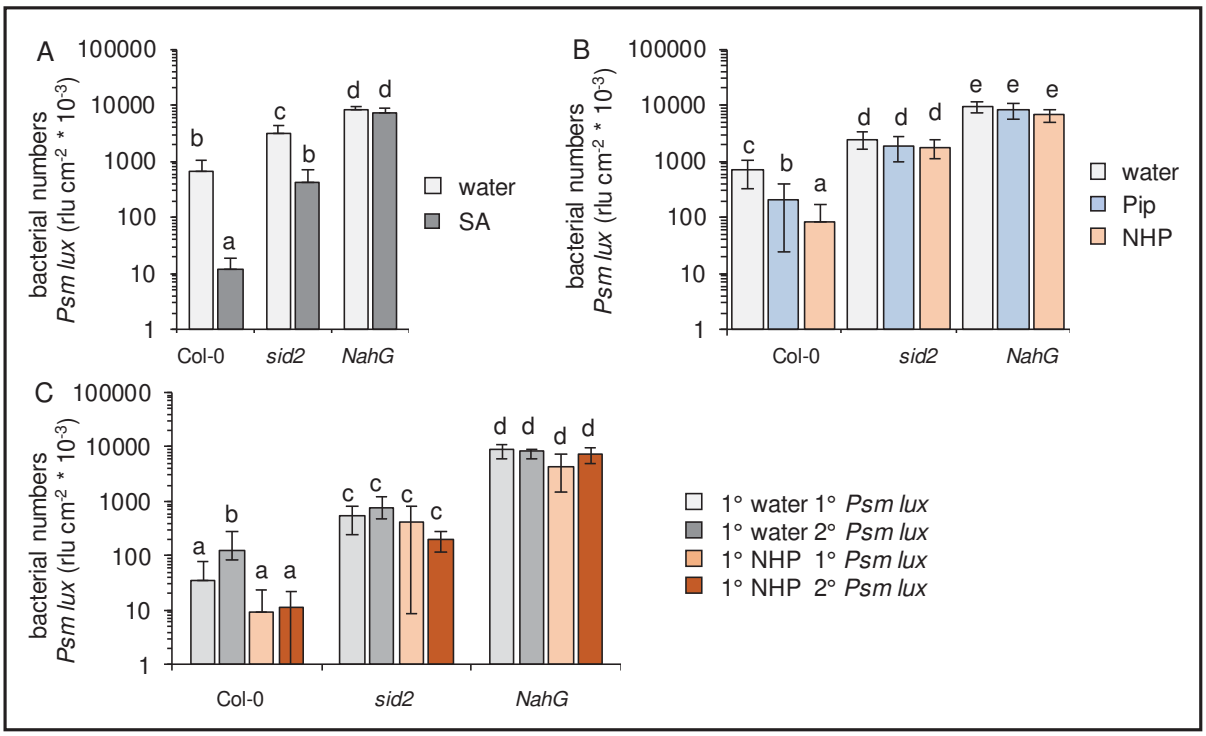

Figure 2.3.1: Exogenously applied SA, NHP and Pip did not lead to an increased resistance in *NahG*

(A) 0,5 mM SA were applied through leaf infiltration, 4 hours after first infiltration same leaves were infected with *Psm lux*. (B) 10 mL of 1 mM NHP and Pip or water as control were exogenously applied to the soil one day before *Psm lux* infection. (C) To examine the influence of NHP more detailed on Col-0, *sid2* and *NahG*, plants were pre-infiltrated with water or 1 mM NHP on local leaves (1°). One day later local and systemic (2°) leaves were infected with *Psm lux*. For A, B, C Bacterial numbers were defined 60 hpi with the bioluminescent virulent *Psm lux* strain and expressed as rlu per cm^2 leaf area. Plants were treated with SA, NHP and Pip one day before infection with virulent *Psm lux* strain (OD_{600}= 0.001). The y-axes have a log_{10} scaling.

The bacterial growth in *sid2* and *NahG* plants was not significantly affected by pre-infiltration of NHP or water. However, we observed a decreased bacterial growth especially in *sid2* plants. In conclusion, these results underline the important role of SA, NHP and Pip to enhance resistance against bacterial pathogens in *A. thaliana*. In SA deficient *sid2* mutants, resistance can be recovered by exogenously applied SA. It is not possible to rescue the salicylate hydroxylase line *NahG* through SA pretreatment, most likely due to its rapid degradation to catechol. The exogenous application of NHP and Pip results in a slight, but not significant decreased bacterial growth in *sid2* and *NahG* plants.

2.3.2 Accumulation of SA and NHP related metabolites in *NahG* plants

Based on the influence of exogenously applied SA, NHP and Pip to *sid2* and *NahG* plants, we were interested in the cellular levels of SA and its glycosylated forms SGE and SAG, NHP and Pip in *NahG* plants after pathogen treatment. Therefore, metabolites of *A. thaliana* Col-0 and *NahG* leaf samples were analyzed 12, 24 and 48 hpi with *Psm vir* (OD_{600}= 0.005) by GC-MS. The key defense metabolite SA, SEG and SAG showed a time-dependent accumulating in *A. thaliana* wild-type Col-0 after *Psm vir* infection (Figure 2.3.2). Compared to uninfected plants all three metabolites were significantly increased 12, 24 and 48 hpi. SA and SGE reached their climax 24 hpi with 2.6 µg*g FW^{-1} for SA and 10 µg*g FW^{-1} for SGE, respectively. After two days, cellular amounts of SA and SGE decreased (SA: 1.0 µg*g FW^{-1}, SGE: 3.5 µg*g FW^{-1}). In contrast, SAG steadily increased over time from 20 µg*g FW^{-1} at 24 hpi to approximately 70 µg*g FW^{-1} at 48 hpi. Compared to Col-0, the transgenic *NahG* line, which degrades SA to catechol, showed no significant accumulation of SA-compounds after bacterial treatment at any time point. The values of *NahG* concur to Col-0 mock treated leaf samples and are about 10-fold lower compared to Col-0 24 hpi (0.24 µg*g FW^{-1}/ 2.58 µg*g FW^{-1}). The SA glycosides SGE and SAG were not detectable in *NahG* plants at any timepoint, indicating a degradation of free SA to catechol before SA is converted to its glycosylated forms. The results are in line with previous studies which reported a lack of SA in *A. thaliana NahG* plants [67].

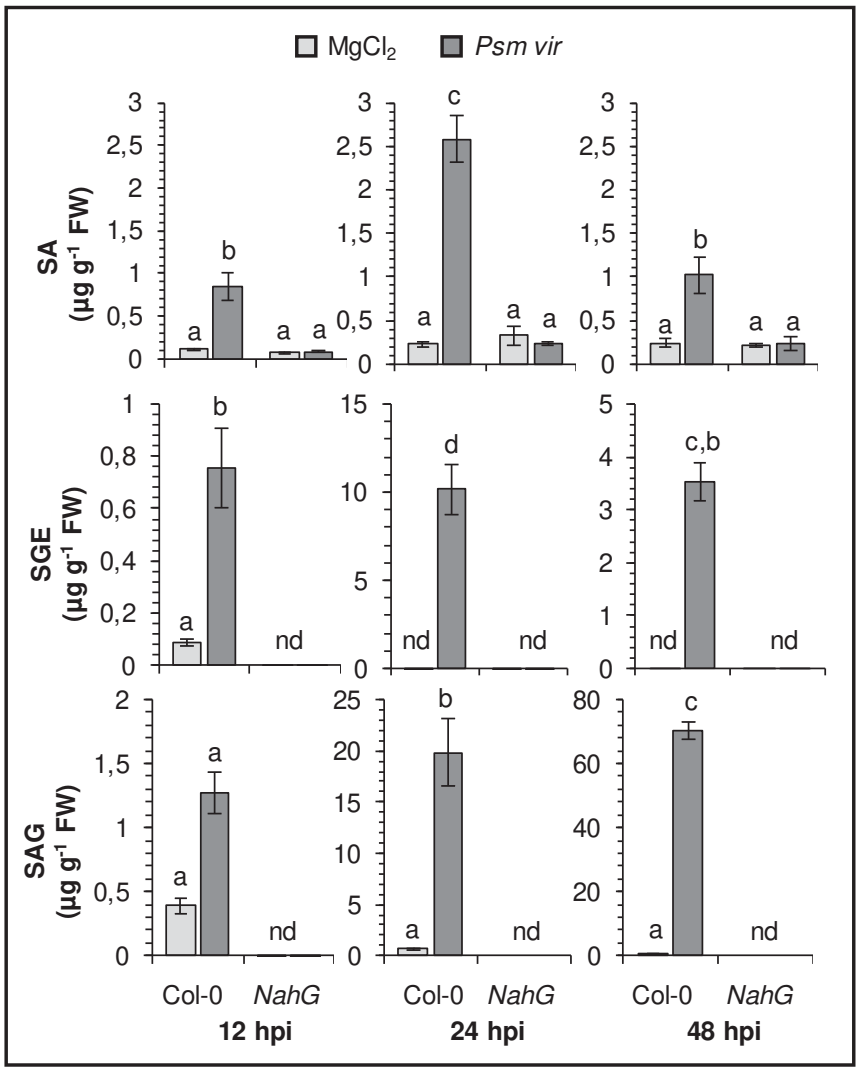

Figure 2.3.2: *NahG* shows no accumulation of key defense metabolites SA, SAG and SGE
The time course analysis shows the accumulation of SA, SAG and SGE after *Psm vir* infection in Col-0 and transgenic *NahG* plants (OD_{600}= 0.005). Infiltration with 10 mM $MgCl_2$ served as mock control. Leaf samples were harvested 12, 24 and 48 hpi and extracted via TMS method. Samples have been silylated for derivatization. Not analyzable traces of metabolites were declared as not detected (nd).

The defense-related metabolite NHP and its precursor Pip as well as the glycosylated form NHPGE accumulate significantly in *A. thaliana* wild-type after *Psm vir* infection (Figure 2.3.3). The non-proteinogenic amino acid Pip increased after pathogen infection over time (12 hpi: 0.95 µg*g FW^{-1}, 24 hpi: 25 µg*g FW^{-1}, 48 hpi: 129 µg*g FW^{-1}). The accumulation of Pip derived NHP and its glycosyl NHPGE is delayed and both metabolites were not detectable after 12 hpi in Col-0 and *NahG* plants. The amount of NHP and NHPGE increased form 24 hpi (NHP: 10 µg*g FW^{-1}, NHP-hexose: 2.1 µg*g FW^{-1}) to 48 hpi (NHP: 20 µg*g FW^{-1}, NHP-hexose: 22 µg*g FW^{-1}) in Col-0 wild-type. NHPGE only accumulated after *Psm vir* infected leaf tissue and was not detectable in mock samples. Interestingly, in *Psm vir* infected plants carrying the salicylate hydroxylase *NahG*, the accumulation of all three

metabolites Pip, NHP and NHPGE is drastically reduced compared to infected wild-type plants (Figure 2.3.2). The amounts of detected Pip in *Psm vir* infected *NahG* plants were significantly lower compared to wild-type plants. The difference of Pip in *NahG* compared to Col-0 reached form a µg*g FW^{-1}) after 12 , to eight-folds (3.04 µg*g FW^{-1}) after 24 hpi and to 13-folds (9.87 µg*g FW^{-1}) after 48 hpi. Like in Col-0, NHP and NHPGE could not be detected 12 hpi in *NahG* plants. Further, the accumulation of NHP is reduced in *NahG* plants compared to Col-0 after bacterial infection. Here, *NahG* 24 hpi samples contained 11 times less NHP (0.99 µg*g FW^{-1}) and in samples after 48 hpi the amount of NHP was six-fold (3.16 µg*g FW^{-1}) reduced compared to Col-0. Moreover, the amounts of NHPGE were four times lower in *NahG* plants compared to Col-0 (24 hpi: 0.5 µg*g FW^{-1}, 48 hpi: 5.47 µg*g FW^{-1}).

In conclusion, we could show that *NahG* plants lack the accumulation of SA after pathogen treatment as previously described. Moreover, the SA glycosides SAG and SGE, were not found in *NahG* at all, most-likely because of the constant SA degradation to catechol. Strikingly, *NahG* plants contain significant lower amounts (up to 13 times) of the defense-related metabolites NHP, NHPGE and Pip, compared to similar treated wild-type plants, indicating a deeper influence of *NahG* on plant metabolic immune response. It its worth mentioning at this point that the lack of NHP, NHPGE and Pip cannot simply be explained by the degradation of SA in *NahG* since *sid2* mutants, which cannot accumulate SA after pathogen treatment, still accumulates Pip and NHP [3,5].

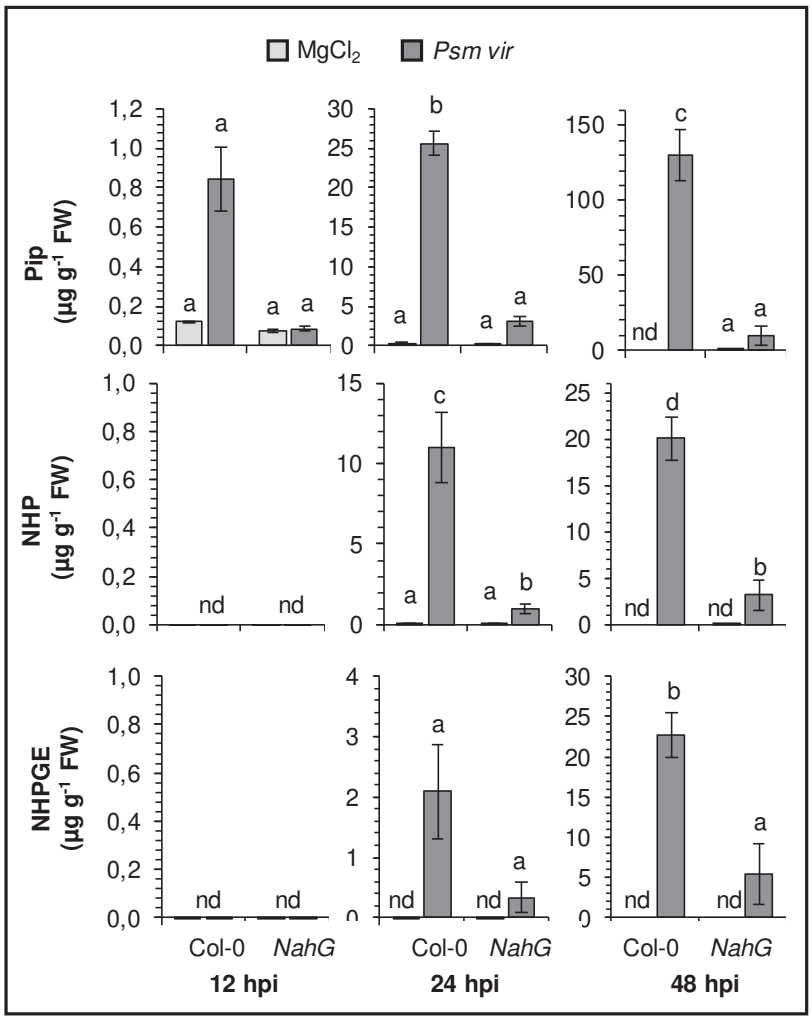

Figure 2.3.3: *NahG* shows a reduced accumulation of key defense metabolites Pip, NHP and NHP-hexose
The time course analysis shows the absent accumulation of molecular species after virulent Psm vir (OD_{600}= 0.005) infection in transgenic NahG plants. Infiltration with 10 mM MgCl2 served as mock control. Leaf samples were harvested 12-, 24- and 48-hpi and extracted via TMS method. Samples have been silylated for derivatization. No analyzable traces of metabolites were declared as not detected (nd).

To studie a deeper influence of NAHG on the Pip-pathway, we analyzed cellular Pip levels of Pip pretreated *A. thaliana* Col-0 and *NahG* plants and pathogen treatment (Figure 2.3.4). Therefore, 10 mL 1 mM Pip was applied to the soil. All plants were infected one day after Pip application with *Psm vir* or 10 mM $MgCl_2$ and were harvested 48 hpi and analyzed by GC-MS. In wild-type plants, we could observe a significant Pip increase after Pip application from 2 µg*g FW^{-1} in water treated mock plants compared to16 µg*g FW^{-1} in Pip treated mock plants. The inoculation with *Psm vir* lead to significant high rise of Pip in pretreated and mock treated Col-0 plants to 138 µg*g FW^{-1} in water treated *Psm vir* plants and to 108 µg*g FW^{-1} in infected plants previously treated with Pip. Interestingly, we observed, that *A. thaliana NahG* still accumulates Pip as wild-type Col-0, however, cellular amounts were drastically reduced indicating a direct influence of *NahG* on cellular Pip levels. In *NahG* control plants only traces

of Pip were detectable (0.2 µg*g FW^{-1}), Pip treated *NahG* mock plants accumulated only as much Pip as detected in Col-0 mock control (2.8 µg*g FW^{-1}). Metabolic analysis of inoculated *NahG* plants showed only a very low accumulation of Pip, which were comparable to Pip treated mock Col-0 plants. Here, exogenously applied Pip inclined a towards more Pip in *NahG* from 14 µg*g FW^{-1} after *Psm vir* infection, to 23 µg*g FW^{-1} in plants previously treated with Pip before infection. If Pip nor NHP, does not induce resistance in *NahG*, and Pip is not accumulating in Pip treated plants, the question is what happens in *NahG* to Pip and its derivate NHP. A second question is, are further metabolic pathway influenced by the introduction of the SA-hydroxylase NAHG. Therefore, further investigations on a metabolic level should help answering these questions.

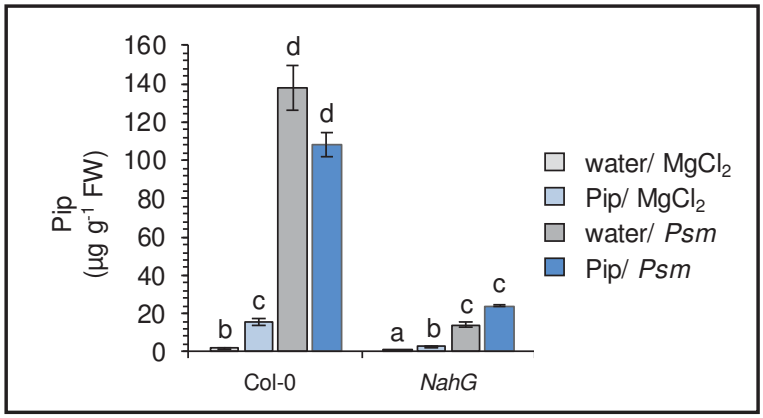

Figure 2.3.4: Pip is drastically reduced in Pip treated *NahG* plants
Col-0 and *NahG* plants were pretreated with 10 mL 1 mM Pip to the soil. One day later inoculated with *Psm vir* (OD_{600}= 0.005) or 10 mM $MgCl_2$. Samples were extracted via EZ:faast amino acid extraction kit and analyzed via GC-MS. Different letters denote significant differences ($p < 0.05$, ANOVA and post hoc Tukey HSD test).

2.3.3 Further metabolic deviations in *NahG*

To understand the influence of the introduced salicylate hydroxylase *NahG* to the metabolic composition of *A. thaliana* immune system, we quantified further defense-related metabolites in *NahG* that differed from wild-type plants 48 hpi (Figure 2.3.5). Heck et al. already observed in 2003 that *NahG* influences more defense pathways independent of SA. Here, they described enhanced JA levels in *NahG* plants. In this study we could confirm these findings. JA was four times more abundant in *NahG* compared to Col-0 (0.43 µg*g FW^{-1}/ 0.11 µg*g FW^{-1}/). We also discovered highly enhanced levels of the JA precourser OPDA in *NahG*. OPDA was 13 times higher in *NahG* compared to Col-0 (0.82 µg*g FW^{-1}/ 0.06 µg*g FW^{-1}).

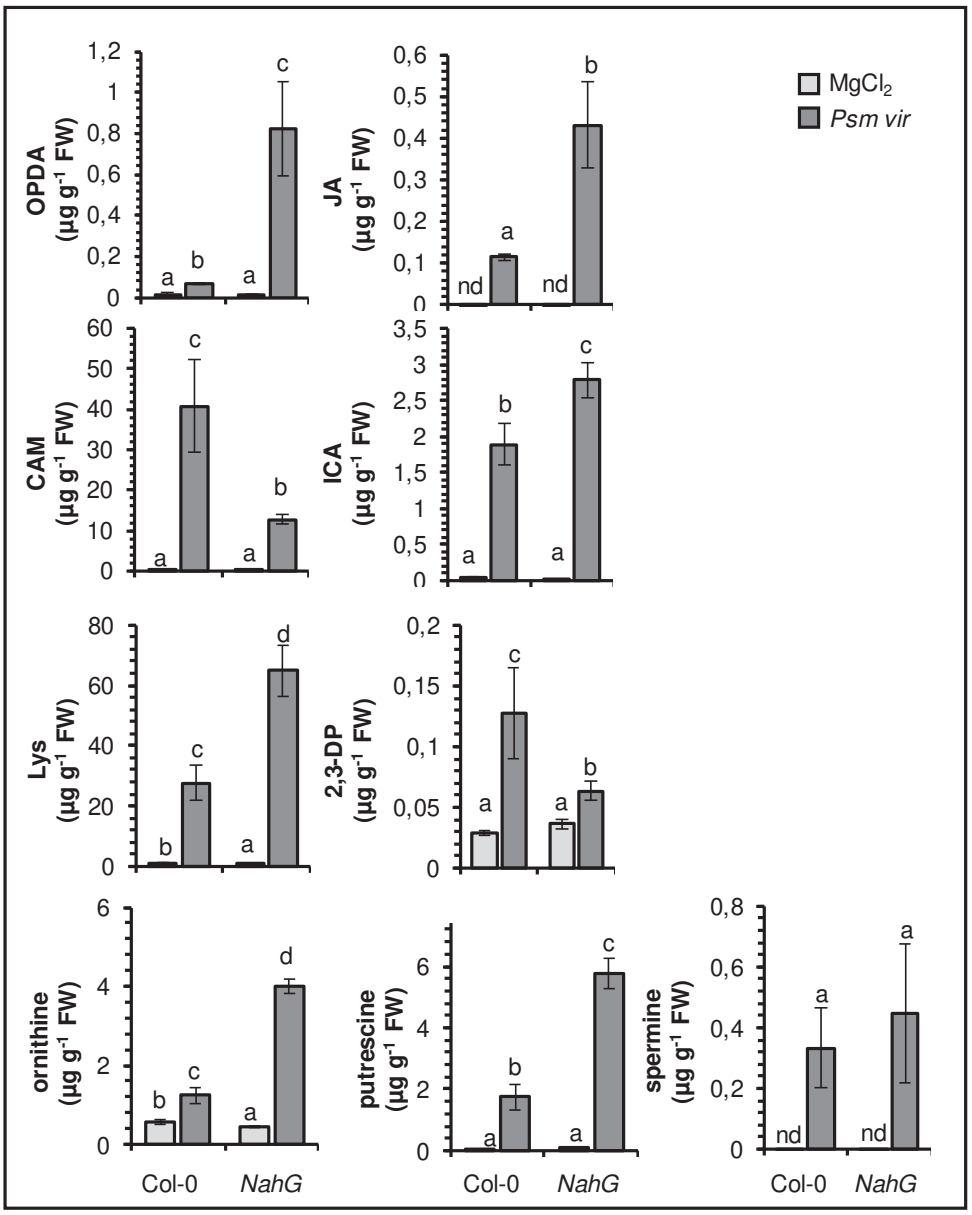

Figure 2.3.5: Metabolic deviations of *NahG*
Endogenous levels of metabolites in *NahG* compared to the wild-type Col-0, 48 hpi *Psm vir* infection, mock plants were infiltrated with 10 mM $MgCl_2$ as control. Samples haven been extracted via VPE and were methylated for derivatization. Lys, putrescine, ornithine and spermine were extracted through EZ:faast (Phenomenex). Different letters denote significant differences ($p < 0.05$).

Further the authors described, that *NahG* is lacking a strong accumulation of the indole CAM after pathogen treatment, which is also consistent with our findings. Accumulation of CAM is three times weaker in *NahG* compared to Col-0 (12.77 µg*g FW^{-1}/ 40.74 µg*g FW^{-1}). On the other hand, the amount of ICA after *Psm vir* treatment was slightly, but significantly higher in *NahG* compared to Col-0 (2.05 µg*g FW^{-1}/ 1.89 µg*g FW^{-1}). L-Lys, as precursor of NHP and Pip, is significantly over twice as much abundant in *NahG* as in Col-0 (64.83 µg*g FW^{-1}/ 27.56 µg*g FW^{-1}). In contrast, the intermediate 2,3-DP (m/z 141), which is catalyzed by the aminotransferase ALD1 from L-Lys, is half as much abundant in *NahG* compared to Col-0 (0.06 µg*g FW^{-1}/ 0.12 µg*g FW^{-1}). *NahG* also seems to have an influence on the polyamides in plants. Here a significant enhancement by three times in *NahG* compared to Col-0 was noticed in putrescine (5.75 µg*g FW^{-1}/ 1.75 µg*g FW^{-1}) and ornithine (4.0 µg*g FW^{-1}/ 1.25 µg*g FW^{-1}). The polyamide spermine did not differ in *NahG* to Col-0.

2.3.4 Summarized results of *NahG* in plant immunity

Investigating salicylate hydroxylase *NahG* regarding its role in plant immunity, we could uncover that NAHG influences more defense pathways than just the degradation of SA to catechol. We found out, that critical defense metabolites SA, NHP and Pip do not have an influence on plant immunity in *NahG* plants. Metabolic analysis of *NahG* displayed a highly reduced accumulation of free SA in *NahG* plants, the SA glycoside conjugations SAG and SGE were not detectable in *NahG*. The measured amounts of NHP, Pip and NHPGE were drastically reduced in *NahG* compared to *A. thaliana* wild-type Col-0. In contrast, Lys as a precursor of Pip is enhanced in *NahG*, were as 2,3-DP is reduced. The introduction of *NahG* to *A. thaliana* lead also to further metabolic deviations. For example, JA and its precursor OPDA were upregulated as well as the polyamines ornithine, putrescine and spermine. Indoles, like CAM and ICA were as well influenced by *NahG*.

3 Discussion

After an infection, a plant reacts on a metabolic level with the accumulation of defense metabolites to combat the pathogen and build up immunity to protect uninfected tissue against further pathogen attacks. Known crucial immune relevant metabolites are SA, NHP, and Pip, but there are still open gabs in the metabolic plant defense network. Through comparative gas chromatographic studies using GC-MS and GC-FTIR analysis, nine previously unknown metabolites in infected leaf tissue of SA-related mutant plants were identified, playing a potential role in plant defense pathways. The following chapter 3.1 will discuss a putative integration of these molecular species into metabolic plant defense pathways. Three of the newly identified molecular species are, besides ICS1-, also PBS3-dependent and accumulate after pathogen infection. This interesting aspect is another important point of discussion. In addition, the central role of PBS3 is controversially discussed in plant defense. In chapter 3.2 PBS3 and its involvement in pathogen induced SA accumulation is one key aspect. Besides SA, NHP and Pip play a central role in plant defense. The transgenic mutant line *NahG*, carrying a bacterial hydroxylase which degrades SA to catechol, has been established to study the influence of SA in plant immunity. The results, however, show that the introduced enzyme has a more severe influence on the metabolic equilibrium, especially on the crucial defense regulators NHP and Pip. These aspects will be discussed in chapter 3.3.

3.1 Extension of the hitherto described IC-pathway by nine newly identified molecular species

In planta, a lot of functional and regulatory metabolites possess BA as basic carbon structures, derived from IC- or PAL-pathway [46]. The major plant hormone SA can be synthesized via both pathways, but it is known that after pathogen infection the shikimate derived IC-pathway is responsible for 90 % of newly formed SA [62]. This present thesis described nine new molecular species, which are all accumulating in pathogen infected wild-type leaf tissue. All these nine molecular species are missing in the SA deficient ICS1-mutant leading to the suggestion to be directly connected to the IC-pathway and/ or SA-biosynthesis. Most of the metabolites share structural similarities with SA and BA underlining their putative origin. The identification of the nine molecular species extends the hitherto described IC-pathway by:

3-formylbenzoic acid (3-FBA)	5-formylsalicylic acid (5-FSA)
3-carboxybenzoic acid (3-CaBA)	5-carboxysalicylic acid (5-CaSA)
3-(carboxymethyl)-benzoic acid (3-CaMeBA)	5-(carboxymethyl)-salicylic acid (5-CaMeSA)
isochorismoyl-glutamate (IC-Glu)	*N*-pyruvoyl-glutamate (*N*-pyr-Glu)

salicylic acid–malate (SA-Mal)

We could unambiguously prove the identity of 3-FBA, 5-FSA, 3-CaBA, 5-CaSA and 3-CaMeBA through commercially available authentic standard substances. Using GC-MS mass spectra combined with analytics of chemical groups due to GC-FTIR we could identify 5-CaMeSA. Latest research results described the conjugation of glutamate to isochorismate by PBS3 forming IC-Glu, which spontaneously decays to *N*-pyr-Glu and releases SA [47,51]. These new findings confirm our achieved results and the identity of IC-Glu and *N*-pyr-Glu as parts of the SA-biosynthesis pathway. Through chemical synthesis and isotope labeling with D_4-SA we could confirm SA-Mal as until yet unknown, newly identified SA derivate.

IC-Glu and *N*-pyr-Glu are directly PBS3 and ICS1-dependent

Since all identified molecular species are clearly ICS1-dependent, their origin has to be involved with the ICS1-pathway. Interestingly, all identified molecular species highly over-accumulate in *pbs3* mutant plants, except for IC-Glu, *N*-pyr-Glu and SA-Mal. The absence of these metabolites in *pbs3* mutants indicate a direct PBS3 dependency. Newest research results

further strengthen these findings. Two research groups recently reported independently on the crucial role of the PBS3 enzyme in the biosynthetic SA-pathway [47,51]. Here, both groups identified IC-Glu as intermediate product in SA-biosynthesis. PBS3 conjugates the amino acid glutamate directly to IC forming the unstable IC-Glu, which spontaneously and/ or with the help of EPS1, decomposes into *N*-pyr-Glu and SA. PBS3 accelerates the chemical decomposition from IC to SA (Figure 3.1.1).

Isoprephenic acid and 3-carboxyphenylpyruvate describe the missing link between novel molecular species and IC

Besides its role in SA biosynthesis, IC serves as a precursor for *m*-carboxy-substituted non-proteinogenic aromatic amino acids in plants [114–117]. Following this pathway, IC is converted to the intermediates isoprephenic acid and 3-carboxyphenyl-pyruvate [118,119]. Both intermediates exhibit strong structural resemblance to the remaining six newly identified molecular species. Isoprephenic acid contains a hydroxy group at the ortho position which is lost through a dehydration reaction step forming 3-carboxy-phenylpyruvate. The same pattern of the *o*-hydroxy group is retrieved in 5-CaMeSA, 5-CaSA and 5-FSA. However, the structurally related molecular species 3-CaMeBA, 3-CaBA and 3-FBA differentiate from the above by a nonexistent *o*-hydroxy group (Figure 3.1.1). Pathogen-related SA accumulation involves a rising IC level. An IC surplus could be degraded through isoprephenic acid and 3-carboxyphenyl-pyruvate explaining an increase of all six molecular species.

There are indications that the formation of isoprephenic acid from IC runs analogous to the enzymatic Claisen rearrangement of chorismic acid to IC performed by chorismate mutase, however, a further isochorismate mutase (ICM) has not been described in Arabidopsis yet [116]. The question if there is an isoprephenate dehydratase (IPDT) *in planta* or if the reaction forming 3-carboxyphenyl-pyruvate proceeds only non-enzymatically is pending to be answered. Nevertheless, it is known, that applied high heat of 60°C to 100°C enhances a non-enzymatic conversion of IC to isoprephenic acid and 3-carboxyphenylpyruvate [118,119].

A decarbonylation of both metabolites through an unknown reaction could catalyze isoprephenic acid to 5-CaMeSA and analogously 3-CaMeBA through the decarbonylation of 3-carboxy-phenylpyruvate (Figure 3.1.1). Here, the carbonyl groups are dissociated under the release of carbon monoxide. Enzymatic decarbonylations have been described *in planta* mainly in the fatty acid and lipid catabolism. In *A. thaliana* two aldehyde decorbonylases CER1 and CER3 (ECERIFERUM 1 and 3) play a role in the biosynthesis of epicuticular waxes [120,121]. It

remains to be determined, which enzyme in particular is responsible for catalyzing this specific reaction.

The next plausible reaction step from 5-CaMeSA to 5-CaSA, and analogously for 3-CaMeBA to 3-CaBA, involves a shortening of the carbon chain of the carboxylic acid group by one carbon. The Barbier-Wieland degradation describes a non-enzymatic reaction of cyclic compounds where higher-order aliphatic acids are degraded to the next lower homologs in four-step consecutive processes [122]. It seems plausible that the reaction is catalyzed enzymatically, however, a putative enzyme is still unknown.

Aldehydes 3-FBA and 5-FSA are oxidized to 3-CaBA and 5-CaSA *in planta*

All newly identified molecular species, except *N*-pyr-Glu, share a related chemical composition. Beyond these similarities we could bring 3-FBA, 3-CaBA, 5-FSA and 5-CaSA in closer context. We observed a strong accumulation of 3-CaBA and 5-CaSA after 3-FBA and 5-FSA infiltration in Col-0 plant leaves. This data indicates an oxidation of the aldehydes 3-FBA and 5-FSA to their corresponding acids 3-CaBA and 5-CaSA *in planta*. Four aldehyde oxidases have been described in *A. thaliana* so far, AAO1 to AAO4 (ARABIDOPSIS ALDEHYDE OXIDASE), which could be involved in this reaction [123–125]. AAOs are involved in the oxidation of a diversity of aldehydes including phytohormones like auxin (IAA) and abscisic acid (ABA). AAO1 has been described to be involved in the indole biosynthesis. Here, AAO1 is, *inter alia*, involved in the hormone regulation of auxin, where indole-3-acetaldehyde is oxidized to IAA. Further, AAO1 together with CYP71B6 catalyzes the formation of ICC and ICA derivates, which also accumulate upon pathogen infection in *A. thaliana* [104,126]. AAO2 forms dimers with AAO1 and AAO3 has been described to be involved in ABA biosynthesis [124,125]. AAO4 was reported to protect the plant form toxic aldehyde formation and has a high activity on oxidizing benzaldehyde derivates to their benzoic acid counterparts, including moderate conversion rates for vanillin, cinnamaldehyde and hydroxy benzaldehydes [127,128]. If one of these AAOs is responsible for the oxidation of FBA to CaBA needs to be determined. For this reaction, good candidates might be the pathogen induced AAO1 or the benzaldehyde oxidase AAO4. These AAOs could directly convert the aldehydes to the corresponding carboxylic acids, but potential intermediate reaction steps cannot be excluded. Therefore, further enzyme families like aldehyde dehydrogenases and certain members of the cytochrome P450 superfamily (CYPs) could also be involved in this kind of reaction. Data analysis of pathogen induced transcriptional profiles, like RNA-Seq and microarray data could provide upregulated candidates.

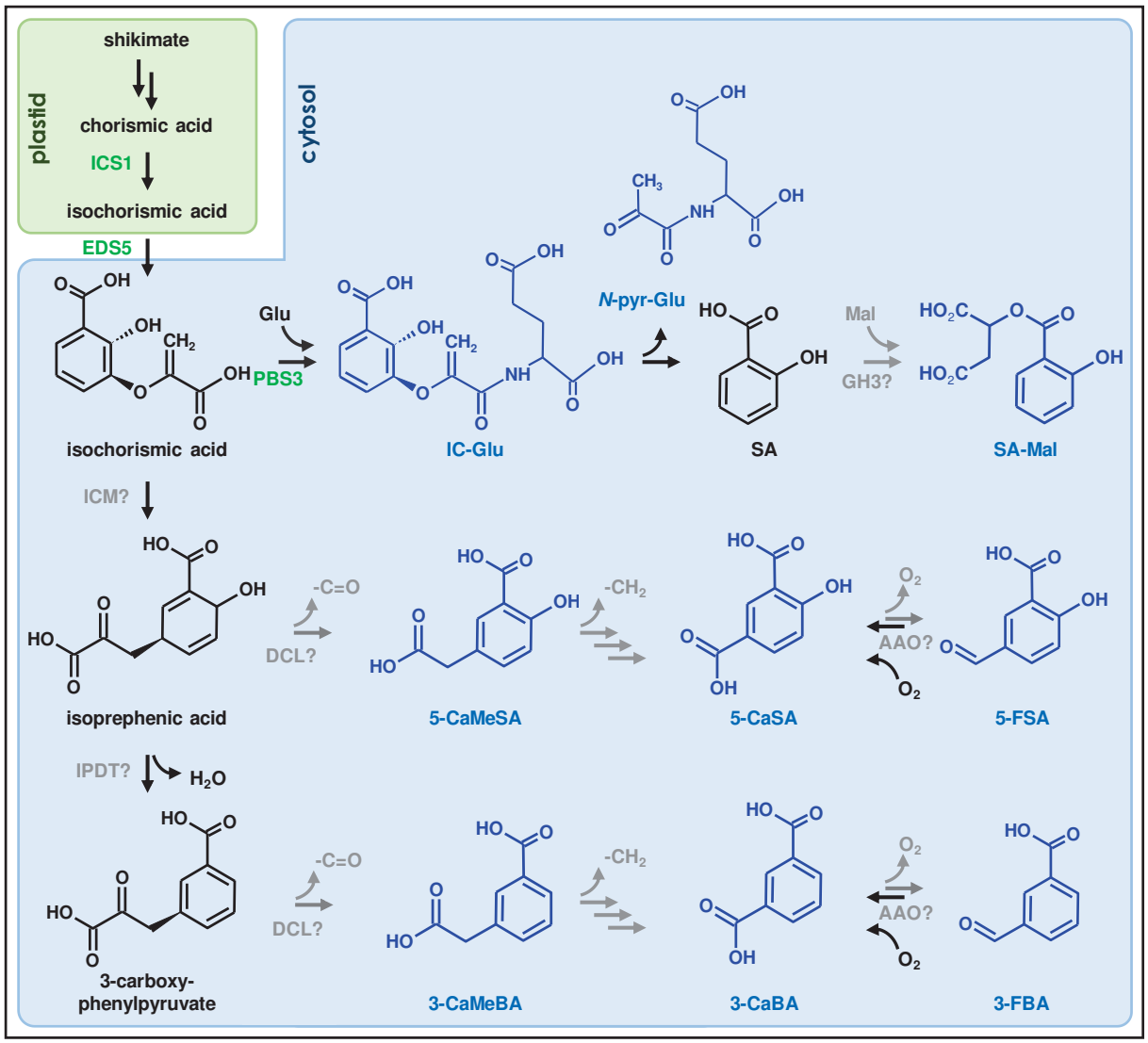

Figure 3.1.1: Integration of the identified molecular species into the IC-pathway
In this thesis identified molecular species are colored in blue, previously known metabolites and characterized reactions are colored in black, specific enzymes are written in green, presumed reactions are depicted in gray. ICM: isochroismate mutase, IPDT: isoprephenate dehydratase, DCL: decarboxylase, AAO: Arabidopsis aldehyde oxidase, GH3: Gretchen-Hagen3.

Integration of the molecular species into the IC-pathway through mutant analysis

The broad analysis of SAR and defense-related Arabidopsis mutants clarified the putative role and integration of the identified molecular species. As mainstay of our hypothesis all identified molecular species are ICS1-dependent and therefore absent in the *sid2* mutant. If ICS1 is inhibited to catalyze chorismic acid to IC, neither a conversion of IC to SA nor to isoprephenic acid and 3-carboxyphenylpyruvate is possible, resulting in a lack of all nine identified molecular species (Figure 3.1.1). The involvement of *eds5* regarding our proposed model has to be discussed, since most of the metabolites seem to be depending on EDS5. Latest research results proposed that EDS5 exports IC rather than SA from the plastid to the cytosol [47].

Once out of the plastid, IC is conjugated to Glu by PBS3 and subsequently decomposes IC-Glu to SA [47]. This theory explains the lack of IC-Glu and *N*-pyr-Glu in *eds5* mutant plants and indicates a probable location of PBS3 to the cytosol. The lack of the remaining molecular species could be explained, if the conversion of IC to isoprephenic acid and 3-carboxyphenylpyruvate is also located in the cytoplasm. Recent literature locates an analogue reaction, forming phenylpyruvate through chorismic acid and prephenate, to the cytoplasm as well [129]. The authors could identify a cytosolic chorismate mutase and a cytosolic prephenate dehydratase strengthening this hypothesis.

The accumulation pattern of the identified metabolites in *pbs3* and *npr1* mutant plant underlines their integration to the portrayed IC-pathway. As mentioned before, PBS3 conjugates Glu to IC forming SA through its precursor IC-Glu and the spontaneous cleavage of *N*-pyr-Glu [47,51]. With the loss of the PBS3 enzyme, the conversion of IC to IC-Glu is restricted, resulting in a strongly enhanced transformation of IC through isoprephenic acid and 3-carboxy-phenylpyruvate to the remaining six molecular species, ending in a high over-accumulation compared to wild-type plants. NPR1 is the master regulator of SA and responsible for SA-signal transduction in plant defense. As SA-receptor, NPR1 is the last link in the SA-pathway [65,66]. In *npr1* mutant plants systemic SA and SAR signaling is restricted, resulting in a local SA over-accumulation in infected tissue. Since SA is not transmitted in *npr1*, also SA-derivates like SAG, SGE, SA-Asp and SA-Mal pile up. The non-reception of SA in *npr1*, could lead to a general over-accumulation of metabolites integrated in the SA and IC-pathway including the newly identified molecular species.

It seems like the positive defense regulators PAD4 and NDR1 modulate the accumulation of 5-CaSA to 5-FSA and 3-CaBA to 3-FBA and vice versa. How the effect of these regulators takes place and how they are involved in the biosynthesis of the molecular species remains to be determined. Moreover, our results show, that the NHP pathway does not change the overall biosynthesis of the molecular species. The NHP deficient mutants *ald1* and *fmo1* depict a similar accumulation scheme compared to wild-type plants.

The accumulation pattern of the transgenic mutant line *NahG*, which carries a SA-hydroxylase underlines the direct SA decent of SA-Mal. Likewise other SA derivates, SA-Mal was not detectable in *NahG* mutants, whereas the remaining identified molecular species were not affected in this transgenetic plant. To ascertain the origin of the identified molecular species, pre-infiltration with isotopic labeled versions of putative metabolic precursors SA, BA and Phe did not yield to any labeling of the characterized substances, except for SA-Mal. These results

support our hypothesis for SA-Mal being a direct SA derivative and strengthen the close connection of all remaining molecular species to the IC-pathway (Figure 3.1.1).
Since, most SAR and defense deficient mutant plants are more susceptible towards pathogen infections, they develop more severe symptoms compared to wild-type plants which results in metabolic over-accumulation [45,57,68,103,130]. The higher loss of water in stronger infected tissue was considered during evaluation of the data.

5-CaSA and 5-FSA occur in microorganisms

In the bacterium *Pseudomonas syringae* pv. *putida* 5-CaSA, there called 4-hydroxyisophalic acid, is an intermediate in the degradation of the toxic pollutant 2,4-xylenol [131]. During the 2,4-xylenol degradation pathway the ortho-methyl-group of 4-hydroxy-3-methylbenzoate is oxidized to 5-CaSA, which is converted to protocatechuate through 4-hydroxyisophthalate hydroxylase (HipH). HipH is very substrate specific and showed no reaction on similar compounds including SA, 2,5-DHBA, 3-CaBA, or 3-formyl-4-hydroxybenzoate, an isoform of 5-FSA [132].
In a recent study 5-FSA was extracted as fungal metabolite of the necrotrophic fungal pathogen *Heterobasidion abietinum*. *H. abietinum* causes 'annosum root rot' in Norway spruce (*Picea abies)*. In co-culture of the pathogen with the rhizosphere bacterium *Streptomyces* AcH 505 the authors described an enhanced accumulation of 5-FSA in the presence of bacteria. Norway spruce seedling did not exhibit an increased vitality due to 5-FSA, nevertheless, seedlings pretreated with 5-FBA had enhanced amounts of ergosterol and the severity of the fungal infection was comparable to *Streptomyces* AcH 505 co-treated plants. Moreover, the authors described, that exogenously applied 5-FBA to *A. thaliana* seedlings results in an upregulation of the defense-related *PR1* gene. Our results with exogenously applied 5-FBA to 5-week old *A. thaliana sid2* mutant plants showed a moderately altered *PR1* expression after application.
We assume that all identified molecular species are true plant metabolites and do not result due to technical artifacts of the applied methods. For 5-CaMeSA and 3-CaMeBA we could verify both molecular species via three distinct methods (VPE, TMS and TMS2, Figure S1, S2). Here, Especially the extraction and derivatization of the TMS2 method involved only a moderate heating of the samples to 37°C for 30 min, because the application of high temperatures could cause a thermal decompositions of chemical structures [118]. Furthermore, does our data underline the *in planta* origin of 3-CaBA and 5-CaSA, since we detected moderate amounts in non-bacteria treated control plants. Moreover, we did not analyze any of the nine identified

metabolites in extractions of *Psm vir* suspensions. But, amounts of IC-Glu, *N*-pyr-Glu, SA-Mal, 3-CaBA and 5-CaSA were detected after treatment with the bacterial flagellin peptide flg22.

Putative role of identified molecular species in plant resistance

The highest accumulation of most molecular species occurs after 48 hpi and respond to the infection of *Psm vir* and *Psm avir*. Therefore, we chose the time point of 48 hpi and an infection with *Psm vir* for all further experimental setups. Only 3-FBA and 5-FSA accumulate stronger after infection with *Psm avir.* Since, the infection of *Psm avir* has been described to trigger a faster response and induces HR in contrast to *Psm vir*. The choice of the sampled time point, and bacterial strain might be a reason why 3-FBA and 5-FSA were only detectable in small amounts. Here, a further examination for the best infection pattern should be conducted to analyze both molecular species.

3-CaBA and 5-CaSA accumulate after necrotrophic fungus infection in *A. thaliana*

The molecular species 3-CaBA and 5-CASA do not only play a role in the combat against (hemi)biotrophic bacteria like *P. syringae*, but also protect against a broader spectrum of phytopathogens. Döring and colleagues detected 2015 an accumulation of both metabolites 3-CaBA, or isophthalic acid, and 5-CaSA, or hydroxyterephthalic acid, upon infection with the necrotrophic fungus *Botrytis cinereal* in *A. thaliana* plants. Furthermore, 5-CaSA accumulated after infection with the oomycete *Hyaloperonospora arabidopsidis* (*Hpa*) and the obligate biotrophic powdery mildew fungus *Golovinomyces orontii* only in small amounts [133]. The accumulation of 3-CaBA and 5-CaSA after infections with a diversity of phytopathogens indicates a general role in plant defense for both metabolites. Interestingly, 3-CaBA and 5-CaSA do not only accumulate on the local side of the infection, but also in non-infected systemic tissue, strengthening their putative role in plant defense.

Direct influence of identified molecular species on plant immunity

We examined the direct influence of the molecular species on plant immunity by applying basal resistance assays using *Psm lux* and *PR1* gene expression in wild-type Col-0 plants and *sid2* mutants. To gain a comparability between the different molecular species, we applied application method and substance concentration how it is commonly used to generate SA induced resistance in *A. thaliana* [15]. We included the SA-derived 2,3-DHBA and 2,5-DHBA as further controls for the basal resistance and *PR1* expression assays, and could verify that both

derivatives induced resistance and *PR1* gene expression, but to a lesser extent compared to a treatment with free SA [88]. Under these conditions we could show that 5-FSA and 5-CaSA influence the bacterial resistance in the wild-type plants positively. The bacterial growth was slightly reduced after 5-FSA treatment and significantly decreased after application of 5-CaSA. None of the tested molecular species was able to induce *PR1* expression. It even seemed like 3-CaBA and 3-CaMeBA had an inhibiting effect on the expression of *PR1*. All metabolites share similarities to the phytohormone and *PR1* inducer SA, but further chemical groups are attached to the basic structure. Therefore, an uptake through the infiltrated apoplast might be an unsuitable application for these larger metabolites. Especially for 3-CaMeBA, which was the largest of the applied molecular species, we could not detect any influence on metabolic level or basal resistance. An application through the root system to plants grown in hydroponic culture or to seedlings, grown on media containing the substances, could display possible approaches to further test an uptake of the identified molecular species.

SA-malate – a novel SA modification to dicarboxylic acids

The detection and identification of SA-Mal might be a milestone in SA-biosynthesis. It broadens the previously known SA modifications like methylation, glycosylation, hydroxylation and AA conjugations, by SA conjugations to small dicarboxylic acids. Malate is a key metabolite in plants and besides its role in carbon fixation it is involved in many other housekeeping functions [134]. Our results revealed a pathogen- and time-dependent accumulation of SA-Mal. Compared to early responses of SA derivates like free SA, SAG and SGE; the accumulation of SA-Mal and SA-Asp rises about two days after pathogen infection. The reason for the delayed accumulation of SA-Mal remains unclear. It is also uncertain whether SA-Mal is a storage, degradation or intermediate form in SA biosynthesis. To prove the influence of SA-Mal on plant immunity, SA-Mal application assays could be performed, but a presumable fast hydroxylation of SA-Mal to free SA and Mal must be considered.

Next to SA-Mal and SA-Asp, we identified the corresponding BA derivates BA-Mal and BA-Asp through GC-MS analytics and chemical synthesis, as new metabolic conjugations accumulating after pathogen infection. Unlike SA-Mal and SA-Asp, BA-Mal and BA-Asp are not ICS1- and PBS3-dependent. Nevertheless, SA-Asp and BA-Asp are conjugated by the same enzyme GH3.5 [54,95]. GH3.5 has previously been described to inactivate the phytohormone IAA or auxin by a conjugating of IAA to Asp [94]. Auxin plays a role in plant growth and development as well as in plant disease susceptibility [135]. A knockout mutant analysis of *gh3.5* could prove

an involvement of GH3.5 in the synthesis of SA-Mal and BA-Mal. Further *in vitro* assays with GH3.5 protein could help clarify this theory.

The broad spectrum of substrate acceptance of GH3.5 raises the question if other Gretchen Hagen family members are active on various substrate combinations *in planta* as well. Breakthrough research findings proved, that GH3.12 or PBS3 conjugates Glu to isochorismic acid *in planta* and Glu to 4-hydroxy-substituted BAs *in vitro,* indicating a broader substance acceptance for PBS3 [47,58,136]. Supporting this argument, we could confirm in total eight *in vitro* PBS3 conjugations between 4-hydroxy-substituted BAs and Glu, Met and Mal and moreover the conjugation of glutaric acid and succinic acid to AA. The putative involvement of PBS3 will be discussed in more detail in the following PBS3 dedicated chapter.

Conclusion and outlook regarding identified molecular species

This study reveals nine newly identified *ICS1* and *EDS5*-dependent metabolites that accumulate after *Psm vir* treatment in wild-type *A. thaliana* plants. The proposed model depicts a viable integration of the nine compounds to the IC-pathway based on gained data and the current scientific background. To validate the established model, it is essential to verify the presence of the precursors isoprephenic acid and 3-carboxy-phenylpyruvate in *A. thaliana*. Since both metabolites are not commercially available a synthesis through IC and its precursor chorismate should follow a detailed analysis through NMR spectroscopy and GC-MS identification. Moreover, achieving an unequivocal structural identification of SA-Mal, IC-Glu and 5-CaMeSA should be one priority. Therefore, a better chemical synthesis of SA-Mal and subsequent spectroscopic characterization through NMR is still pending. To validate the candidate for U5 as 5-CaMeSA, a SPE to enhance the substance concentration to collect enough material for NMR-spectroscopy is needed. Moreover, the impact of the newly identified compounds on resistance against other leaf pathogens such as the oomycete *Hpa* or the fungus *Botrytis cinerea* is an interesting point remaining to be investigated.

3.2 The role of PBS3 in plant defense

PBS3 is an important enzyme in the SA biosynthesis pathway, but until recently it's detailed role in plant defense pathways was uncertain and some aspects of PBS3 are still controversially discussed. The results of this thesis should help to clarify the involvement of PBS3 in SA-biosynthesis and overall plant defense. For a better understanding of the putative role of PBS3 in the complex plant defense pathway, we examined the subcellular localization of the

PBS3 enzyme, the accumulation of metabolites in the PBS3 knockout mutant *pbs3* and studied various substrate combinations through *in vitro* assays with the active PBS3 enzyme. The gained results will be discussed in detail hereafter.

PBS3 is located in the cytosol of plant cells

After pathogen infection, PBS3 is co-expressed in local and systemic plant tissue, together with the crucial SAR regulators ICS1 and FMO1 [17]. ICS1 and FMO1 are responsible for the biosynthesis of the key SAR metabolites SA and NHP [3,43]. ICS1 has been located to the chloroplast, whereas FMO1 was found in the endoplasmic reticulum (ER) [44,137]. A putative interaction between the enzymes could correlate with a sub-cellular spatial proximity. Therefore, we co-expressed 35S-PBS3-CFP transient in *N. tabacum* together with fluorescent markers of important cell compartments like ER, vacuolar tonoplast, plasma membrane and Golgi apparatus. A putative localization of PBS3 in the chloroplast was performed using the autofluorescence of the plastid. PBS3 could not be co-localized with one of the cell compartments tested in this study, which leads to the suggestion that PBS3 might be localized to the cytosol. This hypothesis is strengthened by the findings of Chang et al., 2019, who co-localized PBS3 with EDS1 together to the cytosol [32]. Also, Rekhter et al. could not localize PBS3 to the plastid and proposed PBS3 activity as well to the cytosol [47].

How is PBS3 involved in pathogen induced SA accumulation?

The identified molecular species could be integrated into a metabolic model (Figure 3.1.1). Anyhow, there are still open inquiries concerning the model remaining to be answered. The model does not consider the major questions, how and why *pbs3* mutant plants possess wild-type or even stronger enhanced levels of free SA. Based on the proposed role of PBS3 to conjugate Glu to IC forming IC-Glu which spontaneously decomposes to *N*-pyr-Glu and releases free SA [47,51]. Therefore, the amount of formed SA should be drastically reduced in *pbs3* mutant plants compared to wild-type plants. We could verify the first part of this hypothesis by the loss of IC-Glu and *N*-pyr-Glu in *pbs3* mutants and the *in vitro* synthesis of *N*-pyr-Glu by PBS3 through the conjugation of pyruvate and Glu in small amounts. On the contrary, the analysis of *pbs3* depicted wild-type and even stronger levels of unbound SA after *Psm vir* infection. However, the amounts of glycosylated forms of SA, SAG and SGE were strongly reduced. Interestingly, like SA-Mal, SGE was almost missing in *pbs3* mutants. Therefore, SGE might be dependent on PBS3. Already early studies of *pbs3* mutant plants observed higher amounts of unbound SA and a lack of glycosylic SA, which could be restored by exogenously

applied free SA [52]. These findings rather indicate a role of PBS3 downstream SA biosynthesis and a putative involvement in SA glycosylation. Okrent et al., 2009 proposed that free SA inhibits PBS3, but the authors based their findings on *in vitro* results. This leads to the conclusion that the connection between glycosylic SA production and PBS3 has not been fully understood yet. Here, *in vitro* assays of PBS3 and substrate combinations of SA and glycose could help to understand the connection between PBS3 and SA-glycosylation.

As responsible SA glycosyltransferases UGT76B1, UGT74F1 and UGT74F2 were described. UGT76B1 glycolyzes not only SA to SAG but also NHP to NHPG [36,37]. However, UGT74F1 and UGTF4F2 preferer BA and other substrates over SA [79]. UGT74F1 has been described to be responsible to form SAG, and UGT74F2 to form both, SAG and SGE with a priority to form SGE [80,81]. Like the active PBS3 enzyme, SAG formation and the location of UGT74F2 is supposed to be in the cytoplasm [138,139]. However, to our current knowledge the subcellular location of UGT74F1 has not been unambiguously verified yet. If PBS3 positively influences UGT74F2 activity and therefore as well SGE and SAG biosynthesis, has not been described yet. This could explain the lack of SGE and reduced SAG levels in *pbs3* mutant plants. A reduced *UGT74F2* gene expression in *pbs3* mutants, detected by qPCR analysis, microarray or RNA-seq data, could help to answer this question. Though, database analysis of atted II ver. 11.0 could not detect a co-expression of PBS3 and UGT74F1 or UGT74F2 (https://atted.jp/locus/?gene_id=831173, Figure S12).

The purpose of SAG and SGE *in planta* is still uncertain. However, it is under discussion that SAG is not active in disease resistance and considered a main storage form of SA due to its stable glycosylation [140]. Considering the high-energy-conjugation of SA to the sugar in SGE, SGE might conduce as potential biosynthetic or metabolic intermediate [80]. This interesting aspect about SGE and the absence of SGE in *pbs3* mutants portends a significant role of SGE in plant defense signaling. Albeit, it has been proposed that, especially SAG is stored in the vacuole but a proper subcellular localization of SAG and SGE *in planta* has not been described yet [138]. The localization of SAG and SEG through putative antibodies or molecular labeling might help clarify the role of SA glycosylation in plant defense against (hemi)biotrophic pathogens.

PBS3 conjugates 4-substituted benzoic acids and small carboxy acids to amino acids

Besides the priorly described role of PBS3 in SA biosynthesis, PBS3 has previously been reported to conjugate 4-substituted BAs to AA [58]. In the present thesis, we could broaden the *in vitro* substance acceptance of the PBS3 enzyme by confirming 4-substituted BAs to AA

conjugations and further conjugations between the small aliphatic acids glutaric acid and succinic acid to AA. The conjugated products were gluaric acid-Gly and glutaric acid-Ala, as well as, succinic acid-Ala and succinic acid-Val. Anyhow, the newly identified PBS3 *in vitro* products could not be detected *in planta*. The elevated *in vitro* substrate acceptance of PBS3 could point to a wider role of PBS3 *in planta* and in plant defense. However, evidences supporting this hypothesis remain to be provided.

Conclusion and outlook of PBS3 in plant defense

So far, the results gained in the present thesis about PBS3 confirm and support latest insights into plant research. Moreover, we could broaden the *in vitro* activity of PBS3 by four carboxylic acid and amino acid conjugations. Still, central questions about the involvement of PBS3 in SA glycosylation remain to be answered. For a larger substrate screening and to measure binding affinities of various substrates, including SA and glucose, the use of isothermal titration calorimetry (ITC) is planned. Furthermore, protein interaction studies between PBS3 and ICS1 are under discussion. Here, we plan to purify ICS1 next to PBS3 to examine an interaction of both proteins with putative substrates and the identified molecular species. One further goal was the complementation of PBS3 knockout mutant plant and the generation of an *A. thaliana* over-expression line of PBS3 for further metabolic analysis. Both lines have been established, and the selection for homozygous plants is still open. The PBS3 over-expression line could help to solve the question of PBS3 in plant immunity. Does the over-expression line have a higher pathogen resistance compared to the wild-type? Do the putative PBS3-derived compounds over-accumulate in these plants compared to the wild-type? Studies on *A. thaliana* ecotypes showed, that naturally more resistant ecotypes share the same natural variation in the PBS3 enzyme [141,142]. In this context it would interesting to express this version *in vitro* to look for variation in enzyme activity.

3.3 Is *NahG* an appropriate candidate to study plant immunity?

About a quarter of a century ago transgenic plant lines, carrying the bacterial salicylate hydroxylase NAHG from *Pseudomonas putida* were established to study the influence of SA on plant immunity [67,102,143]. In *P. putida* NAHG is involved in the degradation of naphthalene to pyruvate acetaldehyde and responsible for the decarboxylation and hydroxylation of SA to catechol [102].

In this thesis, we focused on the influence of the introduced NAHG enzyme on the plant immune system and revealed that consequences exceed the salicylate pathway by far. A central question in this thesis is the involvement of the crucial immune regulators NHP and Pip in transgenic *NahG* mutant plants.

Neither exogenously applied SA, NHP nor Pip leads to an increased resistance in *NahG* plants

The enhanced susceptibility of *NahG* plants to *Psm vir* compared to SA deficient *sid2* plants and *A. thaliana* wild-type Col-0 was observed in this study. Earlier studies by van Wees and colleagues proposed 2003 that the produced catechol in *NahG* plants has a negative influence on resistance against non-host pathogen *P. syringae* pv. *phaseolicola* strain 3121 (*Psp*). In their study, they tested SA compromised mutants *sid2*, *eds5*, *pad4* and *npr1* besides *NahG* plants. Like the wild-type, these mutants were resistant to *Psp* infection, leading to the conclusion that the enhanced susceptibility to *Psp* in *NahG* plants relays on other factors besides the absence of SA. The authors showed, that exogenous applied catechol leads to enhanced susceptibility in wild-type and in *NahG* plants [103]. Regarding our results, we observed a stronger effect of enhanced susceptibility in *NahG* against the virulent pathogen *Psm lux* compared to SA deficient *sid2* and wild-type plants. In contrast to Col-0 and *sid2*, the resistance to *Psm lux* could not be restored by exogenously applied SA, probable due to a constant degradation of SA to catechol in *NahG* plants [15].

Important studies performed by our research group, revealed the crucial influence of NHP and Pip in plant immunity [3,5,15]. The exogenous application of NHP and Pip leads to an induced resistance in Col-0 and *sid2* plants. However, the effects were dampened in *sid2* compared to the wild-type, underlining the importance of SA for a full defense against *Psm vir* and the oomycete *Hpa* [3,5]. In this thesis, we could show that resistance of *NahG* plants against *Psm vir* was not altered by the pretreatment of the two crucial immunity regulators NHP and Pip.

NahG plants are lacking endogenous NHP and Pip accumulation

Considering metabolic data of *NahG* plants which were pretreated with Pip before *Psm lux* infection, we observed poor levels of endogenous Pip compared to wild-type plants. Moreover, a pathogen-dependent accumulation of Pip was almost absent in *NahG*. A time course experiment demonstrated the accumulation of SA and Pip derivates after bacterial infection in *NahG* and Col-0 plants. Here, wild-type levels of SA and SA-glycosides steadily increased after pathogen infection. The metabolite analysis through GC-MS showed that transgenic *NahG* plants accumulate only mock levels of free SA and completely lack the ability to accumulate

the SA-glycosides SAG and SGE after *Psm vir* infection, most likely due to the already mentioned constant degradation of SA to catechol in *NahG* [102]. In contrast to SA deficient *sid2* mutant, which over-accumulates NHP and NHPGE [3], in *NahG* plants NHP and its derivates NHPGE and Pip were almost not detectable. The lack of SA in *sid2* plants outlines the fact that NHP biosynthesis is independent of SA [3]. This fact demonstrates, the lack of NHP in *NahG* plants is not only due to the absence of the regulator SA. Analysis of double mutant plants *NahG/ sid2* could provide further clarification of the influence of NAHG on NHP in transgenic *NahG* plants.

Does *NahG* degrade NHP-derivates besides SA?

So far it can be concluded that the exogenous application of the crucial defense-metabolites SA, NHP and Pip does not increase the resistance in *NahG* plants. Moreover, *NahG* plants degrade SA to catechol and accumulate very low levels of NHP and Pip, up to 13-fold less compared to wild-type equivalent, after pathogen treatment. Beyond that, further metabolic analysis revealed that *NahG* plants generally contain lower levels of the NHP and Pip derivate 2,3-DP but exhibit significantly higher amounts of the overall precursor Lys compared to wild-type plants after infection. Previous work showed that Lys significantly accumulates upon pathogen infection in infected leaf tissue to initiate the biosynthesis of NHP and Pip [3,5]. This specific accumulation pattern of *NahG* plants, leads to the suggestion, that the introduced hydroxylase does not only degrade SA to catechol but also accepts structural similar metabolites. In this case all three metabolites 2,3-DP, Pip and NHP are cyclic non-proteinogenic amino acids, sharing basic structural similarities with SA (Figure 3.3.1). Here, especially the six-membered ring, the carboxy group and the location of the *ortho*-hydroxy group of NHP relates to SAs basic structure. Already, Hartman et al. 2018 referred to the similar structure of SA and NHP and pointed to a potential influence towards biological function between both regulators. This assumption is based on the accumulation pattern of *NahG*. The degradation of NHP-derivates could explain the observed over-accumulation of L-Lys as direct precursor to NHP. Moreover, the transformation of NHP to NHP-hexose decelerates with decreasing NHP supply. To substantiate this hypothesis, evidence of the putative degraded end products of 2,3-DP (2-piperidone, CAS: 675-20-7), Pip (2-piperidinol, CAS: 45506-41-0) and NHP (1,2-piperidinediol, CAS: 1823946-50-4) should be determined *in planta* (Figure 3.3.1). For an incontestable evidence of a *NahG* depended degradation of NHP-derivates, *in vitro* analyses of the recombinant expressed NAHG protein are pending to be performed. The putative evolved products could then be analyzed via GC-MS methods and be verified *in planta*.

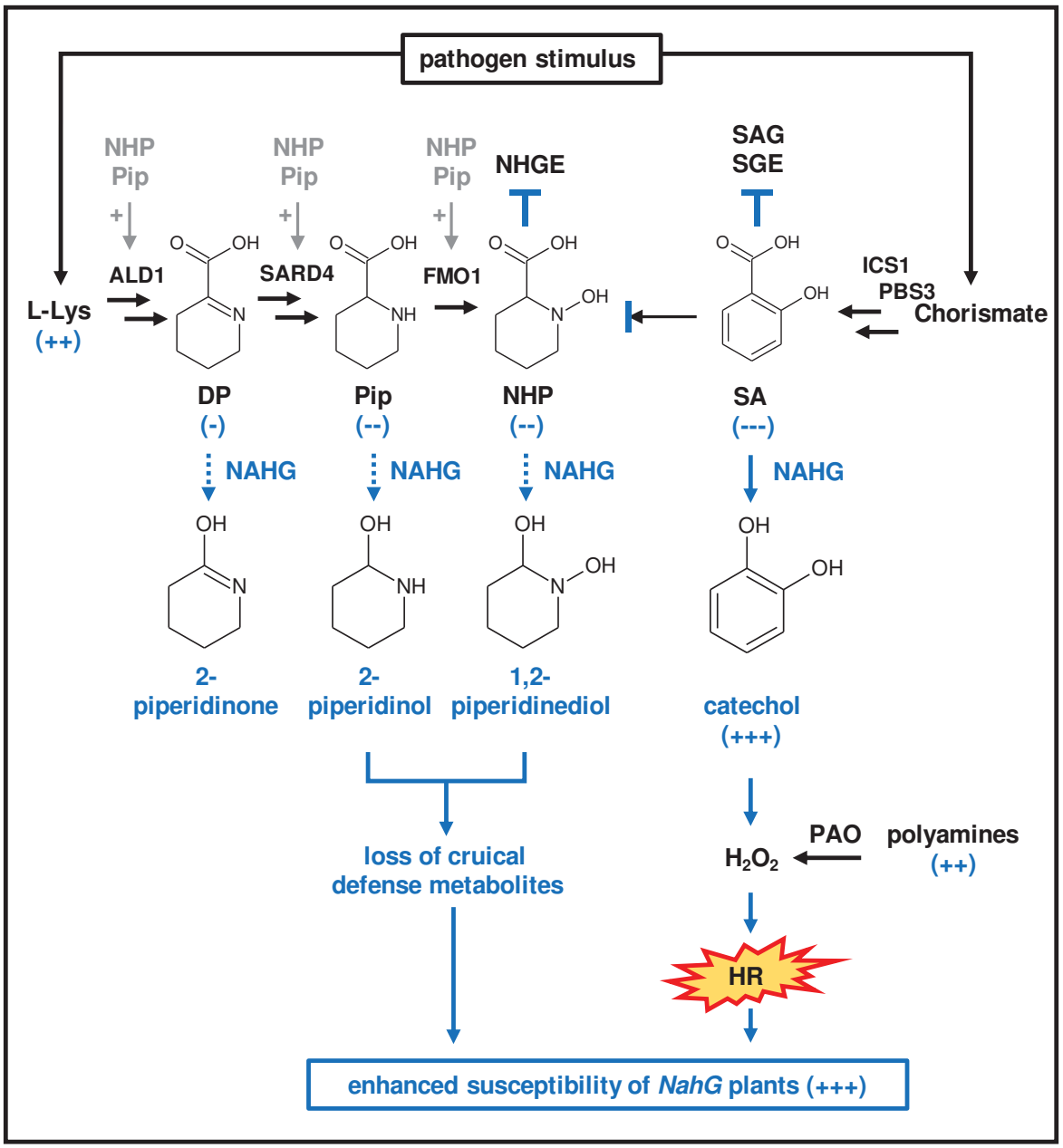

Figure 3.3.1: Putative influence of NAHG on plant immunity
Pathogen infection stimulates the *de novo* synthesis of the crucial defense metabolites SA and NHP. In transgenic *NahG* lines, SA is continuously degraded to catechol, inhibiting the conversion to further SA derivates such as SAG and SGE. With the loss of SA, the influence on NHP signaling pathway is absent. The accumulation of catechol leads to an increase of ROS through H_2O_2. Influence of NAHG on plant metabolism is shown in blue, putative degradation of NAHG is shown in dashed arrows. (-) reduction in *NahG* plants, (+) accumulation in *NahG* plants. Self-amplification of NHP and Pip is marked in gray.

Another aspect explaining the accumulation pattern of NHP-related substances in *NahG* is the positive feedback amplification loop of NHP and Pip, which are able to stimulate their own biosynthesis [5,18,109]. NHP and Pip have a positive influence on their own biosynthesis genes *ALD1*, *SARD4* and *FMO1* [18]. In consequence, the putative degradation of either NHP or Pip by the hydroxylase NAHG could lead to a mutual decrease including their precursor 2,3-DP

(Figure 3.3.1). If all three NHP-related substances are degraded by NAHG or if the hydroxylase prefers the structural similarity between SA and NHP, remains to be determined *in vitro* by performing a recombinant protein assay of NAHG.

The GC-MS analysis of *NahG* revealed further discrepancies of accumulating metabolites after *Psm vir* infection compared to *A. thaliana* wild-type Col-0. As described in literature *NahG* plants accumulate high levels of catechol, leading to a metabolic imbalance after bacterial infection. The accumulated catechol in *NahG* plants has been described to influence the susceptibility to bacterial pathogens [103]. Catechol causes the accumulation of ROS through H_2O_2 thereby inducing a HR and is involved in DNA and protein damage [144]. As defense strategy the HR induces controlled cell death to prevent the spread of attacking non-host and incompatible pathogens [145]. However, uncontrolled cell death is more harmful than protective, explaining the enhanced susceptibility of *NahG* plants.

Moreover, polyamines (PAs) have been described to play an important role in plant-defense. Here, especially ornithine-derived PAs, like putrescine and spermine, are involved in redox processes, hormone crosstalk and the generation of ROS and HR establishment [109]. PAs are oxidized by polyamine oxidases (PAO), which releases extracellular H_2O_2 and in return enhance the HR reaction [146]. In the present study, we observed an accumulation of ornithine, putrescine and spermine in *NahG* plant. The great amounts of the PAs may therefore contribute to *NahGs* enhanced susceptibility (Figure 3.3.1).

Uncontrolled cell death, induced by the (hemi)biotrophic pathogen *Psm vir* in *NahG* plants, resembles cellular damage normally observed after combat with necrotrophic pathogens and herbivores. These severe symptoms provoke the activation of the JA defense pathway, which is antagonistic to SA response. JA is derived from α-linolenic acid and is converted through intermediate steps to the direct JA precursor OPDA (12-*cis*-oxophytodienic acid). The active form of the plant hormone is the JA amino acid conjugation JA-Ile. In *NahG* plants, in contrast to other SA deficient mutant lines like *sid2*, we observed a strong accumulation of ODPA and JA after bacterial infection. These findings are overlapping with previous publications, which observed changes in the *NahG* metabolic defense-household. Especially the work of Heck et al. 2003 described abnormalities in the JA-pathway and alterations of camalexin amounts in *NahG* plants. Our data is concurrent with these findings describing an accumulation of JA in *NahG* plants after infection with *P. syringae* pv. *tomato* (*Pst*). Moreover, this work also showed the accumulation of JA precursor OPDA.

The indoles CAM and indole ICA accumulate after *Psm vir* infection in *A. thaliana*. CAM is a phytoalexin accumulating in plants upon pathogen infection and has antimicrobial functions

against necrotrophic fungi [106]. In *NahG* plants the CAM biosynthesis is restrained, whereas the ICA production is induced compared to Col-0 after *Psm vir* infection. Like *NahG*, the *pad4* mutant does not accumulate CAM after pathogen trigger [45,103,147]. The lipase-like protein PAD4 is known to be a regulator of defense reactions and is important for SA signaling. The pathogen induced CAM accumulation is not affected in other SA-signaling mutants like *eds5* and *sid2*, indicating for CAM to be SA independent [45,148].

It has therefore been proposed that *NahG* and *pad4* share an additional signaling pathway besides SA [103]. Here, the work of Hartmann et al. 2018 adds another aspect by identifying EDS1 and PAD4 as positive regulators in NHP biosynthesis. Both loss-of-function mutants, *eds1* and *pad4*, exhibit reduced levels of NHP and Pip compared to wild-type plants after *Psm* infection [3]. Moreover, the Pip deficient *ald1* mutant is also inhibited in CAM accumulation [5,107]. On the other hand, NHP deficient *fmo1* shows no restriction and accumulates CAM in wild-type levels [149]. SAR relevant mutants compromised in SA, like *sid2* and *npr1*, and Pip, including *ald1* and *fmo1*, pathways accumulate enhanced levels of ICA locally after pathogen infection compared to wild-type plants. ICA was systemically absent in all SAR deficient mutants, pointing towards to a *de novo* biosynthesis of ICA in distant leaves [104]. Moreover, exogenous applied Pip primes the pathogen-induced biosynthesis of CAM and ICA, underlining the connection between Pip and indole biosynthesis [5,15]. This indolic accumulation pattern in SA and Pip deficient mutant plants, goes in line with the observed accumulation of CAM and ICA in *NahG*.

Conclusion and outlook of *NahG* in plant defense

Overall, it can be concluded that the influence of NAHG on plant immunity of transgenic plants is more complex than solely the degradation of SA to catechol. Our data point towards the hypothesis that the hydroxylase accepts further critical defense metabolites like NHP and Pip. However, the final validation of this question is pending to be performed. A good approach to answer it, could be an *in vitro* enzyme assays of NAHG combined with NHP and Pip as putative substrates. Furthermore, double mutants implying *NahG*/ *sid2* could clarify the role of SA and NHP in *NahG* plants. Moreover, our study revealed a broader activation of metabolic defense pathways in *NahG* mutant plants, like PA production and the JA-signaling pathway. The loss of CAM is a further indication for a deeper involvement of NAHG to plant immunity.

3.4 Overall conclusion

In conclusion, this thesis helped to untie the complex system of plant immunity by the identification of nine newly described molecular species in the IC-pathway. Here, isoprephenic acid and 3-carboxyphenylpyruvate describe the missing link between the six identified molecular species and IC-biosynthesis. Furthermore, we identified with SA-Mal a novel SA conjugation to dicarboxylic acids. How SA-Mal is embedded in the SA-biosynthesis pathway and what exact role SA-Mal fullfills, is an interessting goal for future studies.

Moreover, the data veryfies the breakthrough reaserch, that PBS3 conjugates IC to Glu forming IC-Glu, realsing SA and *N*-pyr-Glu, and therefore finally fills a deep gap in SA-biosynthesis, although we could not unambigiously verify IC-Glu. Besides that, we could locate PBS3 to the cytosol of plant cells in agrement to current literature and broaden the *in vitro* subrate acceptance of PBS3 by conjugations of sCA to AA. Anyhow, an unsolved aspect on PBS3 is still pending: Why do *pbs3* mutant plants have reduced SA-glyosides levels and even lack SGE? Does PBS3 even play a further role in SA-glycolysation? These interesting findings remain to be awnserd.

Furthermore we found out, that transgenic *NahG* plants are lacking endogenous NHP and Pip accumulation. Neither exogenously applied SA, NHP nor Pip leads to an increased resistance in *NahG* plants. If NAHG degrades NHP besides SA has to be proven in the future. Therefore, the influence of *NahG* in plants is more severe on an metabolic level than previously expected.

4 Material and Methods

4.1 Biological material

4.1.1 Plant material

Arabidopsis thaliana (L.) HEYNH. plants were grown under the same conditions as described in Hartmann et al., 2018. Seeds were dispersed on soil and seedlings were separated after 10 days. Each plant grew in one induvial pot containing a mixture of soil (Substrate BP3; Klasmann-Deilmann), vermiculite and sand (8:1:1) in controlled growth chambers with 10 h short day conditions (9 AM to 7 PM), and 14 h dark period, with a humidity of approximately 60 % at 20°C. All experiments were performed during the fifth week after seeding, with non-stressed, uniform appearing, naïve plants. All used *A. thaliana* mutants have Col-0 as background.

Nicotiana tabacum (L.) cv "Samsun *NN*"plants were grown in individual pots in appropriate soil. The growth conditions for *N. tabacum* were set to 12 h long day condition with regulated temperature of 25°C day and 22°C night was adjusted. The sources of supply for all plants used in this thesis are listed herin after:

N. tabacum		*Nicotiana tabacum* (L.) cv "Samsun *NN*"
A. thaliana	Col-0	NASC ID: 1092
A. thaliana	*ald1*	SALK_007673
A. thaliana	*eds5* (*sid1*)	[45]
A. thaliana	*fmo1*	[149]
A. thaliana	*NahG*	[150]
A. thaliana	*ndr1*	[151]
A. thaliana	*npr1* (*npr1-2*)	NASC ID: N3801
A. thaliana	*pad4* (*pad4-1*)	[152]
A. thaliana	*pbs3* (*pbs3-2*)	[153]
A. thaliana	*sid2* (*sid1-2/ ics1*)	[154]
A. thaliana	*sid2-ald1* (*sid2-1-ald1*)	[15]

4.1.2 Bacterial strains

Bacterial strains *Pseudomonas syringae* pv. *maculicola* ES4326 (*Psm*), *Psm avir* and *Psm* carrying the *Photorhabdus luminescens* luxCDABE operon (*Psm lux*) were grown ON at 28°C in Kings B media [155] containing appropriate antibiotics (rifampicin 50 µg L^{-1}, kanamycin 50 µg L^{-1}, tetracycline 15 µg L^{-1}). Before *Psm* infiltration, bacteria cultures in log-phase were washed four times with 10 mM $MgCl_2$ and diluted to an OD_{600}= 0.005 for *Psm vir* and *Psm avir*

for metabolic samples and *Psm lux* for bacterial resistance assays to an OD_{600}= 0.001. The sources of supply for all bacterial strains used in this thesis are listed herin after:

Agrobacterium tumefaciens GV3101	GoldBio [156]
Escherichia coli BL21 (DE3)	
Escherichia coli DH5α	Thermo Scientific [157]
Pseudomonas syringae pv. *maculicola* ES4326 avrRpm1	[158]
Pseudomonas syringae pv. *maculicola* ES4326 luxCDABE	[159]
Pseudomonas syringae pv. *maculicola* ES4326	

4.2 Metabolic profiling

4.2.1 Analytical sample preparation

For metabolic profiling, three leaves of 5-week-old, naïve, non-stressed plants were infiltrated with *Psm* (OD_{600}= 0.005). Plant material has been collected 48 hpi *Psm* infection, unless indicated otherwise. At least six plants were used per treatment, and leaf samples of two plants were pooled and served as one replicate, making at least six leaves per replicate, three replicates for each condition. For all analytical methods plant material was shock frozen in liquid nitrogen right after harvesting and stored at –80°C until further extraction. Frozen plant material has been homogenized with a bead mill (tissue lyser II, Quiagen). Samples were handled in liquid nitrogen to prevent thawing until extraction procedure.

4.2.2 Extraction methods

Vapor Phase Extraction

The unknown molecular species identified in this study, were initially extracted via vapor phase extraction (VPE). This method collects volatile organic compounds and is based on an extraction of a water free organic phase and derivatization of free carboxylic acids with trimethylsilyl-diazomethane into the corresponding methyl esters. Through evaporation steps volatile compounds were collected. A detailed procedure description is found in Hartmann et al., 2017, 2018; Návarová et al., 2012; Schmelz et al., 2004.

To prevent enzymatic reactions and unwanted degradations, 600 µL of 70°C pre-heated extraction buffer (H_2O:1-propanol:HCl; 1:2:0.005; (v/v/v)) was added to approximately 100-200 mg shock-frozen and homogenized leaf material and mixed well for homogeneous thawing.

For precise quantification of plant metabolites 30 µL of an internal standard (IS) mixture consisting of 100 ng of D_4-SA (S16796, Sigma-Aldrich), H_2-JA (D3225, TCI) and indole-3-propionic acid (IPA; I3125, Sigma-Aldrich) was added to each sample. Addition of 1 mL dichlormethane (DCM) lead to a phase separation of lower organic phase after mixing >30 sec and subsequent centrifugation at 14,000 x g for 1 min. The organic phase was dried with natrium sulfate and methylated in a new glass vial with 4 µL 2 M trimethylsilyl diazomethane (36.283-2, Sigma-Aldrich) in hexane. The reaction was stopped after 5 min by adding 4 µL 2 M acetic acid in hexane. For the VPE method, the methylated plant sample was heated up to 70°C until complete evaporation. Following an increasement to 200°C for 2 min always under constant nitrogen stream. The VPE setup included a volatile collector trap column packed with Porapak-Q absorbent (VCT-1/4X3-POR-Q; Analytical Research Systems) to collect volatile compounds. The evaporated metabolites were rinsed of the Porapak-Q column with 1 mL methylene chloride. The collection was concentrated to 30 µL under nitrogen stream and transferred to new GC-vials. Appropriate GC-MS setting, and temperature program is summarized in Table 4.2.1.

For the analysis of chemical substances and aqueous protein assays 30-100 µL of the diluted solution was added to 500 µL MeOH. Optionally, the internal standard mixture was added. To ensure a water-free solution, natrium sulfate was added. The methylation and ensuing VPE took place as described above in a new glass vial.

Trimethylsilylation extraction

Through trimethylsilylation (TMS) extraction methods, it is possible to collect a broad range of metabolites including primary metabolites like amino acids and sugars. Here, two variations TMS1 and TMS2, of extraction and derivatization were applied. Both extraction procedures differ in the composition of the extraction buffer (EB), and later in the silylation of the metabolites, whereas the procedure of the extraction method is alike. The first extraction and derivatization method TMS1, is explained in detail in Hartman et al. 2018. The second, TMS2, was modified after Fiehn et al. 2006 and includes methoxyamine hydrochloride (Ma HCl, 22690, Sigma), which forms *O*-methyl oximes of aldehydes and ketones. Both extractions were performed cold and samples were kept on ice the whole time. About 50 mg homogenized frozen leaf tissue were extracted with pre-cooled EB.

TMS1: EB1 for polar metabolites: MeOH/ H_2O = 80:20 (v/v)

TMS2: EB2 for unpolar metabolites: $CHCl_3$/ MeOH/ H_20 = 1:2.5:1 (v/v/v)

For the first extraction step, 1 mL EB containing IS with appropriate final concentration in extraction solvent listed in Table 4.2.3 was added to the frozen samples. Samples were thoroughly vortexed and mixed under constant shaking (150 rmp) for at least 5 min at 4°C. The mixed samples were centrifugated for 2 min at 14,000 x g at 4°C. The supernatant was transferred to a new 2 mL reaction tube. A second extraction step followed with the appropriate EB containing no internal standards. Mixing for 5 min at 150°rmp and centrifugation for 2°min at 14,000 x g at 4°C was performed as described before. The extracted supernatants were combined. At this point samples could be stored at -80°C. For further procedure, aliquots of 400 to 600 µL were transferred to a new reaction vial and completely evaporated using a Scan Speed vacuum centrifuge (Labogene ApS, Denmark).

For the derivatization procedure of TMS1: 20 µL pyridine (82704, Supelco), and 20 µL *N*-methyl-*N*-trimethylsilyl trifluoroacetamide (MSTFA, 7012701100, Macherey Nagel) containing 1 % trimethylchlorosilane ((TMCS) v/v) and 60 µL of hexane were added with Hamilton syringes to the dried sample. Samples were vortexed thorough in between each step. Before and after incubation at 70°C for 30 min samples were shortly spined down and cooled down for 30 min at room temperature. For analysis aliquots of the samples were transferred to a GC-vial and diluted with hexane 5- to 10-fold.

For the derivatization procedure of TMS2: 10 µL of 20 mg/mL methoxyamine hydrochloride (Ma HCl) in pyridine was added to each dried sample. All samples were vortexed and spined down before incubation at 30°C for 90 min. Ma HCl forms oximes upon treatment with ketones and aldehydes. Afterwards, 90 µL MSTFA containing 1 % TMCS were added for silylation and incubated at 37°C for 30 min. The samples were transferred to GC-vials and diluted appropriately 5- to 10-fold in hexane. Appropriate GC-MS adjustments for both TMS-methods like temperature program and silica column is summarized in Table 4.2.1.

Amino acid extraction

The content of free AA was determined by the EZ:faast free amino acid kit (Phenomenex) for GC-MS analysis. The kit is based on the separation and mass spectrometric detection of propyl chloroformate derivatized AA. In a 2 mL reaction vial about 50 mg of homogenized, frozen plant material was dissolved with 500 µL extraction buffer (25 % acetonitrile in 0.01 $_N$ HCl) and homogenized by vortexing. As an IS, 10 µL of heptylamine (2 µg/ µL) was added. The samples were incubated for 15 min at room temperature under constant shaking and then centrifuged for 4 min at 14000 rpm. An aliquot of 100 µL of the supernatant was required for

further processing according to the manufacturer's instructions. The extract was dried over sodium sulfate and completely evaporated under N_2 flow and re-dissolved in 30 µl of CH_2Cl_2 and transferred to a GC-MS vial. Adjustments of the GC-MS program were summarized in Table 4.2.1. The identified molecular species were listed in Table 4.2.4.

4.2.3 GC-MS analysis of metabolites

Metabolic profiling was performed using a gas chromatographic system (GC, 7890 A, Agilent Technologies) that separates analytes due to their volatility and interaction with the specific fused silica capillary column. The GC is associated to a mass spectrometer (MS, 5975 C, Agilent Technologies), which ionized the compounds in the electron ionization mode (EI) and detects the individual mass-to-charge ratio (m/z). For GC-MS analysis different extraction and derivatization methods have been applied to analyze compounds of interest. A constant flow of helium (1.2 mL/min) ensured an even detection of the metabolites. Specific column types and GC-MS temperature programs are listed in Table°4.2.1.

Table 4.2.1: Overview of specific GC-MS adjustments

GC-MS program	VPE	TMS	EZ:faast
injection volume	4 µl	2 µl	3 µl
injector temperature	250°C	250°C	250°C
capillary column	ZB-5 30 m x 0.25 mm	ZB-35 30 m x 0.25 mm	ZB-AAA 10 m x 0.25 mm
manufacturer	Zebron, Phenomenex	Zebron, Phenomenex	Zebron, Phenomenex
initial temperature	50°C for 3 min	70°C for 2 min	70°C for 3 min
1. gradient	8°C/min to 240°C	10°C/min to 320°C	8°C/min to 240°C
2. gradient	20°C/min to 320°C		20°C/ min to 320°C
final temperature	320°C for 3 min	320°C for 5 min	320°C for 2 min
total run time	33.75 min	32 min	30.25 min

4.2.4 GC-MS quantification of metabolites

The metabolites of interest were identified due to a specific RT and characteristic ion fragmentation pattern of the mass spectrum. For the quantitative evaluation of the GC-MS data the corresponding MSD ChemStation software version E.02.01.1177 from Agilent Technologies was used. The areas of substance peaks were manually integrated and related to the corresponding peaks of the appropriate IS. A correction factor (CF) compensated the accumulation ratio of the analyte to the corresponding IS. Here, an unknown accumulation ratio

to the CF was set to 1. Metabolite levels were related to leaf fresh weight (FW). The formula to calculate the amount of substance reads as follows:

$$amount\ of\ substance\ \left({}^{ng}/_{g\ FW}\right) = \frac{area_{m/z\ Substance} * \ IS\ [ng] * \ CF}{area_{m/z\ IS} * \ FW\ [g]}$$

The specific IS to quantify the molecular species of interest were listed in the following tables for VPE and TMS analysis (Table 4.2.2 and Table 4.2.3). The main ion fragment of the integrated peak of interest is printed in bold and is underlined.

Table 4.2.2: Overview of identified molecular species quantified via VPE

	molcecular species	RT (min)	m/z			
IS	D_4-SA	11.5	**124**	156, 96		
IS	H_2-JA	19.0	**156**	153, 83		
IS	IPA	22.0	**130**	203	**CF**	**IS**
	SA	11.8	**120**	121, 152, 92	1.1	D_4-SA
U1	3-FBA	14.8	**133**	164, 105, 77	1.0	
U2	5-FSA	16.8	**148**	92, 119, 120, 121, 180	1.0	
U3	3-CaBA	17.2	**163**	135, 194, 103, 120	1.0	
	2-5-DHBA	17.4	**136**	168, 108, 80	1.0	H_2-JA
U4	3-CaMeBA	18.6	**208**	149, 177,	1.0	
U5	5-CaSA	18.7	**178**	63, 91, 119, 147, 210	1.0	
U6	*N*-pyr-Glu	18.9	**142**	82, 110, 174, 202	1.0	
	JA	18.9	**151**	224, 206, 193, 156, 83	3.0	
U7	5-CaMeSA	19.0	**133**	165, 192, 224, 105, 77	1.0	
	BA-Mal	21.4	**105**	51, 77, 207, 235, 266	1.0	
U8	SA-Mal	22.5	**120**	65, 92, 121, 282	1.0	
	BA-Asp	23.7	**105**	51, 77, 206, 265	1.0	IPA
	SA-Asp	24.8	**121**	65, 92, 249, 281	1.0	
	CAM	26.1	**200**	142	1.0	
U9	IC-Glu	29.8	**142**	82, 110, 174, 202, 379, 396	1.0	

RT and main ion fragmentation of analyzed plant metabolites. IS used for specific molecular species quantification is indicated.

Table 4.2.3: Overview of identified molecular species quantified via TMS-methods

	internal standard (IS)	RT (min)	m/z	IS (ng/µl)	quantified metabolites
IS	norvalin	7.42	261, 246, 218, **144,** 100	1000	AA
IS	D_9-Pip	9.34	239, **165,** 147, 133, 117, 93	1000	Pip
IS	2-CHC-OH	10.64	**273,** 198, 147, 142, 133, 129, 81	1000	NHP
IS	D_4-SA	11.81	**271,** 213, 197, 139, 95	500	SA
IS	ribitol	12.81	**319,** 307, 217, 205, 189, 147, 129, 117, 103	2000	diverse
IS	H_2-JA	15.56	282, 212, 197, **182,** 112	1000	JA
IS	IPA	18.58	333, 215, **202,** 147, 116	1000	indoles
IS	salicin	21.10	**268,** 361	1000	sugars

U	molecular species TMS1 (MSTFA)	RT (min)	m/z	IS	IS (m/z)	CF
	Pip	9.40	230, **156,** 84	D_9-Pip	**165**	0.8
		9.40	**230,** 156, 84	D_9-Pip	**165**	14.9
	NHP	10.70	172, 246	2-CHC-OH	**273**	0.3
	SA	11.93	**267,** 233, 209, 193, 175, 159, 133, 105	D_4-SA	**271**	0.5
	JA	15.82	280, 264, 250, 207, **180,** 148	H_2-JA	**182**	1.0
	ICA	18.20	115, 173, **246,** 216, 290, 305	IPA	**202**	1.0
	CAM	21.33	272, **257,** 227, 200, 172	IPA	**202**	1.0
	NHPGE	21.56	**172,** 361	salicin	**268**	1.0
	SAG	21.63	**361**, 271, 267, 243, 191	salicin	**268**	0.7
	SGE	21.72	**193**, 267, 361	salicin	**268**	0.2
U1	3-FBA	12.38	**207,** 191, 163, 133, 105 77, 222	D_4-SA	**271**	1.8
	2,3-DHBA	14.31	**355,** 193, 370	ribitol	**319**	1.0
	2,5-DHBA	14.49	**355,** 370	ribitol	**319**	1.0
U3	3--CaBA	14.57	103, 140, 205, 221, 251, 279, **295,** 310,	2-CHC-OH	**273**	0.2
U2	5-FSA	15.40	73, 85, 99, 113, 127, 163, 221, 251, **295**	D_4-SA	**271**	1.0
U4	3-CaMeBA	15.42	90, 118, 133, 145, 192, 219, 235, **280,** 309	2-CHC-OH	**273**	0.7
U5	5-CaSA	16.94	147, 191, 221, 251, **383**	2-CHC-OH	**273**	0.2
U7	5-CaMeSA	17.26	228, **412**, 397, 379	ribitol	**319**	1.0
	TMS2 (MSTFA + MA HCl)					
U1	3-formyl-BA	13.90	236, 204, 177, 130, 104, 76, **251**	D_4-SA	**271**	1.0
U2	5-formyl-SA	16.31	324, 291, 266, 219, 148, 105, 73, **339**	D_4-SA	**271**	1.0

Table 4.2.4: Overview of molecular species quantified via amino acid extraction

molcecular species	RT (min)	m/z	CF
norvoline	9.4	**158** 116, 72	IS
Pip	11.7	**170** 128, 84, 55	1.42
putrescine	16.0	**156**	1
ornithine	19.1	**156** 286, 184, 114, 70	0.75
Lys	20.1	**170** 300, 240, 213, 198,128, 84	0.89
spermine	24.0	**156**	1

4.2.5 GC-FTIR analysis of metabolites

A GC combined with a Fourier transform infrared spectroscopy (FTIR) has been applied to identify functional groups of the compounds of interest. GC-FTIR analysis was performed as described in Hartmann et al. 2017 and 2018. To identify the molecular masses as well as the chemical group composition of the molecular species of interest, the exact same plant extract was analyzed through GC-MS and GC-FTIR. Therefore, the gas chromatograph (Hewlett-Packard 6890 Series) was equipped with an identical silica column and used the same temperature program as operated in GC-MS analysis (VPE-Method Table 4.2.1). Through this exact GC comparison, it was possible to retrieve the exact target peaks in the total ion chromatogram (TIC) in both GC-systems. The GC was set in splitless mode using helium as the carrier gas, with a flow rate of 2 mL/min and a column head pressure of 9.54 p.s.i. To the GC an IRD3 IR detector (ASAP Analytical) was coupled and IR spectra were recorded in the mid-IR range from 4,000 to 600 cm^{-1} (wave number = reciprocal value of wavelength) with a resolution of 4 cm^{1} and a scan rate of eight scans per second. The IRD3 method parameters were as follows: resolution= 16; apodization= triangle; phase correction= mertz; zero-fill= 1; co-add= 2. The temperature of the light pipe and the transfer lines were both set to 250°C. Nitrogen was used as the sweep gas. Depending on the nature of the sample, 1 to 4 µL was injected using an Agilent 7863 Series autoinjector.

4.3 Chemical synthesis

4.3.1 Synthesis of SA-Mal

For the chemical synthesis of SA-Mal, 100 µM $_{DL}$ malic acid (3034.1, Roth) in acetonitrile was mixed with 20 µM salicyloyl chloride (CAS: 1441-87-8), dissolved in DCM, at ambient temperature. Samples were taken after 1 h, 2 h and the next day or ON. SA-Mal Synthesis was based on Suzuki et al., 1988. 50 µL of each reaction were dissolved in 500 µL MeOH, dried with natrium sulfate, and methylated with 4 µL trimethylsilyl diazomethane for 5 min. Methylation reaction was stopped adding 4 µL acetic acid in hexane. Further procedure was performed following the VPE protocol.

4.3.2 Synthesis of BA-Mal

For the chemical synthesis of BA-Mal, 100 µmol benzoyl chloride (8018040, Merck) and 100 µmol $_{DL}$ malic acid (3034.1, Roth) were added to 200 µL dry pyridine (CAS: 110-86-1, Supelco). Reaction proceeded at room temperature in a 1 mL Reacti-Vial^{TM} (Thermo Fisher) under constant shaking. A color change has been noticed as soon as benzoyl chloride was added from clear liquid to dark purple. The sample was taken after two hours. The reaction was transferred to a rotary evaporator and was washed twice with 6 mL MeOH at 60°C until evaporation. The product was dissolved in 1 mL MeOH. This method was based on Anderl, 2003. Afterwards, 50 µL were dissolved in 500 µL MeOH and dried with natrium sulfate, and methylated with 4 µL trimethylsilyl diazomethane for 5 min. Methylation reaction was stopped adding 4 µL acetic acid in hexane. Further procedure followed the VPE method.

4.4 Exogenous chemical treatment

4.4.1 Treatment with newly identified molecular species

To investigate the influence of the newly identified molecular species on plant immunity, Col-0 as well as the SA deficient mutant *sid2*, plants were treated with the authentic substance of the molecular species listed in Table°7.4.1. The application of the substance was performed through careful infiltration on the underside of the leaf with a needless syringe. For each substance three leaves of six plants were infiltrated with 0.5 mM authentic molecular species. In this case SA treatment should serve as a positive control, DIW as a negative. For metabolic analysis leaf samples were harvested 4 hours past chemical treatment and analzyed via GC-MS.

Table 4.4.1: Authentic standard substances of identified molecular species

abbrevation	molecular species	manufacturer	item number	CAS number
SA	salicylic acid	Sigma	S5922	69-72-7
3-FBA	3-formylbenzoic acid	Acros	296560010	619-21-6
5-FSA	5-formylsalicylic acid	Sigma	F17601	616-76-2
3-CaBA	3-carboxybezoic acid isophthalic acid	Alfa Aesar	A14445	121-91-5
3-CaMeBA	3-(carboxymethyl)benzoic acid	fluorochem	446214	2084-13-1
5-CaSA	5-carboxysalicylic acid 4-hydroxyisophthalic acid	Sigma	278270	636-46-4
2,3-DHBA	2,3-dihydroxybenzoic acid	Acros	A0350739	303-38-8
2,5-DHBA	2,5-dihydroxybenzoic acid gentisic acid	Fluka	537960	490-79-9

Molecular species induced resistance

To examine a molecular species induced resistance, three pretreated leaves of six plants were challenge infected with *Psm lux* (OD_{600}= 0.001) 4 hpi with 0.5 mM authentic molecular species listed in Table 4.4.1. Infiltration with 0.5 mM SA and DIW served as positive and negative control. Bacterial growth was measured two and a half days later via luminescence.

Molecular species induced *PR1* gene expression

To investigate the regulatory role of identified molecular species, leaves of Col-0 and *sid2* plants were infiltrated with 0.5 mM of authentic substances of the identified molecular species (Table 4.4.1). Here, infiltration with SA and DIW served as positive and negative control. Leaf samples were harvested 4 hpi. Methods for RNA extraction and qPCR were proceeded as described in Bernsdorff et al., 2016 and Návarová et al., 2012.

RNA extraction and cDNA synthesis

For RNA extraction about 1 mL cold RNA extraction buffer (RNAmagic™, my-buget, BioBuget) was added to 50 mg of frozen and homogenized plant material and mixed shortly. Further procedure was performed on ice rags and a cooled to 4°C centrifuge was used. 200 µL of ice-cold chloroform was added and vortexed for 15 s. Samples were centrifugated at 12,000 rcf for 15 min, clear supernatant was transferred to a new 1.5 mL reaction tube containing 500 µL pre-cooled 2-propanol. Samples were inverted for mixture and incubated for 15 min at room temperature and centrifuged for 10 min at 12,000 rcf. The supernatant was discarded, and the pellet was washed twice with 1 mL pre-cooled ethanol 75 %. In between washing steps, samples were centrifuged at 7,600 rcf for 5 min. EtOH was removed completely before the dry pellet was resolved in 44 µL of RNase free water and incubated at 65°C for 10 min. Concentration and RNA quality has been determined via NanoDrop 2000c (Peqlab Biotechnologie GmbH) and 1 % agarose gel ran with 130 mV for 40 min.
For further procedure and cDNA synthesis, remaining genomic DNA had to be digested with DNase I (EN0521, Fermentas). Therefore, the reactants for the digestion were pipetted together and incubated at 37°C for 30 min (Table 4.4.2). Afterwards, 1 µL 2.5 mM EDTA was added and incubated at 65°C for 10 min and quickly chilled on ice.

Table 4.4.2: genomic DNA digestion

RNAse free water	x µL
DNase I buffer	1 µL
DNase I	1 µL
RNA	1 µg
total volume	10 µL

Table 4.4.3: Mastermix cDNA synthesis

GoScript™ 5x buffer	4 µL
RNAse free water	4 µL
GoScript™ Reverse Transcriptase	2 µL
total volume	10 µL

To convert the extracted mRNA to cDNA the GoScript™ (Promega) kit was pipetted together following manufacturer's instructions (Table 4.4.3). 10 µL of the pre-mix was added to the digested RNA samples and incubated at 42°C for 1 hour. Reaction was stopped by heating up the samples to 70°C for 10 min. Samples were diluted with 180 µL RNAse free water. To examine the quality of the cDNA, from 5 µL cDNA a PCR of the abundant protein actin was performed using the GoTaq® Green master mix (Promega). Results were analyzed on an 1.2 % agarose gel running at 130 mV for 40 min before further proceeding.

Quantitative real-time PCR

The expression of *PR1* (AT2G14610) after molecular species treatment, has been analyzed through quantitative real-time PCR (qPCR). As a reference the housekeeping gene of *polypyrimidine tract-binding protein 1* (PTB, AT3G01150) was used. Transcript levels were measured based on technology using Promega GoTaq qPCR master mix according to the manufacturer's instructions (Table 4.4.4). Primer sequences of *PR1* and *PTB* are presented in Table 4.4.5.

Table 4.4.4: qPCR master mix

RNAse free water	1 µL
primer mix (5 µM)	1.5 µL
SYBRGreen	5 µL
cDNA	2.5 µL
total volume	10 µL

Table 4.4.5: qPCR primer sequence

gene	forward primer (5' to 3')	reverse primer (5' to 3')
PTB	GATCTGAATGTTAAGGCTTTTAGCG	GGCTTAGATCAGGAAGTGTATAGTCTCTG
PR1	GTGCTCTTGTTCTTCCCTCG	GCCTGGTTGTGAACCCTTAG

The qPCR reaction was performed in a duplicate of tow replicates of one treatment in a Rotor-Gene Q machine (Qiagen) under the following program cycle: initial temperature 95°C

for 2 min, 45 cycles at 95°C for 15 s and 60°C for 60 s and a final temperature at 72°C for 3 min. The corresponding Rotor-Gene Q 2.0.2 software was used to analyze the gained data. The threshold was set to 0.1 of the normalized fluorescence, corresponding to the exponential phase of the fluorescence signal. Data was analyzed using the $_{\Delta}$CT method. The *PR1* expression levels were normalized to *PTB* as reference gene and were expressed relative to the value of the water control.

4.4.2 Treatment with isotope-labeled metabolites

To determine the origin of the identified molecular species, *npr1* mutant plants were infiltrated with isotope labeled, 2 mM solutions of D_4-SA (Sigma, S16796), D_5-BA (Sigma, 217158) or D_5-Phe (Sigma, 616273). Infiltration of DIW as well as non- deuterium labeled SA, BA and Phe, served as control. A *Psm vir* challenge infection on the same leaves was performed 4 hpi (OD_{600}= 0.005). The samples were harvested 48 hpi bacterial infection and were shock frozen in liquid nitrogen and stored at -80°C until further metabolic analysis via GC-MS.

4.4.3 Treatment with NHP and Pip

Single potted plants, Col-0, *sid2* and *NahG*, were treated with 10 mL of 1 mM (equal to 10 µmol) $_{D,L}$-Pip (Sigma, S47167) or NHP (Hartmann et. al 2018), autoclaved 10 mL DIW was applied as control, one day prior bacterial leaf infiltration. For each treatment, six plants were used. On each plant three fully grown local leaves were infiltrated with *Psm lux* (OD_{600}= 0.001). Bacterial growth has been measured two and a half days past bacterial infiltration. Method has been previously described in Hartmann et al., 2018 and Návarová et al., 2012.

For a Pip priming experiment in Col-0 and *NahG* plants, Pip or DIW was applied to the soil as described previously. One day after Pip treatment, *Psm vir* (OD_{600}= 0.005) or 10 mM $MgCl_2$ has been infiltrated into local leaves. Leaf samples were harvested 48 hpi bacterial infection, and directly frozen in liquid nitrogen and stored at -80°C until further analysis.

To examine the local influence of NHP, local leaves of Col-0, *sid2* and *NahG* plants were infiltrated with 1 mM NHP or autoclaved DIW as control. One day past NHP infiltration, local or systemic leaves where infiltrated with *Psm lux* (OD_{600}= 0.001). Bacterial growth has been measured two and a half days past bacterial infiltration.

4.5 Enzymatic studies of PBS3

4.5.1 Cloning of PBS3

The PBS3 cloning strategy was followed as described in Okrent et al. 2009 and Hartmann et al. 2018. Therefore, the corresponding PBS3 (AT5G13320) cDNA fragment was PCR-amplified using the primer combinations listed in Table 4.5.1 and high-fidelity Phusion polymerase (New England Biolabs), following manufactures instructions. The amplified cDNA sequence was introduced through sticky end cloning to the target vector pET32 (Novagen) coding for a non-native C-terminal ploy-His tag. The plasmid containing the gene were transformed into chemically competent *E. coli* BL21 Rosetta 2 (DE3) pLysS cells (Novagen) and plated onogeny broth (LB)-Agar for selection with appropriate antibiotics. Positive transformed colonies were analyzed by colony PCR using gene specific primers and were subsequentially sequenced for verification.

Table 4.5.1: Primer combinations used for sticky end cloning of *PBS3* into pET32b

primer name	sequence (5' to 3')	length (bp)	temperature (°C)
PBS3-p32b-F1	**TAT GAAGCCAATCTTCGATATCAACGA**	27	55.2-63.7
PBS3-p32b-F2	**TGAAGCCAATCTTCGATATCAACGAAAC**	28	57-65.3
PBS3-p32b-R1	**GAA TAC TGA AGA ATT TGG CTA CCA CAC**	27	56.7-65.3
PBS3-p32b-R2	**TCG AG A ATA CTG AAG AAT TTG GCT ACC**	27	56.7-65.3

Purification of recombinant PBS3 enzyme

A single colony of pET32-PBS3 transformed *E. coli* BL21 cells was cultured in 3 mL ON in LB medium at 37°C under constant shaking, including appropriate selection antibiotics. The *E. coli* culture was used to inoculate 500-1000 mL LB medium and was incubated under the same conditions until OD_{600} was about 0.5 to 0.8. Reaching this point, the culture was given a short ice cooling, the transgene expression was induced with 0.5 mM isopropyl-β-D1-thiogalactopyranoside (IPTG) and grown at 16°C ON under constant shaking (240 rpm). To collect the bacterial pellets, the LB-culture was centrifuged at 3,220 x g for 15 min at 4°C (Eppendorf 5810R). The collected pellets were resuspended in small amounts of binding buffer and grounded using a liquid nitrogen pre-cooled mortar and pestle to fine homogeneous powder. The powder was collected in 2 mL reaction vials and thaw on ice. Supernatant was collected after 45 min centrifugation at 4°C at 20,913 x g (14.000 rpm). The

pooled cell free supernatant was filtered through a low protein binding 0.22 µm nylon filter before application on the His Gravi Trap affinity column (GE Healthcare, Germany). For the elution a 50 mM sodium phosphate buffer, pH 8 with 500 mM NaCl and 200 mM imidazole has been used. After several washing steps, protein elutions of 750 µL have been collected in 1.5 mL reaction vials. Sample clean-up was done using a desalting column (GE Healthcare PD-10) with an appropriate 100 mM potassium phosphate buffer (pH 8.0) containing 10 % glycerol and 1 mM DTT. Collected aliquots were screened with Bradford reagent: 10 µL + 200 µL diluted Bradford to quantify the total protein content. All collected aliquots have been analyzed via 12 % SDS-polyacrylamide gel electrophoresis to determine the protein purity (Table 4.5.2). Pooled purified protein has been stored at -80°C until further usage.

Table 4.5.2: Protocol of SDS gel preparation

A

12% SDS-separation gel	
30% Polyacrylamid	12 mL
1.5 M Tris (pH 8.8)	7.5 mL
10% APS	0.3 mL
10% SDS	0.3 mL
TEMED	0.01 mL
H_2O	9.89 mL
total volume	30 mL

B

5% SDS-stacking gel	
30% Polyacrylamid	1.25 mL
0.5 M Tris (pH 6,8)	2.5 mL
10% APS	0.1 mL
10% SDS	0.1 mL
TEMED	0.01 mL
H_2O	6.4 mL
total volume	10 mL

The components were added as listed. The separation gel was mixed and poured at first in between two thin glass plates (A). After polymerization of the polyacrylamide of the first gel, the stacking gel was prepared and poured on top of the first (B).

4.5.2 PBS3 activity assays

PBS3 protein assays were performed in a 50 mM Tris buffer (pH 8.8) containing 5 mM $MgCl_2$ and 5 mM ATP. For additional enzyme stability 1 mM DTE in H_2O was added as well as 5 % glycerol. The activity of PBS3 was tested with the conjugation of 10 mM AA to 5 mM carboxylic acids. Reaction mixtures were incubated at 30°C ON and stopped by heating up the mixture to 85°C for 10 min. Protein assays were analyzed via GC-MS as described above.

4.5.3 Co-incubation of crude *pbs3* leaf extracts with recombinant PBS3 enzyme

To test whether metabolites like *N*-pyr-Glu and IC-Glu are PBS3 derived or not, *A. thaliana pbs3* plant material was co-incubated with the purified PBS3 enzyme *in vitro* and subsequentially analyzed by GC-MS. Therefore, homogenized *Psm vir* infected leaf material of

pbs3 mutant plants has been extracted twice with ice cold TMS2 extraction buffer (1 mL; $CHCl_3$/MeOH/H_2O; 1:2.5:1; v/v/v), mixed well and centrifuged down at maximum speed (20,913 x g or 14.000 rpm) for 1 min. The supernatant has been evaporated through freeze drying and was resuspended in enzyme buffer (Tris-HCl; pH 8) for an ON incubation with the enzyme. The enzyme-plant extract has been derivatized for further analysis via GC-MS.

4.5.4 Subcellular localization of PBS3

Gateway cloning system

For the subcellular localization of PBS3 the enzyme was cloned using the GATEWAY® cloning system. Therefore, primer pairs containing the attB1 and attB2 site in combination with PBS3 were designed (Table 4.5.3). PCR was performed using the Platinum™ Taq DNA Polymerase High Fidelity (Invitrogen™, 11304011). The master mix was prepared as recommended by the manufacturer. The attB primer specific annealing temperature was 58°C.

Table 4.5.3: attB primer sequence

name	sequence (5' to 3')
attB1	GGG GAC AAG TTT GTA CAA AAA AGC AGG CTC ACC ATG AAG CCA ATC TTC GAT AT
attB2	GGG GAC CAC TTT GTA CAA GAA AGC TGG GTC AAT ACT GAA GAA TTT GGC TAC C

Primer pair for gateway cloning system PBS3 in pDONR207. Composition of the primer sequence: gray: attB sequence; red: pENTR/ D-Topo; black: PBS3 sequence

PCR products were run on an 1 % agarose gel with 1.5 µL ethidium bromide for control. PCR control bands of PBS3 products containing 1728 bp are shown in Figure 4.5.1. The new attB-PBS3 fragment was extracted from the agarose gel using the gel extraction kit QIAquick (Qiagen, Cat No./ID: 28115) following the manufactures instructions.

pDONR 207 entry clones using BP recombination reaction

To integrate the purified PCR sequence into the entry vector pDONR 207 (Gateway™, Invitrogen) the BP reaction was performed. Therefore, 3 µL DNA were pipetted to 1 µL pDONR 207 vector and 1 µL BP clonase®. Mixture was incubated for two hours at room temperature. Then 1 µL Proteinase K was added and incubated at 37°C for 10 min. The total reaction mixture of 6 µL was added to competent *E. coli* DH5α cells on ice (Thermo Scientific) and incubated on ice for 30 min. A heat shock for transformation was set at 42°C for 45 s and cells were directly placed on ice for 2 min. 900 µL S.O.C. media (Thermo Scientific, 15544034)

was added and incubated for 1 hour at 37°C under constant shaking. Cells were gently centrifuged at 3,000 rpm for 2 min. 750 µL of the supernatant was discarded the rest was gently resuspended and plated on pre-warmed LB-agar plates (Luria Bertani: tryptone: yeast extract: NaCl; 2:1:2 (w/w/w); plates contained 1.5 % agar) containing gentamycin and incubated ON at 37°C. Successful transformed colonies were validated via colony PCR. PCR product of pDONR 207-PBS3 is shown in Figure 4.1.1. The plasmid has been extracted from 3 mL liquid LB cultures using Miniprep Wizard® plus SV kit (Promega, TB225) in accordance to the manufacturer's instructions.

pEARLY expression clones using LR recombination reaction

The purified pDONR 207-PBS3 plasmid has been cloned into pEARLEY 102 vector containing a 35 S promoter and coding for the cfp fluorescence protein for the subcellular localization of PBS3. Therefore, 5 µL purified pDONR 207-PBS3 was incubated with 3 µL pEARLEY 102 vector (Gateway™, Invitrogen) and 2 µL LR Clonase™ II (Gateway™, Invitrogen) for at least two hours at room temperature. The transformation into competent *E. coli* DH5α and the plasmid purification was performed as described in the BP recombination reaction with the exception that LB-Agar plates contaiened kanamycin. Control PCR bands of the right PBS3 fragment of 1728 bp are shown in Figure 4.5.1.

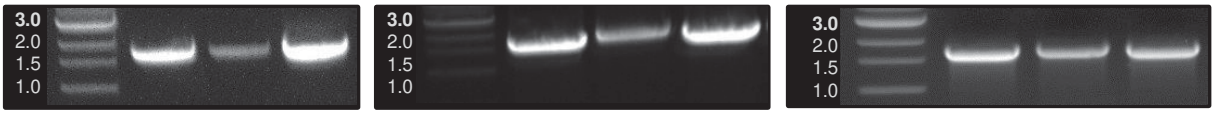

High fidelity PCR for PBS3
product size 1728bp
1 kb DNA ladder (NEB)

Colony PCR for pDONR207-PBS3
product size 1728bp
1 kb DNA ladder (NEB)

Colony PCR for pEARLY102-PBS3
product size 1728bp
1 kb DNA ladder (NEB)

Figure 4.5.1: PCR products of PBS3

Electroporation of *A. tumefaciens*

For the integration of PBS3-CFP into a plant cell, 100 µL electro-competent *Agrobacterium tumefaciens* (C58C1 pGV2260) cells (GV3101) were thaw on ice and 0.5 µL of the pEARLEY 102-PBS3 purified binary vector construct was applied. The mixture was incubated for 30 min on ice before electroporation. Therefore, the culture was transformed to a 1 mm cuvette was placed into a chamber of the electroporation machine (130-200 Ω; charging voltage: 1.44 kV; pulse: 5 ms). Directly after the electroshock, 900 µL S.O.C. media was applied and incubated at 28°C for 1 h. The culture was spread on several LB-agar plates containing kanamycin and grown at 28°C for two days. Presence of plasmid was checked by PCR and Miniprep as described previously.

Transient expression of *PBS3* in *N. tabacum*

For the transient expression in *N. tabacum* single colonies of *A. tumefaciens* containing pEARLEY 102-PBS3 were picked and grown in liquid LB-media at 28°C ON under constant shaking. Already transformed fluorescent marker genes were grown and incubated likewise. Cell cultures were centrifuged at 5,000 rpm for 10 min and the supernatant was discarded. Cells were resuspended in infiltration buffer (10 mM $MgCl_2$; 10 mM MES pH 5.6; 150 µM Acetosyringone). The final optical density was set to OD_{600}= 0.2 for all cultures. *A. tumefaciens* containing pEARLEY 102-PBS3-CFP was mixed 1:1 with the specific marker gene for co-localization. Fully grown and healthy *N. tabacum* leaves were infiltrated with a needleless syringae and the infiltrated leaf area was marked. Infiltrated plants were incubated at normal growth conditions. The fluoresce was observed 48 hpi via a laser scanning confocal microscope (Olympus FlouView-1000SP CLSM; YFP Emission wavelength: 530–555 nm, excitation: 515 nm; RFP emission wavelength: 605–630 nm, excitation: 559 nm; CFP emission wavelength: 475–500 nm, excitation: 458 nm). Microscope set up and subcellular markers were likewise as described in Barbaglia et al., 2016. Pictures were analyzed using the appropriate software (Olympus FV10-ASW 4.2 Viewer) and edited with ImageJ.

5 References

1. Thordal-Christensen, H. Fresh insights into processes of nonhost resistance. *Curr. Opin. Plant Biol.* **6**, 351–357 (2003).

2. Cui, H., Tsuda, K. & Parker, J. E. Effector-triggered immunity: from pathogen perception to robust defense. *Annu. Rev. Plant Biol.* **66**, 6.1-6.25 (2014).

3. Hartmann, M. *et al.* Flavin monooxygenase-generated *N*-hydroxypipecolic acid is a critical element of plant systemic immunity. *Cell* **173**, 456–469 (2018).

4. Hartmann, M. & Zeier, J. L-lysine metabolism to *N*-hydroxypipecolic acid: an integral immune-activating pathway in plants. *Plant J.* 1–17 (2018). doi:10.1111/tpj.14037

5. Návarová, H., Bernsdorff, F., Döring, A.-C. & Zeier, J. Pipecolic acid, an endogenous mediator of defense amplification and priming, is a critical regulator of inducible plant immunity. *Plant Cell* **24**, 5123–41 (2012).

6. Yildiz, I. *et al.* Mobile SAR signal *N*-hydroxypipecolic acid induces NPR1-dependent transcriptional reprogramming and immune priming. *Plant Physiol.* (2021). doi:10.1093/plphys/kiab166

7. Jones, J. D. G. & Dangl, J. L. The plant immune system. *Nature* **444**, 323–9 (2006).

8. Tsuda, K. & Katagiri, F. Comparing signaling mechanisms engaged in pattern-triggered and effector-triggered immunity. *Curr. Opin. Plant Biol.* **13**, 459–465 (2010).

9. Cui, H. *et al.* A core function of EDS1 with PAD4 is to protect the salicylic acid defense sector in Arabidopsis immunity. *New Phytol.* **213**, 1802–1817 (2017).

10. Wang, Y. *et al.* A MPK3/6-WRKY33-ALD1-pipecolic acid regulatory loop contributes to systemic acquired resistance. *Plant Cell* **30**, 2480–2494 (2018).

11. Coll, N. S., Epple, P. & Dangl, J. L. Programmed cell death in the plant immune system. *Cell Death Differ.* **18**, 1247–1256 (2011).

12. Mishina, T. E. & Zeier, J. Pathogen-associated molecular pattern recognition rather than development of tissue necrosis contributes to bacterial induction of systemic acquired resistance in Arabidopsis. *Plant J.* **50**, 500–13 (2007).

13. Durrant, W. E. & Dong, X. Systemic acquired resistance. *Annu. Rev. Phytopathol.* **42**, 185–209 (2004).

14. Shah, J. & Zeier, J. Long-distance communication and signal amplification in systemic acquired resistance. *Front. Plant Sci.* **4**, 30 (2013).

15. Bernsdorff, F. *et al.* Pipecolic acid orchestrates plant systemic acquired resistance and defense priming via salicylic acid-dependent and independent pathways. *Plant Cell* **28**, 102–129 (2016).

16. Sticher, L., Mauch-Mani, B. & Metrauxt, J.-P. Systemic acquired resistance. *Annu. Rev. Phytopathol.* **35**, 235–70 (1997).

17. Gruner, K., Griebel, T., Návarová, H., Attaran, E. & Zeier, J. Reprogramming of plants during systemic acquired resistance. *Front. Plant Sci.* **4**, 252 (2013).

18. Hartmann, M. & Zeier, J. *N*-hydroxypipecolic acid and salicylic acid: a metabolic duo for systemic acquired resistance. *Curr. Opin. Plant Biol.* **50**, 44–57 (2019).

19. Stahl, E., Hilfiker, O. & Reymond, P. Plant– arthropod interactions: who is the winner? *Plant J.* **93**, 703–728 (2018).

20. Hilfiker, O. *et al.* Insect eggs induce a systemic acquired resistance in Arabidopsis. *Plant J.* **80**, 1085–94 (2014).

21. Sewelam, N. *et al.* Spatial H_2O_2 signaling specificity: H2O2 from chloroplasts and peroxisomes modulates the plant transcriptome differentially. *Mol. Plant* **7**, 1191–1210 (2014).

22. Chisholm, S. T., Coaker, G., Day, B. & Staskawicz, B. J. Host-microbe interactions: shaping the evolution of the plant immune response. *Cell* **124**, 803–14 (2006).

23. Knepper, C., Savory, E. A. & Day, B. Arabidopsis NDR1 is an integrin-like protein with a role in fluid loss and plasma membrane-cell wall adhesion. *Plant Physiol.* **156**, 286–300 (2011).

24. Dhar, N. *et al.* Arabidopsis defense mutant *ndr1-1* displays accelerated development and early flowering mediated by the hormone gibberellic acid. *Plant Sci.* **285**, 200–213 (2019).

25. Day, B., Dahlbeck, D. & Staskawicz, B. J. NDR1 interaction with RIN4 mediates the differential activation of multiple disease resistance pathways in Arabidopsis. *Plant Cell* **18**, 2782–2791 (2006).

26. Shapiro, A. D. & Zhang, C. The role of NDR1 in avirulence gene-directed signaling and control of programmed cell death in Arabidopsis. *Plant Physiol.* **127**, 1089–1101 (2001).

27. Wagner, S. *et al.* Structural basis for signaling by exclusive EDS1 heteromeric complexes with SAG101 or PAD4 in plant innate immunity. *Cell Host Microbe* **14**, 619–630 (2013).

28. Feys, B. J. *et al.* Arabidopsis SENESCENCE-ASSOCIATED GENE101 stabilizes and signals within an ENHANCED DISEASE SUSCEPTIBILITY1 complex in plant innate immunity. *Plant Cell* **17**, 2601–2613 (2005).

29. Feys, B. J., Moisan, L. J., Newman, M.-A. & Parker, J. E. Direct interaction between the Arabidopsis disease resistance signaling proteins , EDS1 and PAD4. *EMO J.* **20**, 5400–5411 (2001).

30. Bartsch, M. *et al.* Salicylic acid-independent ENHANCED DISEASE SUSCEPTIBILITY1 signaling in Arabidopsis immunity and cell death is regulated by the monooxygenase FMO1 and the Nudix hydrolase NUDT7. *Plant Cell* **18**, 1038–1051 (2006).

31. Joglekar, S. *et al.* Chemical activation of EDS1/PAD4 signaling leading to pathogen resistance in Arabidopsis. *Plant Cell Physiol.* **59**, 1592–1607 (2018).

32. Chang, M. *et al.* PBS3 protects EDS1 from proteasome-mediated degradation in plant immunity. *Mol. Plant* **12**, 678–688 (2019).

33. Stahl, E., Hartmann, M., Scholten, N. & Zeier, J. A role for tocopherol biosynthesis in Arabidopsis basal immunity to bacterial infection. *Plant Physiol.* **181**, 1008–1028 (2019).

34. Hartmann, M. *et al.* Biochemical principles and functional aspects of pipecolic acid biosynthesis in plant immunity. *Plant Physiol.* **174**, 124–153 (2017).

35. Zeier, J. New insights into the regulation of plant immunity by amino acid metabolic pathways. *Plant. Cell Environ.* **36**, 2085–103 (2013).

36. Bauer, S. *et al.* UGT76B1, a promiscuous hub of small molecule-based immune signaling , glucosylates *N*-hydroxypipecolic acid , and balances plant immunity. *Plant Cell* 1–21 (2021). doi:10.1093/plcell/koaa044

37. Mohnike, L. *et al.* The glycosyltransferase UGT76B1 modulates *N*-hydroxy-pipecolic acid homeostasis and plant immunity. *Plant Cell* 1–15 (2021). doi:10.1093/plcell/koaa045

38. Chen, Y.-C. *et al. N*-hydroxy-pipecolic acid is a mobile metabolite that induces systemic disease resistance in Arabidopsis. *Proc. Natl. Acad. Sci. U. S. A.* **115**, E4920–E4929 (2018).

39. Schnake, A. *et al.* Inducible biosynthesis and immune function of the systemic acquired resistance inducer *N*-hydroxypipecolic acid in monocotyledonous and dicotyledonous plants. *J. Exp. Bot.* **71**, 6444–6459 (2020).

40. Liu, Y. *et al.* Diverse roles of the salicylic acid receptors NPR1 and NPR3/NPR4 in plant immunity. *Plant Cell* **32**, 4002–4016 (2020).

41. Garcion, C. *et al.* Characterization and biological function of the ISOCHORISMATE SYNTHASE2 gene of Arabidopsis. *Plant Physiol.* **147**, 1279–1287 (2008).

42. Vlot, A. C., Dempsey, D. A. & Klessig, D. F. Salicylic acid, a multifaceted hormone to combat disease. *Annu. Rev. Phytopathol.* **47**, 177–206 (2009).

43. Wildermuth, M. C., Dewdney, J., Wu, G. & Ausubel, F. M. Isochorismate synthase is required to synthesize salicylic acid for plant defence. *Nature* **414**, 562–5 (2001).

44. Strawn, M. A. *et al.* Arabidopsis isochorismate synthase functional in pathogen-induced salicylate biosynthesis exhibits properties consistent with a role in diverse stress responses. *J. Biol. Chem.* **282**, 5919–5933 (2007).

45. Nawrath, C. & Métraux, J.-P. Salicylic acid induction- defcient mutants of Arabidopsis express PR-2 and PR-5 and accumulate high levels of camalexin after pathogen inoculation. *Plant Cell* **11**, 1393–1404 (1999).

46. Widhalm, J. R. & Dudareva, N. A familiar ring to it: biosynthesis of plant benzoic acids. *Mol. Plant* **8**, 83–97 (2015).

47. Rekhter, D. *et al.* Isochorismate-derived biosynthesis of the plant stress hormone salicylic acid. *Science (80-.).* **502**, 498–502 (2019).

48. Serrano, M. *et al.* Export of salicylic acid from the chloroplast requires the multidrug and toxin extrusion-like. *Plant Physiol.* **162**, 1815–1821 (2013).

49. Chandran, D. *et al.* Atypical E2F transcriptional repressor DEL1 acts at the intersection of plant growth and immunity by controlling the hormone salicylic acid. *Cell Host Microbe* **15**, 506–13 (2014).

50. Nawrath, C., Heck, S., Parinthawong, N. & Métraux, J.-P. EDS5, an essential component of salicylic acid – dependent signaling for disease resistance in Arabidopsis, is a member of the MATE transporter family. *Plant Cell* **14**, 275–286 (2002).

51. Torrens-Spence, M. P. *et al.* PBS3 and EPS1 complete salicylic acid biosynthesis from isochorismate in Arabidopsis. *Mol. Plant* **12**, 1577–1586 (2019).

52. Nobuta, K. *et al.* The GH3 acyl adenylase family member PBS3 regulates salicylic acid-dependent defense responses in Arabidopsis. *Plant Physiol.* **144**, 1144–56 (2007).

53. Okrent, R. A. & Wildermuth, M. C. Evolutionary history of the GH3 family of acyl adenylases in rosids. *Plant Mol. Biol.* **76**, 489–505 (2011).

54. Zhang, Z., Wang, M., Li, Z., Li, Q. & He, Z. Arabidopsis GH3.5 regulates salicylic acid-dependent and both NPR1-dependent and independent defense responses. *Plant Signal. Behav.* **3**, 537–542 (2008).

55. Lee, M. W., Lu, H., Jung, H. W. & Greenberg, J. T. A key role for the Arabidopsis WIN3 protein in disease resistance triggered by *Pseudomonas syringae* that secrete AvrRpt2. *Mol. Plant. Microbe. Interact.* **20**, 1192–1200 (2007).

56. Wang, H., Tian, C., Duan, J. & Wu, K. Research progresses on GH3s, one family of primary auxin-responsive genes. *Plant Growth Regul* **56**, 225–232 (2008).

57. Jagadeeswaran, G. *et al.* Arabidopsis GH3-LIKE DEFENSE GENE 1 is required for

accumulation of salicylic acid, activation of defense responses and resistance to *Pseudomonas syringae*. *Plant J.* **51**, 234–246 (2007).

58. Okrent, R. A., Brooks, M. D. & Wildermuth, M. C. Arabidopsis GH3.12 (PBS3) conjugates amino acids to 4-substituted benzoates and is inhibited by salicylate. *J. Biol. Chem.* **284**, 9742–9754 (2009).

59. Berens, M. L. *et al.* Balancing trade-offs between biotic and abiotic stress responses through leaf age-dependent variation in stress hormone cross-talk. *Proc. Natl. Acad. Sci. U. S. A.* **116**, 2364–2373 (2019).

60. Rohde, A. *et al.* Molecular phenotyping of the *pal1* and *pal2* mutants of *Arabidopsis thaliana* reveals far-reaching consequences on phenylpropanoid, amino acid, and carbohydrate metabolism. *Plant Cell* **16**, 2749–2771 (2004).

61. Klessig, D. F., Choi, H. W., Dempsey, D. M. A. & Rd, T. Systemic acquired resistance and salicylic acid : past, present, and future. **31**, 871–888 (2018).

62. Dempsey, D. A., Vlot, A. C., Wildermuth, M. C. & Klessig, D. F. Salicylic acid biosynthesis and metabolism. *Arabidopsis Book* **9**, e0156 (2011).

63. Xu, L. *et al.* ABNORMAL INFLORESCENCE MERISTEM1 functions in salicylic acid biosynthesis to maintain proper reactive oxygen species levels for root meristem activity in rice. *Plant Cell* **29**, 560–574 (2017).

64. Bussell, J. D., Reichelt, M., Wiszniewski, A. A. G., Gershenzon, J. & Smith, S. M. Peroxisomal ATP-binding cassette transporter COMATOSE and the multifunctional protein ABNORMAL INFLORESCENCE MERISTEM are required for the production of benzoylated metabolites in Arabidopsis seeds. *Plant Physiol.* **164**, 48–54 (2014).

65. Wu, Y. *et al.* The Arabidopsis NPR1 protein is a receptor for the plant defense hormone salicylic acid. *Cell Rep.* **1**, 639–47 (2012).

66. Ding, Y. *et al.* Opposite roles of salicylic acid receptors NPR1 and NPR3/NPR4 in transcriptional regulation of plant immunity. *Cell* **173**, 1454–1467 (2018).

67. Delaney, T. P. *et al.* A central role of salicylic acid in plant disease resistance. *Science (80-.).* **266**, 1247–1250 (1994).

68. Cao, H., Bowling, S. A., Gordon, A. S. & Dong, X. Characterization of an Arabidopsis mutant that is nonresponsive to inducers of systemic acquired resistance. *Plant Cell* **6**, 1583–1592 (1994).

69. Shah, J., Tsui, F. & Klessig, D. F. Characterization of a salicylic acid–insensitive mutant (*sai1*) of *Arabidopsis thaliana*, identified in a selective Screen utilizing the SA-inducible expression of the *tms2* gene. *Mol. Plant-Microbe Interact.* **10**, 69–78 (1997).

70. Mhamdi, A. NPR1 has everything under control. *Plant Physiol.* **181**, 6–7 (2019).

71. Chen, J. *et al.* NPR1 promotes its own and target gene expression in plant defense by recruiting CDK8. *Plant Physiol.* **181**, 289–304 (2019).

72. Fan, W. & Dong, X. *In vivo* interaction between NPR1 and transcription factor TGA2 leads to salicylic acid – mediated gene activation in Arabidopsis. *Plant Cell* **14**, 1377–1389 (2002).

73. Kinkema, M., Fan, W. & Dong, X. Nuclear localization of NPR1 is required for activation of PR gene expression. *Plant Cell* **12**, 2339–2350 (2000).

74. Zhang, Y., Tessaro, M. J., Lassner, M. & Li, X. Knockout analysis of Arabidopsis transcription factors TGA2, TGA5, and TGA6 reveals their redundant and essential roles in systemic acquired resistance. *Plant Cell* **15**, 2647–2653 (2003).

75. Fu, Z. Q. *et al.* NPR3 and NPR4 are receptors for the immune signal salicylic acid in plants. *Nature* **486**, 228–32 (2012).

76. Attaran, E., Zeier, T. E., Griebel, T. & Zeier, J. Methyl salicylate production and jasmonate signaling are not essential for systemic acquired resistance in Arabidopsis. *Plant Cell* **21**, 954–71 (2009).

77. Liu, P.-P., von Dahl, C. C. & Klessig, D. F. The extent to which methyl salicylate is required for signaling systemic acquired resistance is dependent on exposure to light after infection. *Plant Physiol.* **157**, 2216–26 (2011).

78. Chen, L. *et al.* Methyl salicylate glucosylation regulates plant defense signaling and systemic acquired resistance. *Plant Physiol.* **180**, 2167–2181 (2019).

79. Lim, E. K. *et al.* The activity of Arabidopsis glycosyltransferases toward salicylic acid, 4-hydroxybenzoic acid, and other benzoates. *J. Biol. Chem.* **277**, 586–592 (2002).

80. Dean, J. V. & Delaney, S. P. Metabolism of salicylic acid in wild-type, ugt74f1 and ugt74f2 glucosyltransferase mutants of *Arabidopsis thalian*a. *Physiol. Plant.* **132**, 417–425 (2008).

81. Thompson, A. M. G., Iancu, C. V, Neet, K. E., Dean, J. V & Choe, J. Differences in salicylic acid glucose conjugations by UGT74F1 and UGT74F2 from *Arabidopsis thaliana*. *Nat. Publ. Gr.* **7**, 1–11 (2017).

82. Noutoshi, Y. *et al.* Novel plant immune-priming compounds identified via high-throughput chemical screening target salicylic acid glucosyltransferases in Arabidopsis. *Plant Cell* **24**, 3795–3804 (2012).

83. Seo, S., Ishizuka, K. & Ohashi, Y. Induction of salicylic acid ß-glucosidase in Tobacco leaves by exogenous salicylic acid. *Plant Cell Physiol.* **36**, 447–453 (1995).

84. Hennig, J., Malamy, J., Grynkiewicz, G., Indulski, J. & Klessig, D. F. Interconversion of the salicylic acid signal and its glucoside in tobacco. *Plant J.* **4**, 593–600 (1993).

85. Zhang, K., Halitschke, R., Yin, C., Liu, C.-J. & Gan, S.-S. Salicylic acid 3-hydroxylase regulates Arabidopsis leaf longevity by mediating salicylic acid catabolism. *Proc. Natl. Acad. Sci. U. S. A.* **110**, 14807–12 (2013).

86. Zhang, Y. *et al.* S5H/ DMR6 encodes a salicylic A acid 5-hydroxylase that fine-tunes salicylic acid homeostasis. *Plant Physiol.* **175**, 1082–1093 (2017).

87. Ibrahim, R. K. & Towers, G. H. N. Conversion of salicylic acid to gentisic acid and o-pyrocatechuic acid, all labelled with carbon-14, in plants. *Nature* **4701**, 1803 (1959).

88. Bartsch, M. *et al.* Accumulation of isochorismate-derived 2,3-dihydroxybenzoic 3-O-ß-D-xyloside in Arabidopsis resistance to pathogens and ageing of leaves. *J. Biol. Chem.* **285**, 25654–25665 (2010).

89. Chen, H. & Li, X. Identification of a residue responsible for UDP-sugar donor selectivity of a dihydroxybenzoic acid glycosyltransferase from Arabidopsis natural accessions. *Plant J.* **89**, 195–203 (2017).

90. Huang, X. *et al.* Modulation of plant salicylic acid-associated immune responses via glycosylation of dihydroxybenzoic acids. *Plant Physiol.* **176**, 3103–3119 (2018).

91. Westfall, C. S., Muehler, A. M. & Jez, J. M. Enzyme action in the regulation of plant hormone responses. *J. Biol. Chem.* **288**, 19304–19311 (2013).

92. Staswick, P. E., Tiryaki, I. & Rowe, M. L. Jasmonate response locus JAR1 and several related Arabidopsis genes encode enzymes of the firefly luciferase superfamily that show activity on jasmonic , salicylic, and indole-3-acetic acids in an assay for adenylation. *Plant Cell* **14**, 1405–1415 (2002).

93. Meesters, C. *et al.* A chemical inhibitor of jasmonate signaling targets JAR1 in *Arabidopsis thaliana. Nat. Chem. Biol.* **10**, 830–838 (2014).

94. Leclere, S., Tellez, R., Rampey, R. A., Matsuda, S. P. T. & Bartel, B. Characterization of a family of IAA-amino acid conjugate hydrolases from Arabidopsis. *J. Biol. Chem.* **277**, 20446–20452 (2002).

95. Westfall, C. S. *et al. Arabidopsis thaliana* GH3.5 acyl acid amido synthetase mediates metabolic crosstalk in auxin and salicylic acid homeostasis. *PNAS* **113**, 13917–13922 (2016).

96. Mackelprang, R., Okrent, R. A. & Wildermuth, M. C. Preference of *Arabidopsis thaliana* GH3.5 acyl amido synthetase for growth versus defense hormone acyl substrates is dictated by concentration of amino acid substrate aspartate. *Phytochemistry* **143**, 19–28 (2017).

97. Chen, Y., Shen, H., Wang, M., Li, Q. & He, Z. Salicyloyl-aspartate synthesized by the acetyl-amido synthetase GH3.5 is a potential activator of plant immunity in Arabidopsis. *Acta Biochim. Biophys. Sin. (Shanghai).* **45**, 827–836 (2013).

98. Suzuki, Y., Yamaguchi, I., Murofushi, N. & Takahashi, N. Biological conversion of benzoic acid in Lemna paucicostata 151 and its relation to flower induction. *Plant Cell Physiol.* **29**, 439–444 (1988).

99. Bourne, D. J., Barrow, K. D. & Milborrow, B. V. Salicyloylaspartate as an endogenous component in the leaves of *Phaseolus vulgaris*. *Phytochemistry* **30**, 4041–4044 (1991).

100. Steffan, H., Ziegler, A. & Rapp, A. *N*-Salicyloyl-Asparaginsäure: Eine neue phenolische Verbindung aus Reben. *Vitis* **86**, 79–86 (1988).

101. Venis, M. A. Auxin-induced conjugation systems in peas. *Plant Physiol.* **49**, 24–27 (1972).

102. Gaffney, T. *et al.* Requirement of salicylic acid for the induction of systemic acquired resistance. *Science (80-.).* **261**, 754–756 (1993).

103. Wees, S. C. M. Van & Glazebrook, J. Loss of non-host resistance of Arabidopsis *NahG* to *Pseudomonas syringae* pv. *phaseolicola* is due to degradation products of salicylic acid. *Plant J.* **33**, 733–742 (2003).

104. Stahl, E. *et al.* Regulatory and functional aspects of indolic metabolism in plant systemic acquired resistance. *Mol. Plant* 1–20 (2016). doi:10.1016/j.molp.2016.01.005

105. Glazebrook, J., Ausubel, F. M. & Frederick, M. Isolation of phytoalexin-deficient mutants of *Arabidopsis thaliana* and characterization of their interactions with bacterial pathogens. *Proc. Natl. Acad. Sci. U. S. A.* **91**, 8955–8959 (1994).

106. Glawischnig, E. Camalexin. **68**, 401–406 (2007).

107. Song, J. T., Lu, H., McDowell, J. M. & Greenberg, J. T. A key role for ALD1 in activation of local and systemic defenses in Arabidopsis. *Plant J. cell Mol. Biol.* **40**, 200–12 (2004).

108. Cecchini, M., Ine, M. & Alvarez, E. Proline dehydrogenase contributes to pathogen defense. **155**, 1947–1959 (2011).

109. Zeier, J. New insights into the regulation of plant immunity by amino acid metabolic pathways. *Plant. Cell Environ.* **36**, 2085–103 (2013).

110. Nafisi, M., Fimognari, L. & Sakuragi, Y. Interplays between the cell wall and phytohormones in interaction between plants and necrotrophic pathogens. *Phytochemistry* (2014). doi:10.1016/j.phytochem.2014.11.008

111. Staswick, P. E. & Tiryaki, I. The oxylipin signal jasmonic acid is activated by an enzyme that conjugates it to isoleucine in Arabidopsis. *Am. Soc. Plant Biol.* **16**, 2117–2127 (2004).

112. Glazebrook, J. Contrasting mechanisms of defense against biotrophic and necrotrophic pathogens. *Annu. Rev. Phytopathol.* **43**, 205–227 (2005).

113. Sperschneider, J. *et al.* LOCALIZER: subcellular localization prediction of both plant and effector proteins in the plant cell. *Nat. Publ. Gr.* **7:44598**, 1–14 (2017).

114. Larsen, P. O. & Wieczorkowska, E. Intermediates in the metabolism of m-carboxy-substituted aromatic amino acids in plants. *Biochim. Biophys. Acta* **381**, 409–415 (1975).

115. Larsen, P. O., Onderka, D. K. & Floss, H. G. Biosynthesis of phenylalanine, tyrosine, 3-(3-carboxyphenyl)alanine and 3-(3-carboxy-4-hydroxyphenyl)alanine in higher plants. *Biochim. Biophys. Acta* **381**, 397–408 (1975).

116. Zamir, L. O., Nikolakakis, A., Bonner, C. A. & Jensen, R. A. Evidence for enzymatic formation of isoprephenate from isochorismate. *Bioorganic Med. Chem. Lett.* **3**, 1441–1446 (1993).

117. Gerald Rosenthal. *Plant nonprotein amino and imino acids: biological, biochemical, and toxicological properties*. *Elsevier* (2012).

118. DeClue, M. S., Baldridge, K. K., Kast, P. & Hilvert, D. Experimental and computational investigation of the uncatalyzed rearrangement and elimination reactions of isochorismate. *J. Am. Chem. Soc.* **128**, 2043–2051 (2006).

119. Young, I. G., Batterham, T. J. & Gibson, F. The isolation, identification and properties of isochorismic acid. an intermediate in the biosynthesis of 2,3-dihydroxybenzoic acid. *Biochim. Biophys. Acta* **26**, 389–400 (1969).

120. Aarts, M. G. M., Keijzer, C. J., Stiekema, W. J. & Pereira, A. Molecular characterization of the CER1 gene of Arabidopsis involved in epicuticular wax biosynthesis and pollen fertility. *Plant Cell* **7**, 2115–2127 (1995).

121. Le, A. *et al.* Overexpression of Arabidopsis ECERIFERUM1 promotes wax very-long-chain alkane biosynthesis and influences plant response to biotic and abiotic stresses. *Plant Physiol.* **156**, 29–45 (2011).

122. Zerong, W. Barbier-Wieland degradation. in *Comprehensive organic name reactions and reagents* 210–214 (John Wiley & Sons, Inc., 2010).

123. Garattini, E., Fratelli, M. & Terao, M. Mammalian aldehyde oxidases : genetics, evolution and biochemistry. *Cell. Mol. Life Sci.* **65**, 1019–1048 (2008).

124. Seo, M. *et al.* Abscisic aldehyde oxidase in leaves of *Arabidopsis thaliana. Plant J.* **23**, 481–488 (2000).

125. Koiwai, H., Akaba, S., Seo, M., Romano, T. & Koshiba, T. Functional expression of two Arabidopsis aldehyde oxidases in the yeast Pichia pastoris. *J. Biol. Chem.* **664**, 659–664 (2000).

126. Böttcher, C. *et al.* The biosynthetic pathway of indole-3-carbaldehyde and indole-3-carboxylic acid derivatives in Arabidopsis. *Plant Physiol.* **165**, 841–853 (2014).

127. Ibdah, M., Chen, Y., Wilkerson, C. G. & Pichersky, E. An aldehyde oxidase in developing seeds of Arabidopsis converts benzaldehyde to benzoic acid. *Plant Physiol.* **150**, 416–423 (2009).

128. Srivastava, S. *et al.* Aldehyde oxidase 4 plays a critical role in delaying silique senescence by catalyzing aldehyde detoxification. *Plant Physiol.* **173**, 1977–1997 (2017).

129. Qian, Y. *et al.* Completion of the cytosolic post-chorismate phenylalanine biosynthetic pathway in plants. *Nat. Commun.* **10:15**, 1–15 (2019).

130. Dewdney, J. *et al.* Three unique mutants of Arabidopsis identify eds loci required for limiting growth of a biotrophic fungal pathogen. *Plant J.* **24**, 205–218 (2000).

131. Chapman, P. J. & Hopper, D. J. The bacterial metabolism of 2,4-xylenol. *Biochem. J.* **110**, 491–498 (1968).

132. Chao, H.-J. *et al.* HipH catalyzes the hydroxylation of 4-hydroxyisophthalate to protocatechuate in 2,4-xylenol catabolism by *Pseudomonas putida*. *Appl. Environ. Microbiol.* **82**, 724–731 (2016).

133. Döring, A.-C. Exploring the role of pipecolic acid in defence priming and inducible immunity in *Arabidopsis thaliana* (L.) Heynh. (2015).

134. Finkemeier, I. & Sweetlove, L. J. The role of malate in plant homeostasis. *Biol. Reports* **3**, 10–12 (2009).

135. Zhang, Z. *et al.* Dual regulation role of GH3.5 in salicylic acid and auxin signaling during Arabidopsis-*Pseudomonas syringae* interaction. *Plant Physiol.* **145**, 450–464 (2007).

136. Holland, C. K. *et al.* Brassicaceae-specific Gretchen Hagen 3 acyl acid amido synthetases conjugate amino acids to chorismate , a precursor of aromatic amino acids and salicylic acid. *J. Biol. Chem.* **294**, 16855–16864 (2019).

137. Bernsdorff, F. E. M. On the role of amino acids in plant disease resistance: Interplay between pipecolic acid and salicylic acid in plant systemic acquired resistance. (2014).

138. Dean, J. V & Mills, J. D. Uptake of salicylic acid 2-*O*-ß-D-glucose into soybean tonoplast vesicles by an ATP-binding cassette transporter-type mechanism. *Physiol. Plant.* **120**, 603–612 (2004).

139. Li, W. *et al.* Nicotinate *O*-glucosylation is an evolutionarily metabolic trait important for seed germination under stress conditions in Arabidopsis thaliana. *Plant Cell* **27**, tpc.15.00223 (2015).

140. Ryals, J. A. *et al.* Systemic acquired resistance. *Plant Cell* **8**, 1809–1819 (1996).

141. Mantz, M. Untersuchungen zur pflanzlichen Immunabwehr in Ökotypen von *Arabidopsis thaliana* mit natürlichen Variationen in abwehrrelevanten Genen. (2016).

142. Scholten, N. Die durch Flagellin induzierte Immunantwort in Angiospermen verstärkt durch Pipecolinsäure. (2015).

143. Vernooij, B. *et al.* Salicylic acid is not the translocated signal responsible for inducing systemic acquired resistance but is required in signal transduction. *Plant Cell* **6**, 959–965 (1994).

144. Schweigert, N., Zehnder, A. J. B. & Eggen, R. I. L. Chemical properties of catechols and their molecular modes of toxic action in cells, from microorganisms to mammals. *Environ. Microbiol.* **3**, 81–91 (2001).

145. Zurbriggen, M. D., Carrillo, N. & Hajirezaei, M.-R. ROS signaling in the hypersensitive response. *Plant Signal. Behav.* **5**, 393–396 (2010).

146. Moschou, P. N. *et al.* The polyamines and their catabolic products are significant players in the turnover of nitrogenous molecules in plants. *J. Exp. Bot.* **63**, 5003–5015 (2012).

147. Heck, S., Grau, T., Buchala, A., Métraux, J.-P. & Nawrath, C. Genetic evidence that expression of *NahG* modifies defence pathways independent of salicylic acid biosynthesis in the Arabidopsis-*Pseudomonas syringae* pv. *tomato* interaction. *Plant J.* **4**, 342–352 (2003).

148. Zhou, N., Tootle, T. L., Tsui, F., Klessig, D. F. & Glazebrook, J. PAD4 functions upstream from salicylic acid to control defense responses in Arabidopsis. *Plant Cell* **10**, 1021–1030 (1998).

149. Mishina, T. E. & Zeier, J. The Arabidopsis flavin-dependent monooxygenase FMO1 is an essential component of biologically induced systemic acquired resistance. *Plant Physiol.* **141**, 1666–1675 (2006).

150. Lawton, K. *et al.* Systemic acquired resistance in Arabidopsis requires salicylic acid but not ethylene. *MPMI* **8**, 863–870 (1995).

151. Century, K. S., Holubt, E. B. & Staskawiczt, B. J. NDR1, a locus of *Arabidopsis thaliana* that is required for disease resistance to both a bacterial and a fungal pathogen. *PNAS US* **92**, 6597–6601 (1995).

152. Glazebrook, J. *et al.* Phytoalexin-deficient mutants of Arabidopsis reveal that pad4 encodes a regulatory factor and that four pad genes contribute to downy mildew resistance. *Genet. Soc. Am.* **146**, 381–392 (1997).

153. Warren, R. F., Merritt, P. M., Holub, E. & Innes, R. W. Identification of three putative signal transduction genes involved in R gene-Specified disease resistance in Arabidopsis. (1999).

154. Nawrath, C. & Métraux, J.-P. Salicylic acid induction – deficient mutants of Arabidopsis express PR-2 and PR-5 and accumulate high levels of camalexin after pathogen inoculation. *Plant Cell* **11**, 1393–1404 (1999).

155. King, E., Ward, M. & Raney, D. Two simple media for the demonstration of pyocyanin and fluorescin. *J. Lab. Clin. Med.* **44**, 13184240 (1954).

156. Studier, F. W. Use of bacteriophage T7 lysozyme to improve an inducible T7 expression system. *J. Mol. Biol.* **219**, 37–44 (1991).

157. Ritter, C. & Dangl, J. L. The avrRpm1 gene of *Pseudomonas syringae* pv. *maculicola* is required for virulence on Arabidopsis. *Mol. Plant-Microbe Interact.* **8**, 444–453 (1995).

158. Fan, J., Crooks, C. & Lamb, C. High-throughput quantitative luminescence assay of the growth in planta of *Pseudomonas syringae* chromosomally tagged with *Photorhabdus luminescens* luxCDABE. 393–399 (2008). doi:10.1111/j.1365-313X.2007.03303.x

159. Dong, X., Mindrinos, M., Keith, R. D. & Ausubel, F. M. lnduction of Arabidopsis defense genes by virulent and avirulent *Pseudomonas syringae* strains and by a cloned avirulence gene. *Plant Cell* **3**, 61–72 (1991).

160. Schmelz, E. A., Engelberth, J., Tumlinson, J. H., Block, A. & Alborn, H. T. The use of vapor phase extraction in metabolic profiling of phytohormones and other metabolites. *Plant J.* **39**, 790–808 (2004).

161. Anderl, J. Synthese und Cytotoxizität membranpermeabler Phallotoxine. (2003).

162. Barbaglia, A. M., Tamot, B., Greve, V. & Hoffmann-Benning, S. Phloem proteomics reveals new lipid-binding proteins with a putative role in lipid-mediated signaling. *Front. Plant Sci.* **7:563**, 1–13 (2016).

6 Summary

To combat pathogens, plants have evolved a multi-layered immune system which is based on a complex signaling network controlled by plant hormones and defense-related metabolites. Comparative metabolite-profiling with leaf extracts of *Pseudomonas syringae* (*Psm*) inoculated and uninfected *Arabidopsis thaliana* plants indicate that more than 100, partially uncharacterized, metabolites with a potential function in plant immunity accumulate in leaves upon pathogen challenge. Crucial defense-regulatory metabolites include the phytohormone salicylic acid (SA) and the hydroxylated non-proteinogenic amino acid *N*-hydroxypipecolic acid (NHP) and its precursor pipecolic acid (Pip). In this study, we extended the hitherto described isochorismate pathway by nine previously unknown molecular species. The results were achieved using a combination of gas chromatography with mass spectrometry (GC-MS) and Fourier transform infrared spectroscopy (GC-FTIR). Combining the analytical and spectroscopic data, the chemical structures of the molecular species were reconstructed and identified. The identity of most molecular species was proven by authentic standard substances or chemical synthesis. With SA-Mal we discovered and identified a novel SA derivative *in planta*. However, the involvement of SA-Mal in plant immunity remains to be investigated. Moreover, we proved ICS1 and PBS3 dependency of isochorismoyl-Glu and *N*-pyruvoyl-Glu and thereby underlined the central involvement of PBS3 in SA biosynthesis and plant defense, in agreement with latest research results. Besides the high pathogen-dependent accumulation of all identified molecular species, the remaining six molecular species, 3-formylbenzoic acid, 5-formylsalicylic acid, 3-carboxybenzoic acid, 5-carboxysalicylic acid, 3-(carboxymethyl)-benzoic acid, and 5-(carboxymethyl)-salicylic acid, revealed no severe influence on plant immunity. Since we could prove that none of the six molecular species share a common origin with SA and BA, we propose that isoprephenic acid and 3-carboxyphenylpyruvate describe the missing link to fit all six molecular species into the isochorismate pathway.

The transgenic *NahG* line has been established to study SA-dependent defense in *A. thaliana*. Our data indicates that the introduced SA-hydroxylase, also severely influences the NHP and Pip metabolism and has broader involvement to plant immunity than previously assumed. Whether NAHG directly accepts and hydroxylases NHP and Pip is one important goal to achieve in the future. Overall, the results of this study contribute to unravel the complex metabolic reprogramming induced in plants upon pathogen inoculation and identify novel regulatory metabolites in plant immunity.

7 Appendix

7.1 Supplemental Material

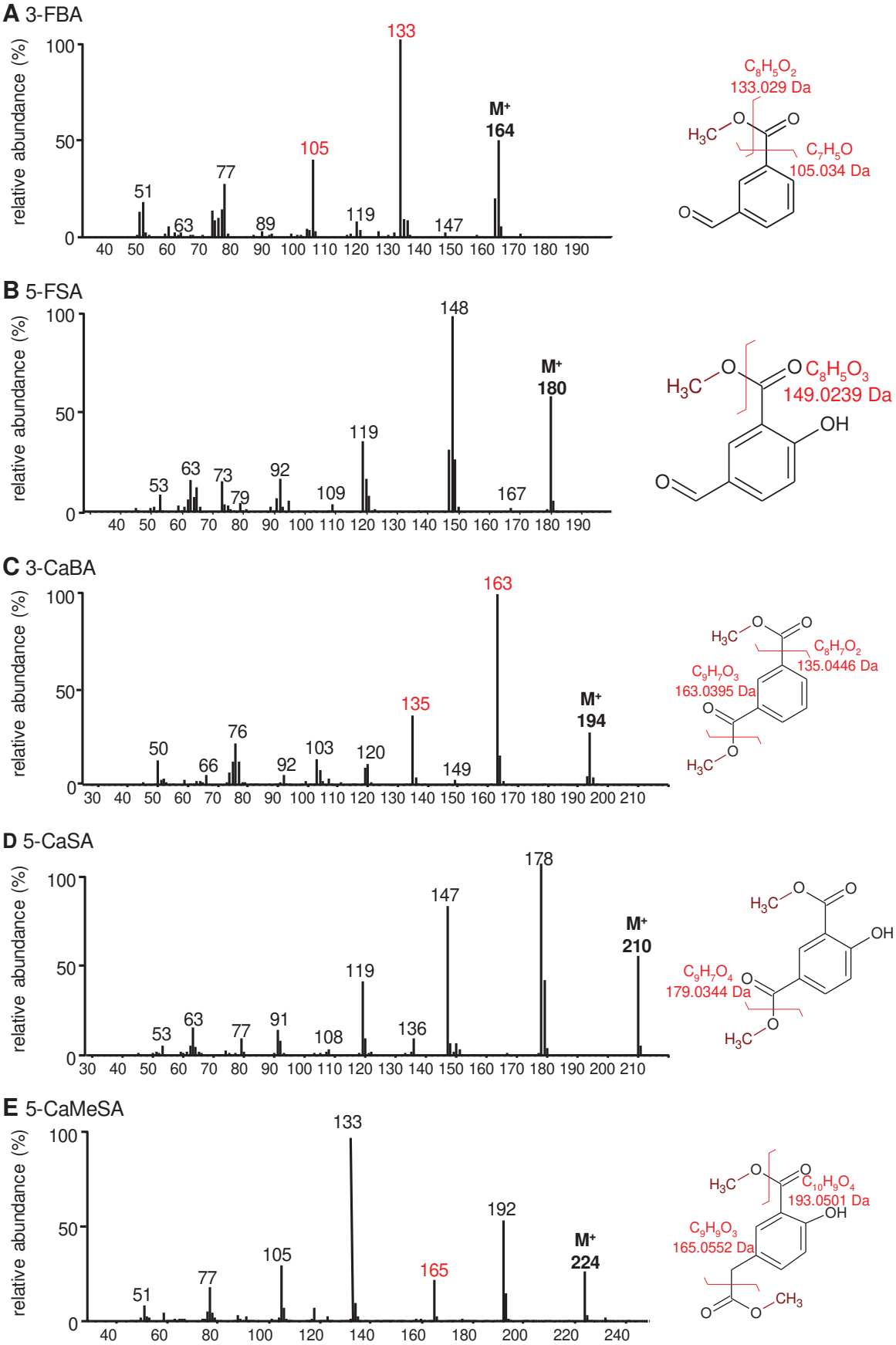

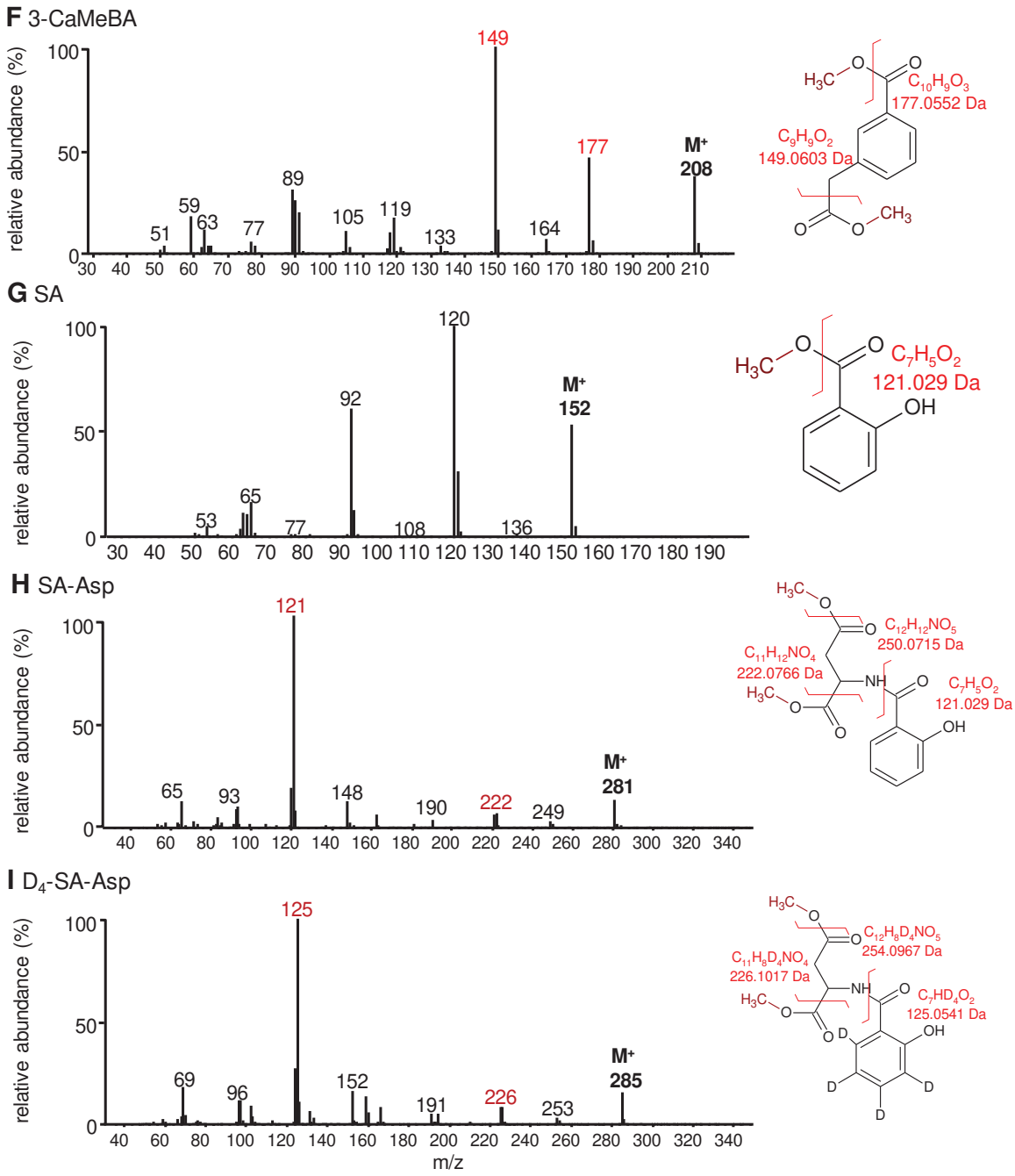

Figure S1: GC-MS mass spectra of methylated molecular species
All substances have been extracted via VPE-method and were methylated with trimethyl diazomethane. Introduced methyl groups were indicated in red. Putative molecular fragmentation and corresponding ion fragments were indicated in red.

A 3-FBA

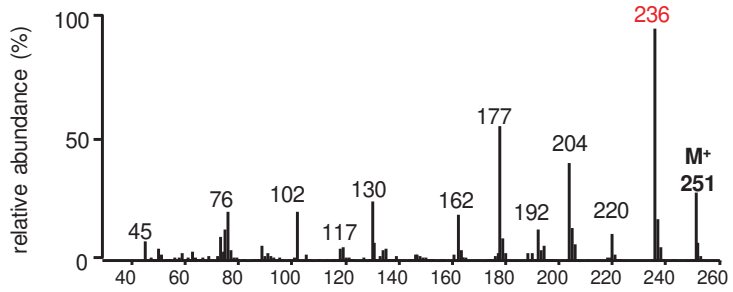

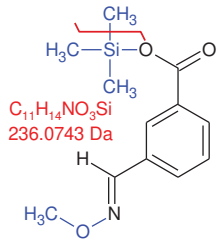

B 5-FSA

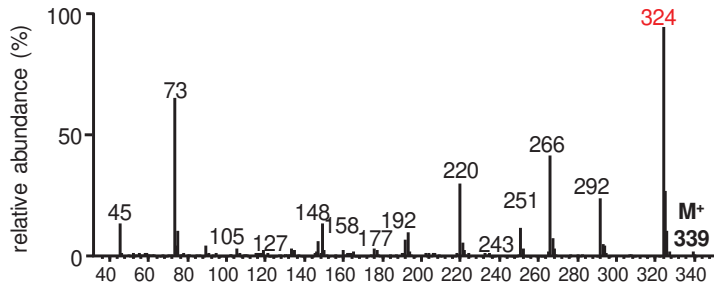

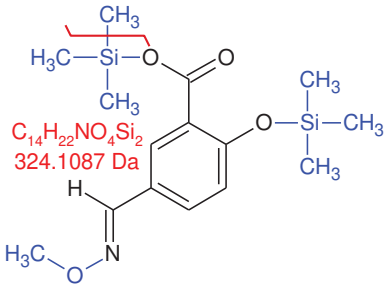

C 5-FSA

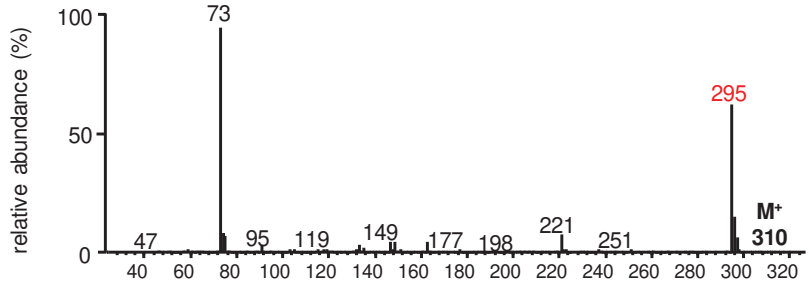

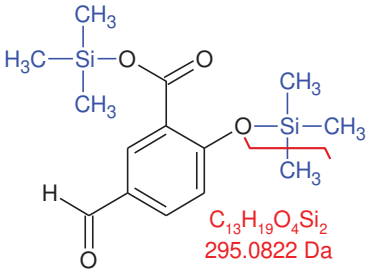

D 5-CaSA

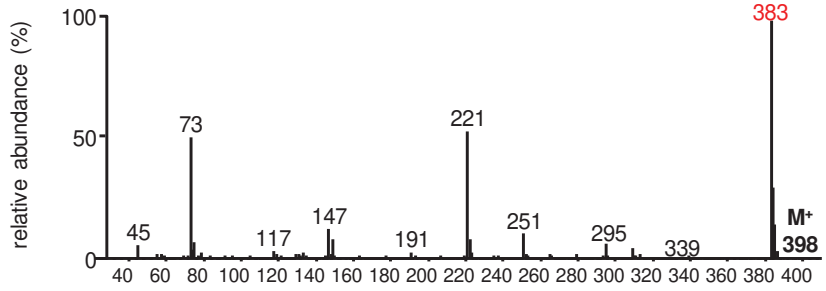

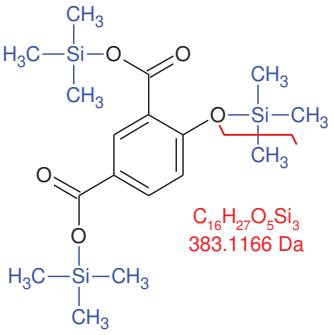

E 5-CaMeSA

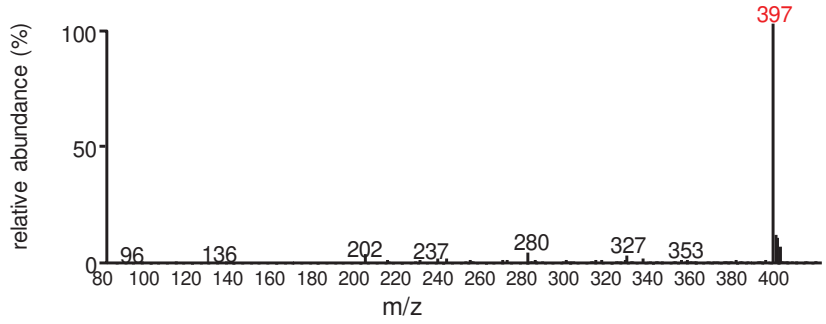

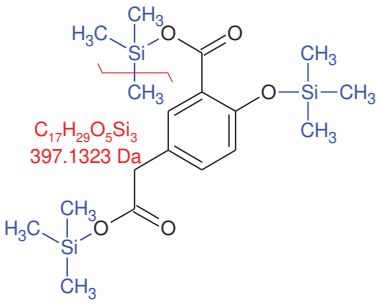

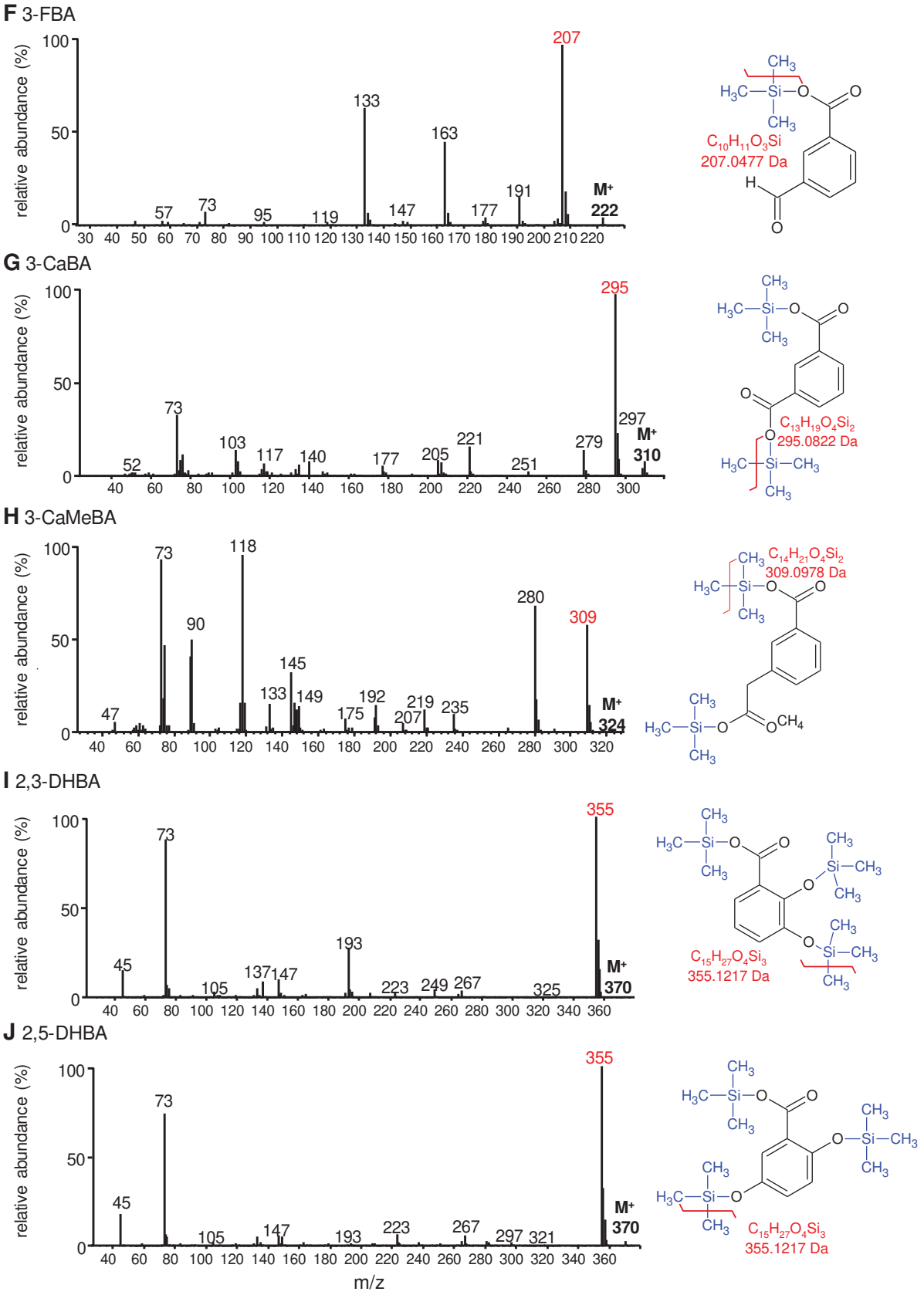

Figure S2: GC-MS mass spectra of silylated molecular species
All substances have been extracted via TMS-method and were silylated with MASTFA or BSTFA. The aldehydes in (A) and (B) were previously treated with MA HCl forming an oxime, which are colored in blue. Introduced trimethylsilyl (TMS) groups are indicated in blue, as well. Putative molecular fragmentation and corresponding ion fragments are indicated in red.

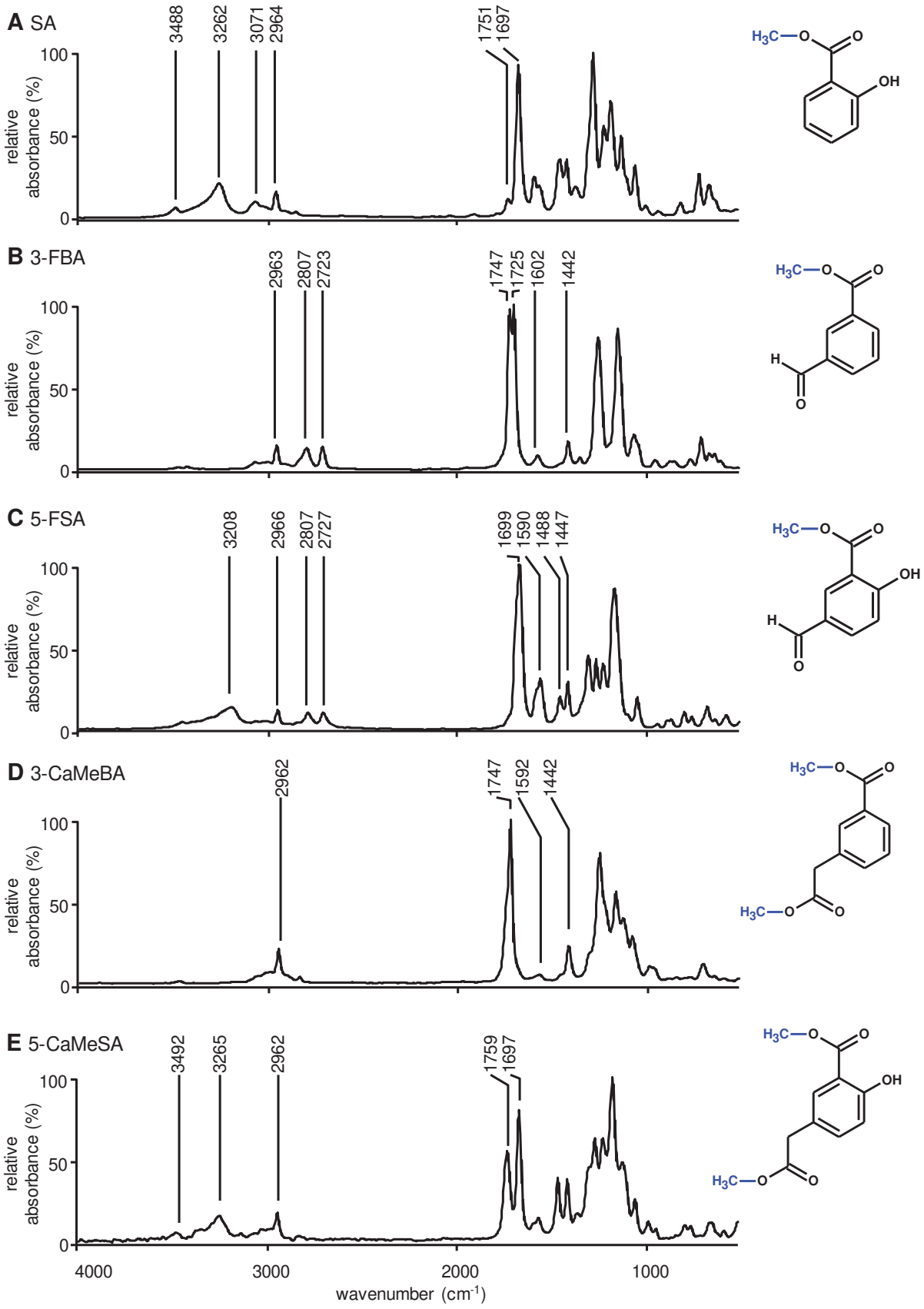
A SA
3488
3262
3071
2964
1751
1697
B 3-FBA
2963
2807
2723
1747
1725
1602
1442
C 5-FSA
3208
2966
2807
2727
1699
1590
1488
1447
D 3-CaMeBA
2962
1747
1592
1442
E 5-CaMeSA
3492
3265
2962
1759
1697
relative absorbance (%)
100
50
0
4000
3000
2000
1000
wavenumber (cm-1)
H3C—O
O
OH
H

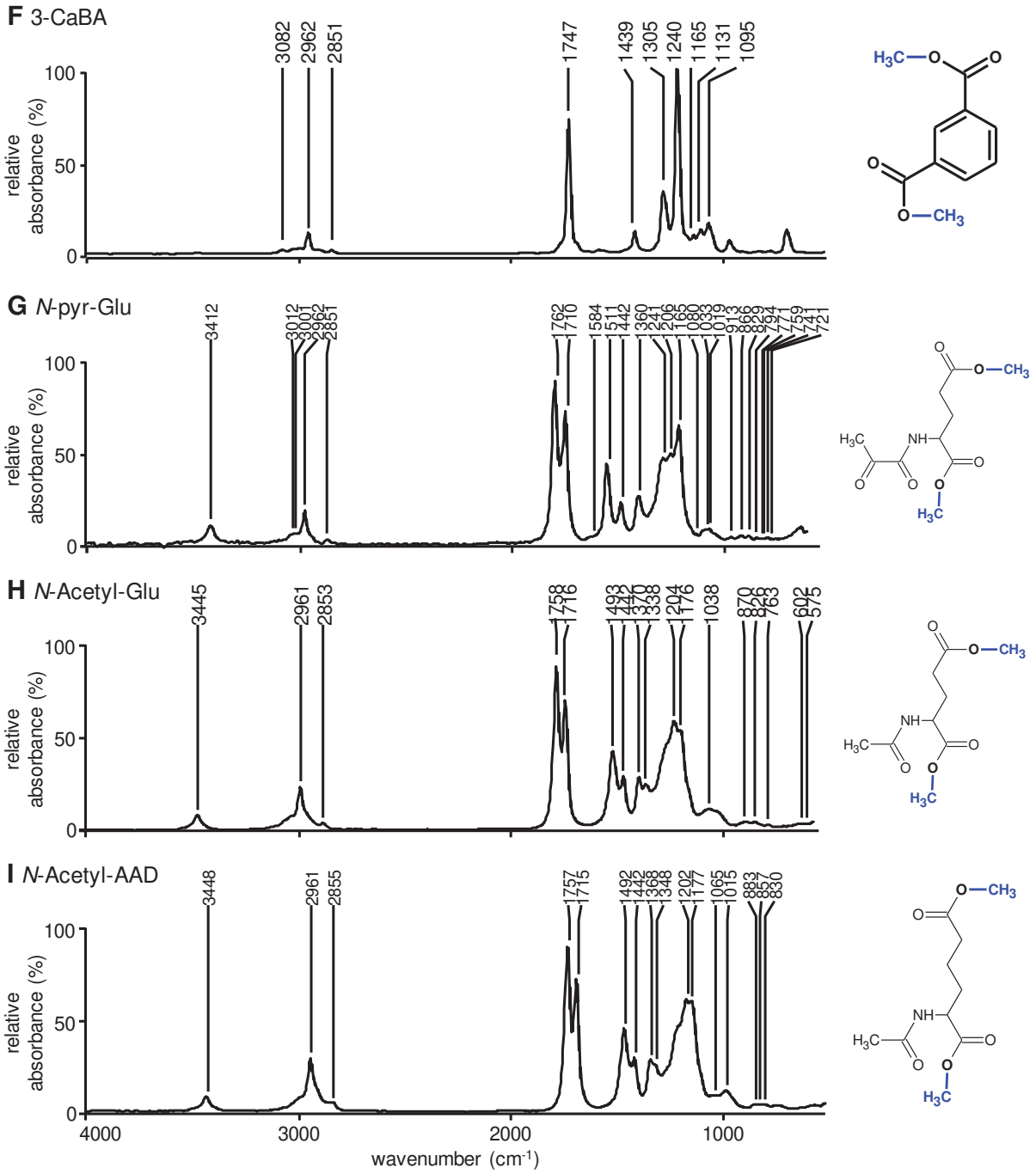

Figure S3: GC-FTIR spectra of methylated molecular species
GC-FTIR chromatograms depict authentic standard substances of molecular species, except 5-CaMeSA (E) and *N*-pyr-Glu (H) which are plant extracts. Samples have been methylated with trimethyl diazomethane for derivatization. Introduced methyl groups were indicated to the molecular structure in blue. Metabolic characteristic vibrations for specific groups were highlighted in the tables on the right (A-E).

Table S1: IR-stretching of chemical groups at certain wavelength (cm^{-1}) and corresponding assignment

ν (cm^{-1})	assignment	
3647	O-H	free strech
3412	N-H	amide strech
3492 - 3488	O-H	free strech in hydrogen bonding
3265 - 3208	O-H	strech in hydrogen bonding
3071	=C-H	aromatic strech
2964 - 2962	-C-H	aliphatic strech
2807 - 2723	O=C-H	aldehyde stretch
1759 - 1747	O=C-	free carbonyl strech
1725	O=C-O	ester conjugated carbonyl strech
1710	O=C-N	amide conjugated carbonyl strech
1699 - 1697	-OH O=C-	carbonyl strech in hydrogen bonding

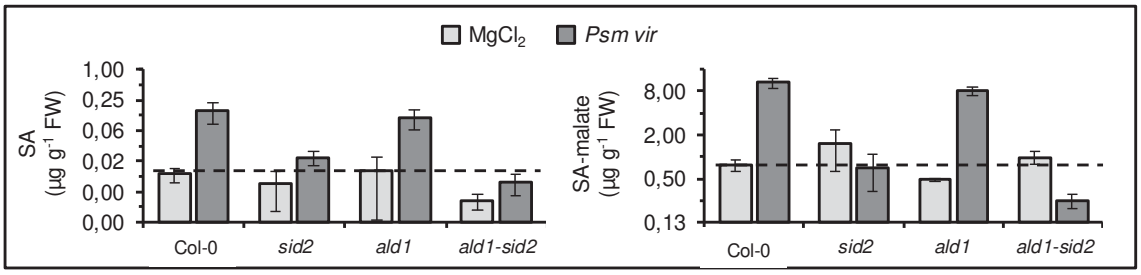

Figure S4: Accumulation pattern of molecular species in defense-related mutants
The figure shows the accumulation pattern of defense-related mutant, *pbs3, fmo1* and *ald1,* 48 hpi with *Psm vir* and mock control infiltrated with 10 mM $MgCl_2$. Data represents experiment RB30, including three biological replicates (three leaves of six plants per treatment were harvested). Samples have been methylated for derivatization. Not analyzable traces of metabolites were delcared as not detected (nd). The y-axes have a log_2 scaling. Experiment was conducted by Fredericke Bernsdorff (RB30) and analyzed by Nicola Scholten.

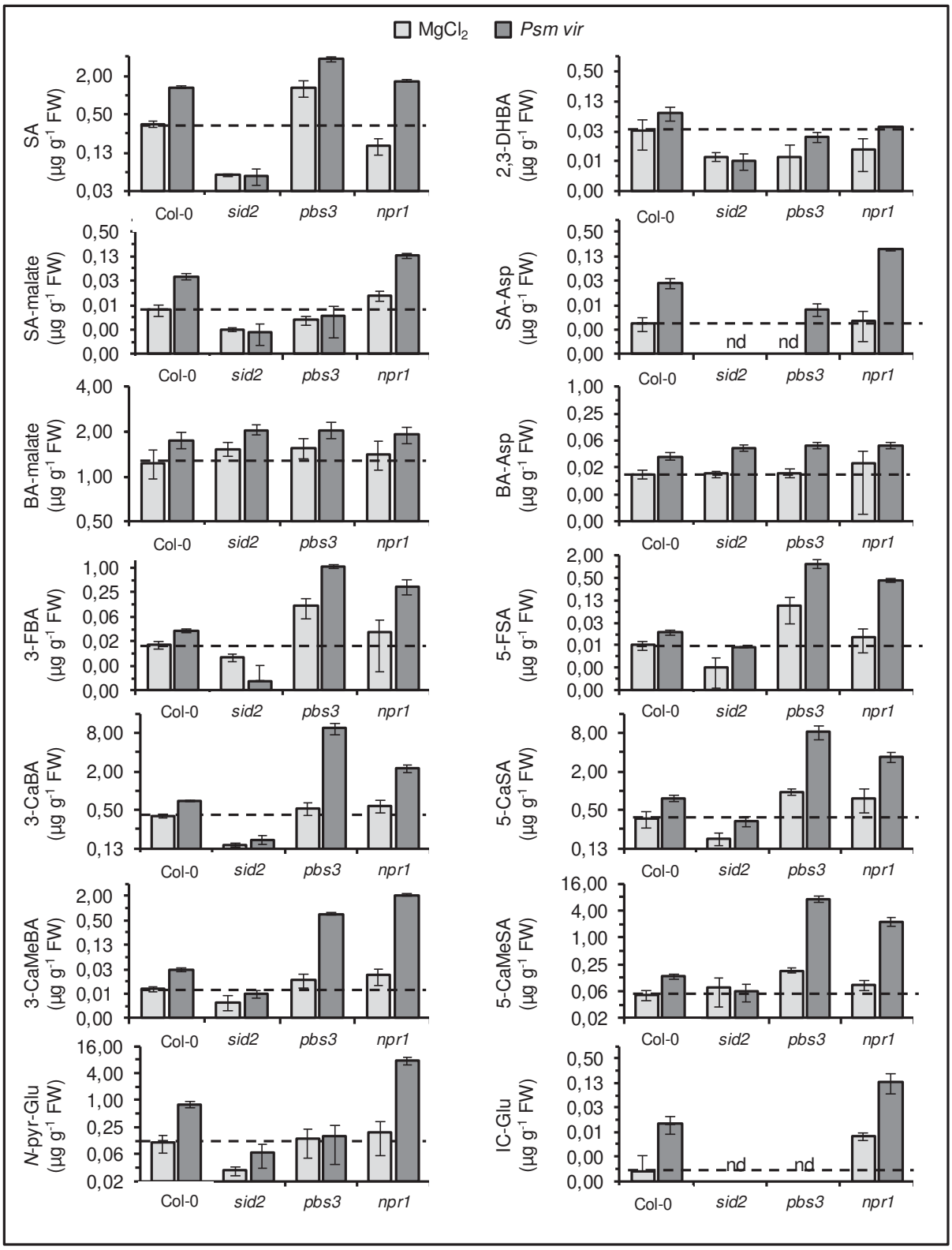

Figure S5: Accumulation pattern of molecular species in defense-related mutants
The figure shows the accumulation pattern of defense-related mutant, *sid2*, *pbs3* and *npr1,* 48 hpi with *Psm vir* and mock control infiltrated with 10 mM $MgCl_2$. Data represents experiment NiS09, including three biological replicates (three leaves of six plants per treatment were harvested and for each replicate leaves of two plants were pooled to one sample). Samples have been methylated for derivatisation. Not analyzable traces of metabolites were declared as not detected (nd). The y-axes have a log_2 scaling.

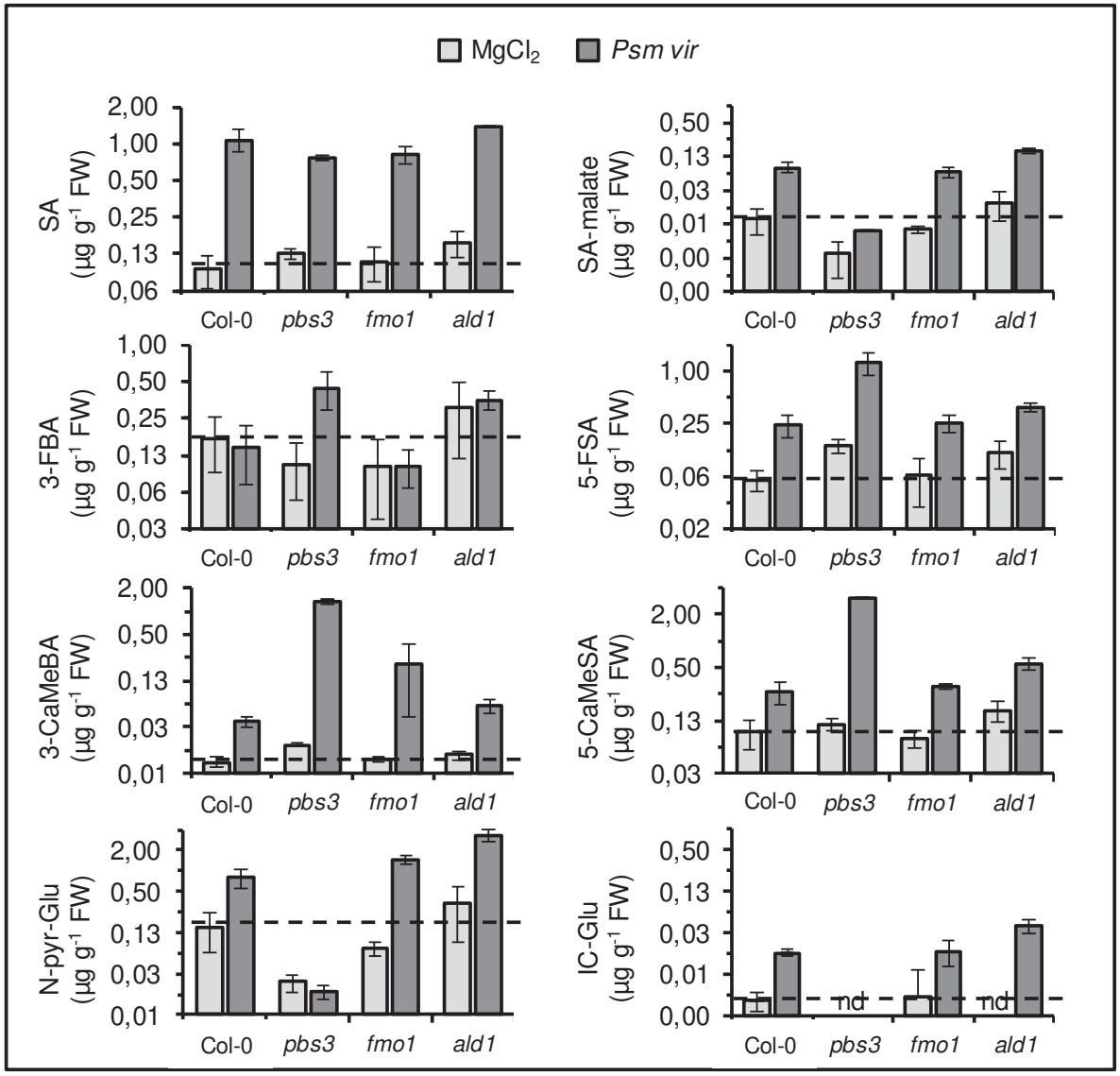

Figure S6: Accumulation pattern of molecular species in defense-related mutants
The figure shows the accumulation pattern of defense-related mutant, *pbs3, fmo1* and *ald1,* 48 hpi with *Psm vir* and mock control infiltrated with 10 mM $MgCl_2$. Data represents experiment RB01, including three biological replicates (three leaves of six plants per treatment were harvested). Samples have been methylated for derivatization. Not analyzable traces of metabolites were delcared as not detected (nd). The y-axes have a log_2 scaling. Experiment was conducted by Fredericke Bernsdorff (RB01) and analyzed by Nicola Scholten.

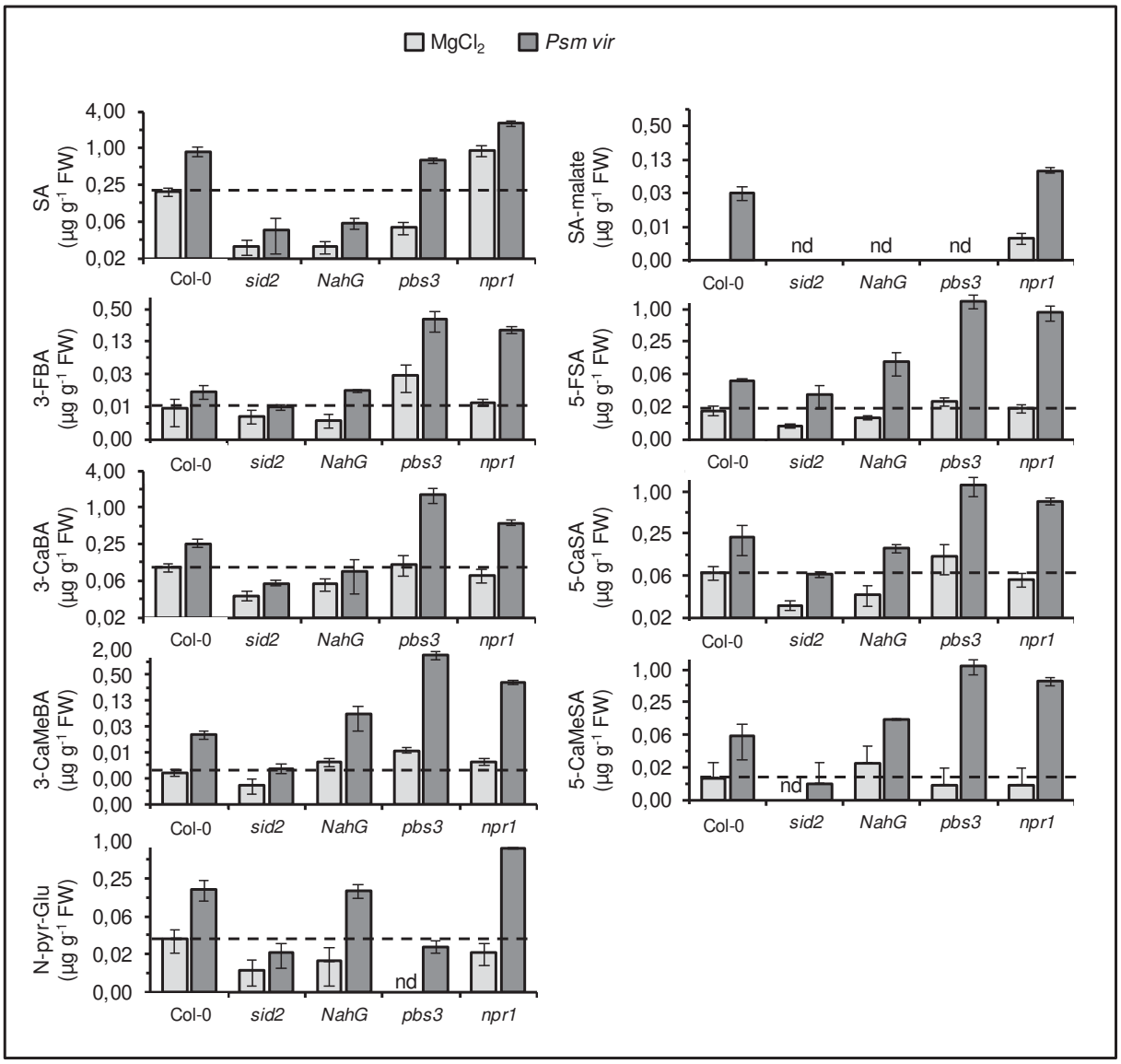

Figure S7: Accumulation pattern of molecular species in defense-related mutants
The figure shows the accumulation pattern of defense-related mutant, *sid2*, *NahG*, *pbs3* and *npr1,* 48 hpi with *Psm vir* and mock control infiltrated with 10 mM $MgCl_2$. Data represents experiment NiS10, including three biological replicates (three leaves of six plants per treatment were harvested and for each replicate leaves of two plants were pooled to one sample). Samples have been methylated for derivatization. Not analyzable traces of metabolites were declared as not detected (nd). The y-axes have a log_2 scaling.

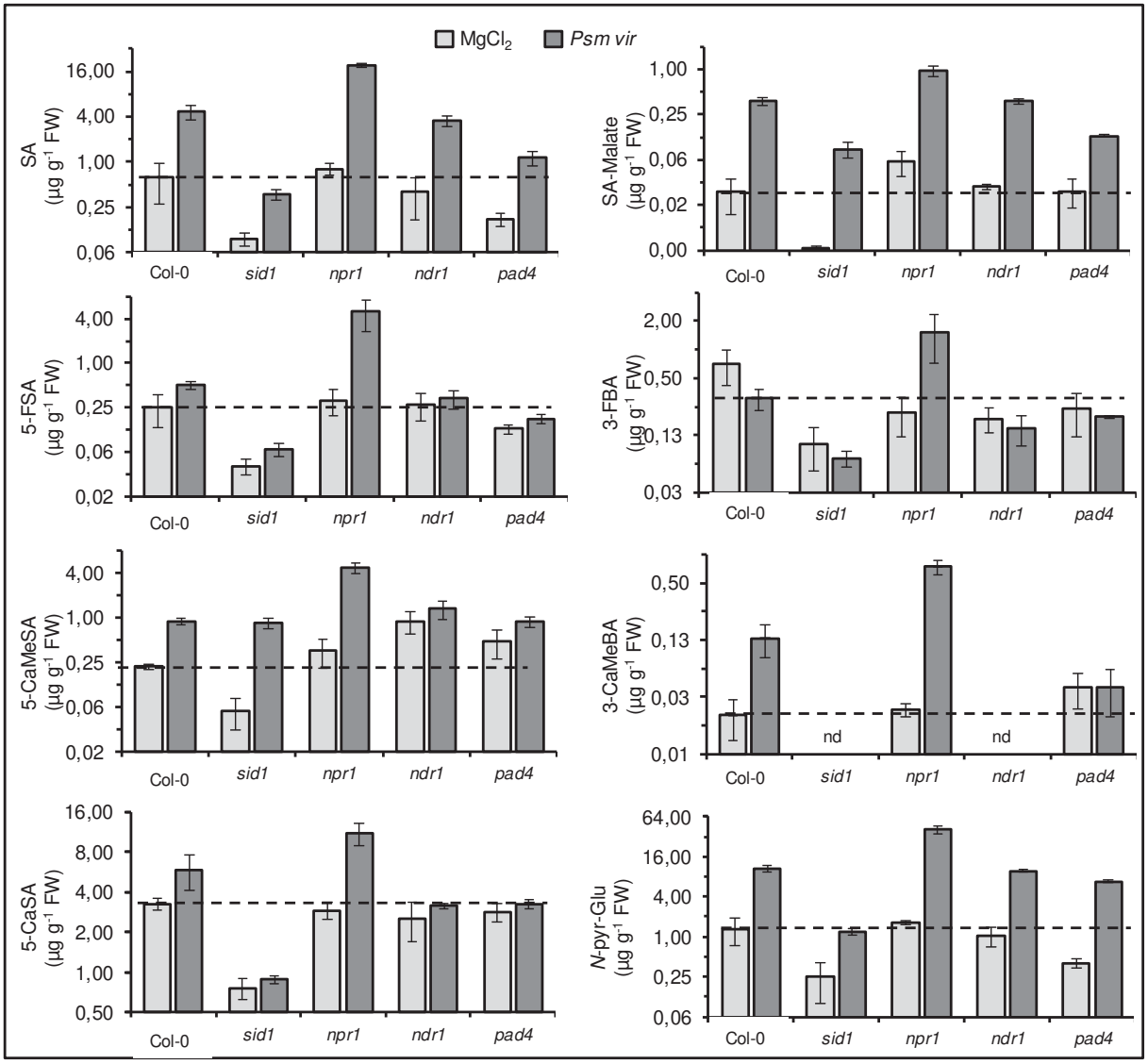

Figure S8: Accumulation of identified molecular species in important plant defense knockout mutants

The accumulation pattern of the identified molecular species shows the metabolites in important defense-related *A. thaliana* mutants after virulent *Psm vir* infection and infiltration with $MgCl_2$ as mock control. Col-0 leaves were infiltrated with a bacterial solution of OD_{600}= 0.005 or 10mM $MgCl_2$. Leaf samples were harvested 48 hpi and extracted via VPE. Experiment was conducted by Stefan Huber (SH_130412) and analyzed by Nicola Scholten. Samples have been methylated for derivatization. Not analyzable traces of metabolites were declared as not detected (nd). Data is shown in log^2.

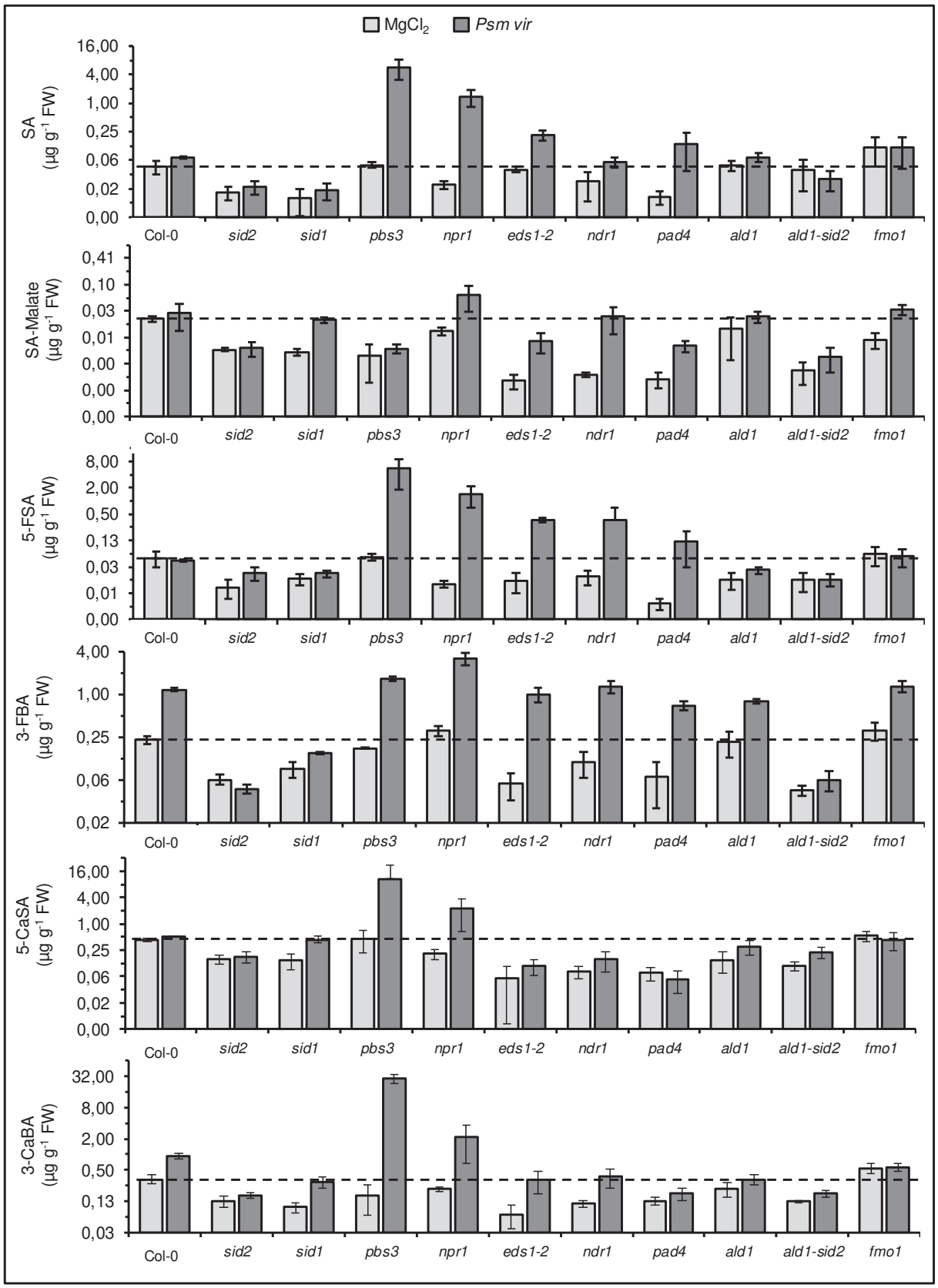
MgCl2
Psm vir
SA (µg g-1 FW)
16,00
4,00
1,00
0,25
0,06
0,02
0,00
SA-Malate (µg g-1 FW)
0,41
0,10
0,03
0,01
0,00
0,00
5-FSA (µg g-1 FW)
8,00
2,00
0,50
0,13
0,03
0,01
0,00
3-FBA (µg g-1 FW)
4,00
1,00
0,25
0,06
0,02
5-CaSA (µg g-1 FW)
16,00
4,00
1,00
0,25
0,06
0,02
0,00
3-CaBA (µg g-1 FW)
32,00
8,00
2,00
0,50
0,13
0,03
Col-0
sid2
sid1
pbs3
npr1
eds1-2
ndr1
pad4
ald1
ald1-sid2
fmo1

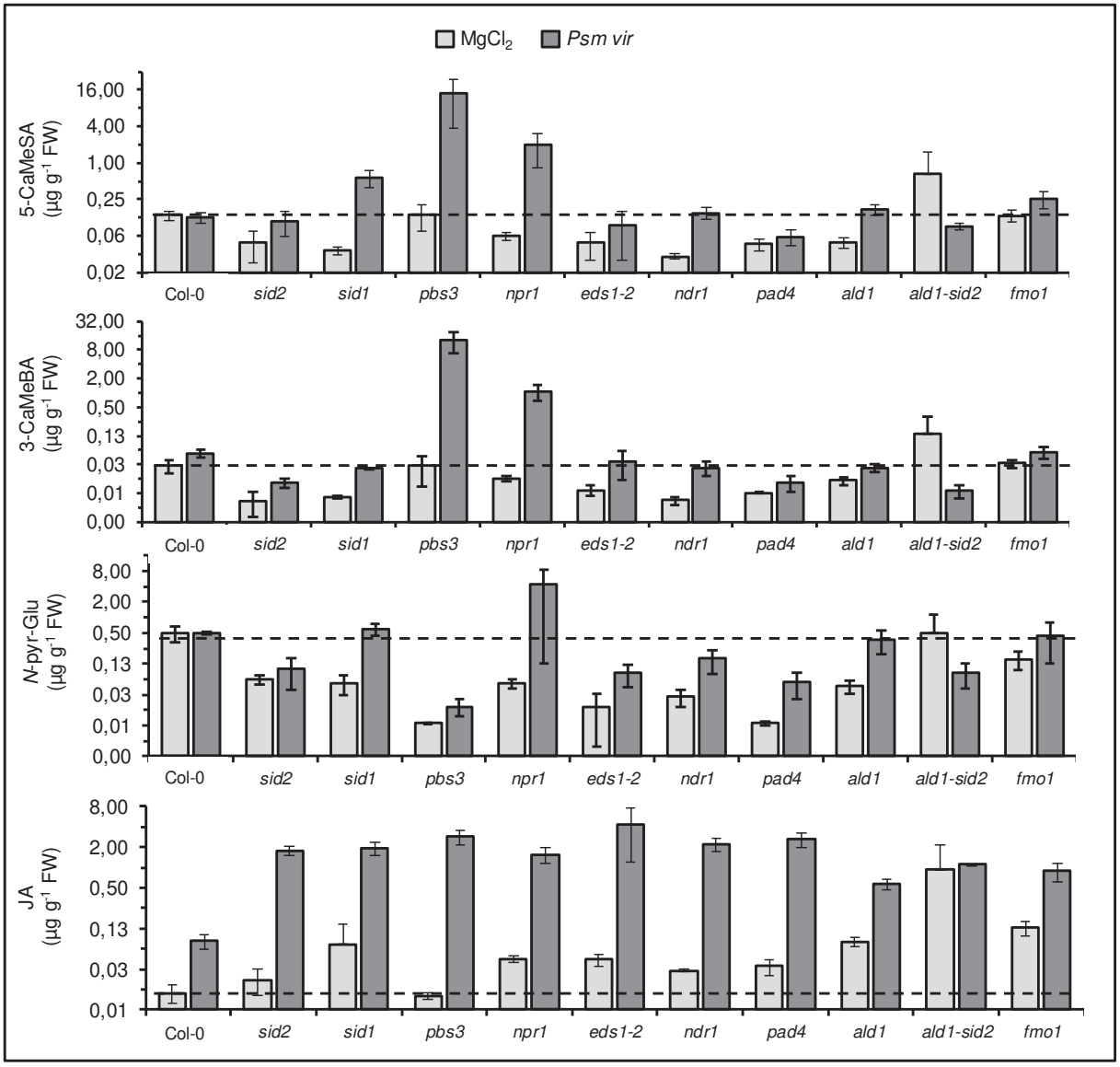

Figure S9: Accumulation of identified molecular species in important plant defense knockout mutants

The accumulation pattern of the identified molecular species shows the metabolites in important defense-related *A. thaliana* mutants after virulent *Psm vir* infection and infiltration with $MgCl_2$ as mock control. Col-0 leaves were infiltrated with a bacterial solution of OD_{600}= 0.005 or 10mM $MgCl_2$. Leaf samples were harvested 48 hpi and extracted via VPE. Samples have been methylated for derivatisation. Data represents experiment NiS06, including three biological replicates (three leaves of six plants per treatment were harvested and for each replicate leaves of two plants were pooled to one sample). Data is shown in log^2.

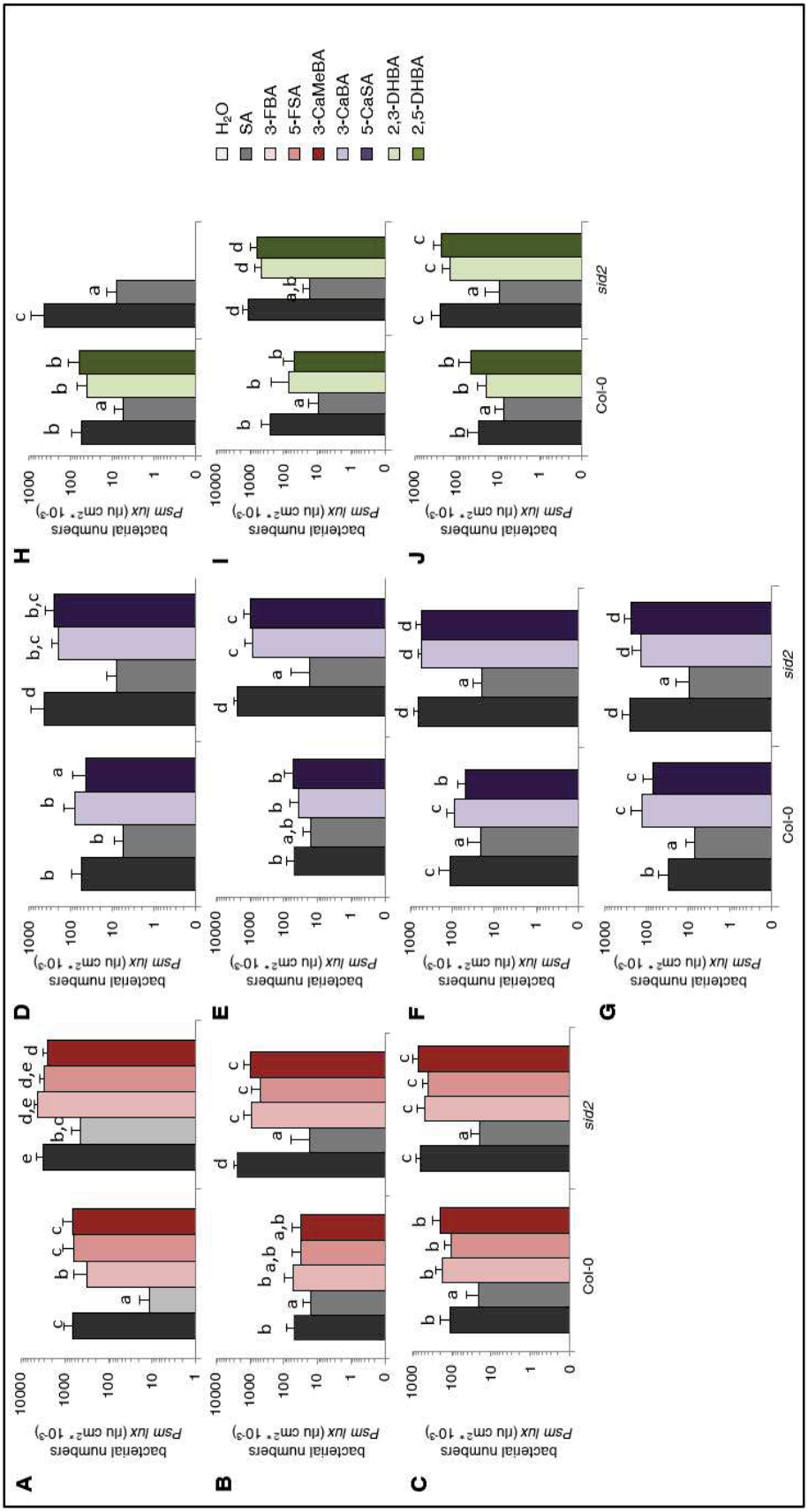

Figure S10: Replicates of the influence of identified molecular species on bacterial resistance
For bacterial resistance assays (A, B, C) plants were pretreated with the previously mentioned substance concentrations. 4 hours later the same leaves were infected with *Psm lux* (OD_{600}= 0.001). Bacterial growth has been measured 2 ½ days later. To examine the influence of the identified metabolites to plant resistance, authentic standard substances of the molecular species were infiltrated into Col-0 wild-type and *sid2* mutant plants with aqueous solutions of 0.5 mM 3-FBA, 5-FBA, 3-CaMeBA (A- C), 3-CaBA and 5-CaSA (D- G) and 2,5-DHBA, 2,3-DHBA (H-J). SA has been infiltrated as a positive control, autoclaved deionized water as a negative. Bars represent means ± SD an individual experiment, consisting of at least 15 leaves. Letters above bars indicate statistically significant differences ($p < 0.05$, ANOVA and posthoc Tukey's honestly significant difference [HSD] test

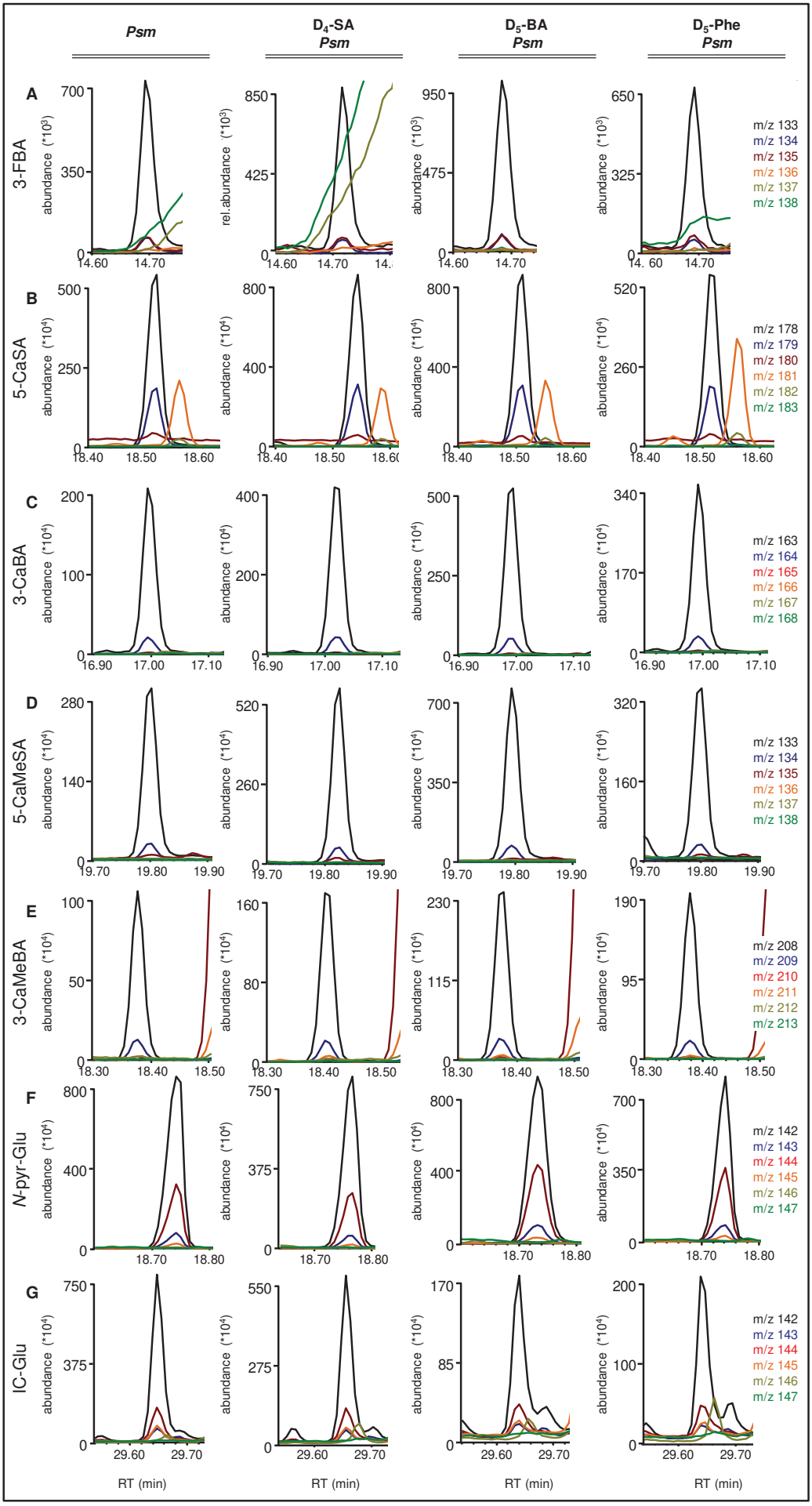
Psm
D4-SA Psm
D5-BA Psm
D5-Phe Psm
A
3-FBA
B
5-CaSA
C
3-CaBA
D
5-CaMeSA
E
3-CaMeBA
F
N-pyr-Glu
G
IC-Glu
abundance (*10³)
rel.abundance (*10³)
abundance (*10⁴)
m/z 133
m/z 134
m/z 135
m/z 136
m/z 137
m/z 138
m/z 178
m/z 179
m/z 180
m/z 181
m/z 182
m/z 183
m/z 163
m/z 164
m/z 165
m/z 166
m/z 167
m/z 168
m/z 208
m/z 209
m/z 210
m/z 211
m/z 212
m/z 213
m/z 142
m/z 143
m/z 144
m/z 145
m/z 146
m/z 147
RT (min)

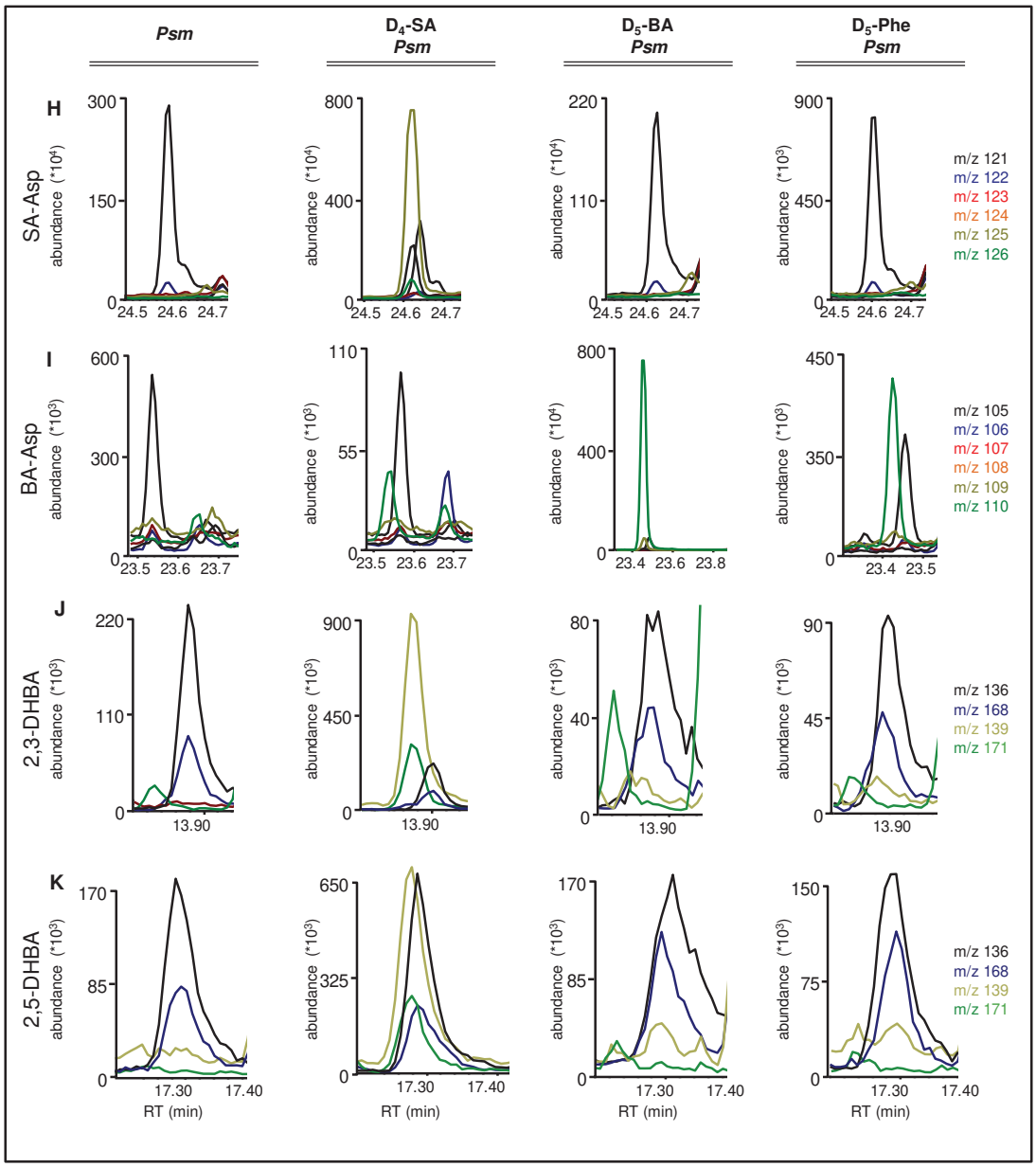

Figure S11: Pre-infiltration with labeled D_4-SA, D_5-BA and D_5-Phe
Fully grown leaves of five weeks old *npr1* plants were pre-infiltrated with 2 mM of the potential precursors SA, BA and Phe as well as isotopic labeled varieties D_4-SA, D_5-BA and D_5-Phe or water for control. Same leaves were infected with *Psm vir* (OD_{600}= 0.005) 4 h later. Infiltrated leaves were harvested 48 h after second treatment. Plant material has been extracted, methylated for derivatization and was analyzed by GC-MS.

Table S2: Tested *in vitro* substrate combinations of PBS3

AA	second acid		m/z	identification
Ala	α-ketoglutaric acid	(sCA)	n.d.	
Ala	glutaric acid	(sCA)	**129**	this thesis
Ala	succinic acid	(sCA)	**115**	this thesis
Asp	acetic acid	(sCA)	n.d.	
Asp	pyruvate	(sCA)	n.d.	
Glu	pyruvate	(sCA)	**142**	this thesis
Glu	4-HBA	(BA)	**121**	Okrent et al.
Glu	*p*-ABA	(BA)	**120**	Okrent et al.
Gly	glutaric acid	(sCA)	**129**	this thesis
Gly	α-ketoglutaric acid	(sCA)	n.d.	
Ill	oxalate	(sCA)	n.d.	
Ill	malonic acid	(sCA)	n.d.	
Leu	malonic acid	(sCA)	n.d.	
Leu	oxalate	(sCA)	n.d.	
Mal (sCA)	SA	(BA)	n.d.	
Mal (sCA)	3-HBA	(BA)	n.d.	
Met	4-HBA	(BA)	**121**	Okrent et al.
Met	*p*-ABA	(BA)	n.d.	
Val	malonic acid	(sCA)	n.d.	
Val	oxalate	(sCA)	n.d.	
Val	succinic acid	(sCA)	**115**	this thesis

21 potential *in vitro* substrate combinations were tested with active PBS3 enzyme. PBS3 conjugated amino acids (AA) to benzoic acids (BA) and small carboxylic acids (sCA). Here, we could show that PBS3 was active on eight substrate combinations. The mass to charge ratio (m/z) of the identified product is marked in bold and underlined. Substrates were extracted via VPE and methylated for derivatization. Five of the combinations were initially described in this thesis. not detected (n.d.).

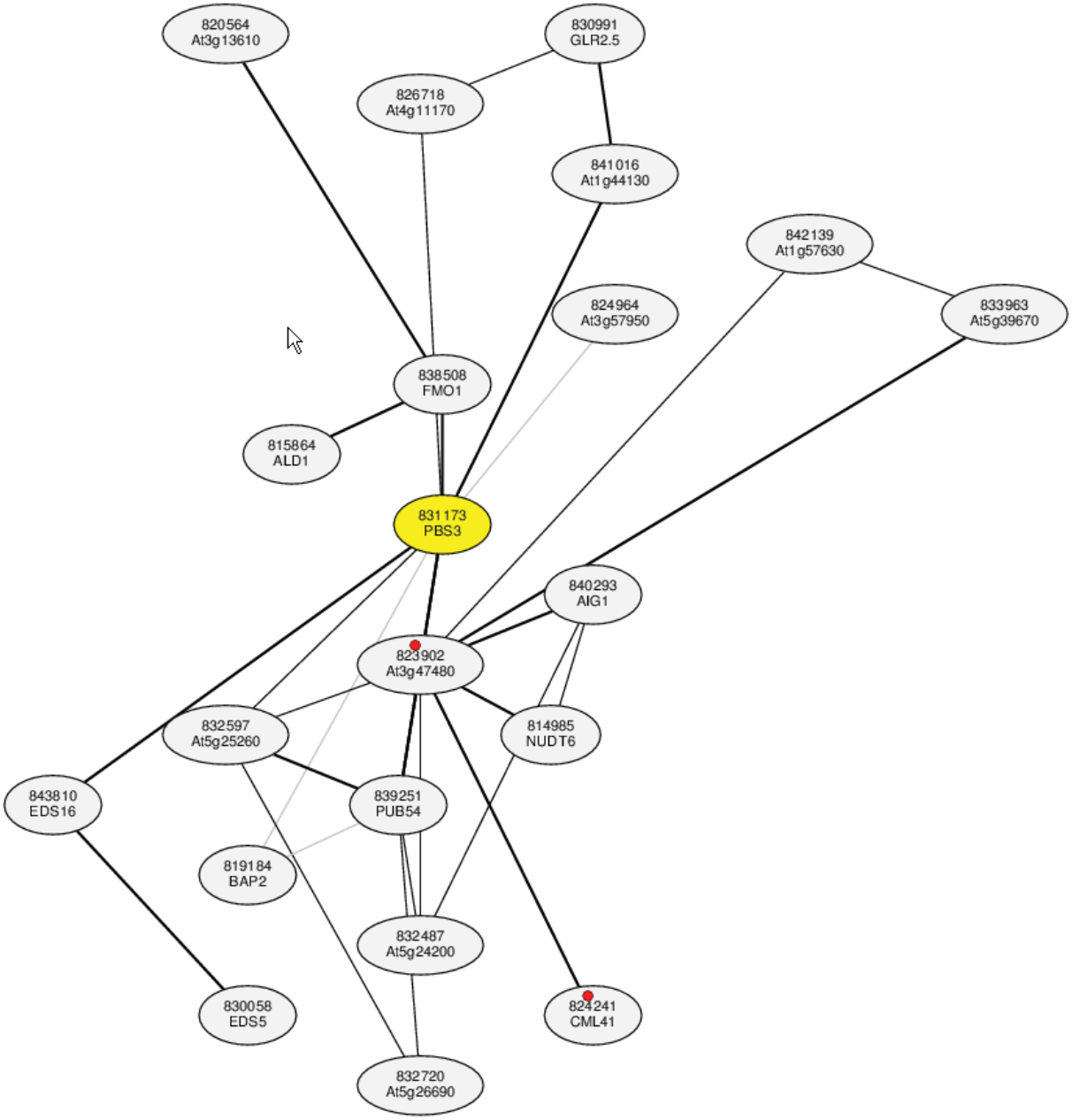

Figure S12: Coexpressed gene network around At5g13320 (Microarray)
Network of coexpressed genes of PBS3/ WIN3
source: https://atted.jp/locus/?gene_id=831173 downloaded: 02.05.2021 16:23

7.3 Eigenständigkeitserklärung

Hiermit erkläre ich, dass ich die heute eingereichte Dissertation selbständig verfasst und keine anderen als die angegebenen Quellen und Hilfsmittel benutzt sowie Zitate kenntlich gemacht habe. Bei den vorliegenden Dissertationen handelt es sich um in Wort und Bild völlig übereinstimmende Exemplare.

Weiterhin erkläre ich, dass digitale Abbildungen nur die originalen Daten enthalten und in keinem Fall inhaltsverändernde Bildbearbeitung vorgenommen wurde.

Düsseldorf, den 6. April 2021

_____

Nicola Scholten